Experimental Thermonuclear Installation - TOKAMAK - 20 – Preliminary Study

V.V. Alikaev, V.A. Glukhikh, U.N. Dnestrovskii, D.P. Ivanov, B.B. Kadomtsev, S.B. Mirnov, N.A. Monoszoh, V.S. Mukhovatov, G.N. Popkov, N.N. Semashko, V.S. Strelkov, G.F. Churakov, V.D. Shafranov; Translated by I.N. Sviatoslavsky

June 1975

UWFDM-129

FUSION TECHNOLOGY INSTITUTE

UNIVERSITY OF WISCONSIN

MADISON WISCONSIN

Experimental Thermonuclear Installation - TOKAMAK - 20 – Preliminary Study

V.V. Alikaev, V.A. Glukhikh, U.N. Dnestrovskii, D.P. Ivanov, B.B. Kadomtsev, S.B. Mirnov, N.A. Monoszoh, V.S. Mukhovatov, G.N. Popkov, N.N. Semashko, V.S. Strelkov, G.F. Churakov, V.D. Shafranov; Translated by I.N. Sviatoslavsky

Fusion Technology Institute
University of Wisconsin
1500 Engineering Drive
Madison, WI 53706

http://fti.neep.wisc.edu

June 1975

UWFDM-129

- 129

Experimental Thermonuclear Installation

TOKAMAK - 20

Preliminary Study (First draft)

Vol. 1
Basis for the Physics

National Committee for the Utilization of Atomic Energy Soviet Ministry, USSR.

I. V. Kurchatov Atomic Energy Institute
D. V. Yefremev Scientific Research Institute for Electrophysical Aparatus.

MOSCOW 1975

Translated by Igor N. Sviatoslavsky
University of Wisconsin Fusion Design Study Group.

FDM-129

Participants in the preparation of the "Basis for the Physics"

Section of T-20

V. V. Alikaev

V. A. Glukhikh

U. N. Dnestrovskii

D. P. Ivanov

B. B. Kadomtsev

S. B. Mirnov

N. A. Monoszon

V. S. Mukhovatov

G. N. Popkov

N. N. Semashko

V. S. Strelkov

G. F. Churakov

V. D. Shafranov

Note from the translator.

This report was translated hastily without benefit of proper editing. I would therefore like to beg the indulgence of the readers, if certain portions of it read more like Russian than English.

I am grateful to my wife Wanda, who typed late into the night to get this report done.

I.N.S.

TABLE OF CONTENTS

INTRODUCTION

T-20 is an experimental thermonuclear installation intended for the study of physical processes in plasma with thermonuclear parameters of ($n\tau_E \approx 10^{14}$ cm^{-3} sec, $T > 7$ KeV) and which will allow fairly lengthy operation under D-T conditions. Besides solving problems of physics, T-20 will make it possible to perform modeling and the selection of basic engineering solutions which must be faced before the design of an energy producing thermonuclear reactor based on the Tokamak principle can be completed.

The main parameters of the installation (plasma size, plasma current, total power expended and methods of supplementary heating) are selected in such a way that the energy produced by the thermonuclear reaction in a D-T plasma, in the form of neutrons, is the same order as the amount expended on the plasma.

The $n\tilde{\tau}_E$ and T plasma parameters in T-20 are almost identical to those needed in a hybrid Tokamak reactor with a uranium blanket and can be directly extrapolated (without any intermediate steps) to a "clean" energy producing reactor.

1.2. The rapid growth of research on Tokamaks and the general conclusion that plasma confinement time must scale with dimension have dictated the next step in the program for Tokamaks. This step will be implemented with the coming on line by mid 1975 of two large installations; T-10 (IAE) and PLT (Princeton).

On T-10 as compared to T-4, the plasma radius was doubled and the current is up by almost a factor of 4 (from 0.2 to 0.7 MA). It is anticipated that T-10 may have an $n\tilde{\tau}$ up to 10^{13} and an ion temperature of 1.5-2 KeV.

1.3 At the present time there are designs for three large Tokamaks of the next generation: JET (Joint European Torus), TCT (Two-component Torus, Princeton) and JT-60 (60m3 plasma Tokamak in Japan). JET is figured for a current of 3 MA (with the possibility of going to 5 MA), TCT up to 2.5 MA and JT-60 to 3 MA. The JET and TCT machines are planned as last stages in experiments for achieving a thermonuclear reaction in a DT plasma. We assume that all these machines will be built and brought on line by 1980.

2. The T-20 Installation and its Aims

2.1 Based on the consecutive steps $n\tau \approx 10^{12}$ (T-4), $n\tau \approx 10^{13}$ (T-10) it appears reasonable to aim at $n\tau \approx 10^{14}$ during the next step, namely T-20. At a plasma temperature T = 8-10 KeV, the value of $n\tau \approx 10^{14}$ will insure a power output from the DT reaction (with 14.1 MeV neutrons) greater than that expended on the plasma. In other words Q, the ratio of power out to power in will be greater than unity. The value of $n\tau \approx 10^{14}$ is entirely adequate for a commercial breeder reactor with Uranium in the blanket. This is somewhat lower than Lawson's criterion of $n\tau = 3 \times 10^{14}$ for igniting a thermonuclear reaction but is entirely reasonable from a standpoint that a 3-5 extrapolation to a "clean" energy producing reactor can be made from $n\tau = 10^{14}$ without any intermediate steps.

Thus, one of the main aims of T-20 is the attainment of $n\tau_E \approx 10^{14}\ cm^{-3}\ sec$ (τ_E is the confinement time) for a plasma temperature higher than 7 KeV, namely, the realization of a demonstration experiment where the energy output from a DT reaction is of the same order as that expended in the plasma.

2.2 On attaining a plasma with thermonuclear parameters ($n\tau_E \approx 10^{14}$ cm^{-3} sec, $\bar{T} > 7$ keV) the T-20 installation will allow investigation of the physical processes in a reacting DT plasma. In particular it would be possible to study the confinement processes of charged thermonuclear reaction products, namely, α particles and their effect on the reaction, a point which is imperative to the understanding of ignition and a self-sustaining reaction in a DT plasma.

2.3. Upon attaining a mode of rapid rate pulses and by operating for a long period in such a mode, T-20 will permit the study of blanket modules of different construction for neutronic experiments and will allow modeling work on future energy producing thermonuclear reactors based on the Tokamak principle.

3. Choice of Main Parameters for T-20

3.1. The parameters of T-20 are determined by the pre-set goal, namely the possibility of long term operation with a reacting DT plasma and by the technical limitation for achieving these parameters.

3.2. One of the main parameters of a Tokamak type device is the current I in the plasma. According to optimistic evaluations, the quantity $n\tau = 10^{14}$ can be attained only with a current which is greater than 3 MA. Such a current is planned for JFT and JT-60, and the same order of current will be attained in TCT. If we included a factor of uncertainty based on inadequate knowledge, then we should pick a higher current value. Planning as well the possibility of long term operation with a DT plasma and the performance of engineering and technical studies on the

T-20, it seems reasonable to pick a current value of I = 5-6 MA.

3.3. At a current I ≳ 3 MA, not all the α particles from the DT reaction are confined in the system with the result that a noticeable amount will immediately hit the wall. In order to confine a substantial portion of the α particles and to retard their motion in the plasma toroid, it is reasonable to increase the current I higher than 3 MA. At a plasma current of 6 MA, more than 90% of the α particles will be confined.

3.4. The main parameters of T-20

1 - Major radius of the toroid: R = 5m

2 - Minor radius of the plasma toroid to the limiters: a = 2m

3 - Plasma volume 400m^3, plasma surface area $S = 400\,m^2$.

4 - Maximum plasma current: I = 6 MA

5 - The magnetic field at plasma center: $H_z = 35\,KG$

6 - Pulse length in the plasma: $t_y = 20\,sec.$

7 - Expected values

Plasma temperatures

Due to ohmic heating: T = 3 KeV

Due to supplementary heating: T = 10 KeV

Confinement time $\tau_E = 2\,sec.$

Confinement parameter $n\tau_E = 10^{14}\,cm^{-3}\,sec$

Average density $n = 5 \times 10^{13}\,cm^{-3}$

β_p poloidal for T = 10 KeV $\beta_p = 1$

Stability factor $q = 2.3$

Number of particles in machine $N_e = 10^{22}$

8 - Energy stored in the plasma $W_p = 10^8$ J.

Anticipated power losses $P = W_p/\tau_E = 50$ MW

Average heat load on the wall $p_w = P/S = 12.5$ w/cm^2

9 - The anticipated number of neutrons per pulse for a DT mixture is $10^{20} - 10^{21}$ (neutron fluence is up to 10^{13} neutr/cm^2 sec).

4. Plasma Confinement in T-20

4.1. Let us present now those considerations which have led us to the proposed parameters for T-20. The main indicator of the effectiveness of magnetic plasma confinement is the confinement time τ_E. This value can be obtained either on the basis of extrapolating existing empirical relationships or the reliance on one or another theoretical Model. We will now discuss the different possible options.

4.2. A straight empirical extrapolation can be made based on the empirical equation $\tau_E = 7 \times 10^{-9} a I$ (i.e. $\tau_E \sim a^2 H_\theta$ where $H_\theta = I/5a$ is the electric field at the edge of the plasma in oersteds, and I is the current in A). This relationship produces the best results for plasma confinement in Tokamaks and in this sense it provides an upper limit for τ_E. For the selected parameters of a and I, the empirical formula gives the value of $\tau_E = 8.4$ sec. There is already experimental data in which τ_E is a factor of two or three smaller than empirically predicted by $\tau_E \sim a I$. For this reason it is more realistic to take $\tau_E = 3-4$ sec which for a stored energy of $W_p = 10^8$ J corresponds to a power loss of 25-30 MW.

It should be mentioned that the empirical equation $\tilde{\tau}_E \sim a^2 H_\theta$ does not have any physics basis and besides, it does not take into account any losses due to radiation by impurities which will become greater as the temperature is increased.

4.3. The other approach is based on one or another theoretical model, which gives an adequate agreement with existing data. Some of these models are discussed in Appendix 1. Thus, for example, a rather optimistic model which proposes a pseudoclassical diffusion of electrons and a neoclassical diffusion of ions (with an entry into a deep collisionless banana regime) gives a confinement time of several tens of seconds. A more pessimistic "six regime" model which takes account of theoretical predictions but experimentally unverified instabilities due to trapped particle orbits, gives for H_z = 35 KG and a current I = 6 MA a value of $n\tilde{\tau}_E \approx 10^{14}$ for T = 7 KeV, β_p = 1 and $\bar{Z}$ = 1, further, $n\tilde{\tau}_E$ grows very rapidly with a decrease in the temperature and an increase in the density (besides this, $n\tilde{\tau}_E$ increases linearly with $\bar{Z}$).

4.4. In discussing the question of extrapolating existing data to larger devices, it is reasonable to make use of similarity considerations in Tokamak type systems. We can show that the density of an ionized plasma in a Tokamak is described by eight dimensionless parameters. During ohmic heating, two of these parameters for example β_p and $\theta = T_e/T_i$ are dependent, namely, they are functions of the remaining six. Of these six parameters the Debye number Nd (number of particles in a sphere of Debye radius) is not pertinent to the investigated round of problems, but the

ratio of the electron mass to the ion mass, $\mu = m_e/m_i$, may be considered constant. Four of the remaining parameters are the aspect ratio A = R/a, the confinement factor $q = a H_z/R H_\theta$ and two parameters which represent the longitudinal and transverse plasma confinement: $\nu = qR/\lambda_e$ and $K = \rho/a$ where λ_e is the average mean free path of electrons and ρ the Larmor radius of the ions (it can be easily related to the electron temperature). A and q are parameters with a limited variation and can thus be considered constant. In this way only ν and K are the determining parameters.

The value of ν, even in existing devices varies within a large range and it characterizes the degree of the collisionality in the banana regime. In T-20, the proposed parameters correspond to a plasma well into the banana regime so that existing data concerning ions in the plateau regime cannot be directly extrapolated.

The dependence of the K parameter is apparently less critical. Existing machines have proved that the diffusion characteristic of the leakage corresponds to the dependence $\tau_E \sim K^{-2}$ and this will not likely change in T-20 where the parameter $K \sim \sqrt{T}/I$ will decrease only by a factor of five over TFR and a factor of three or four over T-10.

In this way the largest uncertainty in predicting τ_E for T-20 comes from the ions entering the banana regime. This uncertainty will be partly alleviated and possiby eliminated by imminent experiments on T-10 and PLT.

4.5. For further discussion, it is convenient to introduce a group of numerical values for some of the important quantities. Let us begin with the σ, the electrical conductivity of the plasma. Taking into account the trapping of electrons due to the toroidal geometry and the possible presence of impurities, we will introduce into the Spitzer equation for σ the anamoly factor A_R:

$$\sigma = \frac{1.1 \times 10^{13}}{A_R} T^{3/2} sec^{-1} = \frac{12}{R} T^{3/2} ohm^{-1} cm^{-1}$$

where T is the temperatue in eV. Assuming $A_R = 10$ we obtain for T = 10 KeV a value of $\sigma = 1.2 \times 10^{6} ohm^{-1} sec^{-1}$ and for T = 3 KeV a value of $\sigma = 1.6 \times 10^{5} ohm^{-1} sec^{-1}$ (skin time of the plasma is 90 sec. and 15 sec. respectively). In this way the power from ohmic heating $P_g = 2RI^2/\sigma a^2 = 1 MW$ for T = 10 KeV and P_g = 5 MW for T = 3 KeV; in other words it is very small.

Further for (T = 10 KeV): electron-ion collisional mean free path $\lambda_{ei} \approx \frac{3 \times 10^{12} T^2}{A_R n} \approx 6 \times 10^{5} cm$

Electron thermal velocity $v_e = 6 \times 10^{7} \sqrt{T} = 6 \times 10^{9} cm/sec$

Electron-ion collision frequency $\nu_{ei} = v_e/\lambda_{ei} \approx 10^{4} sec^{-1}$

Charge exchange time $\tau_{eq} \approx 0.8 sec$

Collision parameter $\nu = qR/\lambda_e \approx 2 \times 10^{-3}$

Time to slow down an 80 KeV ion $\tau_D \approx 0.3 sec$

Let us note that the boundary between the "plateau" regime and the "banana diffusion" regime is $\nu \approx (r/R)^{3/2} \sim 10^{-1}$, and thus at 10 KeV the T-20 plasma enters well into the banana regime (about two orders of ν).

We will also introduce the Bohm time $\tau_B = \frac{\pi a^2 H_z e}{cT} =$ 5×10^{-3} sec for T = 10 KeV and the ion thermal diffusion time on the plateau $\tau_{pi} \cong \frac{a^2 R}{6q\rho^2 v_i} \cong 0.1$ sec for $T = 10$ KeV (here ρ is the ion Larmor radius, v_i is their thermal velocity). At a temperature of 3 KeV, this value is $\tau_{pi} = 0.5$ sec., greater than the charge exchange time between electrons and ions which is $\tau_{ei} \approx 0.2$ sec.

The slowing down time of α particles, τ_α, is the order of one sec. The power loss due to them at 10 KeV is $P_\alpha \approx 15$-20 MW.

4.6. Power losses from a plasma can be by electron and ion thermal conductivity, neutral charge exchange, radiation by pure hydrogen plasma (Bremsstrahlung and synchrotron) and radiation from the impurities. In a pure plasma of large dimensions all the energy loss mechanisms except the thermal conductivity losses are small (see Appendix 1). We will thus examine the thermal conductivity losses.

On all the existing experiments on Tokamaks there is a dominating energy loss channel by means of electrons. Correspondingly, in T-20, during ohmic heating, when ion thermal conductivity does not exist, one might expect the same kind of plasma condition as exists in present experiments. In fact, within a large interval of the variation in the parameter $\nu = qR/\lambda e$ the value β_p changes slowly and as a rule does not fall below 0.2 - 0.3. With guarded optimism let us assume that β_p in T-20 during ohmic heating and an absence of ion thermal conduction reaches a value $\beta_p = 0.3$ which corresponds to a plasma stored energy $W_p = 3 \times 10^7$ J and a temperature T = 3 KeV. Under these conditions $\tau_E = W_p/P_\gamma = 3 \times 10^7 / 5 \times 10^6 = 6$ sec.

As the plasma temperature is increased, the time τ_E and the power loss by the electron channel mechanism varies somewhat. For instance, if the pseudoclassical relationship $\chi_e \sim \rho_{e\theta}^2 \nu_e$ is correct, then the electron lifetime must scale with temperature as $\sqrt{T}$ and correspondingly, the power loss $\sim nT/\tau_E \sim \sqrt{T}$ can rise to 10 MW.

4.7. Let us now turn to the ions. In all contemporary Tokamaks the ions are in the plateau regime of the neoclassical theory of diffusion processes and the value of their thermal conductivity is in good agreement with theory. If in T-20 the rate of diffusion remains in the plateau regime, then the power loss from ions would be $P_i = W_p/2\tau_{pi} = 100\,MW$ for $T = 3\,KeV$ and P_i = 500 MW at T = 10 KeV which is unreasonably high. For this reason, in order to be able to carry out experiments at 10 KeV it is imperative to achieve an ion thermal conductivity at least an order of magnitude lower than the plateau value. Neoclassical scaling at the anticipated $\nu \sim 10^{-3}$, namely well into the banana regime, predicts a value which is two orders of magnitude larger than τ_{pi}, i.e. $\tau_{Ei} \approx 10$ sec and the corresponding power loss $P_i \sim 5\,MW$.

These values appear to be optimistic, since at this depth into the banana regime, there may be ion instabilities due to thermal drift and trapped ions. In a toroidal geometry such as T-20 where the aspect ratio A = R/a = 2.5, the thermal drift instability will produce an increase in τ_{Ei} of several times relative to τ_{pi} and the trapped ion instability will permit the attainment of $n\tau_E \cong 10^{14}\,cm^{-3}sec$ for $T = 7\,KeV$ & $\beta_p = 1$, $\bar{Z} = 1$.

Accounting for a rather large uncertainty on this point (which could be eliminated by imminent experiments on T-10 and PLT), we have picked the values $\tilde{\tau}_E$ = 2 sec. and $n\tilde{\tau}_E = 10^{14}$ cm^{-3} sec but we should keep in mind that these values can change by two or three factors in either direction from the real values on T-20.

4.8. While analyzing ion thermal conductivity, one must account for the neoclassical thermal conduction by ions trapped in non-homogeneous (wavy) regions of the toroidal magnetic field. Let us designate the ripple by δ = (Hmax - Hmin)/2H. Thus, according to neoclassical theory, the thermal conduction in the ripple must lead to a time $\tilde{\tau}_{\delta i} \approx \nu\delta^{-3/2}\tau_{pi}$. For $\nu \sim 10^{-3}$ and $\tau_{pi} \approx 10$ sec the value of δ must be less than 1% so that $\tilde{\tau}_{\delta i}$ could rise to a value of the order of several seconds. In this way, the value δ in the main portion of the plasma toroid must be undoubtedly less than 0.1%.

4.9. Radiation from impurities in a high temperature plasma is one of the main channels of energy leakage. According to the latest theoretical data (see Appendix 3) the average radiated power from impurities at T = 10 KeV is relatively weakly dependent on temperature and may be approximated by $P_r = 6 \times 10^{-30} n_e n_z Z^2$ w/cm^3, where n_z is the density of the impurity which has an atomic number Z. At a density $n_e = 5 \times 10^{13}$, we obtain for the whole volume $P_r = 6\bar{Z}$ MW, where $\bar{Z} = \sum_z \frac{n_z}{n_e} Z^2$, is the effective atomic number of the charged ions. From this it is evident that at higher $\bar{Z}$, the radiation losses from impurities become

larger, reaching 30 MW for $\bar{Z} = 5$. It would seem that the value $P_r \approx 30$ MW should be a reasonable upper limit for allowable losses due to radiation (we remind you that the energy from the α particles from the DT reaction can reach 15-25 MW.)

5. Impurities

The problem of plasma contamination by impurities is a big problem in most stationary systems including Tokamaks. Besides plasma confinement and heating, the problem of impurities is one of the three main problems standing in the way of a thermonuclear reactor. Since T-20 is a short pulse device (pulse length does not exceed several energetic times) and is intended to solve only the first two problems, plasma heating and confinement, nevertheless, in order to do this it must have a relatively clean plasma. Existing experimental data on the level of plasma contamination in Tokamaks and the behavior of impurities in the plasma toroid are not completely determined. A common quantity that might be considered is several percent of light impurities and a fraction of a percent of heavy impurities, such that the value of $\bar{Z}$ might reach 3-4. From the standpoint of radiation from the impurities, this level seems acceptable for T-20.

The process of accumulating impurities during a discharge is not completely understood. The accumulation of impurities during a discharge and their concentration on the axis of the toroid were discovered during stable discharges on the T-4 Tokamak. On the other hand, for example on TFR, for a small increase in the plasma density with time, one observes a constant in time impurity concentration corresponding to a $\bar{Z} = 4$, from which the authors have concluded that the rate of impurity accumulation is two

orders less than the rate of impurities coming from the wall of the chamber and entering the plasma surface.

5.3. In T-20 the average energy deposition on the chamber wall is taken as 12.5 watt/cm^2 (during ohmic heating at T = 3 KeV, this value is an order of magnitude less). This value is the same order of magnitude as that in contemporary large Tokamaks such as T-4 and TFR. Thus it might be expected that the rate of plasma contamination in T-20 at 10 KeV will be about the same as in T-4 and TFR (if the chamber and the limiters will be made of the same materials as are used presently). But since the minor radius of the plasma torus in T-20 is an order of magnitude larger than in T-4 and TFR then we may expect that the rate of plasma contamination per cubic centimeter will be an order of magnitude less. In TFR the value $\bar{Z}$ = 4 is maintained for 0.4 sec. which leads us to think that in T-20, we may expect several seconds before the impurities reach a value of $\bar{Z}$ = 4 - 5. This gives adequate time for the performance of an experiment.

5.4. In the first version of the vacuum chamber for T-20, we do not propose to have a diverter in order to reduce the level of impurities (although such a possibility is considered for future stages of the effort). We also concede that the first version of the chamber will not be optimised as to the choice of materials for its various components which might interact with the plasma. These are the chamber itself, the limiters (stationary and movable), screens etc. For this reason the design must allow for the possibility of replacing the chamber and its elements during experi-

mentation. The design of the chamber and its elements must also take into account the peculiarities of energy transfer in the plasma and the means of its contamination by impurities.

5.5. During the interaction of the plasma with the walls there exist several means by which impurities are liberated so that they can contaminate the plasma:

1 - Scorching and possibly ablation of chamber elements from the intense heat.

2 - Physical sputtering by energetic ions.

3 - Gas desorption and the destruction of chemical bonds from the impact of electrons.

4 - Knock-out of impurity atoms by gamma and ultraviolet radiation.

5 - Physical sputtering by neutrons from the DT reaction

6 - Blistering, namely exfoliation of material, mainly due to the action of α particles from the DT reaction

5.6. These mechanisms are not identical in their effect on the plasma. Blistering, for example, begins with doses the order of 0.1 coulumbs, namely, with an α particle fluence of 10^{13}-10^{14} per pulse per cm^2 of surface, blistering begins to appear after $\sim 10^3$ DT pulses. Thus for the initial series of experiments with a small number of pulses it is not dangerous, but may become very significant on further use. Since α particles are charged and will undoubtedly accumulate on protruding sections of the chamber (limiters), a plan must be implemented for replacing them if the need arises (we should point out that for very large doses,

blistering diminishes). We can also hope that for the T-20 parameters, a large portion of the α particles will have time to give up their energy to the plasma.

5.7. As concerns neutron sputtering, there does not seem to be a full understanding of the process, since the corresponding data for sputtering coefficients S_n oscillates from 10^{-3} to 0.25. Even with $S_n \sim 10^{-1}$ the flow of impurities will be the order of 10^{12} particles/cm^2 sec. (for a neutron flux of 10^{13} n/cm^2 sec.), which is small.

5.8. The liberation of impurities due to the bombardment of the wall surface by γ quantas appears to be the least damaging of all the mechanisms and thus, the radiation from these impurities is the most favorable from the standpoint of a plasma energy loss mechanism. This mechanism of contamination can be neglected.

5.9. The flow of impurities due to electron bombardment can be reduced to acceptable levels by means of proper preparation of the chamber. If a coefficient of desorption $C \sim 10^{-5}-10^{-4}$ can be achieved (a very high level of cleanliness of the wall) then one joule of energy transferred to the wall by 100 eV electrons will liberate the order of 10^{12} impurity particles, which implies 10^{14} particles/cm^2 per pulse and is a permissable quantity.

In all existing Tokamaks, the energy which is dissipated on the limiters is mainly in the form of 100 eV electrons. This process removes energy from the plasma by means of the most favorable mechanism from the standpoint of material sputtering.

This advantage should also be preserved in the construction of the chamber and limiters for T-20.

5.10. Physical sputtering by fast ions is one of the most serious means of contaminating the plasma. In T-20, sputtering will occur first of all by ions of 30-100 eV on the plasma boundary (for example, those that hit the limiters), secondly by neutrals of 1-3 KeV coming from charge exchange with cold gas atoms reaching the plasma boundary, and thirdly, by neutrals of 10 KeV coming from charge exchange with externally injected atoms (with energy of 80 - 160 KeV) in the inner regions of the plasma. (Besides this, the wall area across from each injector will be bombarded by 80 - 160 KeV neutrals, but that portion of the wall can be made deeper and can be preferentially cooled in order to absorb the sputtered impurities). The flow of energy from 10 KeV atoms can comprise several percent of the injector power, amounting to 1 watt/cm^2. Since the sputtering coefficient for stainless steel at this energy comprises about 2%, then the corresponding flow of impurities can be of the order of 10^{13} particles/sec cm^2, such that during an injection pulse lasting 10 sec, the surface of the plasma will receive 10^{14} particles/cm^2, which is 2% of the hydrogen ions. Such a level of impurities in the plasma is unacceptable, and here we can only depend on the experimentally observed mechanism of screening the plasma from the impurities, so that the flow of impurities to the center of the discharge is considerably less than the flow of impurities to the plasma boundary.

Even a more serious problem exists in the softer region of the ion spectrum. In the energy range of 100 eV to several KeV, the

sputtering of stainless steel by ions can liberate about 10^{14} particles/joule. If these ions transfer the order of 10% of the energy to the wall, then the impurity rate to the plasma surface will be about 10^{14} particles/cm^2 sec.

5.11. Consequently, the anticipated flow of impurities from the stainless steel to the surface of the plasma is very high. The experimentally observed phenomenon of plasma screening from impurities, (namely, that the rate of impurity flow to the center of the plasma is lower than the rate of flow to the plasma boundary) can substantially improve the situation, nevertheless, there exists a dire need for the selection of more suitable materials for the chamber and the limiters.

5.12. Scorching of the walls and ablation of chamber elements under very high thermal fluxes can present a much more serious problem in T-20 than in all the contemporary Tokamaks. The choice of the thermal parameters of the chamber walls and the heat removal elements (limiters) must be performed in the earliest stages of the project design.

6. Initial and Final Stages of the Process

6.1. It should be expected that the initial stage of discharge in T-20 will be noticeably different from that of existing Tokamaks.

The main reason for this is the large size of the device and the consequent skin effect of the plasma current. In contemporary Tokamaks, breakdown occurs along the total cross section of the chamber and the plasma current increases to its nominal value

in 3-30 m sec. at a rate $\sim 10^7$ A/sec . This produces a tendency for skin effect However, the skin effect configuration of the plasma current appears to be unstable due to the development of spiral resonance perturbations with integer values of $q(a)$.

6.2. The development of these instabilities, apparently causes the current to penetrate into the plasma. On the other hand, these instabilities lead to increased interaction between the plasma and the walls, producing more impurities.

6.3. The amount of energy that is thus deposited on the wall can be evaluated as $\sim \frac{\Delta L I^2}{2}$ where ΔL is the change in the plasma inductance during the transition from the skin distribution j(r) to a parabolic. For T-20 this value can reach $\sim$ 100 MJ. If we take into account the pulsed nature of instability development, then we can expect a pulsed energy deposition on the wall the order of hundreds of MW. In such a case, it is possible to evaporate some parts of the discharge chamber.

6.4. Calculations show (Appendix 1) that the skin effect cannot be approximated by simply introducing an anamolous resistance with a coefficient $A_R = 10$ (this is all that is needed in existing Tokamaks, so that the calculations would not give excessive skineffect). Even $A_R = 50$ does not help. Both calculations indicate a deep skin effect which prevails during a considerable portion of the initial stage of discharge $\left(\tau_{sk} = 0.9 \frac{\sigma a^2}{c^2} \right)$.

6.5. To avoid the skin effect in T-20 we are proposing a different means of plasma breakdown, namely, the use of movable limiters, which will make it possible to change the plasma minor radius during the rise of the discharge current. We are assuming that in the shadow of the limiters, the electrical conductivity is low and the current density is negligible.

6.6. The function of movable limiters could have been performed by the chamber wall together with a transverse magnetic field appropriately programmed in time.

6.7. A necessary condition for such a method to work is the supply of fuel (D_2 , T_2) to the expanding plasma boundary. The gas will ionize near the plasma boundary and this will give us the means to program the distribution of $n_e(r)$.

6.8. It is proposed that the initial plasma radius be picked the same order as present Tokamaks, 30 - 50 cm and a density $n_e \sim 10^{13}$ cm^{-3}. The rate at which the limiters increase in radius should be picked to correspond to the diffusion rate ($\sim$ 10m/sec.). We can expect that the heat load on the limiters (or the wall) in this case will be minimal.

6.9. In order to improve the conditions for making the plasma, there should be provision for preliminary ionization on the axis of the chamber. If a plasma of $n_e \sim 10^{12}$ cm^{-3} and $T_e \sim$ 30 eV can be created at the axis of the chamber then at a current rate of 10^7 A/sec., in $\sim$ 100 m sec. the current will reach a value needed for confining such a plasma. During this time the radial transverse

dimension of the plasma will not increase appreciably. Localized ionization on the axis of the chamber can be obtained by a system for plasma heating which utilizes the electron-synchotron resonance.

6.10. At the final stage of discharge when the heating mechanism is turned off, 2 - 3 sec. are needed for cooling the plasma to a temperature of 1 - 2 KeV, namely, its thermal energy will appear to be relatively low.

The problem here is to remove, in the order of several seconds, the magnetic energy $\frac{L_i I^2}{2}$, which is within the plasma, without reversing the current on the boundary and conserving the energy in the plasma.

6.11. It would appear this can be accomplished by lowering the current and by simultaneously injecting some inert gas, such as argon on the boundary of the plasma toroid. (It is hoped that it can be subsequently removed from the wall by baking at 600°C). Cooling the periphery is imperative in order to reduce the electrical conductivity close to the boundary to a value $I \sim 3 \times 10^{16}$ sec.$^{-1}$.

It may be assumed that such a scheme can be effective if the amount of argon makes up about 10% of the total initial number of electrons.

6.12. Further, a negative current at the plasma boundary can be avoided by lowering the electrical conductivity in the external layers of the plasma by introducing mechanical limiters, or by squeezing the plasma to the wall by tranverse fields. This operation is the reverse of the initial stage. It is possible to use all three methods simultaneously.

7. Plasma Heating Methods in T-20

7.1. Ohmic heating in the initial 2 sec. can raise the temperature of the plasma to $T \approx 3$ KeV. On reaching this temperature, the effectiveness of ohmic heating diminishes, since the current value is limited by the condition of hydrodynamic stability and the plasma resistance decreases rapidly with temperature. Further heating must be done by methods which are effective independently of plasma temperature. Of all the various heating methods, the most promising and the most experimentally developed at the present time is the injection of fast atoms and the use of high frequency and ultra high frequency methods.

For the selected parameters $n = 5 \times 10^{13}$ cm^{-3}, $\tau_E = 2$ sec., raising the temperature from 3 - 10 KeV can be accomplished by expending $\sim$ 50 MW of power on the plasma within 2 - 3 sec. Let us assume that the energy coupling efficiency of the ions is 85%, then the total power needed is 60 MW.

7.2 The time sequency of the plasma heating phase is: the first two sec. ohmic heating the plasma to 3 KeV; during the next 2 - 3 sec, expending 60 MW of power on the plasma by either atom injection or by RF methods and reaching a plasma temperature of 10 KeV. Further power input (the quantity and length) is dependent on the experiment, but not exceeding 15 sec.

7.3. Heating by means of fast atom beams (Deuterium). The energy of the atoms is taken at 80 KeV, and the quantity is 750 equivalent atoms, which corresponds to an injection of 4.5×10^{21} particles/sec. The initial number of particles in the 400 m^3 volume is 2×10^{22}

and during injection the number is doubled within 5 sec. This may limit the injection pulse at 80 KeV and force the transition to more energetic atoms at 160 KeV.

7.4. The injection system consists of the following types of injectors:

Energy of Deuterium atoms	KeV	80	160
Total power in the atoms at injector exit	MW	12.5	16
Number of atoms	Equiv. atoms	160	100
Power supply to the injectors:			
High Voltage	MW	32	64
Low Voltage	MW	5.4	5.4

In order to produce 80 KeV atoms and supply 60 MW, 5 injectors will be needed with an overall power supply of 190 MW. Three injectors for 160 KeV atoms will supply about 50 MW of power to the plasma with a total expended power by the injectors of 210 MW.

The total power transmitted by the atom beams at 80 and 160 KeV simultaneously is 110 MW, while the total power expended by all the injectors is 400 MW.

If necessary, three of the 160 KeV injectors can be converted to 80 KeV. In that case the injected power at 80 KeV will be 110 MW and the expended power will reach 300 MW.

7.5. Let us note that neutral beam injection at 160 KeV has several advantages:

1 - The number of particles injected into the chamber of a Tokamak for the same expended power is one half that at 80 KeV.

2 - The capture of the injected atoms in the plasma is mainly due to ionization (not charge exchange) and as a result, the flow of charge exchange atoms to the walls is decreased. However, 80 KeV injectors will be available sooner and therefore the initial stages of experimentation will take place with them.

7.6. Transfer of energy by neutral beams is accomplished by means of several injectors which have independent power supply and vacuum systems. Such a scheme insures simultaneous injection of atoms with several energies (80 and 160 KeV) and also allows adjustment of the injected power.

In view of the geometric configuration of the toroidal magnets, we have selected four sectors (90^{o} apart) to locate eight injectors (two in each sector, pointing opposite to the direction of the plasma current). The direction of the injected beam is tangent to the circumference of radius $R - \frac{a}{2} \simeq 4m$. The length of the beam in the plasma is 12 m.

The flow of atoms through the plasma is slowed down in intensity by a factor of 20 for the 80 KeV injector and a factor of 13 for the 160 KeV. At the same time, the chamber wall opposite the beam port will receive concentrated power at the rate of 125 w/cm^2 for the 80 KeV case and 250 w/cm^2 for the 160 KeV.

At a beam energy of 90 KeV the ionization cross section for ions and charge exchange are about equal, such that half of the

atoms injected into the plasma will exchange charge, and the neutrals thus formed which have an energy of 10 KeV can exit from the plasma onto the wall. In this way, about 5% of the power injected into the plasma can end up on the wall in the form of 10 KeV neutrals. (The corresponding wall loading is about 1 watt/cm^2).

7.7. Heating by RF Methods.

The most promising methods are:

1 - UHF heating, close to the electron-cyclotron frequency

2 - UHF heating in the range of the lower hybrid frequencies

3 - Heating with the aid of ion-cyclotron resonance and its harmonics, as well as by magnetic sonic resonance

For the selected plasma parameters, the time for energy exchange between ions and electrons is less than one sec, and it is therefore immaterial into which component of the plasma this energy is transferred.

7.8. Electron-cyclotron plasma heating.

For the indicated magnetic field of 35 KG, it is imperative to utilize the frequency range $\lambda \simeq$ 3mm. According to calculations, an ordinary wave propagating from outside the plasma torus at an angle of $\sim 60^{o}$ to the main magnetic field can be almost totally attenuated in the area of cyclotron resonance. The main difficulty in the way of using the mm wavelengths for plasma heating is the necessity for developing high power UHF generators. However,

it is also possible to use a large number of generators with the energy of each transferred to the plasma through as many ports. For HF energy radiation at an angle of 60^{o} to the magnetic field, there exists a total absorption of the RF energy with a single pass of the wave through the cyclotron resonance area, thus the heating of the "runaway" electrons can be considerably decreased by the correct choice for the direction of the current.

In order to use HF energy, it would be necessary to have 100 ports distributed between toroidal magnets. Between each toroidal magnet on the outside of the torus, there will be several round tubes which will radiate HF energy focused on the axis of the toroid at an angle of 60^{o} to the magnetic field.

It should be pointed out that with electron heating there will be less plasma contamination, since the chamber wall surface sputtering by electrons is two orders less than with ions. Further, with HF heating, there is no flow of neutral particles into the chamber and therefore, there are no 10 KeV atoms due to charge exchange.

7.9. UHF heating in the range of the lower hybrid frequencies.

The effective linear mechanism of absorption has to do with the transformation of an electromagnetic wave to a plasma wave. In order to insure the penetration of the plasma by the waves, it is necessary to use longitudinal absorption. Such a situation would produce heating of both ions and electrons in the neighborhood of the lower hybrid resonances. HF energy can be routed by phased waveguides, situated in ports which can also be used as

injectors of fast atoms. At this frequency ($f \sim$ 1000 MC) the problem of developing the necessary high power generators is considerably easier than in the millimeter range.

7.10. Heating in the area of the ion-cyclotron resonance and its harmonics.

The preliminary design does not call for special development of a system for HF energy transfer. These systems can be developed at the technical stage of the project in connection with the use of HF heating and ports for the injection of neutral beams.

7.11. For providing the power to the HF and UHF generators and injectors, it is reasonable to use a common high voltage electrical system. In the case of plasma heating with HF alone, the total 400 MW of power will be available. This would give 80 MW of HF power if the generator will have a duty factor of 20%, which is common to most types.

For operation with a two component plasma and with both UHF heating and 160 KeV atomic injection, the power supply for the 80 KeV injectors can be used to drive the UHF generators with a total available 400 MW. In this case, to obtain 60 MW of UHF power, the generators should have an efficiency of no less than 30%.

7.12. The planned complex of heating methods for T-20 allows for a large range of maneuverability depending on the obtained value of $n\tau_E$:

1 - Heating the DT plasma at the given conditions of $n\tau_E = 10^{14}$ cm^{-3} sec the expended power of 60 MW and a

T = 10 KeV will insure a value of Q = 2 (Q is the ratio of power out from the DT reaction to power into the plasma). Besides, out of 100 MW obtained from the DT reaction, about 20 MW comes from α particles which could produce supplementary heating in the plasma. Consequently, the power needed in this case may be reduced after 2 - 3 seconds of heating.

2- If the confinement time τ_E is less than 2 sec. say about one sec., then by maintaining a power input of 60 MW and a plasma temperature T = 10 KeV ($n\tau \approx 2.5 \times 10^{13}$) one might expect a Q = 1.

3 - If for τ_E = 1 sec., plasma temperature does not exceed 5 KeV, then for a nominal value of $n = 5 \times 10^{13}$ cm^{-3} ($n\tau = 5 \times 10^{13}$) the value of Q will fall to 0.3. In such a case plasma heating can be accomplished by 80 KeV neutral beam injection or one of the RF methods.

4 - By heating the plasma with 160 KeV neutral beams and expending 60 MW of power, one might expect $Q \approx 4$.

5 - For the same conditions as in (4) but a confinement time τ_E = 1 sec. $Q \approx 1.5$.

6 - If at a higher plasma temperature, the ion thermal conductivity will not decrease and will not enter the "banana" regime (ion confinement time $\tau_{Ei} \ll$ 2 sec.), then there is a possibility of maintaining the electron temperature at 5 KeV by electron-cyclotron resonance at a power level of 60 MW with simultaneous 160 KeV neutral beam injection giving an additional 50 MW. In this regime of two-component plasma, one might

expect a value of $Q > 1$. Under these conditions, the virtues of both heating methods will be taken advantage of with respect to the vacuum and wall loading conditions, however, it does strain the collective effects on the chamber wall.

8. Research Program and the Operating Modes

8.1. Experiments on the T-20 device can be divided into the following:

1 - Investigation of the physics of confinement and heating of a hydrogen plasma with thermonuclear parameters

2 - Investigation of a reacting DT plasma with α particle confinement

3 - Electrodynamic investigation

4 - Neutron physics and study of materials

5 - Technological investigations

These various investigations, to a certain extent, can be conducted in parallel, which indicates that a well developed system of diagnostics will be needed and good coordination of the experiments maintained.

8.2. Investigation of a Thermonuclear Hydrogen Plasma.

This part of the investigation is proposed to be done on hydrogen in order to avoid strong activation of the chamber. The natural content of deuterium in hydrogen will give a dose of $10^{11} - 10^{12}$ neutr./pulse for the projected parameters.

Such a dose is harmless from the standpoint of protecting operating personnel, material activation and instrument operation.

The main aim of this investigation must be directed at determining thermal conductivity and diffusion in a thermonuclear plasma, which will be obtained by means of RF heating and neutral beam injection. During these investigations, it is important to determine the causes which limit heating and produce energy losses from the plasma, in particular the degree of plasma stability or instability and the rate of contamination by impurities. On the basis of these studies it would be necessary to conduct an optimization of the operating mode, such as determining the mode which produces the least amount of plasma wall interaction, experimenting with various limiters and if the need arises, diverters as well.

The results obtained should serve as the basis for calculating the parameters of a thermonuclear power reactor and its energy balance.

8.3. Investigation of a DT Plasma.

Experiments on a DT plasma will, first of all, concentrate on the confinement of α particles and the transfer of their energy to the plasma. On the basis of the obtained results, it would then be possible to arrive at the conditions for a reactor operating in a self-sustaining mode. Since a self-sustaining mode does not appear to be entirely feasible, these investigations will establish parameters for obtaining a reactor with continuous supplementary heating or a two component reactor. To do this, will require experiments in two-component mode operation and continuous supplementary heating mode operation.

8.4. Future thermonuclear power reactors should have the highest possible energy duty cycle. Investigations on T-20 should produce recommendations for the realization of such a duty cycle. In this connection, such problems as DT fueling during operation, purifying the plasma of reaction products and means of producing a stable thermodynamic mode of operation should be solved.

8.5. Electrodynamic Investigations.

The aim of such investigation is to determine the plasma interaction with external magnetic fields and the current distribution in the plasma. Dealing with the problem of the skin effect during the initial stage of discharge and the plasma transition into a thermonuclear regime must be learned. Experience on contemporary Tokamaks has verified the possibility of operating these devices with various coefficients of confinement down to $q \gtrsim 2$. However, lowering q from 3 to 1 or 2 produces a smaller confinement time. It is also necessary to determine the limits of β_p and methods of maintaining the plasma temperature mode in the regions of β_p which are close to the critical value of β_p. The large amount of stored energy in the plasma, in particular the inductive component, requires a thorough study of the means for quenching the plasma. Special experiments will be needed to do this.

8.6. Neutron Physics and Material Selection Studies.

This area of study will deal with the development of blanket modules for future thermonuclear power reactors, both "clean" and "hybrid". This will involve, first of all, the determination of the tritium breeding ratio for different configurations of the

blanket, measurement of neutron flux, and testing of front wall materials under a full complement of existing factors (neutron radiation, α particle and fast ion bombardment, as well as electron, gamma and synchrotron radiation). Results of these studies should lead to the testing of different cooling configurations and materials of construction. It should be noted that the T-20 device is not intended for the testing of materials and construction at the maximum allowable integrated neutron flux.

8.7. Technological Investigations.

In as much as most of the engineering systems on T-20 will be prototypes of future power reactors, it is proposed that a broad program for technological investigations be implemented. These would include handling of the tritium cycle, such as tritium extraction from the blanket and vacuum system, preparing the fuel, and thermodynamic testing with operating blanket modules. The experiments should also lead to the development of automatic control systems, determination of the reliability of the thermonuclear reactor systems and the optimum tolerance on them. In addition there should be a complete diagnostic complex for the thermonuclear reactor which would permit its reliable operation with minimal effort.

8.8. Operating Model

The operating modes can be divided into the technological development of the device and the operating modes.

We anticipate two modes for the technological development, namely, baking the vacuum chamber at 600^{o}C and training it with a current of 1.5 MA.

There will be two stages for the experimental program.

Operation in mode "a" (first 1.5 - 2 years).

10,000 pulses on hydrogen plasma at 15 minute intervals, we envisage a possibility of making a series of 50 pulses at a rate of one pulse/minute).

Operation in mode "b" (0.5 - 1.5 years).

1000 pulses on DT plasma at intervals of 15 minutes between pulses.

Operation in mode "c" (2 - 3 years)

100,000 pulses on DT plasma at intervals of no greater than 5 minutes with continuous pulsing for 3 - 5 hours.

The above indicated stages will be taken consecutively. The possibility of replacing certain chamber elements between modes of operation is taken into account.

Appendix 1

A Short Review of Energy Balance Calcuations for T-20

Yu. N. Dnestrovskii

Based on one dimensional energy balance models, calculations were performed on plasma heating during discharge. In these calculations we used pseudoclassical scaling for the electrons, neoclassical sealing for the ions and Bohm thermal conductivity. Such factors as neutral beam heating of the plasma, cooling of the plasma by cold neutrals from the vacuum chamber, Bremsstrahlung and synchrotron radiation, and transfer of energy to the plasma by α particles were taken into account.

For the main calculated version, the following dimensions were used

R = 400, a = 150, H = 40 KG

For a value of q = 2,these parameters give I = 5.6 MA, the value used in the original version of the device.

In the first series of calculations we have taken the current rise as 600 m/sec. Calculations show that even for $Z_{eff} = 10$ the plasma heats rapidly and current concentration near the edge begins to occur. Electron temperature rises to Te $\sim$ 3 KeV in $t \sim$ 1 sec and the current distribution becomes fixed. Even if Z_{eff} increases by a factor of five, the process does not change appreciably. The current soak-in time in this case exceeds 10 - 20 sec.

For this reason, in order to produce a uniform current distribution in the plasma cross section, special steps have to be taken, such as the use of movable limiters or the formation of the plasma

with the aid of a transverse magnetic field. In further calculations, it was assumed that these steps were implemented and the initial current distribution was considered parabolic.

We have ignored the effect of plasma particle diffusion in these calculations and have assumed a density distribution described by $n(x) = n_{max}(1 - 0.8\, r^2/a^2)$.

Calculations using an optimistic "psuedoclassical" scaling model show the following behavior of the discharge. At a density $n_{max} = 6 \times 10^{13}$ cm^{-3}, if the supplementary heating is not present, the plasma temperature for the next 10 - 15 sec stabilizes at $T_i \sim T_e \sim 3$ KeV. In order to reach $T_i \sim 12$ KeV in $\Delta t \sim 5$ sec, supplementary power equal to $W \sim 3 \times 10^7$ J must be supplied.

At particle temperature less than 10 - 15 KeV, the primary energy loss mechanism is by ion thermal conductivity and the confinement time τ_E is about 10 sec. At higher electron temperatures, synchrotron radiation begins to take effect. For $T_e > 40$ KeV synchrotron radiation losses exceed all other losses from the plasma. The total confinement time is halved, to a value of $\tau_E \simeq 5$ sec as T_e rises from 15 - 40 KeV. Synchrotron radiation losses are $W_{ce} = 4$ MW at Te = 20 KeV, and $W_{ce} = 11$ MW at Te = 40 KeV. (See Fig. 1).

In studying the problem of the possibility and reliability of ignition in a DT reaction, we introduce into the calculations a phenomenological paramteter K_α, which determines the amount of energy transferred by the α particles to the plasma electrons. We assume that 3-5 x 10^7J of energy is injected into the plasma in Δt = 5 sec by means of neutral beams (the energy of the injected particles is E_0 = 100 KeV, and the current $i \approx 100$ A).

After the injectors are turned off, the reaction continues to self-heate. even at $K_\alpha = 0.5$. Equilibrium condition is reached in t = 30 - 40 sec for $K_\alpha = 1$ and in t = 60 - 80 sec for $K_\alpha = 0.5$. For small values of transfer coefficients, say $K_\alpha \simeq 0.01$, plasma temperature falls in a characteristic time of the order 20 - 30 sec.

Small losses by the ion route in the investigated model (without taking into account field ripple) cause relatively high particle temperatures in the stationary case:

for $n = 6 \times 10^{13} cm^{-3}$, $T_e \sim 60$ KeV and $T_i \sim 50$ KeV;

for $n = 12 \times 10^{13}$ cm^{-3}, $T_e \sim T_i \sim 80$ KeV

In the latter case, a supplementary energy of $W \approx 10^8$J supplied in the order of $\Delta t = 5$ sec will produce ignition in the plasma. However, the spontaneous heating for $n = 12 \times 10^{13}$ cm^{-3} leads to large values of $\beta_I \sim 8 - 10$, and to the loss of equilibrium and plasma stability in the torus.

Lowering the field to H = 30 KG and the corresponding reduction in I to 4.2 MA increases ion thermal conductivity and lowers their temperature. The result is that the conditions of self-sustainment of the reaction for $n = 6 \times 10^{13}$ cm^{-3} become more critical. After the injectors are turned off, the reaction ignites for $K_\alpha = 1$, but for $K_\alpha = 0.5$, it "smolders", spreading very slowly.

If the minor radius of the chamber is reduced to a = 100 cm, then no ignition will occur. After the injectors are turned off, for $T_i \sim 25$ KeV, the ions cease to be heated even for $K_\alpha = 1$. For $K_\alpha = 0.5$ the reaction goes out in $t \sim 10 - 15$ sec.

For calculating the "Bohm" model, it was assumed that the

coefficients of thermal conductivity were determined by

$$\chi_{i,e} = \frac{1}{\mathcal{H}} \chi_{i,e}^{B}, \quad \left(\chi_{i,e}^{B} = \frac{c\,\overline{T_{i,e}}}{16eH}\right)$$

where $\mathcal{H}$ is a phenomenological coefficient. In contemporary machines $\mathcal{H} \sim 30 - 100$.

Energy calculations for the initial version (1) were made with $\mathcal{H} = 10^2 - 10^3$. It was also assumed, that supplementary plasma heating took place by means of continuous injection of hot neutral beams at $E_0 = 100$ KeV and at $i = 100$ A.

For a density of $n = 6 \times 10^{13}$ cm^{-3} calculations have shown that for $\mathcal{H} \sim 600$ the reaction is not self-sustaining. In $t \sim 5$ sec, the beam heats the plasma to $\overline{T_i} \sim 10 - 12$ KeV, however, $n\overline{\tau_E} \sim 8\text{-}9 \times 10^{13}$ which is insufficient to sustain a reaction. Only for $\mathcal{H} \sim 600 - 700$ does the energy supplied by the α particles become equal to the energy of the hot neutral beam. By increasing the plasma density to 12×10^{13} cm^{-3} and the current injected to $i = 200$ A, the ignition threshold for the parameter $\mathcal{H}$ goes down by a factor of 2 - 2.5.

In the calculations we took account of the cold neutrals coming from the chamber walls and their rôle in the energy balance. In the peripheral plasma layer of $\ell \sim 20 - 30$ cm, where the temperature of the neutrals is not very high, there is a rapid decrease in their density by two orders of magnitude. On the inner plasma layers, the density of the neutrals is well described by the diffusion approximation. At $\overline{T_i} \sim 10$ KeV, the density of neutrals at the plasma center is five orders of magnitude less than on the edge.

In the energy balance, cold neutrals begin to have a noticeable effect, starting with a density in the vacuum region.

$N_0 \sim 10^9$ cm^{-3}. Their influence is particularly felt at the plasma edge. At $N_0 \sim 10^{10}$ cm^{-3} plasma ions remain cold due to charge exchange $(T_i \sim T_i^{wall})$ in the next to the uppermost layer of 10 cm thickness. With the "Bohm" model for thermal conductivity in the stationary mode at $\mathcal{H} = 800$, neutrals which have a density of $N_0 = 10^{10}$ cm^{-3} lower $T_{i\ max}$ from 15 - 10 Kev, while the total confinement time goes down by 30 - 40% (from $\tau_E \sim 1.8$ sec to $\tau_E \sim 1.2$ sec).

For evaluating the effect of magnetic field ripple on the energy balance, the following models for the coefficients of thermal conductivity were used

$$\chi_i = \chi^{neo} + \chi^{ripple} \quad \text{и} \quad \chi = \frac{1}{\mathcal{H}}\chi^{Bohm} + \chi^{ripple}$$

Calculations using the first model show that for a ripple of 2δ from 0 to 0.2 the confinement time in the range $T_i = 10 - 30$ KeV goes from $\tau_E = 7\text{-}8$ sec to $\tau_E = 3.5\text{-}4$ sec. Calculations using the second model were performed for $\mathcal{H} = 800$. In this case for $T_{i\ max} = 10$ KeV, confinement time decreases from $\tau_E = 2.6$ sec ($\delta = 0$) to $\tau_E = 1.6$ sec ($2\delta = 0.1$).

In both models, the partial confinement time in the ripple for $2\delta = 0.2$ and $T_{i\ max} = 10$ KeV is $\tau_E^{ripple} \simeq 8 - 15$ sec. Consequently the value of $\delta = 0.01$ on the plasma boundary is the maximum allowable, producing a ripple which does not appreciably effect the energy balance.

Appendix 2

Calculations of the Effective Energy Attenuation of an Ordinary Wave in T-20

Yu. N. Dnestrovskii, G.V. Pereverzev, V.V. Parail

We solve the problem of the attenuation of an ordinary electromagnetic wave having a frequency Ω which is equal to the electron-cyclotron frequency (at the plasma center) in T-20. The plasma was considered collisionless with the following parameters: $n_e = \frac{3}{2} n_0 \left(1 - \frac{r^2}{a^2}\right)$, $(n_0 = 5 \times 10^{13} cm^{-3})$, $T_e = \frac{3}{2} T_0 \left(1 - \frac{r^2}{a^2}\right)$ $(T = 3, 5 \text{ \& } 10 \text{ KeV})$, $H = H_0 \left(1 - \frac{r}{R} \cos\varphi\right)$, $(H_0 = 35 KG)$ $R = 5m$, $a = 2m$, $\Omega = \omega_{He}(r=0)$.

It was assumed that the wave attenuation occured by means of a linear cyclotron damping mechanism. Since an ordinary wave has almost a circular polarization with respect to its direction of rotation which is opposite to the rotation of the electrons in the magnetic field, the damping decrement is very small $(\partial\ell/k \leq 10^{-3}$ for $\Omega \simeq \omega_{He})$. An electronic computer was used to calculate the wave trajectory, entering the plasma from the low field side and its energy attenuation along the beam as a function of the angle θ on the plasma edge; $\theta = \{\vec{k}\hat{\vec{H}}\}$.

It was shown that for $\theta \gtrsim 50°$, refraction does not appreciably affect the wave propagation and the trajectory passes close to the center of the plasma column. For $\theta \lesssim 60°$, only one traverse is required for the wave energy to be completely dissipated (thus for To = 10 KeV and $\theta = 60°$, $\ln \frac{W_{INIT}}{W_{FIN.}} = 4.1$; for $\theta = 70°$, $\ln \frac{W_{INIT}}{W_{FIN}} = 1.8$).

It turns out that the major portion of the energy is absorbed by electrons of $E \lesssim T_0$, namely, heating occurs in the main plasma component. The heating zone is localized in the region

$$\frac{\Omega - \omega_{He}}{\Omega} \ll 1 \text{ , i.e. } \frac{\Delta r}{a} \leq \frac{1}{4}$$

which in principle will make it possible to change the heating zone by varying the field Ho or the wave frequency. The calculations took into account the possibility of the presence in the plasma of an accelerated electron beam at an energy $T_\beta \simeq 250$ KeV and $n_\beta/n_e = 10^{-2}$. Results indicate that for To $\gg$ 3 KeV the portion of energy transferred to the beam is neglibibly small compared to the energy going into heating the main plasma component.

Appendix 3

Radiation Losses in a Thermonuclear Plasma as a Function of the Atomic Number of Impurities and Temperature

V.I. Gervidz, V.I. Kogan

Calculations are made on radiation losses in a thermonuclear plasma as a function of the atomic number of the impurities and the electron temperature T_e . A determination is also made of the dependence on Z of a "lethal" relative concentration of impurities in a DT reactor. Such results are needed (with respect to finding the sputtering coefficients as a function of Z) to make the best possible selection of materials for the chamber and limiters in a fusion reactor.

The Model. The calculations were made on a model based on corona equilibirium for constant and homogeneous (n_e, n^*, ξ^* T_e/n_e $\xi^* n^*$ concentrations of electrons and impurities. The corona model itself, as shown by comparison with a more general colissional-radiation model, is suitable for low n_e , high T_e and large values of Z , peculiar to fusion reactor plasmas, and its steady state limit / $t \to \infty$ / is insured by the satisfaction of the Lawson criterion , $n_e \tau \gtrsim 10^{14}$ cm^{-3} sec.

Ionization State of the Impurities. The degree of "stripping" of the various impurities is indicated in Table I for T_e = 10 KeV by the relative concentration of titanium, iron, molybdemun and tungsten, respectively. The starred values indicate representative ion concentrations.

Table I

Z	Ion Charge $K = Z - N$							
	Relative Ion Concentration							
22	22 0,66*	21 0,30	20 0,04					
26	26 0,28	25 0,48*	24 0,23	23 0,01				
42	42 0,00	41 0,01	40 0,47*	39 0,37	38 0,13	37 0,02		
74	65 0,03	64 0,013	63 0,24	62 0,29*	61 0,18	60 0,08	59 0,03	58 0,01

From Table I it is evident that for the investigated temperatures even the atoms of the heaviest impurities are capable of holding about $N \leq 10$ electrons, such that $N << Z$. This in effect, considerably simplifies accounting for the screening effect of Bremsstrahlung.

Radiation Losses. On Fig. 1 - 3 is shown the results of calculations of radiation power losses due to Bremsstrahlung, recombination and line radiation (and their sum), using a single impurity particle and a single electron. The bumps in the curves are due to

presence of helium and neon shells. The weak dependence of the total losses Q^{sum} on Te is due to the averaging effect of increasing and decreasing terms as functions of Te. The slowly changing characteristic of Q^{sum} as a function of the atomic number Z (first a $\sim Z^4$ then $\sim Z^3$ and finnaly as $\sim Z^2$) is due to the changes in Bremsstrahlung, recombination and line mechanisms of radiation.

As is evident from Fig. 3, for relatively low Z (when impurity stripping appears to be total) $Q^{sum}(Z)$ is well approximated by the three term equation

$$\frac{Q^{sum.}}{n_e n^*} = 1.5\times10^{-25} Z^2 Te^{\frac{1}{2}} + 6\times10^{-24} Z^4 Te^{-\frac{1}{2}} + 8\times10^{-23} Z^6 Te^{-3/2}$$

(Vasiliev, Dodgov-Saveliov, Kogan, 1962) which accounts for Bremsstrahlung and recombination radiation for a stripped atom by $Q^{Brem} \sim Z^2 Te^{1/2}$, $Q^{rec.} \sim Z^4 Te^{-\frac{1}{2}}$, and for line radiation by the approximation $Te \gg Z^2 Ry\ eV$ when the relative concentration of hydrogen type ions is already low ($Q^{line} \sim Z^6 Te^{-3/2}$).

The two term equation

$$\frac{Q^{Sum}}{n_e n^*} = 1.5\times10^{-25} Z^2 Te^{\frac{1}{2}} + 5\times10^{-24} Z^4 Te^{-\frac{1}{2}}$$ (Kogan, 1959)

corresponds to an almost 100% stripped atom; its apparent order of accuracy is due to the partial mutual compensation caused by the incomplete accounting of Q^{line} and the rise in Q^{rec}.

"Lethal" Concentrations. We will use our results to determine the dependence of a "lethal" concentration of impurities Z, defined as the concentration at which the total radiation losses

exceed the energy output of the DT reaction (by α particles) for any temperature. It is assumed that $T_e = T_i$ and n_e is fixed (it is dependent on n^*). Results indicate that $C(Z)$ for $10 \leq Z \leq 80$ can be well approximated by the equation $C(Z) \approx 2.75 \times Z^{-1.67}$. For C, Fe, Mo and W, we get C (6) $\approx$ 13%, C (26) $\approx$ 1.3%, C (42) $\approx$ 0.6% and C (74) $\approx$ 0.2% respectively.

Figure Captions

Fig. 1 Dependence of the various radiation on Te.
Q^{Brems} (curves 1 and 5), $Q^{recom.}$ (2 and 6), Q^{line} (3 and 7).
Q^{total} (4 and 8) for carbon (solid curves 1-4)
and Iron (dotted curves 5 - 8).

Fig. 2 Same as Fig. 1, for Molybdemums (solid curves 1 - 4) and Tungsten (dotted curves 5 - 8).

Fig. 3. The dependence of Q^{total} on Z.
(1) Te = 10 KeV, (2) Te = 20 KeV, (3) Te = 40 KeV
— · · — · · — two term equation (Kogan 1959)
— x — x — three term equation (Vasiliev, Dolgov, Savelov and Kogan, 1962). The last two curves are for Te = 10 KeV

Fig. 4 The dependence of W_α, W_e, T_e on temperature.

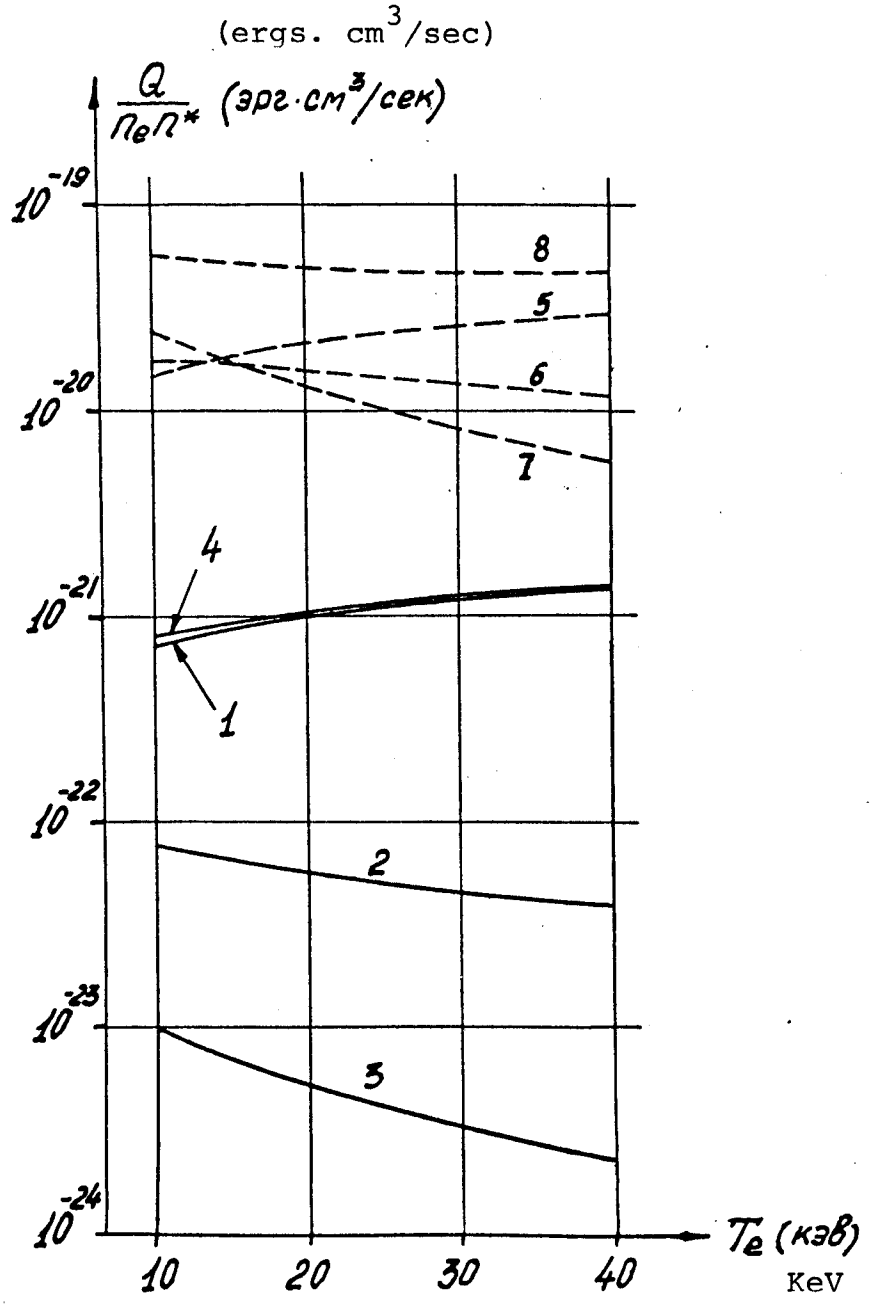

Рис.1

Figure 1

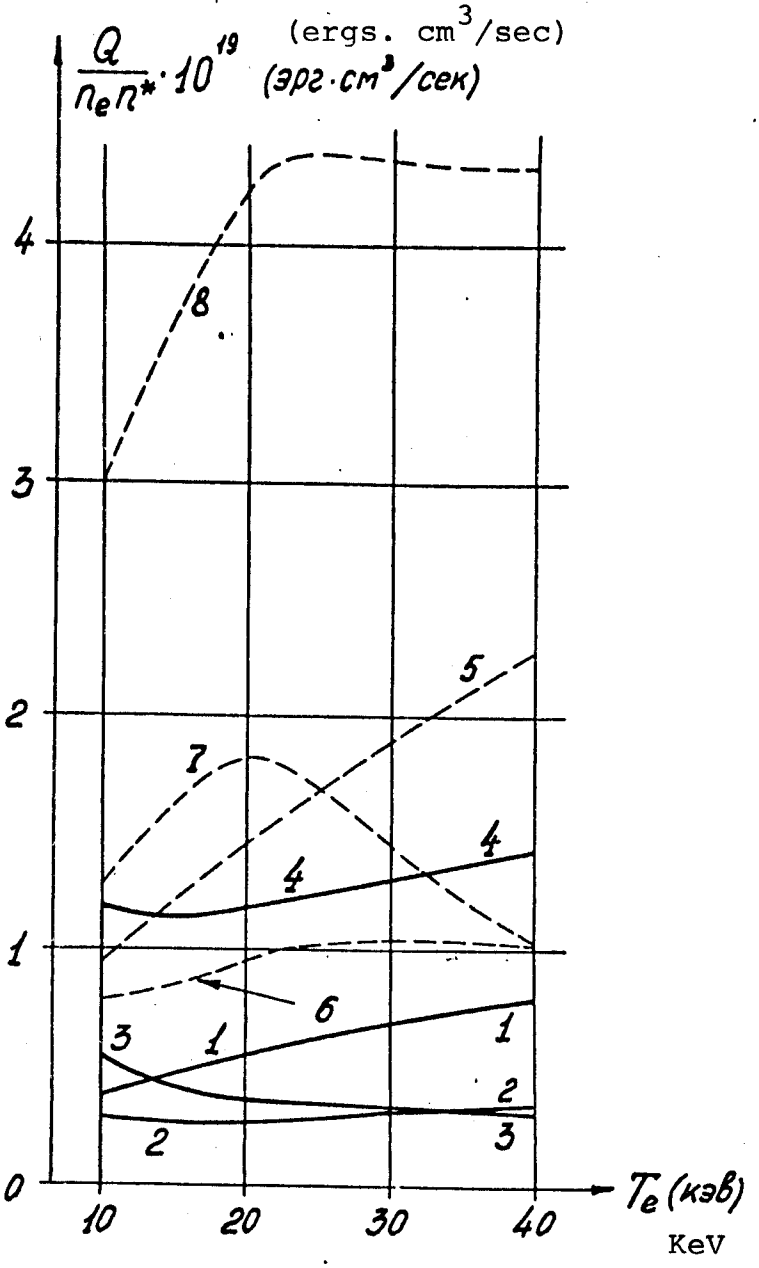

Рис.2

Figure 2

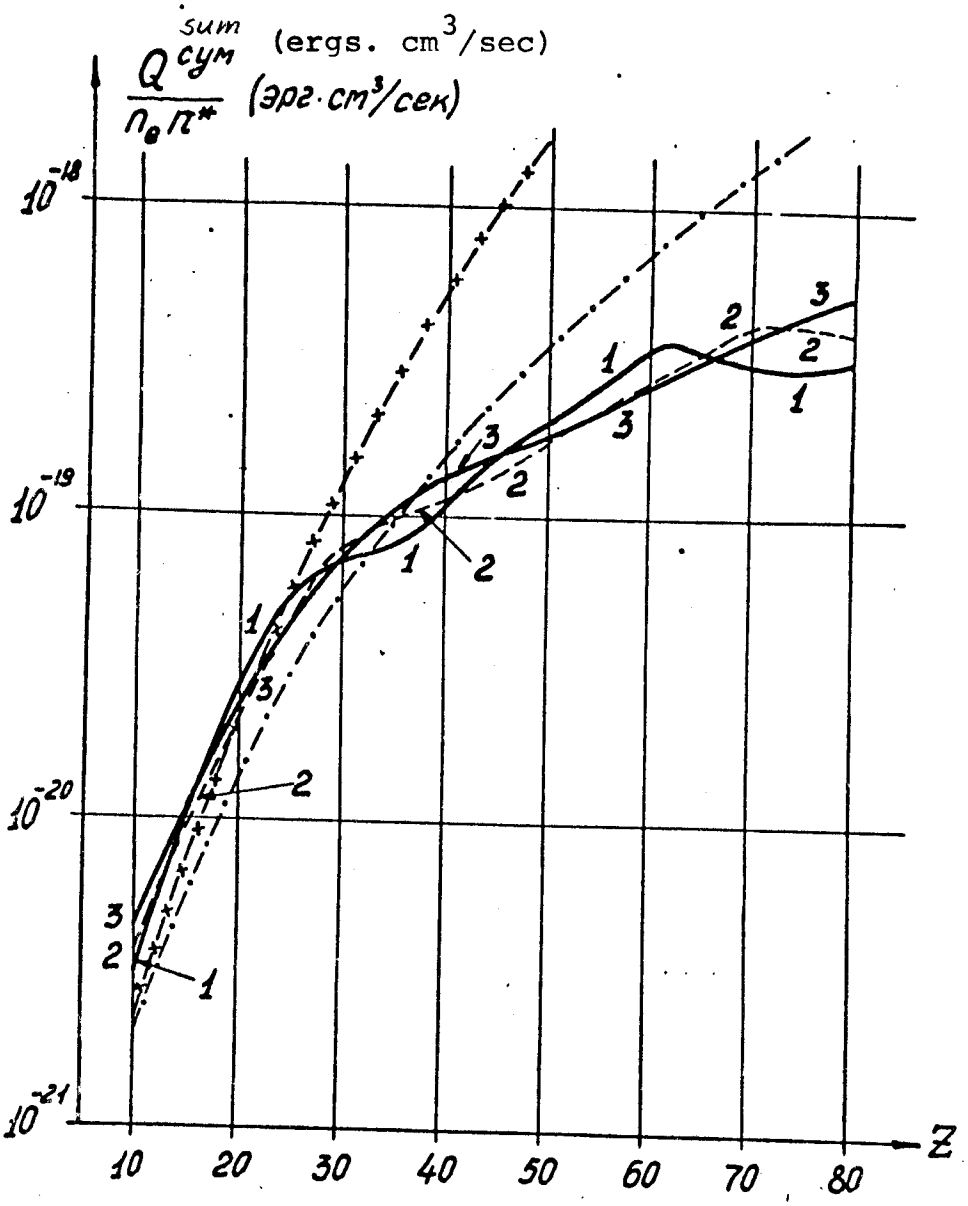

Рис.3
Figure 3

T-20
R = 400
a = 150
H ≅ 40
$n_{max} \cong 6 \cdot 10^{13}$

W_α - power from DT reaction removed by α particles

W_{ce} - cyclotron radiation from plasma

τ_E - confinement time

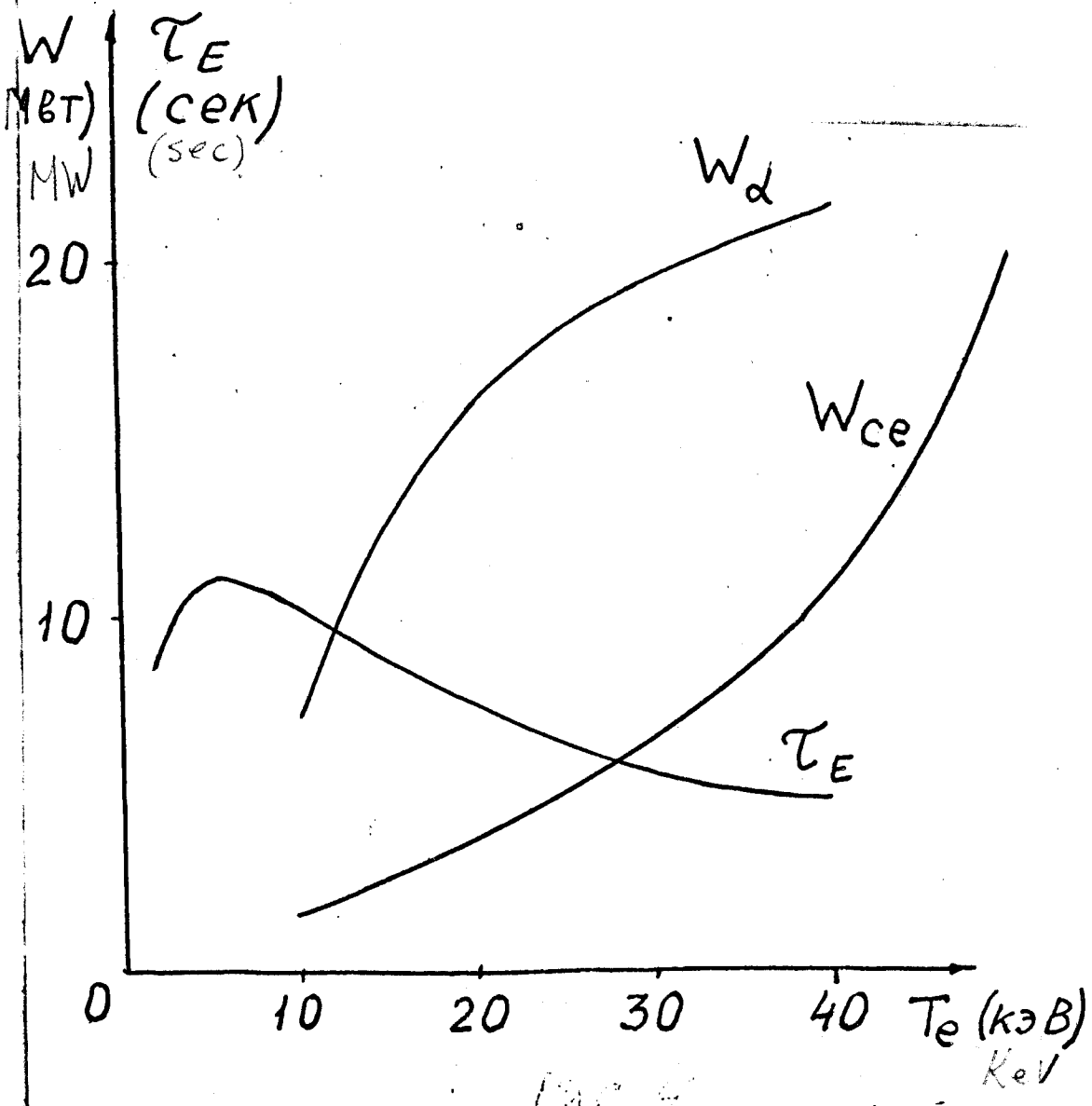

Figure 4

- 129

Experimental Thermonuclear Installation

TOKAMAK - 20

Preliminary Study (First draft)

Vol. II, part 1
Engineering Solutions

National Committee for the Utilization of Atomic Energy Soviet Ministry, USSR.

I. V. Kurchatov Atomic Energy Institute
D. V. Yefremev Scientific Research Institute for Electrophysical Apparatus.

MOSCOW 1975

Translated by Igor N. Sviatoslavsky
University of Wisconsin Fusion Design Study Group

Experimental Thermonuclear Installation

TOKAMAK - 20

Preliminary Study (First Draft)

Vol. II, part 1
Engineering Solutions

National Committee for the Utilization of Atomic Energy Soviet Ministry, USSR

I. V. Kurchatov Atomic Energy Institute
D. V. Yefremev Scientific Research Institute for Electrophysical Apparatus

MOSCOW 1975

Translated by Igor N. Sviatoslavsky
University of Wisconsin Fusion Design Study Group

UWFDM-129

In this volume are presented reports of a preliminary investigation of the main engineering systems for the Tokamak-20 (T-20) installation.

The question of shielding the surroundings has been treated in a very preliminary way and the question of plasma diagnostics does not appear in this volume, but will be treated on subsequest stages of the project.

The preliminary investigation of the T-20 project (First Edition, Vol. II) besides N.I.I.E.F.A. of D.V. Efremov and I.A.E. of I.B. Kurchatov, there was participation by L.F.T.I and IK, ASC, USSR

Participants

Alikayex, V.V.
Bondarchiuk, E.N.
Burtsev, V.A.
Vasiliev, M.P.
Vinogradova, N.K.
Glukhikh, V.A.
Golant, V.E.
Golubiov, V.P.
Gubariov, V.F.
Gusev, O.A.
Dnestrovskii, Yu.N.
Doinikov, N.I.
Yevgrafova, D.I.
Yershov, B.D.
Yershova, Z.V.
Ivanov, V.V.
Ivanov, D.P.
Ivkin, V.G.
Kadomtsev, B.B.
Kapishev, V.K.
Karasev, B.G.
Kolerov, E.P.
Komarov, V.L.
Kornakov, E.V.
Konstantinov, Yu.A.
Krivonoc, Yu.G.
Lebedev, A.P.
Malishev, I.F.
Mingalev, B.S.
Mirnov, S.B.
Mozin, I.V.
Monoszon, N.A.
Mukhamet-Galeyev,S.Sh.
Nekrilov, Yu.N.
Odintsov, B.N.
Ostroumov, Yu.N.
Parail, V.V.
Pereversev, G.B.
Peregoud, V.I.
Pilia, A.D.
Popkov, G.D.
Puzinovich, Yu.T.
Pustovoit, Yu.M.
Ratnikov, B.K.
Roife, I.M.
Saksaganskii, G.L.
Samoilenko, Yu.I.
Svinin, M.P.
Semashko, N.N.
Serebrennikov, D.V.
Seredenko, E.V.
Simakov, A.S.
Simonov, V.A.
Snegur, A.A.
Spevakova, F.M.
Spirchenko, Yu.V.
Stolov, A.M.
Strelkov, V.S.
Feodorov, V.D.
Feodorov, V.I.
Churakov, G.F.
Shatalov, G.E.
Shafranov, V.D.
Shenderovskii, S.P.
Scherbinin, O.N.

TABLE OF CONTENTS

I. Main Technical Features of T-20

1. As has already been mentioned (Vol. 1), the T-20 device is intended for the study of physical processes of a DT thermonuclear plasma ($n\tilde{\tau}_E = 10^{14}$ sec cm^{-3}, $T > 7$ KeV) as well as verification of engineering solutions which could be implemented for the design of a fusion reactor. The plasma parameters of T-20 are identical to those needed for a hybrid Tokamak reactor with uranium in the blanket, and can be directly extrapolated to a "clean" fusion power reactor.

After investigating several versions with plasma current from 5 - 6 MA, R = 4 - 8 m and a = 1.5 - 2.5 m, we have settled on the following main parameters for T-20:

Major radius	5 m
Minor radius	2 m
Maximum plasma current	6×10^6 A
Length of current pulse	5-20 sec.
Current rise	1-2 sec.
Initial rate of current rise (to 6×10^5 A)	10^7 A/sec
Plasma density	$5 \times 10^{12} - 5 \times 10^{13}$
Toroidal field at chamber center	3.5 T
Confinement time	2 sec.
Plasma temperature without supplementary heating	3 KeV
Plasma temperature with supplementary heating	10 KeV
Stored energy in the plasma	10^8 J
Power losses from plasma	50 MW
Neutron wall loading	10^{13} cm^{-2} sec^{-1}
Shield thickness	0.5 m
Shield attenuation	$10^3 - 10^4$

In accordance with the established goals, the following operating modes are being planned:

First Stage

10^4 pulses on hydrogen plasma

10^3 pulses on DT plasma, a neutron flux of 10^{20} - 10^{21} per pulse at a density of 10^{13} cm^{-2} sec^{-1}

Pulsing rate will be every 5-15 min.

Second Stage

10^5 pulses on DT plasma at a rate of one pulse in five min.

2. The T-20 installation will have the following main systems:

1. Magnets system and power supply
2. Vacuum system and apparatus for handling tritium
3. Plasma heating system
4. Control system, with an arrangement for diagnostics and analysis of experimental data
5. Radiation shield system
6. Power and water supply system

The following principles were used as a basis for the engineering decisions:

a - The use, wherever possible, of solutions suitable for fusion reactors which have been experimentally tested and are economical.

b - The design should facilitate relatively easy disassembly and assembly under experiments with both hydrogen and DT plasmas.

c - The design should provide flexibility for the redesign and addition of components, which might be necessitated during the course of the experiments.

3. Figure 1.1 shows two views of the T-20 installation. In this version there will be no iron core. This decision was arrived at from the standpoint of simplifying the construction, providing access to the plasma chamber and making easier disassembly. However, it means that more power will be needed for inducing the plasma current and will cause high magnetic fields to be present in the surroundings. The magnet and vacuum system is divided into 8 blocks. Each block has three toroidal magnets, one vacuum chamber section and shield, and fast acting control windings. Each block can be rolled out radially for disassembly. They are joined together by mechanical means and by welding of the vacuum chamber sections.

The D shaped toroidal field coils are almost totally constant tension with no bending moments produced by the interaction of the current with the toroidal field.

The first two stages of experimental operation will be performed without a diverter, however, the clearance in the D shaped section was picked such that a diverter may be added in the future without replacing the toroidal field coils.

During the design of the magnet system, three different versions of toroidal coils were looked at - superconducting, cryogenic and conventional.

Since the total actual operating time of the device is not very long (600 hrs.) the question of power economy, which is paramount with fusion power reactors necessitating superconducting coils, is not applicable.

The lower cost of the power supply for superconducting coils as compared to conventional coils does not justify the use of

superconductivity. Further, the lack of experience in building large superconducting magnets for Tokamaks can delay the project. Comparative studies of cryogenic and conventional copper coils has shown that the latter are more suitable for T-20.

Based on these considerations, we have selected water cooled copper coils to be used in the device. However, taking into account the need for superconducting magnets for fusion reactors and the rapid progress in applied superconductivity, we should not exclude the possibility of revising this decision.

On the outer surface of the D shaped toroidal magnets are distributed vertical field and ohmic heating coils. Vertical field coils are used to create the field needed to maintain equilibrium in the plasma torus which varies as a function of plasma current and temperature. The field generated by these coils is inadequate to drive the plasma current. The main portion of the vertical field is supplied by the ohmic heating coils. The space current distribution in the ohmic heating coils is selected such that the field variation at the plasma center does not exceed 3×10^{-4} of the toroidal field. The vertical field and ohmic heating coils were placed on the outside of the D coils in order to reduce the electro-mechanical interaction between them and to facilitate disassembly. In order to maintain plasma equilibrium, it is necessary to be able to vary the field with extreme accuracy, as a function of plasma current and temperature. A more reasonable way of achieving this is to have an automatic system with feedback. In order to reduce the power in the automatic feedback coil system in T-20, we intend to augment it with three relatively low power fast acting tuning coils distributed on the chamber surface (these coils are integral with each block

and will come out on disassembly along with the three toroidal coils). It is proposed to program the current in the main vertical field coils and compensate for inaccuracies by using feedback on the fast acting internal coil system. To insure the independence of the fast acting compensating coils from the transformer coils the coupling coefficient between them was picked equal to zero.

4. The vacuum chamber in T-20 is made of two concentric toroidal systems; a main discharge and an intermediate chamber. The inner discharge chamber is a specially constructed bellows made of a thin cooled material with a hardened surface. On its inner surface are situated limiting plates which protect the bellows from direct contact with the plasma and which will receive the brunt of the heat loading within the chamber. The outer intermediate chamber is a massively constructed device which includes the radiation shield and which will have insulated gaps to prevent the formation of closed current loops. The intermediate vacuum chamber and the limitation of the outer chamber wall temperature (to 100°C) will serve to reduce the diffusion of tritium to the surroundings. Joining of adjacent chamber sections will be accomplished by welding on the outer periphery. To facilitate assembly and disassembly, while conducting experiments on hydrogen plasma, the shield can be left out in the vicinity of the joints. The construction of the chamber will permit the replacement of the limiters within the plasma chamber during the first stage of the operation without its disassembly.

It is proposed to investigate the construction of limiters made of different materials such as graphite, refractory metals

and others. The chamber will have provisions for neutral beam injection, RF heating and diagnostic probes.

5. Chamber evacuation will be by means of turbo-molecular pumps and titanium getters, each block being self sufficient and possessing a pumping speed, for N_2 , of 4×10^4 ℓ/sec. These pumps will maintain, after high temperature baking of the chamber, a background pressure of 2×10^{-8} torr and will pump it down to 5×10^{-8} torr between pulses.

The intermediate chamber will be maintained at a pressure of 5×10^{-6} torr.

For pumping down the neutral beam injectors we intend to use cryopanels and getter pumps with a pumping speed of 5×10^7 ℓ/sec (for deuterium). For pumping helium and regenerating the cryopanels, conventional turbo-molecular pumps will be used.

There will be a closed tritium cycle which will insure the cleanup of the DT mixture from other gasses, separate the protium and helium, and prepare the new DT mixture for injection into the chamber.

For controlling and monitoring the vacuum parameters, there will be multichannel vacuum gauges and gas analysers, well shielded against parasitic signals, operating in conjunction with the computer regulated automatic control system.

6. Plasma heating to 3 KeV will be accomplished by the energy dissipated in the plasma by the ohmic heating coils as they drive the discharge current to 6 MA and maintain it at this value for 2 sec. Two methods are envisaged for heating the plasma

to 10 KeV; neutral beams and RF systems. The final choice for this heating will be made on the basis of initial experiments on T-20.

7. For neutral beam heating, there will be 5 injectors of deuterium atoms at 80 KeV energy with a total power of 60 MW.

Two component plasma can be realized with the use of three injectors of deuterium atoms at 160 KeV, with a power of 50 MW.

The maximum injection time for neutral beams is about 13 sec.

There will be 8 ports for neutral beam injection, two each at four locations between toroidal field magnets.

The positive deuterium ions will be generated in 32 modular ion sources with ion-optical systems (4 sources per each injector).

The total power expended with all the injectors in simultaneous use is about 400 MW. The dimensions of each injector are 6 x 8 x 11m.

8. From all the possible choices of RF heating we are planning to use three systems at the frequencies ω_{He}, $\sqrt{\omega_{He} \cdot \omega_{Hi}}$ and ω_{Hi}. Further, more attention is directed at the electron-cyclotron and the lower hybrid resonance frequencies. In the preliminary stages of this project, no investigation of the ion-cyclotron resonance heating is contemplated.

Generators operating at ω_{He} and $\sqrt{\omega_{He} \cdot \omega_{Hi}}$ will have to be developed at an early stage of the project. This development appears to be within the state of the art, judging from the available world-wide literature. We can expect that the efficiency of these generators operating at the troublesome millimeter wavelength will be about 20% (these are total losses, including plasma and waveguide). This implied a total power needed for the RF system of 400 MW.

9. In order to prevent the skin effect, it is proposed to produce the discharge throughout the whole section of the plasma by reducing its minor radius and allowing it to grow with increasing current. This can be accomplished either by movable limiters or by shifting the plasma center against stationary limiters towards the inner radius of the chamber. The inital radius of the plasma is $a = 0.5$ m. It is proposed that the gas within this volume be ionized with an RF system prior to discharge. To insure a current rise rate of 10^7 A/sec, which is common in existing machines, a potential of 250 V will be needed across the plasma circumference. This potential, according to experimental data, is sufficient to compensate for both active and inductive potential drops. As the discharge current rises, this voltage can be reduced.

After the current rises to a value which corresponds to a $q = 2.3$ for $a = 0.5$ m, further current rise will take place as the radius (a) increases and q remains = 2.3.

In order to improve the conditions for discharge, it is planned to vary the particle density from the initial value of $n = 5 \times 10^{12}$ cm^{-3} to a final value of $n = 5 \times 10^{13}$ cm^{-3} as the current reaches a maximum.

10. The operating mode of the magnet system has been designed with the process of producing the plasma current in mind. To insure this operating mode, requires a rise in the vertical field coupled to the plasma at a rate of $\approx$ 71.5 V.sec. The input from the vertical field coils is $\approx$ 25 V. sec and from the ohmic heating coils $\approx$ 46.5 V. sec.

In order to reduce the coil size, magnetic forces and the power supply needed, the current in the coils will be varied from -120 KA to + 120 KA. In order to achieve a current rise rate of 10^7 A/sec, the power input to the coil will have to be 3.45×10^9 watts.

11. The maximum power loss in the toroidal field coils is about 8×10^8 watts. In order to reduce the average power needed by T-20, it seems reasonable to use voltage peaking at the time the toroidal field is energized, which would require a slight increase in the peak power.

12. To reduce the total amount of power used by T-20 and to insure an adequate supply needed to energize the vertical field coils at the time of the plasma current rise, we have adopted a system which will allow us to use a portion of the power from the toroidal magnet power supply to energize the vertical field coils. This will be accomplished in the following way.

After the toroidal field builds up to the prescribed level, a portion of the power supply will be disconnected from the toroidal coils and will be used to energize the ohmic heating coils with a current of --120 KA at the start of the discharge pulse. As the plasma is formed, the ohmic heating coil will be used as an inductive power storage system, which along with its own power supply and that of the vertical field coil, will insure the proper rise in the plasma current. After the plasma current reaches its nominal value, the borrowed part of the power supply will be disconnected and re-instated into the toroidal power grid

13. The operating mode of T-20 and the main technical features are presented below.

Time in sec	Designated Operation
-18 to -0.8	Toroidal field rise $P_{Tot} = 0 - 12 \times 10^8$ watt
-0.8 to -0.1	Ohmic heating coil energizing to I = 1200 KA $P_{OH\ MAX} = 6 \times 10^8$ watt; $P_{TOT}\ 6 \times 10^8$ watt
-0.1 to 0	Injection of D^o , T^o, $n = 0 - 5 \times 10^{12}$ cm^{-3} $P_{TOT} = 6 \times 10^8$ watt, $P_{OH} = 10^8$ watt
0 to 1.1	Plasma formation and current rise to $I = 6 \times 10^6$ A; $P = 6 \times 10^8$ watt $P_{OH\ MAX} = 34.5 \times 10^8$ watt $P_{VF\ MAX} = 2.2 \times 10^8$ watt injection of D^o and T^o , $n = 5 \times 10^{12} - 5 \times 10^{13}$ cm^{-3}
1.1 to 3.1	$I = 6 \times 10^6$ A, Ohmic heating to T = 3 KeV $P_{TOT} = 8 \times 10^8$ watt $P_{OH} = 10^8$ watt $P_{VF} = 0.8 \times 10^8$ watt
3.1 - 16	$I = 6 \times 10^6$ A, plasma heating and maintaining at T = 10 KeV with RF or neutral beams. $P_{TOT} = 8 \times 10^8$ watt, $P_{OH} = 10^8$ watt, $P_{VF} = 0.8 \times 10^8$ watt, $P_{HEAT} = 4 \times 10^8$ watt
16 to 20	Plasma quenching by injection of an inert gas and by lowering the current.
20	Turning off the toroidal field and pumping down the chamber

Technical Parameters of T-20

1. Chamber and Shield

Major radius	5 m
Minor radius	2 m
Chamber radius to the first wall	2.1 m
Outer chamber radius to the shield	2.7 m
Chamber design - double wall with intermediate vacuum.	
Residual pressure in chamber	5×10^{-8} torr
Intermediate chamber pressure	5×10^{-6} torr
Operating temp. of the discharge wall	500^{o} C
Operating temp. of the discharge wall during chamber bake-out	600^{o}C
Power needed for bake-out	10 MW
Power supply needed for induction heating of the chamber	80 MVA

2. Toroidal Field Coils

Number of coils	24
Field at chamber center	3.5 T
Length of flat top	5 - 20 sec
Stored energy	6000 MJ
Maximum ohmic losses	800 MW
Maximum voltage	5 KV
Maximum current	120 KA
Peak power	1200 MW
Weight	1600 tonnes

3. Ohmic Heating Coils

Current	120 KA
Energy stored	220 MJ
Maximum voltage	28 KV
Peak power	3450 MW
Maximum ohmic losses	100 MW
Weight	300 tonnes

4. V.F. Coils (Control Coils)

Field at chamber center	0.45 T
Current	120 KA
Stored energy	460 MJ
Voltage	25.5 KV
Weight	800 Tonnes

5. Power Supply for Magnets

Peak power for toroidal field magnets	1200 MW
Peak power for ohmic heating coils	600 MW
Peak power for V.F. coils	220 MW
Peak power for correction coils	60 MW
Total peak power for magnet system power supply	1480 MW
Energy dissipated by magnets per pulse	30,000 MJ
Average power in magnet system	100 MW
Power losses in the switches	3000 MW
Average power losses in T-20	150 MW

6. System of Plasma Heating

Power dissipated in the plasma for heating	60 MW
Pulse length	2-3 sec
Power dissipated in plasma to maintain temperature	60 MW
Pulse length	10 - 11 sec

Heating system - neutral beams and RF

a) Neutral beam injectors

Number of injectors	5
Energy of injection	80 KeV
Power needed	190 MW

b) RF System

Power needed for electron-cyclotron resonance heating (λ = 3mm)	400 MW
Power needed for the lower hybrid resonance heating (λ = 30 cm)	200 MW
Power needed for ion-cyclotron resonance heating (RF band)	200 MW

Heating parameters for two-component plasma mode

Power needed for neutral beam injection injection at 80 KeV	190 MW
Power needed in 3 injectors at 160 KeV	210 MW

7. Vacuum System

Total pumping speed of the high vacuum system for the chamber (for deuterium)	10^5 l/sec
Pumping time between pulses to reach 5×10^{-8} torr	100 sec

Type of high vacuum pumps - Turbo-molecular and ion getters

Wall surface area required for vacuum ports and neutral beam ports	2.2%

Total effective pumping speed of the intermediate chamber	5×10^3 l/sec
Total pumping speed of the liquid helium pumping cryopanels in the neutral beam ports (on deuterium)	4.4×10^7 l/sec
Liquid helium boil off rate	360 l/hr
Power needed for pumps	1 MW

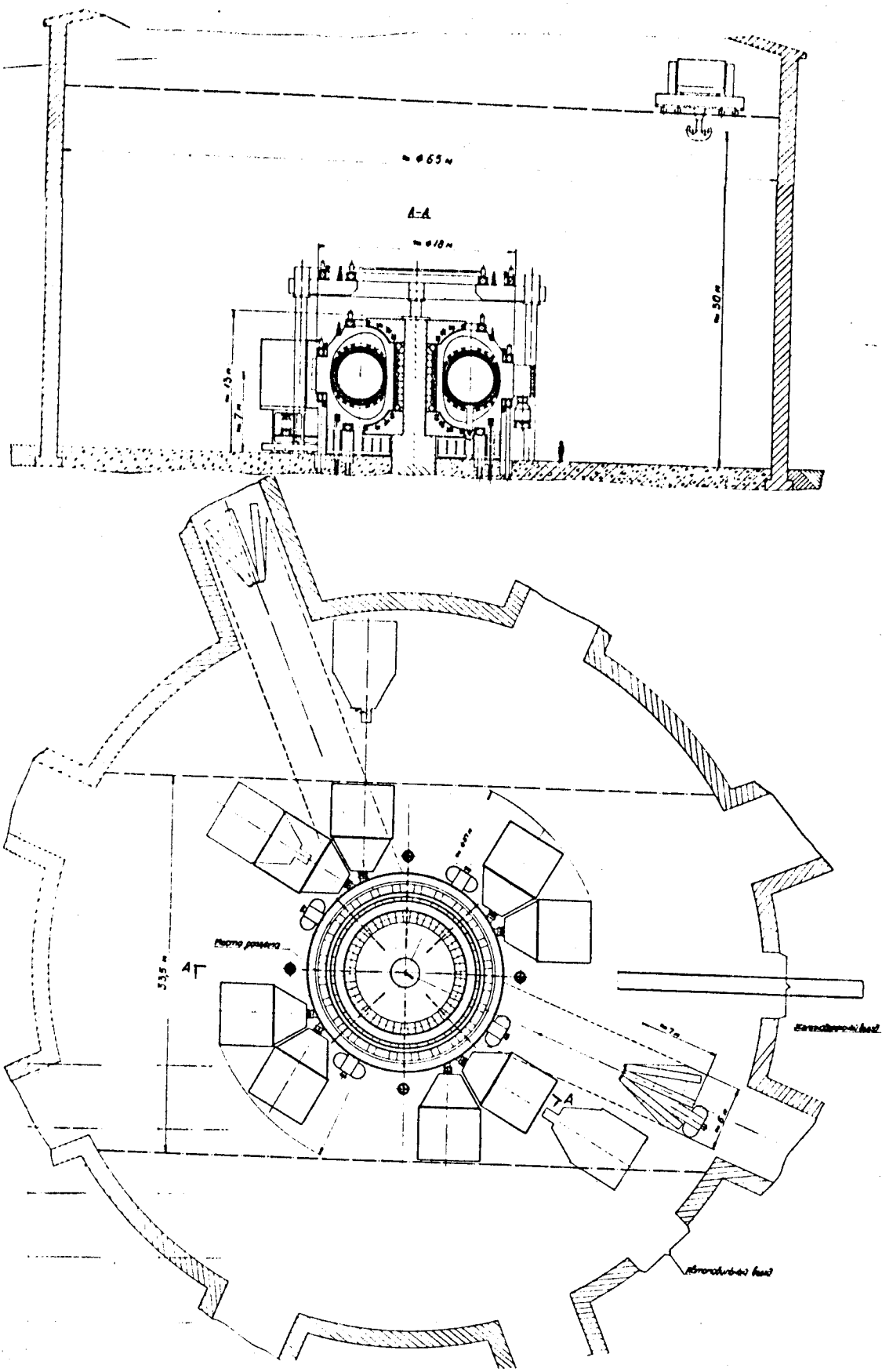

Рис.I.I. Конструктивная схема установки Т-20

Figure I.1.1 Construction Schematic of T-20

II. Magnet System

1. Construction

In accordance with the adopted philosophy, the magnet system was designed to operate reliably under conditions of DT experiments, to be easily assembled and disassembled and to provide access for servicing the chamber during experiments. A schematic drawing of T-20 is shown in Fig. 1.1. The magnet system includes the following elements:

Toroidal Field Coils (TF)

This coil generates a field of H_{TOR} = 35 KG at the axis of the chamber. This value was obtained by the Kruskal-Shafranov method for the given sizes (R = 5 m, a = 2 m) a plasma current I_{PL} = 6 MA and a q = 2.3. Field tolerance on the plateau of the plasma current ±5%. The toroidal field can be varied from (0.1-1) H_{TOR}. Toroidal field ripple on the chamber axis is not greater than ±0.1%.

Ohmic Heating Coils (OH)

The ohmic heating coils along with the vertical field coils produce the needed plasma current of I_{PL} = 6 MA in t = 1 - 2 sec, and maintain this current at a tolerance of ±10% for 5 - 20 sec. The OH coils power supply provides the possibility for regulating the plasma pulse within (0.1 - 1) I_{PL} . Current rise to 0.1 I_{PL} is at a rate of 10^7 A/sec. Current decay depends on the parameters of the plasma toroid when the electric field is lowered and an inert gas (Ar) is injected simultaneously. The design of the OH coils take into account the possibility of overloading due to a sharp

rise in the plasma resistance during current quenching.

Programmed Vertical Field Coils (VF) and Automatic Compensating Coils (AC).

These coils comprise the system for regulating the position of the plasma toroid and maintaining it in an equilibrium position in the center of the chamber both in the vertical and the horizontal directions by using feedback signals to compensate with vertical field. Further, these coils are used to displace the plasma center within the discharge chamber in accordance with a certain operating mode. In order to maintain plasma equilibrium in the vertical direction, a system is needed to create a horizontally steering field of the order of several hundred oersteds. Similarly, for horizontal equilibrium, these coils must create a vertical field $H_{\perp}$ of a value equal to the plasma self field H_{ω}. For creating $H_{\perp}$, two subsystems will be used: (1) VF coils which will give a programmed controlling field $H_{\perp}^{(1)} \approx 0.9H_{\perp}$ and (2) AC which will create a field of $H_{\perp}^{(2)} \approx 0.1\ H_{\perp}$ by means of feedback from the plasma.

Construction of the Magnet System

In accordance with the above plasma requirements and the requirements of the different magnet systems, calculations were performed to determine the main technical parameters of the coils and their construction. A general view of the magnet system is shown in Fig. II.1. The toroidal field magnet (TF) consists of 24 flat D shaped coils, distributed every 15^{o} around the discharge chamber. Each coil is made up of two panckaes, wound from a hollow, water

cooled copper conductor 27 x 280 mm^2. The number of turns in one disc is 30 as is the number of parallel cooling paths. The copper conductor of each coil is wound inside a structural frame made of stainless steel, which is square in cross-section. The number of coils (24) and their flat shape was selected for the following reasons. First of all, the magnetic field ripple at the plasma dictated that there be no less than 24 coils. Secondly, the need for neutral beam injectors situated between the TF coils pointing tangent to the plasma axis dictated that there could not be more than 24. If there were more than 24 TF coils, the neutral beam injectors would have to be radial to the plasma, which is contrary to physics requirements.

To facilitate assembly and disassembly, the TF coils are divided into 8 blocks, such that each 3 coils together with their section of vacuum chamber and shield, constitute a single element which can be preassembled and then transported for mounting in the machine. Such block construction of the TF coils makes it possible to assemble and disassemble only one or two blocks, in the event of a breakdown of a magnet or a vacuum section without disturbing the rest of the device.

Ohmic Heating Windings (OH) and Programmed Vertical Field Coils (VF)

These coils are external to the toroidal magnets making it possible to disassemble the machine with relative ease. To do this, it would be necessary to raise or lower the outer OH and VF coils vertically, undo the seals between vacuum chamber sections and then roll out the TF coil blocks radially.

The OH and VF coils are made of water cooled hollow copper conductors wound within a stainless steel structural frame.

Automatic Compensating Coils (AC)

These coils are mounted locally within each block on the outer surface of the shield. They are arranged such that any part of them will essentially compensate a mangetic disturbance in the neighboring blocks. They are, however, separated by a free zone of 10 cm to make room for the joint between blocks.

There are three types of coils in the (AC) system

(1) Horizontal control field coil

(2) Quadrupole control field coil

(3) Vertical control field coil

The proposed magnet system for T-20 is designed to allow quick and easy remote disassembly of its components and vacuum chamber blocks. A careful analysis has to be done, however, to determine the interaction between all the different elements and to establish their limitations.

The Mechanical Aspects of the Magnet System

An important limitation of the magnet system is the mechanical strength of the elements while operating in different modes and during the shake down period, when various combinations of interacting fields can produce substantial forces between the elements on the system. The following are some of these force interactions:

a - When the toroidal field magnets are energized independently, producing a field of 3.5 T in the discharge chamber axis, there will be tensile electromagnetic forces in the plane of the coils putting the copper and the steel structure in tension. In order to substantially reduce the bending moments acting on the coil it was designed in a D shape. The level of stresses in the TF coils

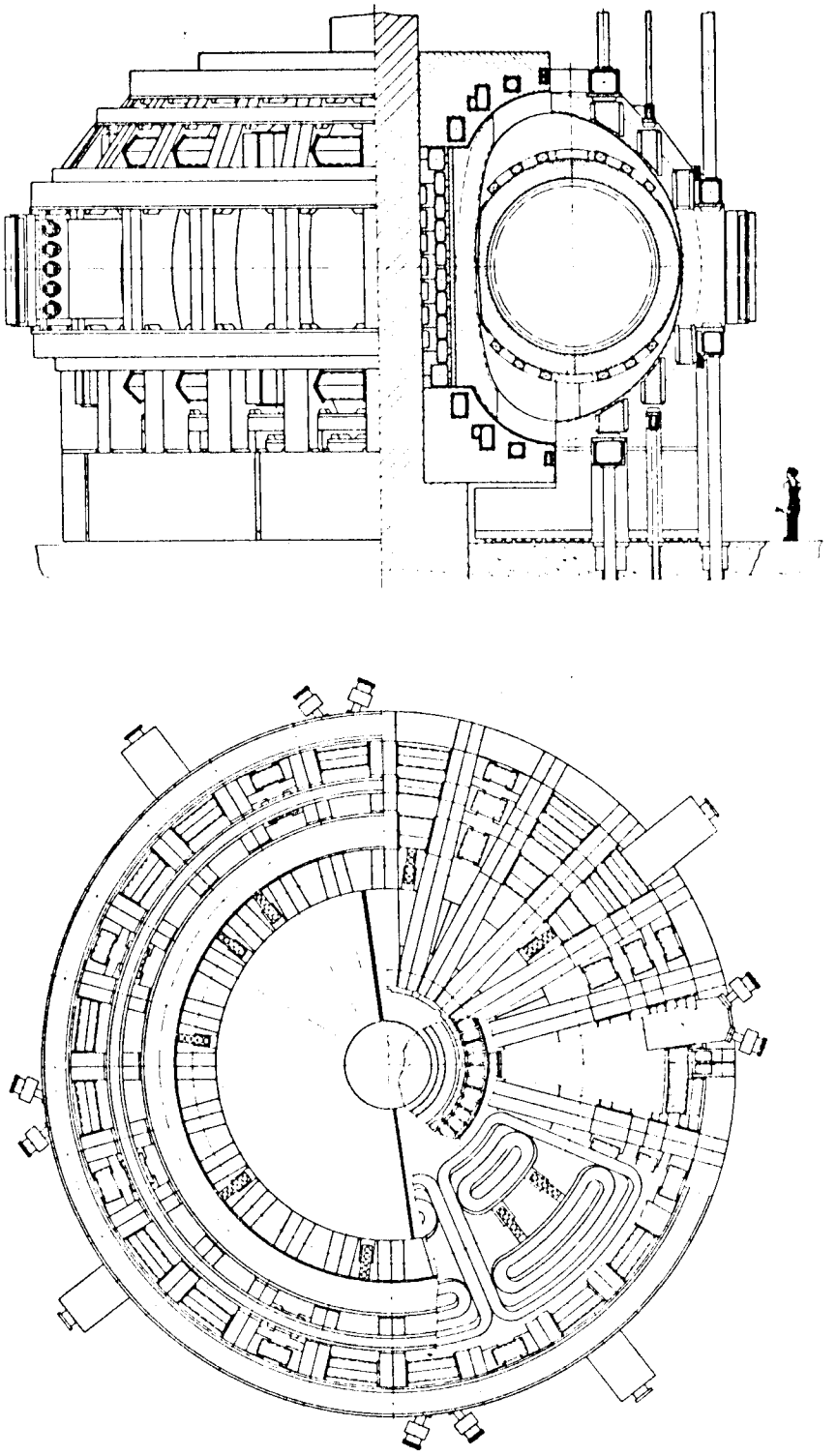

Рис.П.I. Электромагнитная система установки Т-20
Figure II.1 Magnet System for T-20

at a field of 3.5 T on the chamber axis is $\sigma_c \approx 300 Kg/cm^2$ (4267 psi) in the copper and $\sigma_{ST} \approx 600\ Kg/cm^2$ (8535 psi) in the steel. In T-20 the radial force on each coil is equal to 6000 t and is taken up by a structure located at the center of the machine, which is this case (air core), is comprised of the ohmic heating coils reinforced with steel rings and insulated from each other. The location of the ohmic heating coils has been determined analytically such that the poloidal magnetic field, at the initial stage of the discharge, did not exceed the design value. In calculating the stresses in the toroidal magnets, the thermal stresses produced by the temperature rise of the coil to a 100^o C during a pulse and subsequent cooling to 30^o C were taken into account. Assuming that the braze joint between the copper and the steel remains intact, these thermal stresses can reach $\sigma_c = -750\ Kg/cm^2$ (-10,668 psi) in the copper and $\sigma_{ST} = 650\ Kg/cm^2$ (8245 psi) in the steel.

b - The ohmic heating coils along with their reinforcing rings represent an independent structure which is the foundation for the location and adjustment of the TF coils. The magnetic field set up by the ohmic heating coils generates forces which are perpendicular to the planes of the TF coils, with the resulting tendency for them to be literally tossed off. The magnitudes of the forces on the OH and the VF coils are given in Table II - 4.

c - The vertical field coils (VF) produce a poloidal magnetic field which is programmed to vary with the plasma current and temperature. Interaction between this vertical field and the toroidal field produces bending forces on the TF coils which are not balanced within the magnet system and therefore the TF coils undergo a rotation through an angle determined by the equilibrium between the

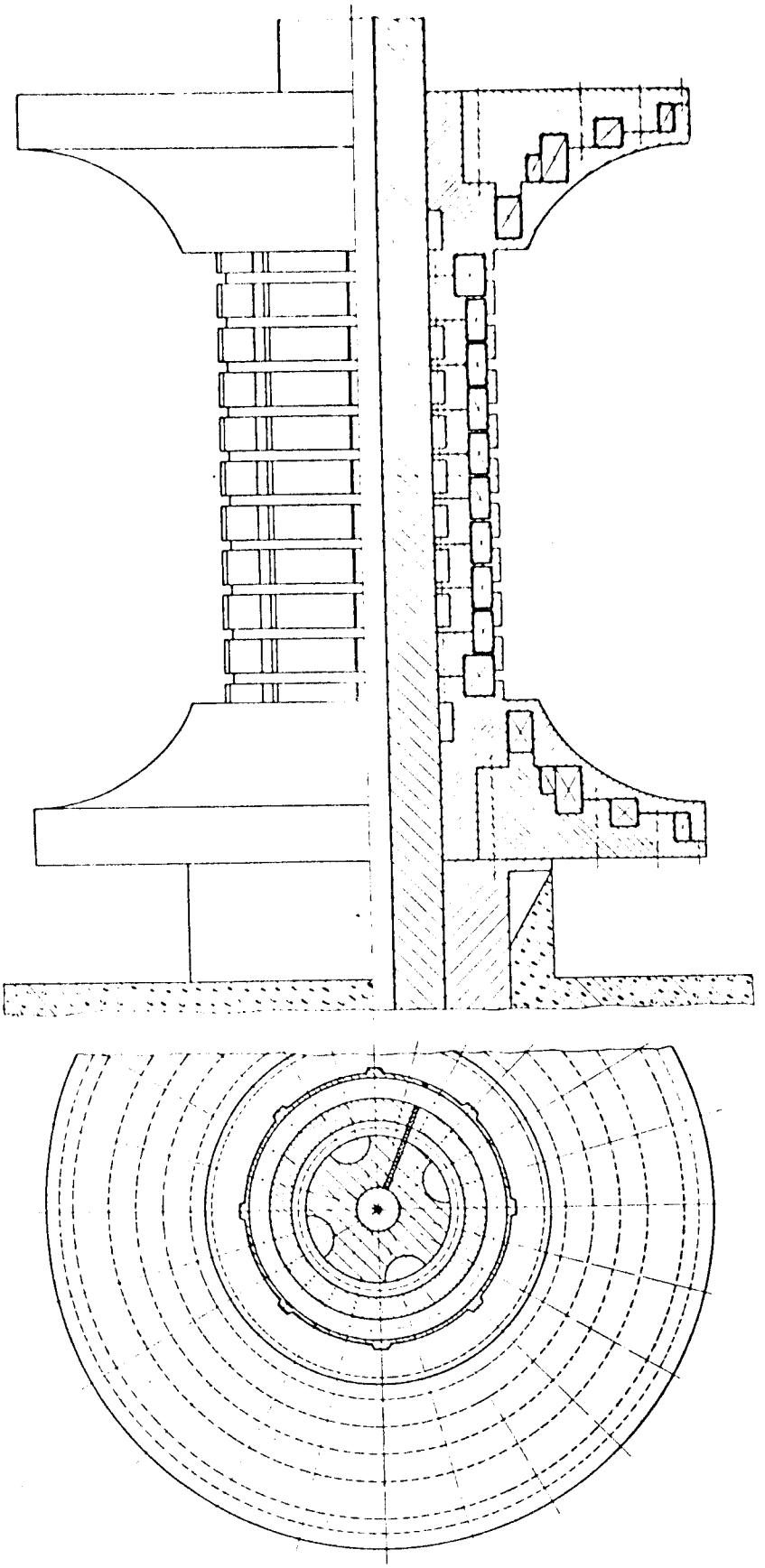

Figure II.2 Ohmic Heating Coils for T-20

Рис.П.2. Индуктор установки Т-20

bending moment of the vertical field and the supporting moment of the toroidal field. Since the tolerance on the vertical component of the toroidal field is very tight, the order of 3×10^{-4} the twisting of the TF coil cannot exceed 3×10^{-4} radians. To provide the rigidity needed by the TF coils to withstand the twisting moment of 800 m tonnes acting on each coil, the following measures were taken: (1) The toroidal field coils were wound solidly inside steel structural frames which are interconnected by solid bridges forming a torsionless structure capable of resisting a torque of 800 m tonnes. (2) The solid coupling between the coils is insured by the bridgework joining the steel frames of the TF coils together as well as by the steel structural rings which contain the vertical field coils, situated on the top and bottom of the TF coils and tightly clamped to them, providing additional restraint against twisting. In the highest stressed areas of the TF coil, the stresses do not exceed σ_{ST} = 2000 Kg/cm^2 (28,446 psi) in the steel and σ_C = 450 Kg/cm^2 (6400 psi) in the copper. The action of all the investigated forces produce a maximum stress of σ_{ST} = 3500 kg/cm^2 (49,780 psi) in the steel and σ_C = -900 kg/cm^2 (12,800 psi) in the copper.

Electrical Insulation

The electrical insulation in T-20 is an important part of the machine and its selection is determined by many considerations, some of which are:

(a) Radiation conditions

(b) Mechanical and thermal effects

The primary factors which will effect the integrity of the electrical insulation are given in Table II.1.

Table II.1

	Operating Conditions	Toroidal Field	Ohmic Heating	Vertical Field
1	Maximum operating voltage KV	5	30	30
2	Maximum temperature of insulation ^{o}C	100	100	100
3	Maximum pressure on insulation KG/cm^2	200	100	100
	Total neutron dose after 10^5 pulses in n/cm^2	2.5×10^{15}	2.5×10^{15}	2.5×10^{15}

At the present time we propose to use a fiberglass impregnated with polyamid resin insulation in the toroidal field coils. For the ohmic heating and vertical field coils, a mica base insulation with an organic-silicon binder will be used. This decision is not final and may be revised if better insulations are developed. To provide protection for the OH and VF coils against a sharp voltage rise due to a sudden plasma quench, there will be spark gaps situated at the coil terminals.

Temperature of Coils

The toroidal and polidal field coils were designed such that the maximum temperature in the conductor during a pulse never exceeds 100 °C and cooling is accomplished between pulses by means of water circulating within the hollow conductors. This circumstance determines the current density in the conductor ($j \approx 1600$ A/cm^2) and its cross-sectional area. For this current density, the temperature in the conductor does not exceed 100 °C, and the temperature rise during a pulse is 70 °C. The cyclic nature of the thermal loading on the coils was taken into consideration during the design.

Main Technical Features of the Magnet System

Table II.2

		Toroidal Field Coil	Ohmic Heating Coil	Vertical Field Coil
1	Current, KA	120	120	120
2	Voltage , KV	5	28	25.5
3	Resistance, Ohms	0.055	0.0075	0.0063
4	Inductance, Henrys	0.85	0.031	0.07
5	I^2R MW	800	100	90
6	Water flow m^3/hr	5000	500	400
7	Weight of copper, tonnes	1100	150	500
8	Weight of structure, tonnes	500	150	300
9	Total weight, tonnes	1600	300	800

2. Calculations

Toroidal Field Coil Calculations

The toroidal field is generated by 24 flat D shaped magnets. The dimensions of the TF coils were dictated by the minor plasma radius, the radial clearance needed for the double walled discharge chamber and shield as well as the mechanical strength of the coils themselves. The modified "D" shaped TF coil was designed such that the straight section, which bears on the central column, is a circular arc. Such a shape, aside from being easier to fabricate, reduces the stored energy in the coil, reduces the inductive losses and improves the coupling between the coil and the plasma. Further, it allows space for a possible future diverter.

Main Parameters of the Toroidal Coil

Table II. 3

R_1 and R_2, the minimum and maximum distance from center of machine to the center line of the magnet leg.	R_1 = 2.25 m R_2 = 8.04 m
Thickness of the copper coil windings	C_c = 0.43 m
Thickness of the structural steel	C_{ST} = 0.05 m
Minimum and maximum cross-section of the copper conductor in a toroidal coil	F_{min} = 0.182 m^2 F_{max} = 0.200 m^2
Maximum toroidal field Field on axis of plasma	7.77 T 3.5 T

Table II. 3 (Cont.)

Tensile force in the toroidal coils	N = 1467 tonnes
Circumference of the center line of a toroidal coil	S = 21.5 m
Ohmic losses in the toroidal system	P_{ohm} = 800 MW
Stored energy in the toroidal field coil	W_T = 600 MJ
Time constant of a toroidal coil	τ_T = 15 sec.

The parameters of the axial line of the TF coil are given in Table II.5.

Calculations

The ohmic heating and vertical field coils are situated on the outside of the TF coils. The OH coils create a varying magnetic flux which is coupled to the plasma and does not produce a magnetic field in the vicinity of the plasma, while the VF coils produce a vertical magnetic field at the plasma with an index of n = 0.5, and at the plasma axis is equal to

$$B_z = \frac{I_{PL}}{4\pi R^2}\left[L_{PL} + (0.5+\beta)\mu_0 R\right] \qquad (2.1)$$

where L_{PL} is the self inductance of the plasma toroid.

$$L_{PL} = \mu_0 R\left(\ln\frac{8R}{a} - 2 + \frac{l_i}{2}\right) \qquad (2.2)$$

β is the ratio of the kinetic plasma pressure to the magnetic field pressure, created by the plasma current $B_\omega = \frac{\mu_0 I_{PL}}{2\pi a}$.

In the calculations we have assumed the following model for the plasma discharge. At the start of the preliminary ionization, conditions are promoted for the propagation of the discharge in the center portion of the vacuum chamber R = 5 m, a = 0.5 m. The current in the plasma increases to 0.1 $I_{PL\ max}$ ($I_{PL\ max}$ = 6 MA) at a rate $\frac{dI_{PL}}{dt}$ = 10^7 A/sec. Further current rise is produced only by increasing the minor radius of the plasma such that $a \approx \sqrt{I_{PL}}$. The presence of active losses in the plasma was accounted for by assigning a potential $U_{PL.ACT}$ on the plasma circumference based on extrapolations of existing experimental data.. In the interval $0 \leq t \leq 0.04$ sec (t = 0 corresponds to the start of the discharge I_{PL} = 0), it was assumed $U_{PL.ACT} = 50V$. Subsequently, for $0.04 \leq t \leq 0.6$ sec $U_{PL.ACT}$ decreases linearly such that at the start of the interval $U_{PL.ACT}$ (0.06) = 20 V and at the end $U_{PL.ACT}$ (0.6) = 1 V. For the rest of the pulse we assumed $U_{PL.ACT}$ = 1 V. Since there is no iron core, the inductive characteristics of the plasma toroid, OH coils and VF coils can be expressed by the symmetric matrix of their coefficients of self induction and mutual induction $M_{ik}(\mu H)$ $(W_{OH} = W_{VF} = 1)$:

$$M_{ik} = \begin{pmatrix} 10.5 & 1.185 & 3.66 \\ 1.185 & 1.162 & 1.10 \\ 3.66 & 1.10 & 7.04 \end{pmatrix} \qquad 2.3$$

In order to produce a plasma current rise from zero to the nominal value in time t, it is necessary to insure a rise in the magnetic flux which is coupled to the plasma current, $\psi_{PL}(t)$:

$$\psi_{PL}(t) = I_{PL}\mu_0 R\left(\ln\frac{R}{a} + 0.75 + 0.23\right) = 71.4\ V\cdot sec \qquad (2.4)$$

(the first term in the brackets describes the external inductance, the second describes the internal inductance and the third describes the scattering of the magnetic flux at the active surface of the plasma toroid). The rise in the magnetic flux is accomplished by the OH and VF windings. The contribution of the VF coil is:

$$\psi_{VF}(t) = \frac{\partial\ell}{4} I_{PL}\left[L_{PL} + (0.5+\beta)\mu_0 R\right] = 25.2 \text{ V.sec} \qquad (2.5)$$

where the coefficient $\partial\ell$ depends on the vertical magnetic field drop-off index n, and for n = 0.5 it is equal to $\partial\ell$ = 1.23. The contribution of the OH winding to the total change in the magnetic flux is equal to

$$\psi_{OH}(t) = \psi_{PL}(t) - \psi_{OH}(t) = 46.2 \text{ V.sec} \qquad 2.6$$

and is proportioned to the initial current in the OH winding $I_{OH}(0)$, since it is useful to make the OH winding operate with a total current reversal

$$I_{OH}(0) = \frac{\psi_{OH.max}}{2 \times 1.185} = 20 \text{ MA} \qquad 2.7$$

In figuring out the power supply needed for the OH and VF windings, it is necessary to take into account the change in the coefficient of plasma self-inductance $L_{PL}(t)$ as a result of the increase in its radius, which is varied such that the average current density over the whole cross-section remains constant after it reaches its nominal value. The first 10% rise of the plasma

current at a rate $\frac{dI_{PL}}{dt}$ = 10 MA/sec can be insured by using the OH winding as an inductive storage unit with a time constant of τ = 0.168. In this way the maximum power available to breakdown the plasma is

$$P_{BR} = \frac{L_{OH} I_{OH}^{2}(0)}{\tau} = 2767\ MW \qquad (2.8)$$

The voltage applidd to the OH winding is

$$U_{OH} = L_{OH} \frac{dI_{OH}}{dt} = - R_{OH} I_{OH} + U_{o} \qquad (2.9)$$

where U_o = 30 V is the constant voltage in the OH winding power supply and which, to a large degree, is independent of the emf induced in the OH winding by the VF coil and the plasma currents, since these emfs are mutually compensating. The time constant of the OH winding is $\tau \approx 4$ sec. The emf induced in the VF coil by the OH and plasma currents during the fast rise in the plasma current adds substantially to the voltage U_{VF} applied to the VF coils and for this reason, to reduce the power supply needed by the VF coils, they are energized in parallel with the breakdown resistance in the OH winding circuit. (see Fig. II.17). By properly choosing the correct ratio of OH winding to VF windings $\frac{W_{OH}}{W_{VF}}$ it is possible to achieve a condition whereby the voltage in the power supply need not exceed 30 V:

$$U_{VF} = L_{VF} \frac{dI_{VF}}{dt} + M_{OH,VF} \frac{dI_{OH}}{dt} - M_{VF,PL} \frac{dI_{PL}}{dt} \qquad 2.10$$

$$= \frac{L_{OH}\left[I_{OH} \frac{W_{OH}}{W_{VF}} - I_{VF}\left(\frac{W_{OH}}{W_{VF}}\right)^{2}\right]}{\tau} + 30$$

On Figures II.3, II.4 and II.5 is shown the time dependence of the voltage for the total amper-turns of the OH and VF coils. AT t = 0.23 sec, the current in the OH winding falls to the level of the VF winding, at which time the two circuits are separated. The plasma current reaches the nominal value at t = 1.1 sec. After the plasma current reaches the nominal value, supplementary heating is turned on and as the temperature and kinetic pressure rises in the plasma, the current in the VF coils increases, reaching a value of 12 MA at t = 5.1 sec.

Calculations and Formation of the Poloidal Field

The sources of the poloidal field are the OH coils, VF coils and the plasma toroid. Since there is no iron core, the field is generated by them independently so that in the calculations we can use super position, which can also be used in the presence of iron when it is not saturated: $B < B_s$. On the other hand, for $B > B_s$ such a division of sources of magnetic field would be superficial, since the magnetic state of the iron is determined by all the currents.

In the following sections we present the calculations and the results for two versions of OH systems: I. air core system and II. iron core system. The two versions differ in the potential needed on the plasma circumference.

(I) Calculations for an Air Core System

The role of the OH coil is to generate and support the plasma current producing simultaneous ohmic heating of the plasma.

(в)	$(-a)^{10}$	(сек)	(сек)	(сек)
30	20	0,168	0,23	1,100

$t\left(\frac{sec}{сек}\right)$	0÷0,23	0,23÷1,1	1,1÷5,1	5,1÷16
U_y (в)	254÷30	30	4,6	0

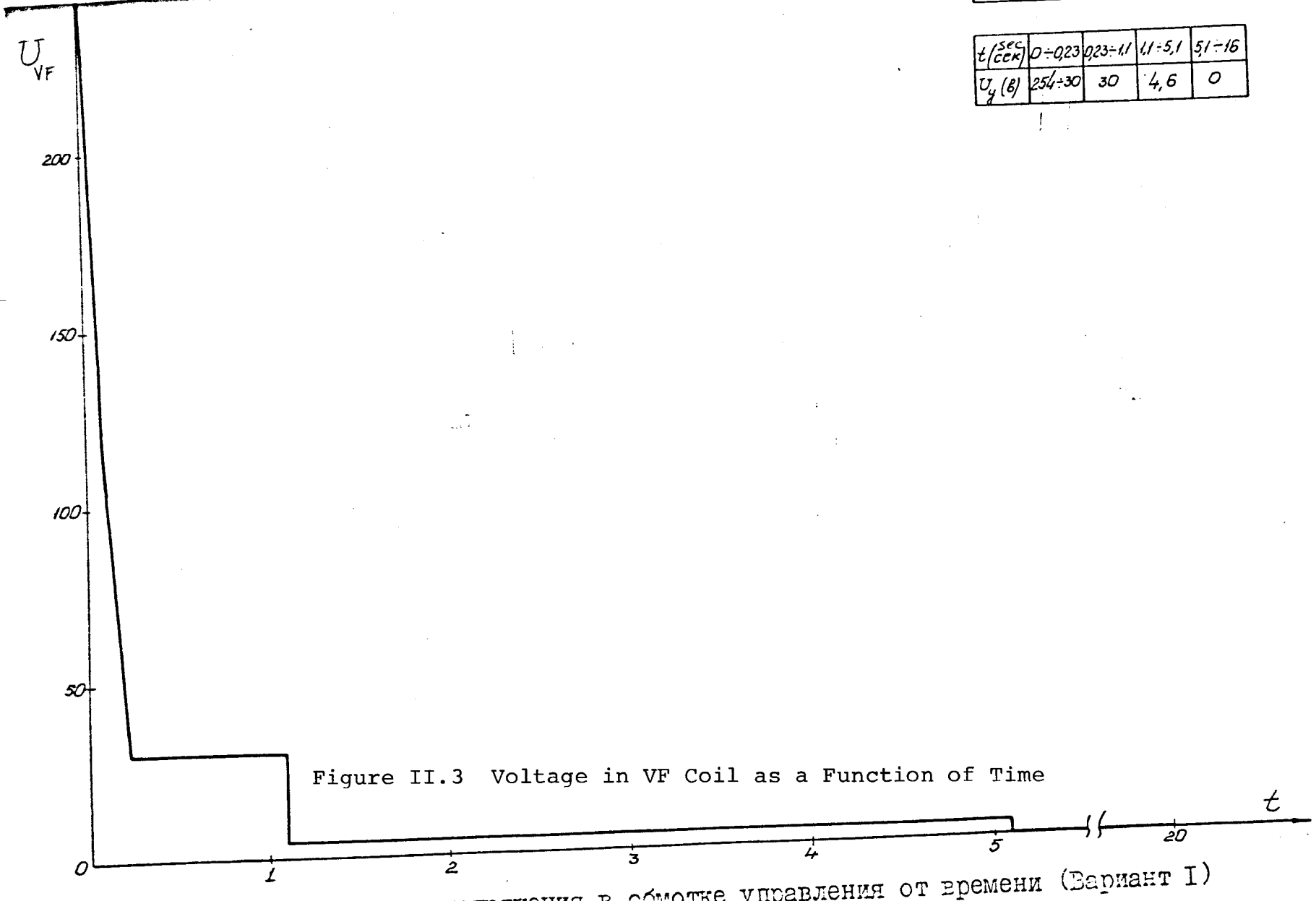

Figure II.3 Voltage in VF Coil as a Function of Time

Рис.П.3. Зависимость напряжения в обмотке управления от времени (Вариант I)

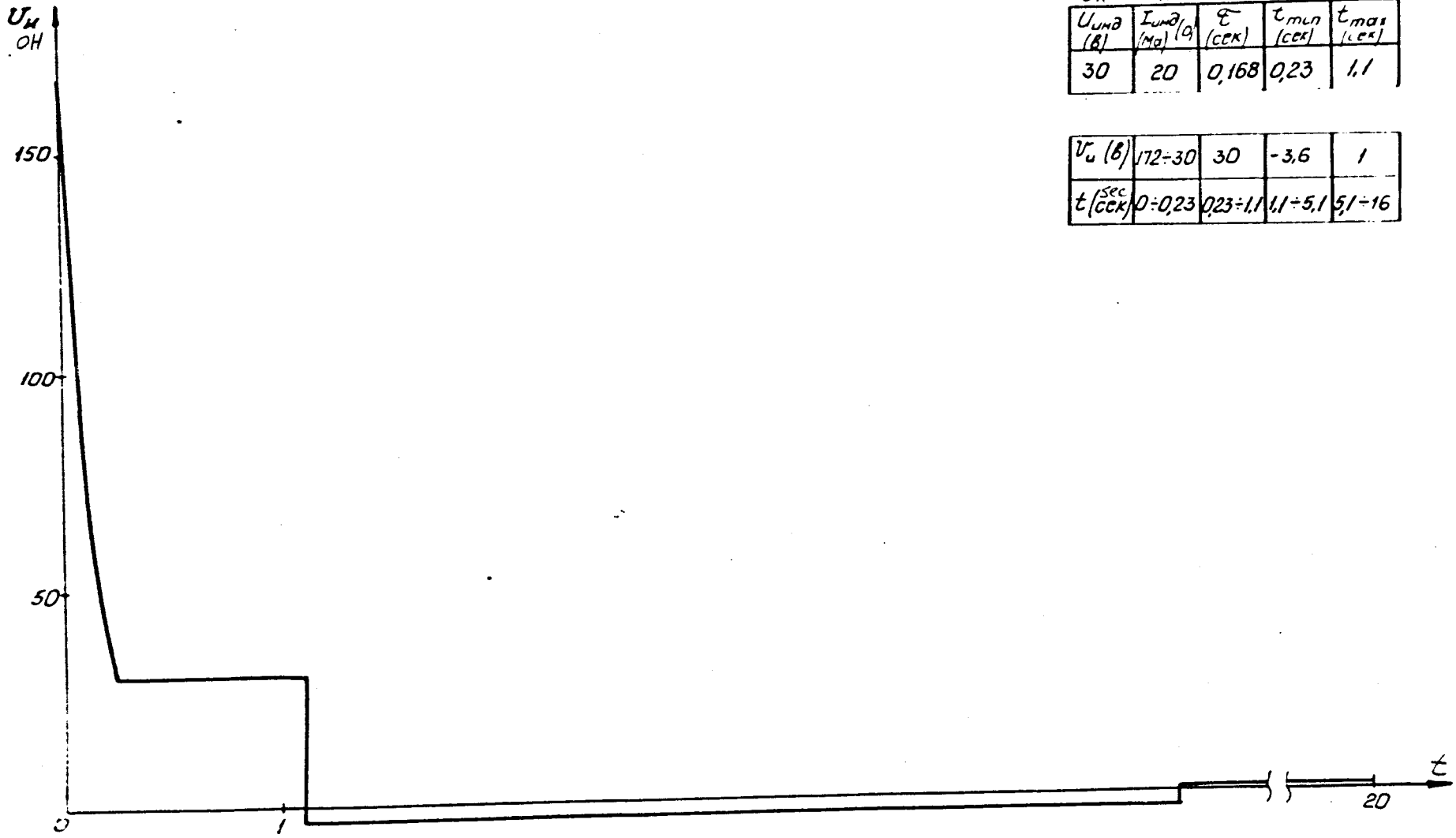

U_{OH} J_{OH} τ_{sic} t_{min} t_{max}

$U_{инд}$ (В)	$I_{инд}$ (мА)	τ (сек)	t_{min} (сек)	t_{max} (сек)
30	20	0,168	0,23	1,1

V_u (В)	172÷30	30	-3,6	1
t (sec / сек)	0÷0,23	0,23÷1,1	1,1÷5,1	5,1÷16

Figure II.4 Voltage in OH Coil as Function of Time (Version I)

Рис.П.4. Зависимость напряжения в обмотке индуктора от времени (Вариант I)

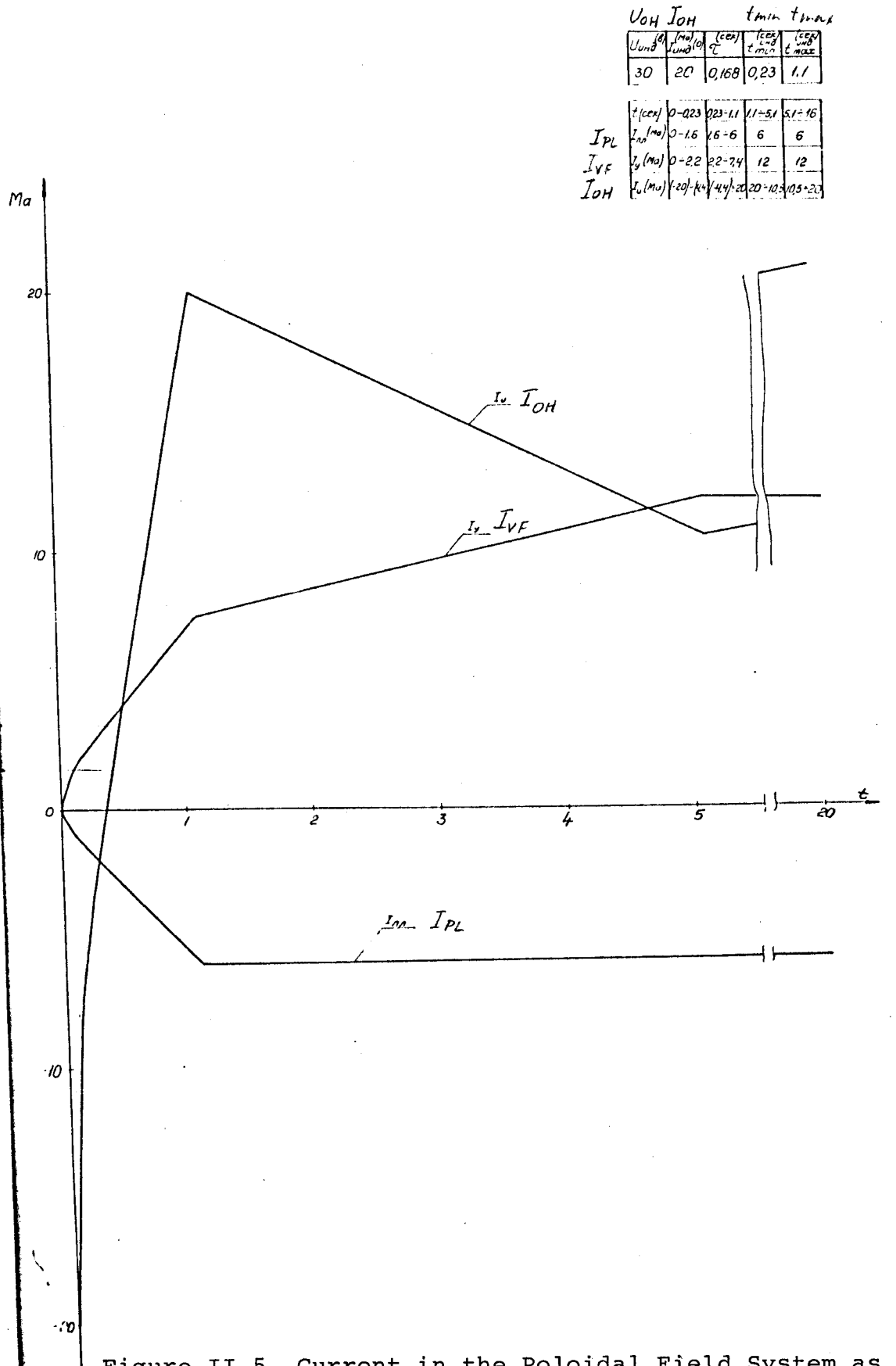

Figure II.5 Current in the Poloidal Field System as a Function of Time (Version I)

Рис.П.5. Токи в системе полоидального поля в функции времени (Вариант I)

At the start of a pulse when there is no plasma yet, and the OH winding is carrying a maximum negative current, the winding should be designed such that the stray field in the plasma region does not exceed 3×10^{-4}, namely $\langle B_{\perp} \rangle \approx 10$ G, averaged over the plasma cross section. The value of this current depends on the total reversal in the coupling of the magnetic flux $\Psi_{pl\ max}$ with the plasma, needed to induce the active and reactive components of the potential on the plasma circumference. Thus, in order to find the maximum OH flux $\Psi_{OH\ max}$ it is necessary to subtract from $\Psi_{pl\ max}$ the contribution of the VF coil (see Eq. 2.6).

The configuration of the OH coil becomes more complicated by the presence of forbidden zones, situated in the vertical and horizontal directions from the plasma which are about 1 - 3 m wide. In addition, it is necessary to take into account the physical location of the OH and VF winding.

Of particular importance in this project is the presence of subtantial transverse field in the region of the toroidal coils, and the consequent manifestation of large twisting moments. However, since the OH windings are located outside the TF coils, their stray field can be minimized. It is true that with this geometry, the coupling between the OH winding and the plasma is reduced, but this is compensated by several advantages such as the ease of assembly and disassembly, mounting of the OH windings etc.

The procedure for calculating the OH winding was the following. On a meridional section of the machine (plane r, z on Fig. II. 6) at some distance away from the "D" shaped toroidal coil surface, 34 current threads were located at equal intervals. The distance from the toroidal surface was determined on the basis of construc-

Figure II.6 Locations of OH and VF Coils (Version I

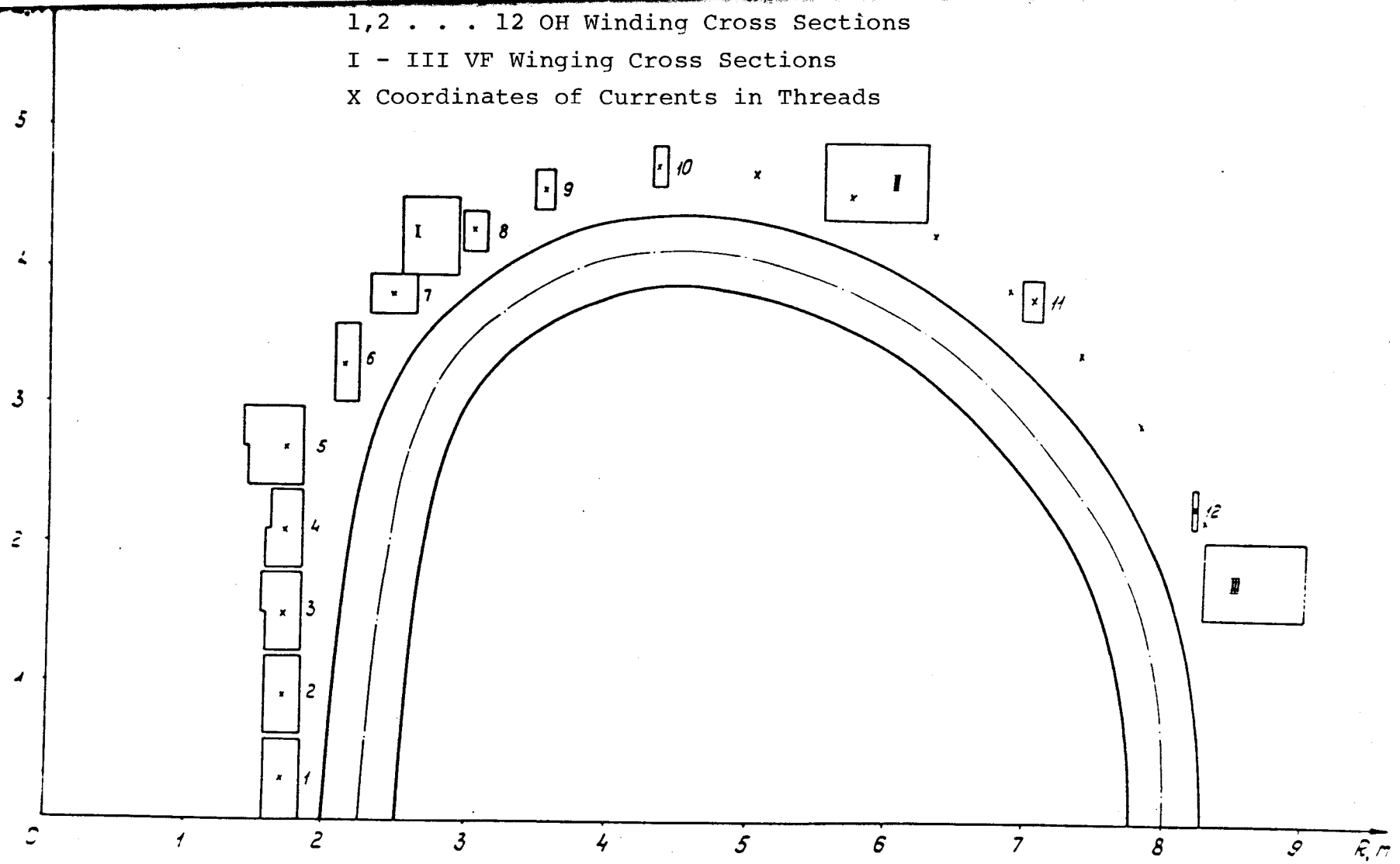

Рис.П.6. Геометрия индуктора и обмотки управления (Вариант I):
I,2,...,I2 - секции обмотки индуктора, I÷III - секции обмотки управления, x - координаты токовых нитей

tional problems and an anticipated coil thickness. Observation points r_i , z_i , i = 1, 2, - - - - , 56 were selected on the center line of the "D" coil. The currents in the threads were determined by the method of least squares according to the condition

$$2\pi r_i A\varphi(r_i ; z_i) = 0.5\,\Psi_{OH\,max} = const.,\quad i = 1, 2 \cdots 56$$

where A_φ is the component of the vector potential different from zero.

For more effective calculations, the distance between adjacent current threads were taken roughly equal to their distance to the closest observation points.

From constructional restrictions, threads i = 1,2 --- 5, all have r_i = const. In the first iteration, the forbidden zones were neglected and the currents were assumed to go in the same direction. With such a configuration, the sum of the currents in the discrete threads was somewhat larger than would have been in an ideal continuous current layer.

In the second stage of calculations the currents in i = 1,2 - - - , 10 were assumed given and the rest were replaced by two threads in which the current was determined by the method of least squares taking into account the requirment for minimizing the average cross section of the plasma toroid. We analyzed several versions of possible current distributions in these threads and the most suitable was selected to be used in further calculations.

In the final stage of calculations, we replaced the threads with finite section d x h = .03 x .28m^2 windings with a t = 1.5mm insulating layer. The results of this approximation are given in Fig. II.6. Each coil was assumed to be a current point in the center of the coil and in this way the field plot and the coil parameters were derived.

On Fig. II.7 is shown a family of curves B = const. At the start of the discharge when a $\leq$ 0.5m (a is the plasma minor radius), the requirement that $\langle B_\perp / B_{TF} \rangle \approx 3 \times 10^{-4}$ was observed, where B_{TF} = 3.5 T at the plasma center. The maximum OH field at this time is $B_{OH\ max}$ = 4T, and the total current in all the coils is (Aw) = 30.2×10^6 A. The coefficient of self inductance of the OH winding is L_{OH} = 1.162 H, its mutual inductance with the plasma M_{OH-PL} = 1.185 H, its mutual inductance with the VF coil is M_{OH-VF} = 1.097 H (single turn coils were assumed). In calculating M_{OH-PL} we assumed that the current distribution in the plasma was parabolic, falling off from the center to the edge.

In Table II.4 are given the number of turns per OH coil and the forces F_r and F_z acting on them per unit length. The self fields of individual coils were taken for calculating Fr, but not for F_z .

Stray field from the OH windings in the regions of neutral beam injectors and their transport tubes is shown in Fig. II.8. It is interesting to note that during the main portion of the pulse, the OH and plasma fields, in a first approximation, cancel each other out.

Calculations for Vertical Field Coils

The vertical field is generated by six groups of windings situated symmetrically about the plane z = 0. The upper half of the coils is shown in Fig. II.6. Maximum current in the coils is 120 KA. Like the OH coils, the VF coils are made of four layers of water cooled copper conductors of 30 x 70 mm^2 cross section.

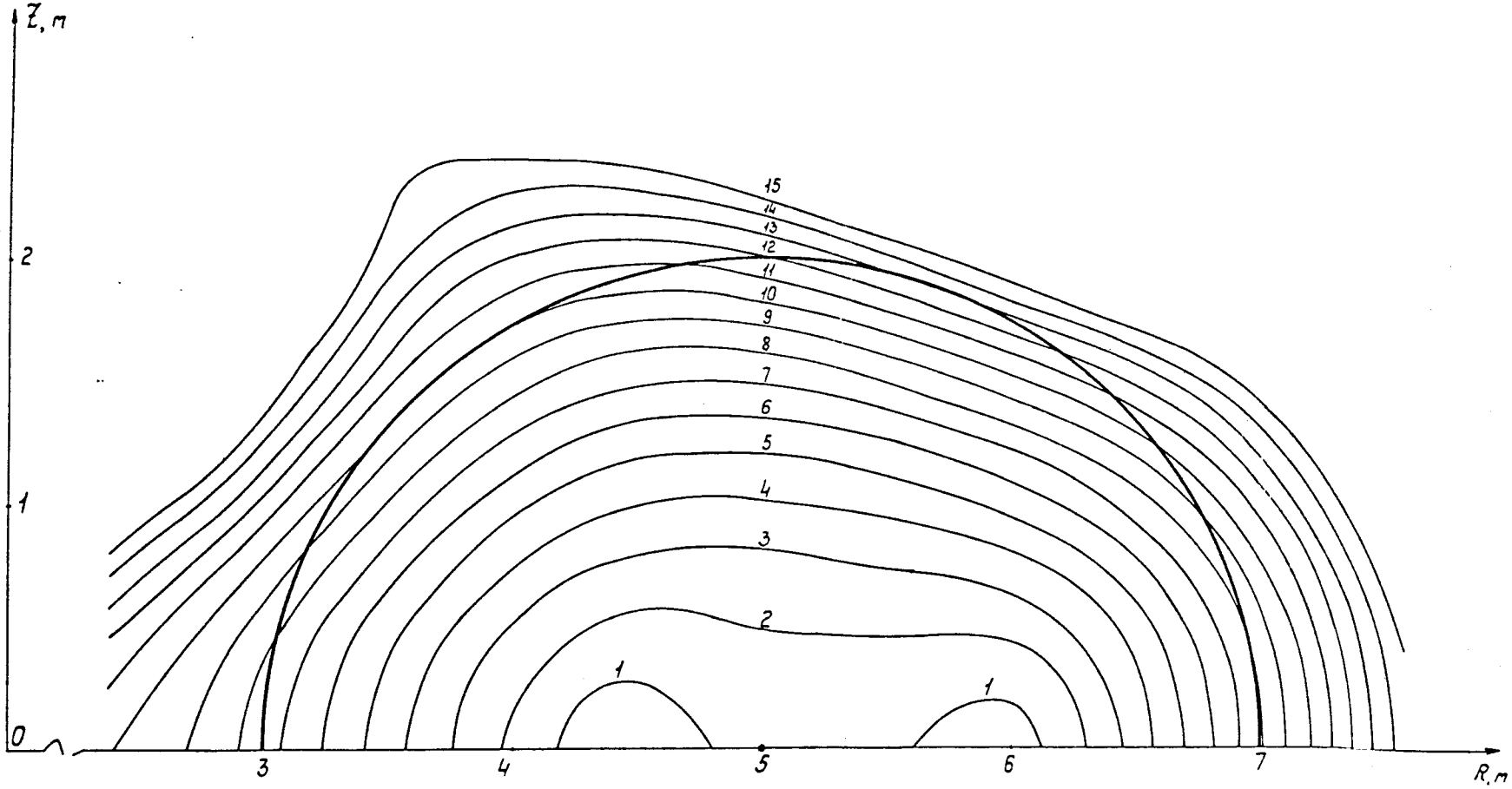

Рис.П.7. Поле рассеяния индуктора в области плазмы (Вариант I):
Линии B = const (тл): I - 0,00I; 2 - 0,002; ...; I5 - 0,0I5

Figure II.7 OH Stray Field in Plasma Region (Version I)
B = const. lines (T) I = 0.001; 2 = 0.002; . . . 15 = 0.015

Table II.4

Section No.	No. of windings per section	Forces from self-fields of OH Coils		Forces from VF Coils		Resulting Forces	
		$F_r .10^{-5}$, N/m	$F_z .10^{-5}$, N/m	$F_r .10^{-5}$, N/m	$F_z .10^{-5}$, N/m	$F_r .10^{-5}$, N/m	$F_z .10^{-5}$, N/m
I	I6	39,60	0,04	I0,90	0,I7	50,50	0,2I
2	I6	39,50	0,20	II,20	0,53	50,70	0,73
3	I7	42,80	-0,06	I2,40	I,0I	55,20	0,95
4	I5	33,90	-0,90	II,60	I,38	45,50	0,48
5	25	75,00	-20,40	2I,60	3,I0	96,60	-I7,30
6	I0	6,30	-5,80	9,80	2,62	I6,I0	-3,I8
7	I0	I0,00	-7,60	I2,00	6,50	22,0	-I,I0
8	5	2,64	-2,65	-0,06	-0,59	2,58	-3,24
9	4	0,87	-2,05	2,03	-0,78	2,90	-2,83
I0	3	0,I3	-0,88	2,26	-0,48	2,39	-I,36
II	4	0,I6	-0,30	I,67	-0,04	I,83	-0,34
I2	I	-0,03	0,002	0,48	-0,62	0,45	-0,62

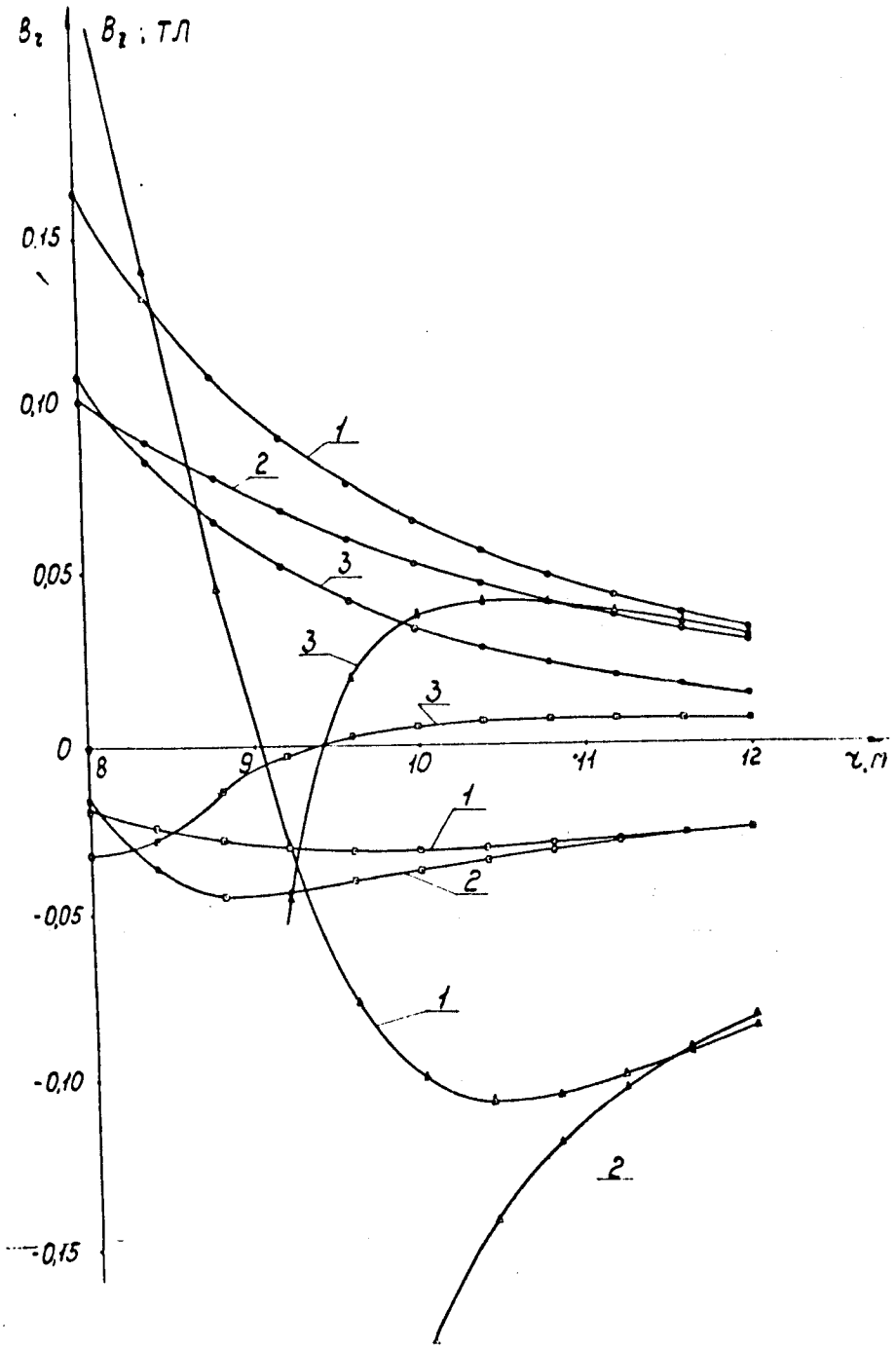

Figure II.8

Poloidal field in the neutral beam injector region and distribution of neutral beams.

1 - B_z (r, o), 2 - B_z (r, 1.6m), 3 - B_r (r, 1.6m)

from plasma (I = -6 MA)
from OH (I = 30 MA)
from VF (I = 11.2 MA)

Calculations for the VF coils were performed in a special way, utilizing linear programming methods (Appendix I). The VF coils had to be situated externally to the "D" TF coils at a distance not less than 0.15m, at $r \geqslant 5.5$m and $Z \gtrless 1.5$m ($Z \leq -1.5$m). The region $4.5\text{m} < r < 5.5\text{m}$ and $-1.5\text{m} < Z < 1.5\text{m}$ was reserved for other purposes; the region $r < 4.5$m, although available, was crowded with OH coils and thus was not suitable.

The field at the center of the vacuum chamber is 4.2 KG with a tolerance of $\Delta B = 0.3$ KG over the whole region occupied by the plasma. Field index $n = -\frac{r}{B} \cdot \frac{\partial B}{\partial r}$ was equal to ≈ 0.5. The position of the coils are shown in Fig. II.9 and the field shape in Fig. II.10.

The self inductance of the VF coils as calculated on the basis of a single winding is 7.04 μH, and the mutual inductance with the plasma is 3.66 μH.

We also calculated the magnetic field from the VF coils at the central line of the toroidal coil in order to determine the twisting moment acting on the TF coil. Results are given in Table II.5 and Fig. II.9. These moments are 3.85×10^3 Tonne-m from the VF coil, 88 Tonne-m from the OH coil and 1.17×10^3 Tonne-m from the plasma. They were calculated with each of the coils at its maximum current value.

Figure II.8 contains the complete picture of the fields in the vicinity of the neutral beam injectors. Approximate values of the forces acting on the VF windings from their self fields are given as follows:

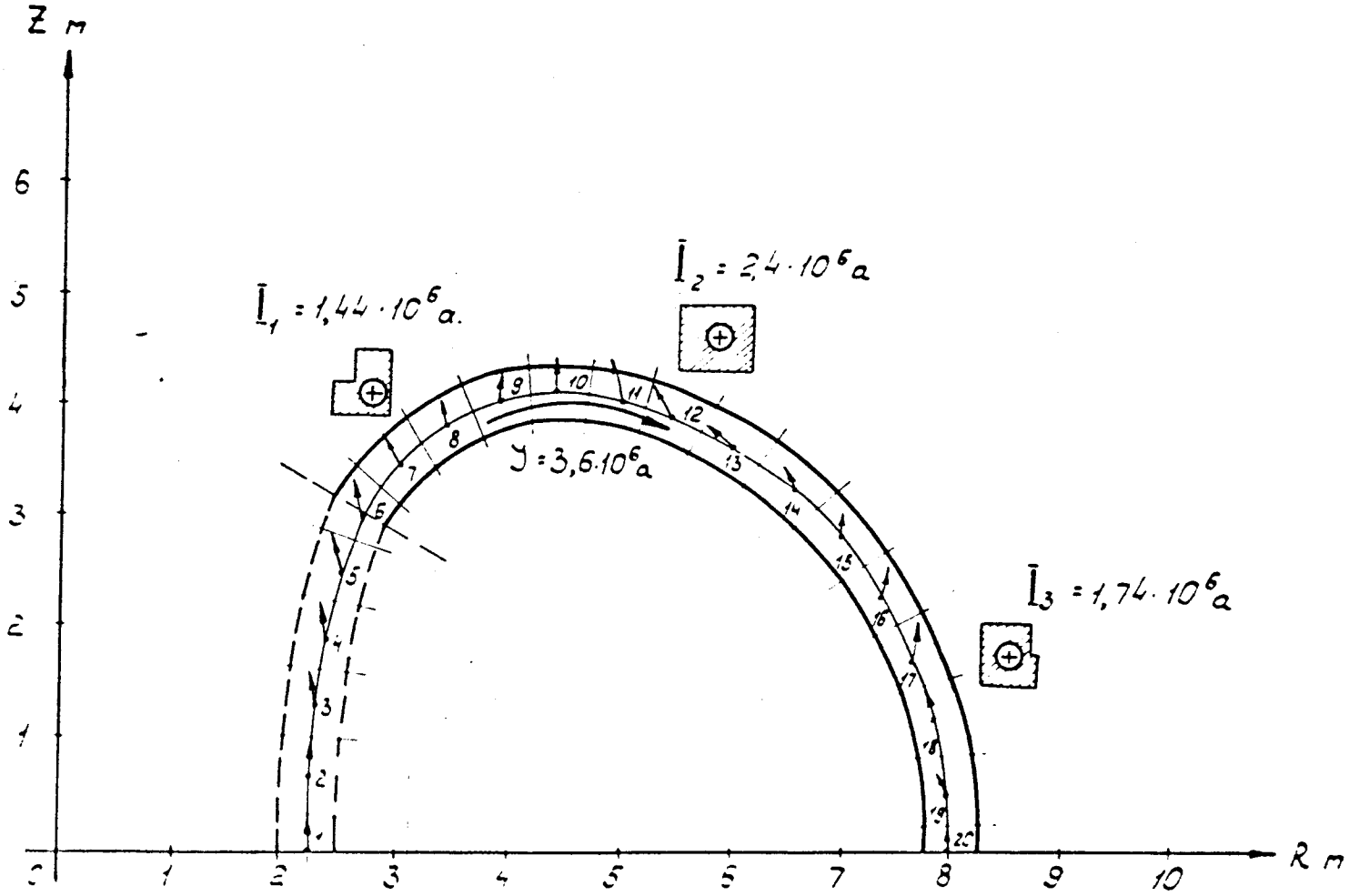

Рис.II.9. К расчету опрокидывающего момента
Figure II.9 Diagram Used for Calculating Twisting Moments

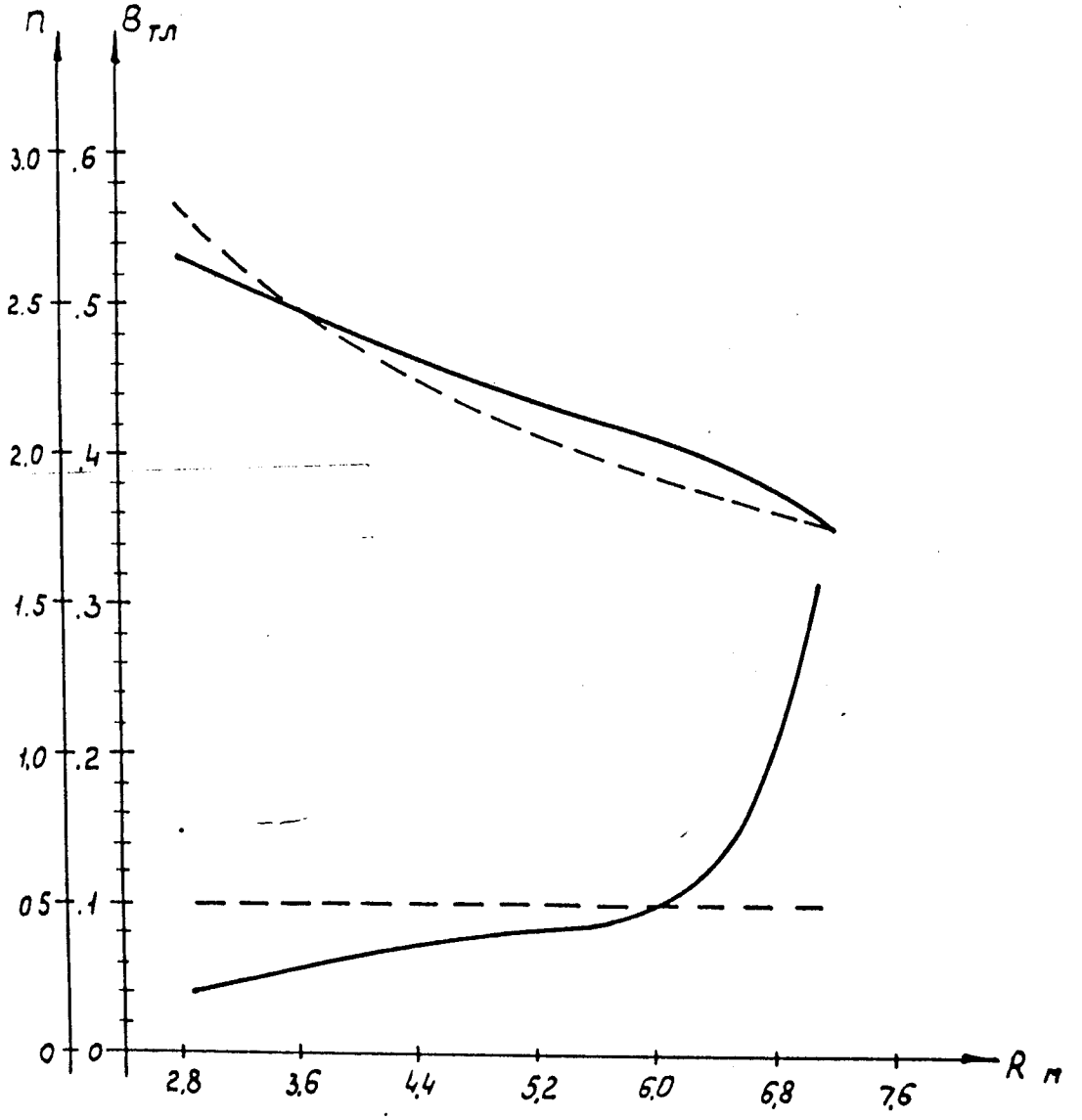

Рис.II.IO. Поле обмотки управления в плоскости z = 0:
- - - n = 0,5; B_o = 0,42 тл;
——— результаты расчета

Figure II.10
The field from VF coils on plane z = 0
--- n = 0.5, B_o = 0.42 T
—— CALCULATED RESULTS

I. F_r = 130 T/m F = -4 T/m

II. F_r = 120 T/m F = -29 T/m

III. F_r = 20 T/m F = -10 T/m

Similarly, the forces from the OH windings are:

I. F_r = 106 T/m F = 0120 T/m

II. F_r = 7.5 T/m F = -34 T/m

III. F_r = -8.7 T/m F = 5.3 T/m

Iron Core Magnetic System (II)

The peculiarity of an iron core magnet system for a project like this, is that unlike other similar systems for Tokamaks the iron can exist for a long period in a saturated state $B > Bs$. Under these conditions, analysis of the magnet system should take into account saturation of the iron as a result of simultaneous operation of all the poloidal field coils.

The amount of iron in the external flux return path is not limited and can be made adequate to carry the flux unsaturated, $B < Bs$. Thus, the only nonlinear element in the system is the central iron column. Figure II.11 shows a cross section of the upper half of the magnet system. Coil number one which bears against the central column takes the place of the OH windings. Its configuration, as a first approximation, insures the absence of fields at the plasma (2) at t = 0 (flux reversal regime). Supplementary correction of stray fields in this region can be accomplished either by special coils or by coils 31, 32 and 33, which were originally intended as VVF coils.

The aim of the magnet system calculations has been to find the laws governing the changes with time of current and voltage at all

Table II.5

Distribution of twisting moment and magnetic field strength along the central line of the TF coil (from the VF coils).

	r (M)	Z (M)	M (T.M)	H, Koersd. x)	Angle (degrees) xx)
I	2,25	0	0,00	5,506	90,00
2	2,26	0,68	II,I8	5,565	92,53
3	3,30	I,32	26,07	5,729	95,I8
4	2,37	I,90	77,35	5,978	98,I3
5	2,50	2,50	I63,93	6,336	I02,47
6	2,70	3,02	289,28	6,625	I09,07
7	3,00	3,48	439,66	5,994	II9,85
8	3,44	3,82	34I,58	4,266	I06,74
9	3,90	4,06	435,26	5,060	92,I4
I0	4,40	4,I4	566,02	6,2I8	92,92
II	5,00	4,08	606,9I	7,644	I04,28
I2	5,46	3,94	36I,52	7,444	I25,I0
I3	6,00	3,70	42,96	4,203	I42,86
I4	6,54	3,34	70,50	2,I77	II5,7I
I5	7,00	2,88	I48,78	2,622	8I,56
I6	7,40	2,34	I88,34	4,028	73,II
I7	7,70	I,80	I26,54	5,824	85,89
I8	7,90	I,24	-28,89	5,27I	II3,75
I9	8,00	0,54	-I3,22	2,865	II3,82
20	8,04	0	0,00	2,258	90,00

ΣM = 3853,77 T.M

Notes: x) The vector direction H is shown in Fig. II.9

xx) This is the angle between the vector H and the central plane.

regions, which insure the given conditions for the plasma current $I_{pl}(t)$, magnetic flux coupling with the plasma $\Phi_{pl}(t)$ and the equilibrium conditions for the plasma toroid.

The potential balance on the plasma toroid circumference is

$$\rho_{PL} I_{PL} + \frac{d\Phi_{PL}}{dt} = 0,$$

where ρ_{pl} is the plasma active resistance, giving

$$\Phi_{PL}(t) = \Phi_{PL}(0) - \Phi_{PL}(t) \tag{2.11}$$

where $$\Phi_{PL}(t) = \int_0^t \rho_{PL} I_{PL}\, dt$$

It follows that to get $\Phi_{pl}(t)$ it is necessary to assign $U_{pl}(t) = \rho_{pl} I_{pl}$ or $\rho_{pl}(t)$. In the calculations, we made use of the $I_{pl}(t)$ and $\Phi_{pl}(t)$ relationships given in Fig. II.12. Thus, the first term in Eq. 2.11 is the flux coupling with the plasma at the initial moment, and the second term is the flux change associated with plasma heating.

Analysis of the equilibrium condition in an axisymmetric geometry can be used to solve the magnetostatics for the two term boundary problem of the flux function $\psi = r A$*). The longitudinal component of the plasma current density can then be described by the equation

$$j_{PL} = A(\psi)\frac{r}{R} + B(\psi)\frac{R}{r} \tag{2.12}$$

*See V.D. Shatranov, JETP, 33, 710, 1957.

Figure II.11

Geometry of iron core magnet system (Version II)

S - effective coil area

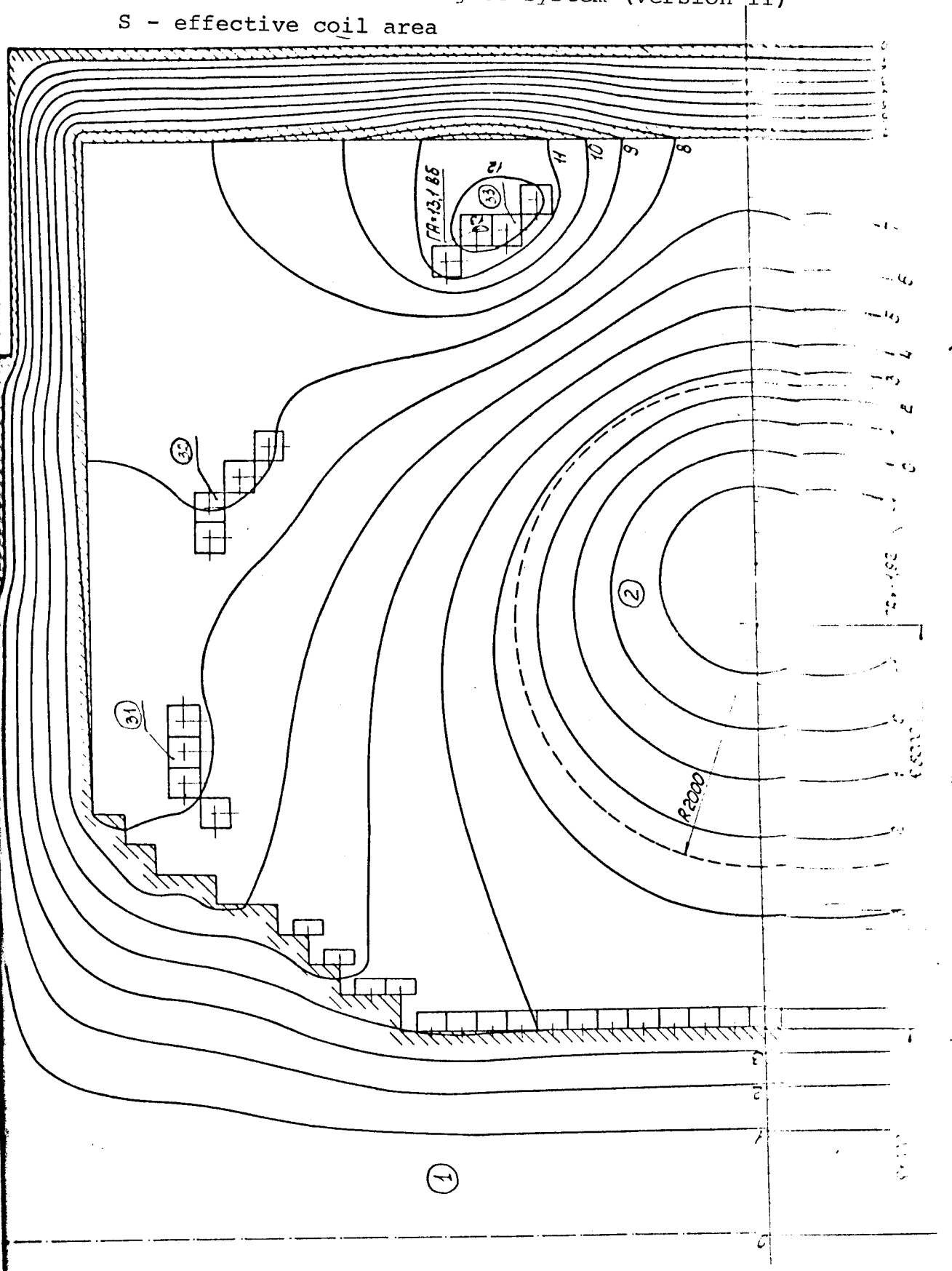

Рис.II.11. Геометрия магнитной системы с железом (Вариант II):
S - эффективная площадь витка

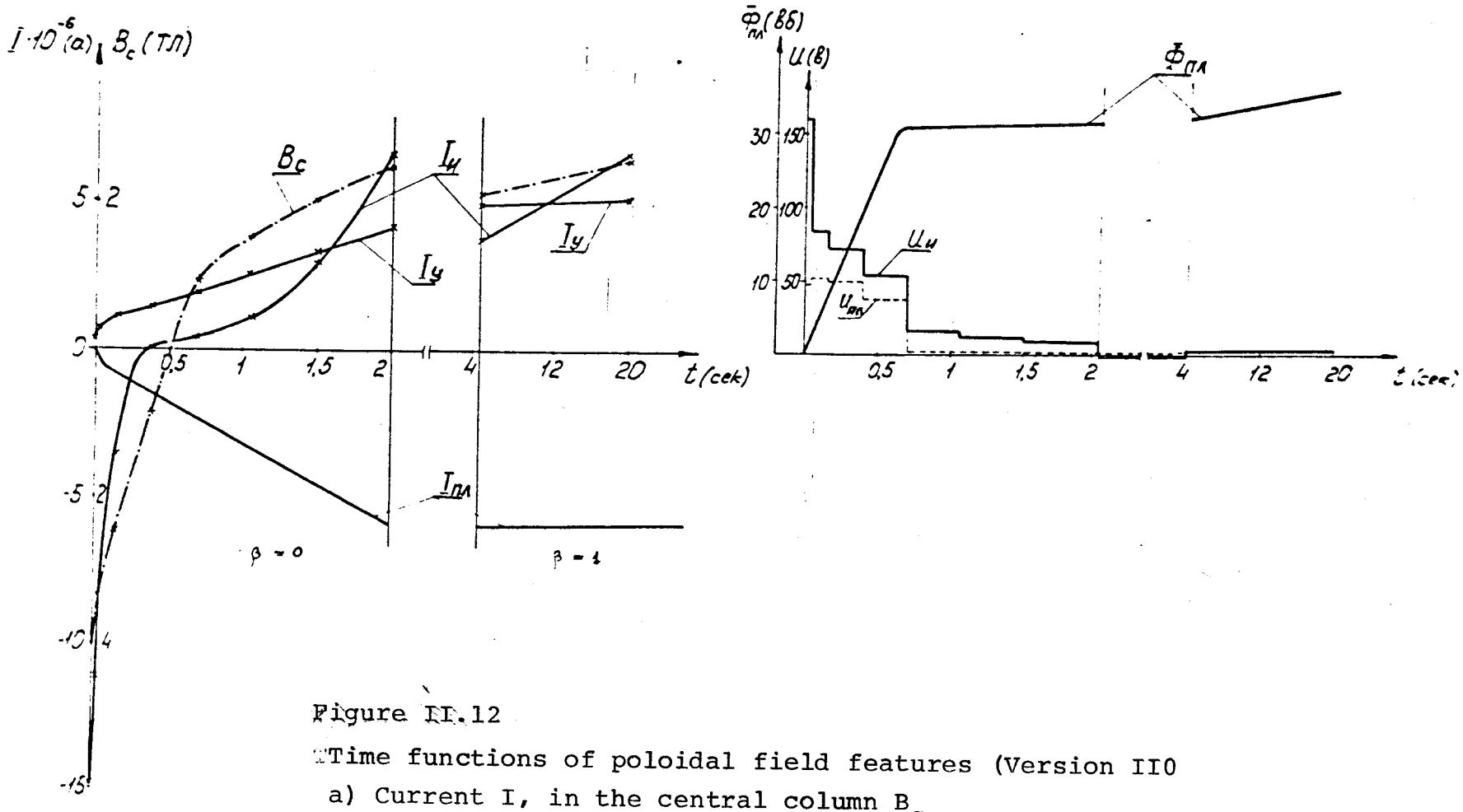

Figure II.12

Time functions of poloidal field features (Version II0

a) Current I, in the central column B_c

b) Voltage in OH coil and voltage across the plasma circumference

where R is the plasma major radius, A (ψ) and B (ψ) are given functions. The plasma boundary r_{pl} should be a constant current line, i.e.

$$(\psi)_{rpl} = \text{const.} \tag{2.13}$$

Since the magnetic flux path is closed and it is not saturated in the outer return leg, the region in question can be limited by the outer radius of the iron r, making $(\psi)_r = 0$.

An anlytic solution of the equilibrium problem in this device, taking into account saturation effects in the steel, does not appear to be possible. Even approximate solutions are suspect. However, as will become obvious, a solution to the problem can be found with the aid of numerical modeling by means of a simple modification of the mesh method used for analyzing DC magnets*. The condition in Eq. 2.13 carries the same value as the requirement that ψ be equal at several points M on r_{pl}.

For each instant under investigation, the values I_{pl} and $\bar{\Phi}_{pl}$ are given

$$I_{PL} = \int_{S_2} j_{PL}\, dS$$
$$\Phi_{PL} = 2\pi \int_{S_2} \psi\, j_{PL}\, dS / I \tag{2.14}$$

and the unknowns are I_1, I_{3i}, - - i = 1,2,3. A solution exists if $M < 4$. Otherwise, the number of VF coils has to be increased.

In ordinary problems of numerical modeling, the sources of the field are given. In this problem, finding many of them is based on the given properties and parameters of the field. This peculiarity is characteristic of the reverse boundary problem. The

---

* See N.I. Doinikov, A.S. Simakov, JTP, 39, 1463. 1969.

solution can be obtained by straight forward methods, namely by calculations which give the dependence of given field characteristics on the unknown values and consequent setting up and solving of the linear algebraic system of equations. The length of the calculation depends on the closeness of the "first guess" to the correct solution. However, numerical tests have shown, that the unknown should be obtained by completing one iteration of the cycle and then by making certain relaxations based on the results obtained.

Equation 2.12 was given in the form

$$j_{PL} = j_o \left[\beta \frac{r}{R} + (1-\beta)\frac{R}{r}\right]\left[1 - \left(\frac{\psi_{max} - \psi}{\psi_{max} - \psi_{r_{PL}}}\right)^2\right] \qquad (2.15)$$

where jo is a coefficient obtained for Eq. 2.13 after 2.15 was substituted in it, β is the ratio of plasma pressure to the pressure of the field on the edge due to the plasma current and ψ_{max} is the largest value of ψ inside the plasma. Besides 2.15 we also used the relationship

$$j_{PL}(r, z) = j_o \left[1 - \left(\frac{r-R}{a}\right)^2 - \frac{z^2}{a^2}\right] \qquad (2.16)$$

which is in agreement with 2.15 for $\beta = 0$. Along with the values of current and a complete flux plot (see Fig. II.11, where the flux plot is shown for t = 20 sec and for $\beta = 1$), the solution makes it possible to establish the Φ_i fluxes coupled to the various coils. By selecting short time intervals one can calculate, as accurately as he wishes, the total flux contour in each coil $d\Phi_i/dt$, for the whole plasma current pulse.

Figure II.13

Current (a) and Voltage (b) in the VF Coil

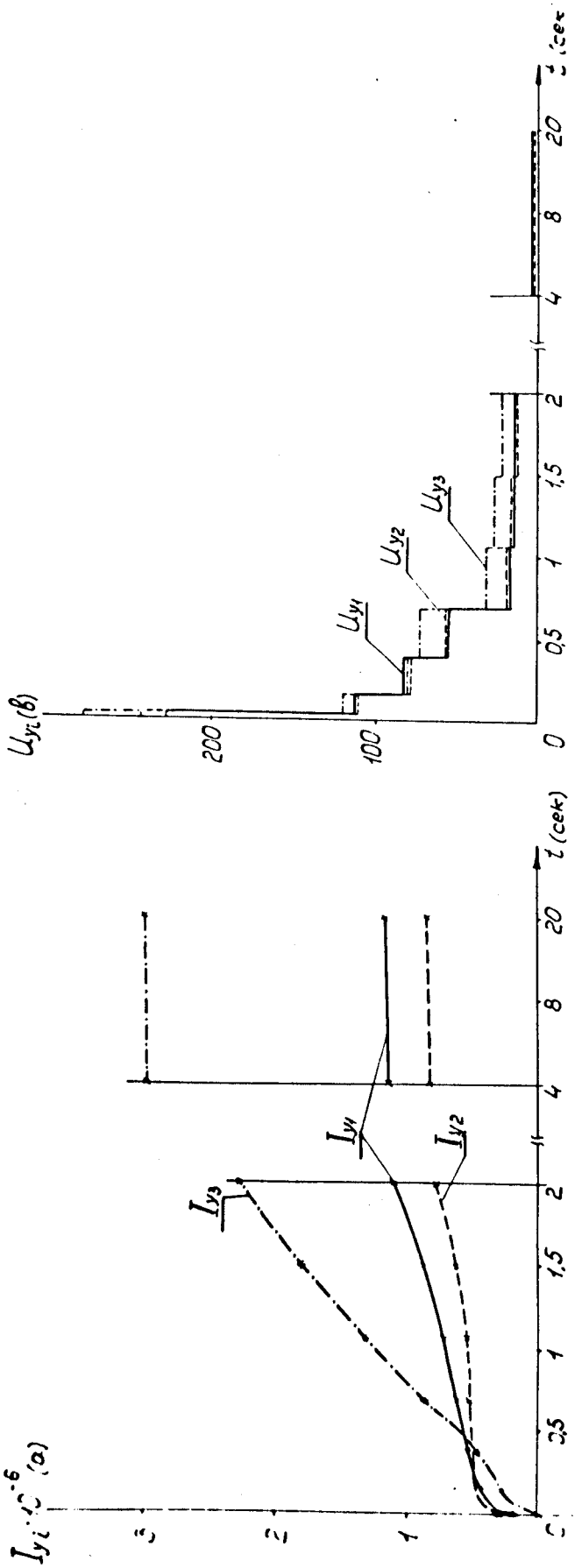

Рис.П.I3. Токи (а) и напряжения (б) в обмотке управления

On Figs. II.12 and II.13 are given the results of calculations for a toroidal model with a varying minor plasma radius a (t). Fixed values of a were taken within the range (0.5 - 2m) at 0.25 m intervals. Conditions of equilibrium were taken as the requirement for the passage of a flux line through four points: $r, z = (R \pm a; 0)$ and $(R; \pm a)$. The allowable deviation of the flux line from these points did not exceed $\delta = .02a$. The largest deviation of Φ_{pl} from the given value was less than 0.5%.

Calculations indicate, that the iron core variety displays values of current and power that are lower by a factor of two, in all the coils.

It is proposed that a similar calculation be performed in the near future for the case of a short iron central column without an iron return yoke, a scheme which has definite constructional advantages. Comparison of all three systems will allow us to make a final selection.

3. Power Supply

The power supply system will feed the following elements of the magnet system:

1 - Toroidal field coils

2 - Ohmic heating coils

3 - Vertical field coils

The external VF coils can be essentially lumped into one coil with equivalent parameters. The power supply for the inner automatic compensating coils which are used to provide plasma equilibrium by using feedback to control its position, will be investigated in the appropriate section of this report.

The coils of the magnet system can be described by the following parameters:

	Self-Inductance (H)	Resistance (Ohm)	Max. Current (A)	Max. Power MW
TF Coil	0.85	0.0555	120,000	1200
OH Coil	3.1×10^{-2}	7.5×10^{-3}	±120,000	3450
VF Coil	7×10^{-2}	6.3×10^{-3}	120,000	3100

The power supply for the TF coils must generate pulses which are trapezoidal in shape, come every five minutes, have a rise and decay time of 13 sec, and a flat top of 20 sec.

During the shakedown period, the TF coil pulses have a repetition rate of one every 20 sec at the full current of 120,000 A.

In the OH coil power supply, the current undergoes a total reversal in order to lower the power needed and the electrodynamic forces on the coils. Curves of the currents and the voltages in the OH coils, VF coils and the plasma during operation are shown in Fig. II.14 - II.16.

As can be seen from the table above, the total pulsed power needed for the magnet system reaches 7700 MW. It is proposed that these pulses be generated with the aid of power tube controlled transformers. The power to the transformers could come directly from the grid or be supplied by ganged electric generators with flywheels.

Direct supply from the power grid involves the need for powerful step-down substations as well as a filtering network to

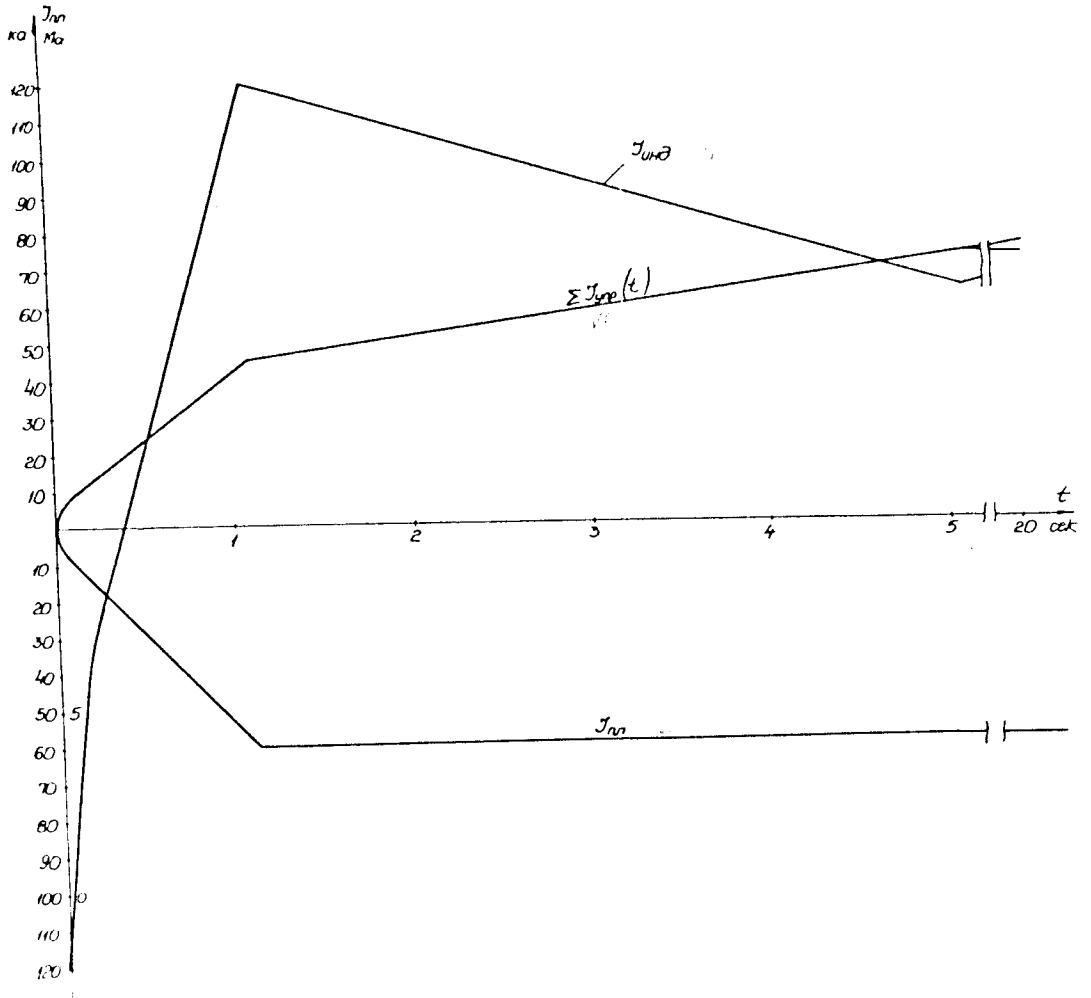

Рис.П.I4. Кривые изменения токов плазмы, индуктора и управляющей обмотки

Figure II.14 Currents in plasma, OH and VF windings

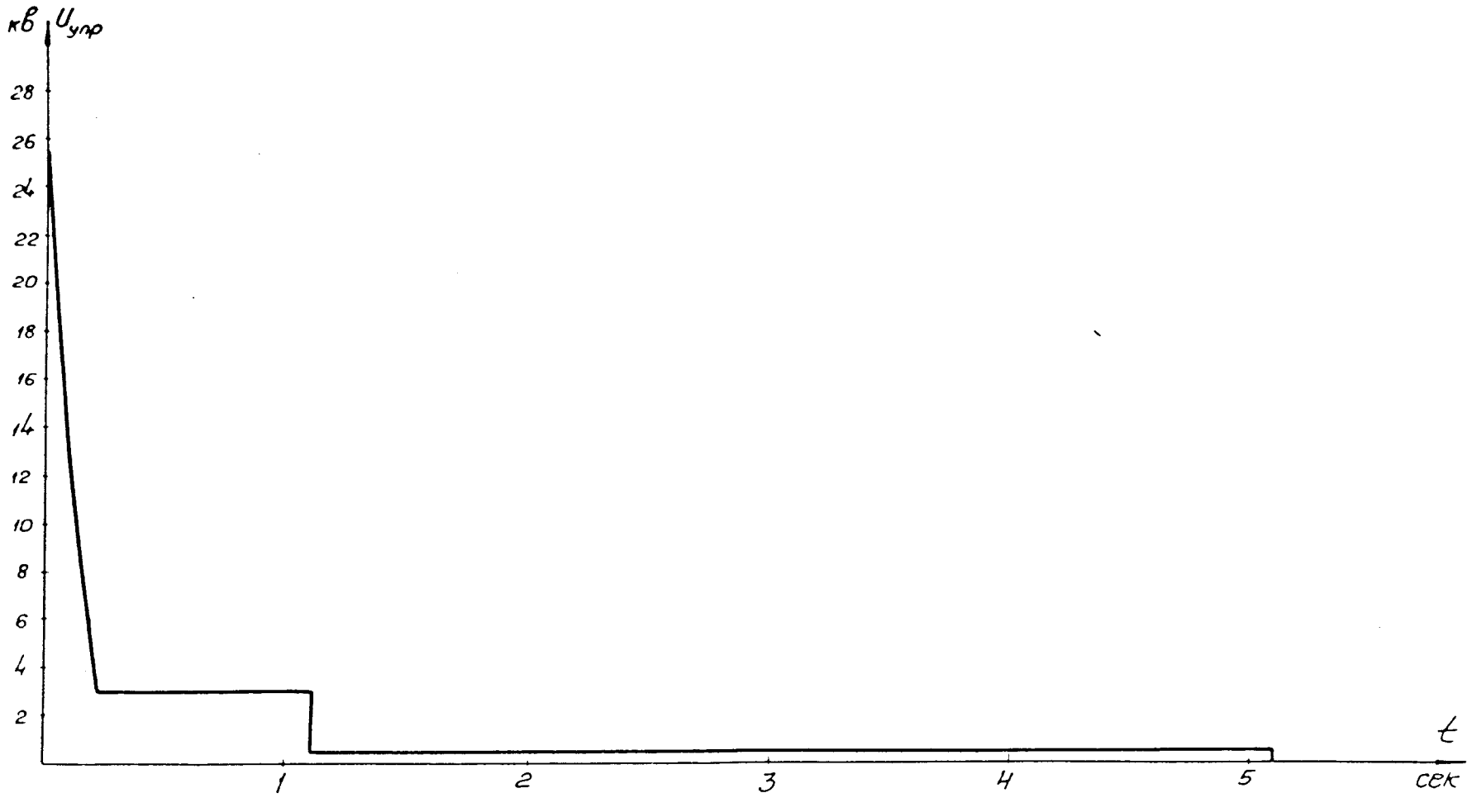

Рис.П.I5. Напряжение управляющей обмотки
Figure II.15 Voltage in the VF Coil

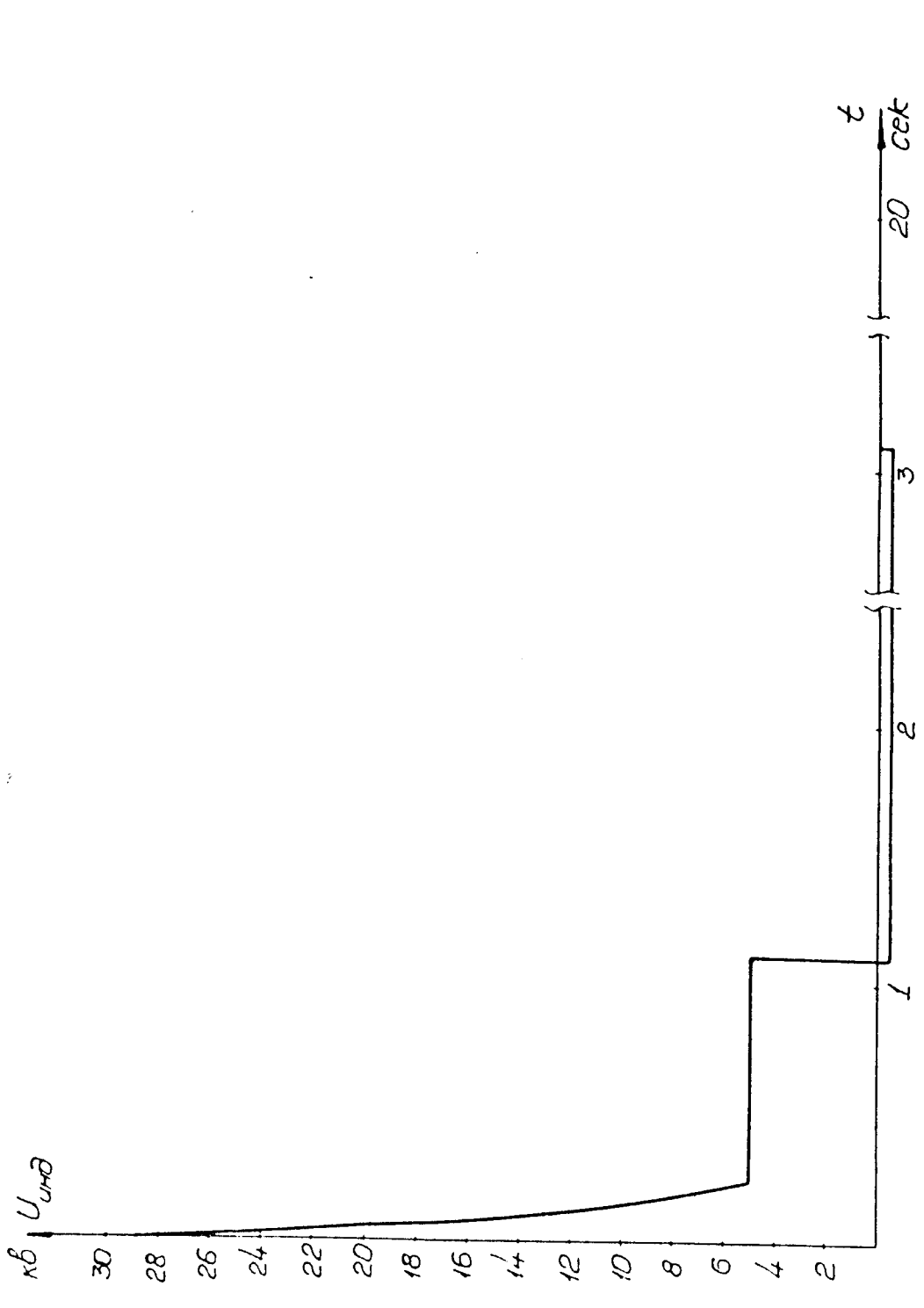

Рис.П.16. Напряжение индуктора
Figure II.16 Voltage in the OH Coil

compensate the reactive power and its harmonics arising from the operation of the pulsed power transformers.

Using gauged electric generators means building special control systems for regulating, filtering and energizing the elements, however, this scheme will substantially reduce the pulsed power drain on the grid.

The choice of the proper power supply scheme will be based on a careful economic analysis of both versions. This will be done during the second stage of the design, after a site has been selected and available power evaluated.

In view of the large power pulses needed for the device, there was a tendency to design complex systems to generate the pulses for the different coils, involving multiple uses of pulse generators.

On Fig. II.17 is shown a simplified method of power supply for the TF coils, the OH coils and the vertical field coils VF1, VF2 and VF3.

Because of the large time constant of the TF coil (15 sec) and the need to limit the rise time of the current to 15-20 sec we intend to use ramping of the coil during the rise time with the power requirement from the pulsed transformer amounting to 1200 MW. To lower the voltage in the coil relative to the machine and to alleviate the possibility of breakdown, it is reasonable to subdivide the coil and connect the pulsed power transformers to the various sections at different points along the circumference. In order to avoid voltage surges during a fault condition, a scheme was selected utilizing two sections of the coil and two pulsed power transformers.

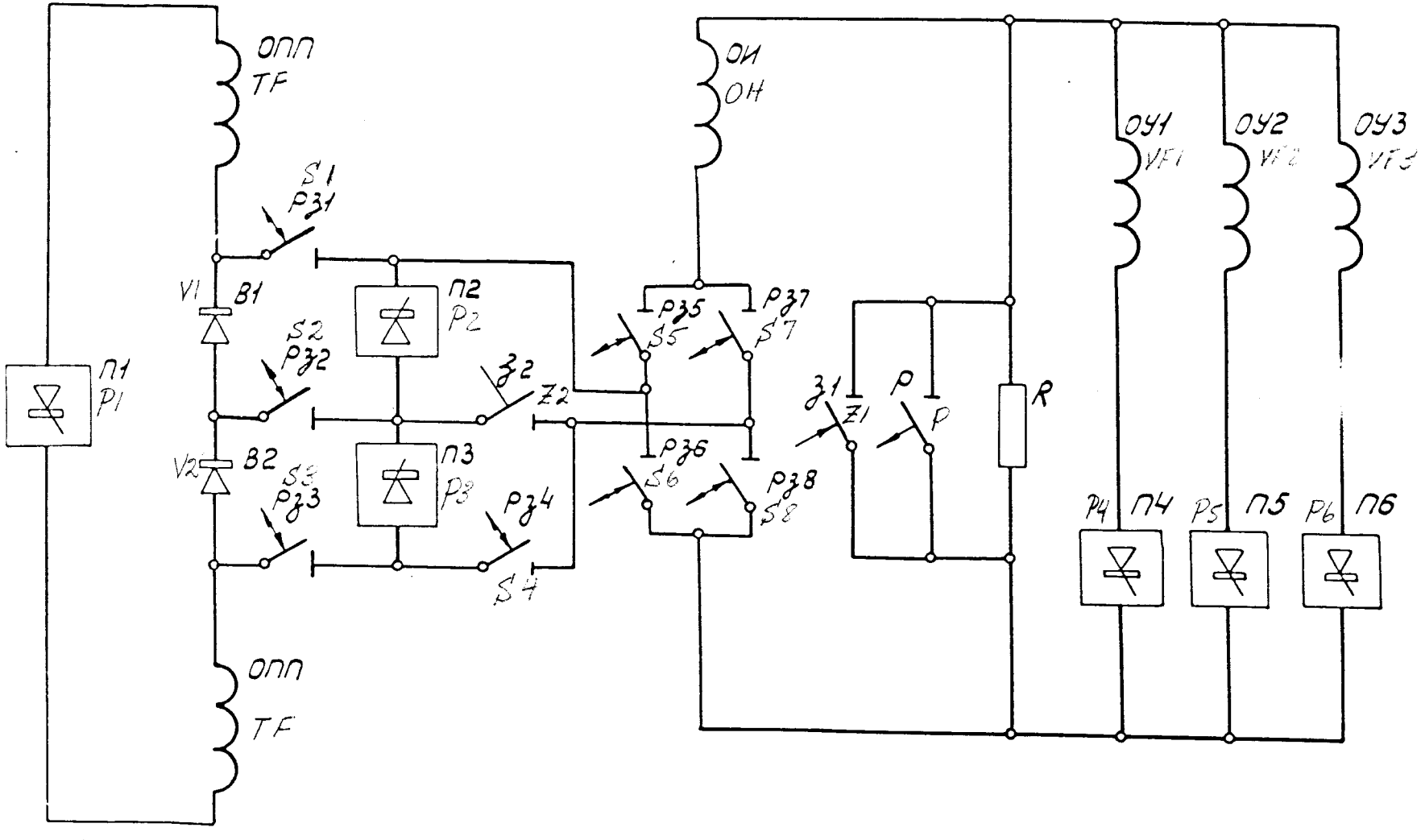

Рис.П.17. Принципиальная схема питания обмоток установки Т-20

Figure II.17 Power supply schematic for the coils of T-20

At the start of a power pulse cycle, switches S1 and S2 are closed. This produces two current loops in the TF coil and the pulsed power transformers P1, P2 and P3. When these transformers receive the signal to start the pulse, a current begins to build up in the TF coil. The power output of P1 is 600 MW at 5 KV, while P2 and P3 supply 300 MW at 2.5 KV each. When the current in the TF coil reaches 120,000 A (17 sec after start of the pulse), it is then necessary to maintain it constant at that level and to start the pulse for the OH coil.

A negative current build-up in the OH winding in one sec is accomplished by switching a 600 MW power transformer into the OH winding circuit. This is done with P2 and P3. These power transformers are switched out of the TF coil circuit by reversing their voltage (at which time the current in the TF coil is shunted through tubes V1 and V2) and by opening the de-energized switches S1 and S3. By closing switches S5, S8 and S4, power transformers P2 and P3 enter the OH winding circuit (switch P is closed and switch Z1 is open at this time). After the signal for putting P2 and P3 back in the mode is received, the current in the OH coil builds up negatively until it reaches -120,000 A in one sec. In order to insure the rapid current rise in the plasma, switch P is closed and the voltages in power transformers P2 and P3 are reversed. This negative voltage along with the drop in the potential across the resistance, maintains the voltage on the OH coil at 28 KV. The potential across the resistance R, along with the potential from power transformers P4, P5 and P6, also appears across the VF coils. The voltage from P4, P5 and P6 is 2.5 KV.

From the moment switch P is closed, the current in the OH coil drops, while the currents in the plasma and the VF coils rises. The correct current shape in the OH and VF coils is obtained by the proper selection of the number of windings in these coils and by the proper use of the power transformers P2 - P6. The correct action of the power transformers is maintained by a programmed controller, while the fine tuning of the conditions of plasma equilibrium is accomplished with the automatic compensating coils using feedback from the plasma toroid. The maximum voltage on power transformers P4, P5 and P6 must be 3 KV at the current level of 120 KA. For the given current and voltage requirements of these transformers it is reasonable to use two steps to perform the needed function, which would lower the power requirement for the transformers feeding the coils to 220 MW. After 0.12 sec had elapsed since the start of the plasma current, switch Z1 is closed and the supply of the OH and VF coils becomes independent of the transformers in question. When the current in the OH winding drops to zero, switches S5 and S6 are opened while S6 and S7 are closed after which the power transformers P2 and P3 are put back in the forward mode, and the current in the OH coil starts to rise in the positive direction to +120,000A in 1.1 sec. When the OH current reaches 120,000 A, the power supply from its power transformer can be reduced to 100 MW.

During the time when the P1 and P3 transformers were in the OH coil circuit, the current in the TF coil which was supplied only by the P1 transformer drops to 3% of its nominal value, namely 3500A. To prevent further erosion of the current in the TF coil, transformer P3 is reinserted in the circuit while P2 stays on the OH winding. To accomplish this, the voltage in P3 transformer is

reversed and simultaneously, switch Z2 is closed. Transformer P3 and switch S4 become de-energized. Switch S4 is opened, switches S2 and S3 are closed and P3 is activated in the forward mode. The current from tube V2 is shunted into P3 and thereafter the current in the TF coil is maintained constant with P1 and P3. To insure that the current decays in the TF coil at the end of the pulse, the voltage in P1 is reversed and the current falls off in 20 sec. Decay of the current in the VF coils is insured by reversing transformers P4, P5 and P6.

The described system will use thyristor controlled transformers as the sources of pulsed power.

The shunting apparatus used in the system consists of four types:

1 - Switches S1 - S8 which can accomplish current transfer in a de-energized state

2 - Switch Z2 which can be used in the energized state up to 2.5 KV

3 - Switch Z1 designed for 25 KV

4 - A switch with a power capacity of 3000 MVA

This apparatus is not available commercially and thus will have to be developed. It seems that the development of one switch to serve all the functions of the circuit would be adequate. This switch should be rated at a current of 35000 A, and should have opening and closing times of several milliseconds. For speeding up such switches, the distance between poles in the open position should be small. This can be accomplished by making the pole environment a pressurized gas. If elegas is used at 5-10 torr, the

the contacts can withhold the necessary voltage at a separation of 3 - 5mm. Actuation can either be electrodynamic or pneumatic.

One of the problems in developing such a switch is the need for fast separation of the contacts without sparking and also the need for continuous pressure on the contacts in the closed mode.

Switch Z1 is intended to operate at 5 KV, and should withstand a total of 25 KV in the open mode as well as pass 120,000 A in 20 sec.

Switch Z2 is intended to operate at 2.5 KV passing a maximum current of 102,000 A in 20 sec.

To make this switch faster and to decrease the erosion of the contacts, it is reasonable to employ a two step switching operation using an ignitron as the first step and a modified version of the S switch as the second.

A more complex apparatus is switch P, which is designated to operate across 3000 MW at a voltage of 25 KV and 120,000 A. In the closed condition, the switch should pass current at a rate of 70 KA/sec. One of the possible directions for developing such a switch is the following:

1. Achieving an essentially arcless opening by creating a "current pause" at the exact moment of the opening of the contacts, for a period of time during which the contacts separate enough to prevent arcing. To decrease the needed separation of the contacts, they could be contained in a pressurized gas chamber. The current pause could be created with a bank of discharge capacitors. The energy of the capacitors is

$$W_c = \frac{P \cdot}{4}$$

where P is the power at the switch, τ is the length of the current pause. For example if τ = 0.5 -1.1 x 10^{-3} sec, W = 400 -800 KJ. Actuation of the switch can either be electrodynamic or pneumatic.

2. Performing the switching with an arc at the opening of the contacts in pressurized gas, and the arc being extinguished by creating an opposite current with the aid of a bank of capacitors. In this scheme, contact erosion will be greater than in the above case, but the bank of capacitors can be substantially smaller.

It may also seem reasonable to develop a two step switch, where the current first passes through massive contacts, but is shunted temporarily into smaller fast acting switches at the moment the massive contacts are opened.

III. Vacuum System and the Tritium Cycle

1. Construction and Main Features

The vacuum system in T-20 consists of a group of different subsystems and elements (see Fig. III.1) which insure the needed physical conditions for creating the plasma toroid with the required parameters and the design of a closed cycle for the tritium. The system consists of:

A discharge vacuum chamber.

An intermediate vacuum chamber.

Independent pumping systems for the discharge and the intermediate vacuum chambers.

A means for injecting fuel (H_2, D_2, equal quantities of D and T) and inert gas for cooling the plasma at the end of a pulse.

A tritium cycle (separation of reaction products and the injected gasses, separation and clean-up of the tritium, clean-up and disposal of the remaining products).

A vacuum system for the neutral beam injectors.[1]

A differential pumping system for the waveguides for RF preionization and heating of the plasma.

Control systems for the vacuum parameters.

A system for evacuating blanket modules.

An automatic operation control system.

The vacuum system is characterized by the following main parameters:

Background pressure in the discharge chamber	2×10^{-8} torr
The total effective pumping speed of the high vacuum pumps for the discharge chamber (for D_2)	10^5 l/sec
The total pumping speed of the different constituents of the high-vacuum system for the discharge chamber (for D_2)	
(a) Compressive	2×10^5 l/sec
(b) Active surface	2×10^5 l/sec
Chamber volume	4.3×10^8 cm^3
Chamber surface area	4.1×10^6 cm^2
Pressure of inert gas immediately after injection for cooling the plasma at the end of a pulse	8×10^{-3} torr
Partial pressure of the tritium	1.9×10^{-3} torr
Upper limit of the pressure in the discharge chamber between pulses	5×10^{-8} torr
Pumping time of the discharge chamber to the indicated pressure range	100 sec
Surface area of the chamber devoted to vacuum ports, including neutral beam ports	2.2%

[1]The description of the vacuum system for the neutral beam injectors is contained in the section entitled "Supplementary Plasma Heating Methods".

Chamber temperature during operation	500 C
Upper limit on the pressure in the intermediate chamber	1×10^{-7} torr
The total effective pumping speed of the high vacuum pumps for the intermediate chamber	5×10^{3} l/sec
Total pumping speed of the cryopanels in the neutral beam injector ports (for D_2)	4.4×10^{7} l/sec
Total surface area of the cryopanels	560 m^2
Liquid helium boil-off	360 l/hr.
Total power needed for vacuum pumping	1 MW

A trace showing the pressure in the chamber as a function of time is shown in Fig. III.2.

2. Vacuum Chamber

The construction of the vacuum chamber should comply with a series of vacuum technology, electrophysical and experimental requirements, many of which are mutually contradictory. Besides the obvious needs for mechanical strength and leak tightness under the electromechanical forces, atmospheric pressure and thermal cycling, the chamber must be radiation safe during operation and shake down periods under DT conditions (tritium and a large neutron flux), and must withstand distributed and localized heat loads up to 50 MW.

In order to avoid shorting out of the plasma, the electrical resistance of the chamber along the toroidal circumference must be not less than $2\text{-}3 \times 10^{-3}$ ohms. The need for reducing the flow of impurities from the wall under the action of electromagnetic and corpuscular radiation from the plasma requires that the chamber surface area be minimized and the conditions governing the contact

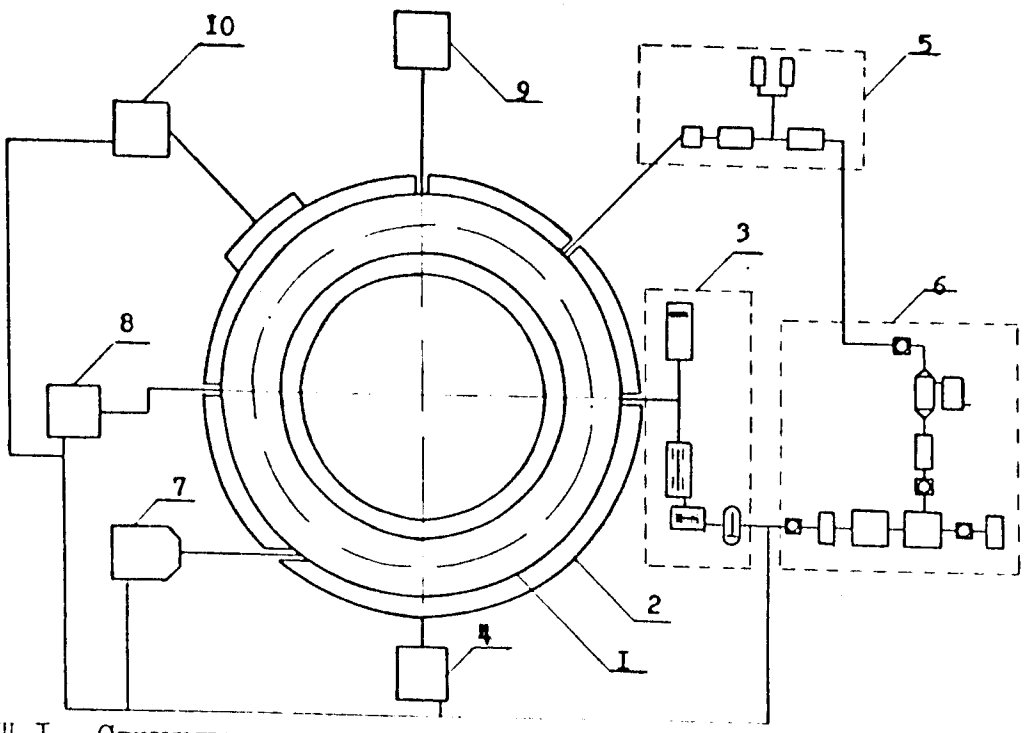

Рис.Ш.I. Структурная схема вакуумной системы установки Т-20:
I - разрядная камера; 2 - промежуточная камера; 3 - система откачки разрядной камеры; 4 - система откачки промежуточной камеры; 5 - система напуска газа; 6 - тритиевый контур; 7 - вакуумная система инжекторов; 8 - система дифференциальной откачки волноводов ВЧ-устройств нагрева плазмы; 9 - система контроля вакуумных параметров; I0 - система вакуумирования модулей бланкета

Figure III.1 Schematic of vacuum system for T-20
1 - discharge chamber, 2 - intermediate chamber, 3 - vacuum pumps for discharge chamber, 4-vacuum pumps for intermediate chamber, 5-gas injection, 6-tritium cycle, 7-injector vacuum system, 8-differential pumping for RF system, 9-vacuum control system 10-blanket module vacuum system

between the plasma and the wall be very closely controlled. Finally, the construction of the chamber must provide for penetrations into the operating zone of electric and magnetic fields, neutral beams and RF radiation for supplementary heating of the plasma, pumping ports, measuring and diagnostic probes etc.

To accomplish these requirments, the following principles of construction were adopted:

(a) A double walled arrangement with independent seals and pumps for each of the toroidal chambers, the discharge and the intermediate.

(b) The discharge chamber is made of a thin walled, continuous (no insulating gap) flexible and stable membrane which has forced cooling.

(c) The inside of the discharge chamber wall contains easily removable and relatively massive metal limiters which prevent direct contact of the plasma with the chamber wall.

(d) Maintaining the intermediate chamber wall at a temperature of 50 - 80 ^{0}C, thus virtually eliminating the diffusion of tritium to the outside.

(e) Integrating the intermediate chamber with the radiation shield situated inside the TF magnets.

Following these construction principles, it will be possible to use relatively simple, technologically feasible solutions for the various systems and thus insure the attainment of the above requirements.

Chamber Assembly

The assembly of the chamber is related directly to the assembly of the magnet system. The chamber consists of eight blocks (octants) (See Fig. III.3) each of which contains three sections, each within

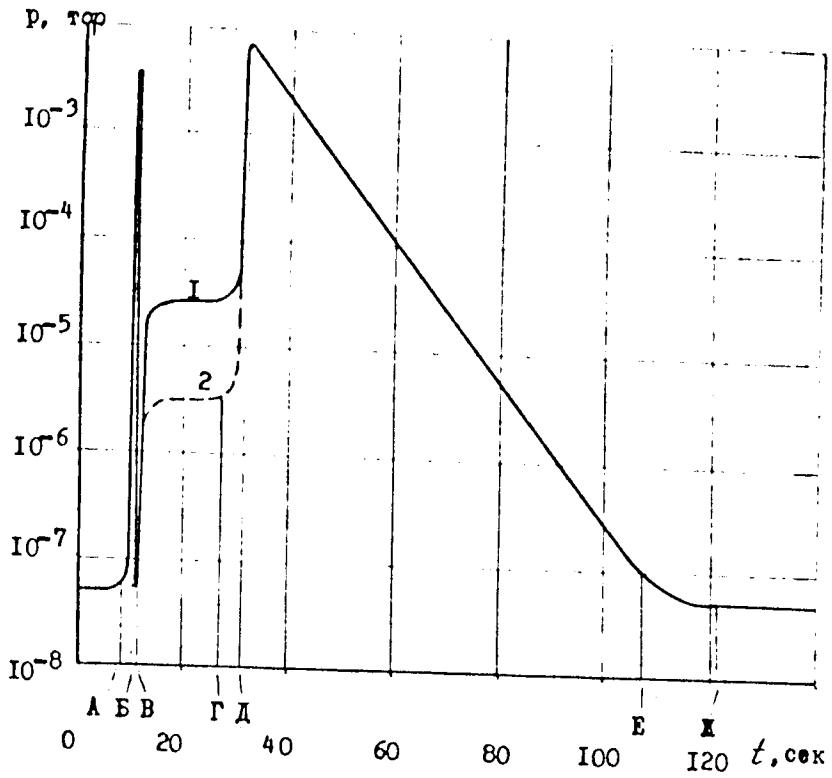

Рис.Ш.2. Циклограмма откачки разрядной камеры:

АБ – напуск рабочей смеси; БВ – предионизация; ВГ – разряд (1 – инжекция быстрых нейтральных атомов, 2 – высокочастотный нагрев); ГД – напуск инертного газа; ДЖ – откачка

Figure II.2 Vacuum trace in discharge chamber

AB Injection of fueld; BC-preionization
CD Ignition (1-neutral beam injection, 2-RF heating)
DE Inert gas injector FF-pumpout

a TF magnet coil. The end sections and the corresponding gaps between blocks are designed for joining the sections to each other.

The following is a list of the various penetrations into the discharge chamber:

- vacuum ports for the discharge chamber
- diagnostic ports
- vacuum ports for the intermediate chamber
- neutral beam ports
- RF waveguides
- inert gas inlets
- diagnostic, vacuum gauge, measuring and controlling apparatus ports

In all, the various ports take up 40% of the available surface area of the discharge chamber.

Discharge Chamber

The thin walled, vacuum tight discharge chamber is electrically insulated from the intermediate chamber wall but is electrically continuous around the circumference of the toroid. One of the investigated designs is shown in Fig. III.4.

The discharge chamber is assembled from sections made in the form of shells of revolution of a negative gaussian curvature (surfaces of revolution with saddle points). The axis of revolution of the shells is coincident with the chamber axis. The shape of the chamber is such as to be capable of sustaining the radial forces on it. Since the wall is in tension, it does not experience the loads which would make it lose stability. The load carrying capability of the shell is due to reinforcing rings attached to it which

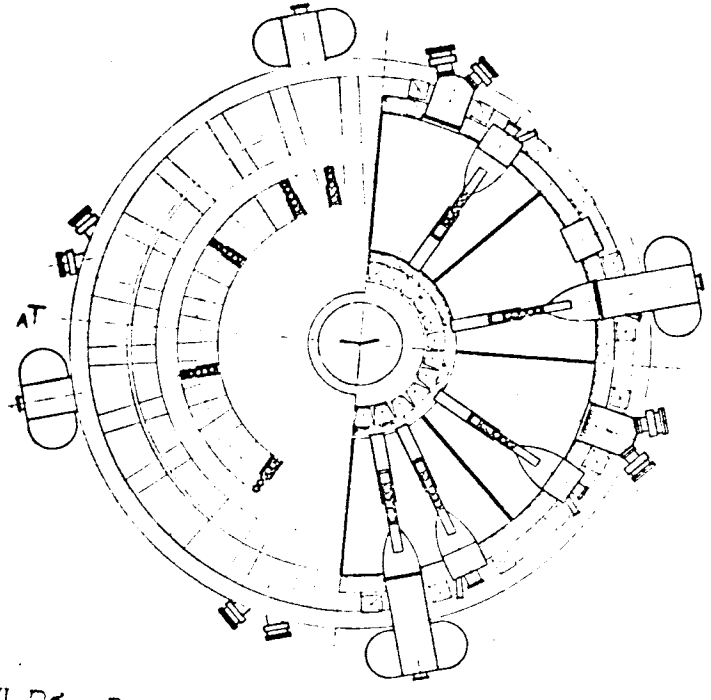

Рис.Ш.3б. Экваториальный разрез установки

Figure III.3b Top view with section removed

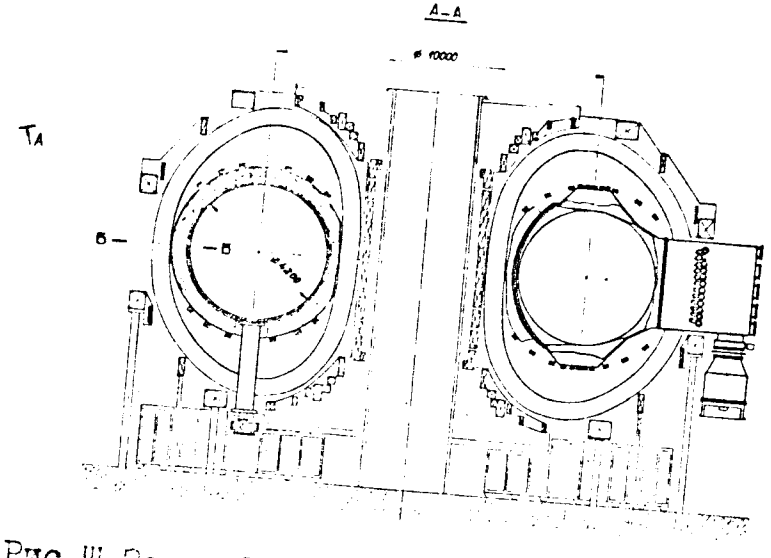

Рис.Ш.3а. Компоновочная схема установки

Figure III.3a Assembly diagram

transfer the loads to the wall of the intermediate chamber. The corrugated portion of the chamber increases its total electrical resistance.

On Fig. III.5 is shown a different version of a wall for the discharge chamber. It represents an attempt to construct a cooled and relatively compact chamber wall which takes advantage of the corrugated shell principle.

The wall is designed such that the relatively thin portion of the corrugations do not actually see the plasma but are shielded by the cooling tubes. In places where the heat load is too high, it is protected with screens. These screens which are fairly massive and have a high thermal inertia, protect the chamber wall from burn-through, and prevent overheating in places of excessive heat load in the event of an uneven plasma energy dump due to a fault condition. At the same time these screens act as limiters, both azymulthal and poloidal. It is proposed that the surfaces of the screens be covered with removable plated sections which would be in direct contact with the plasma. This experiment will aid in selecting proper materials for such functions.

Intermediate Chamber

The intermediate chamber wall is the structural member which will carry the atmospheric loading as well as part of the load on the discharge chamber.

It is made to be an integral part of the radiation shield which gives the following advantages:

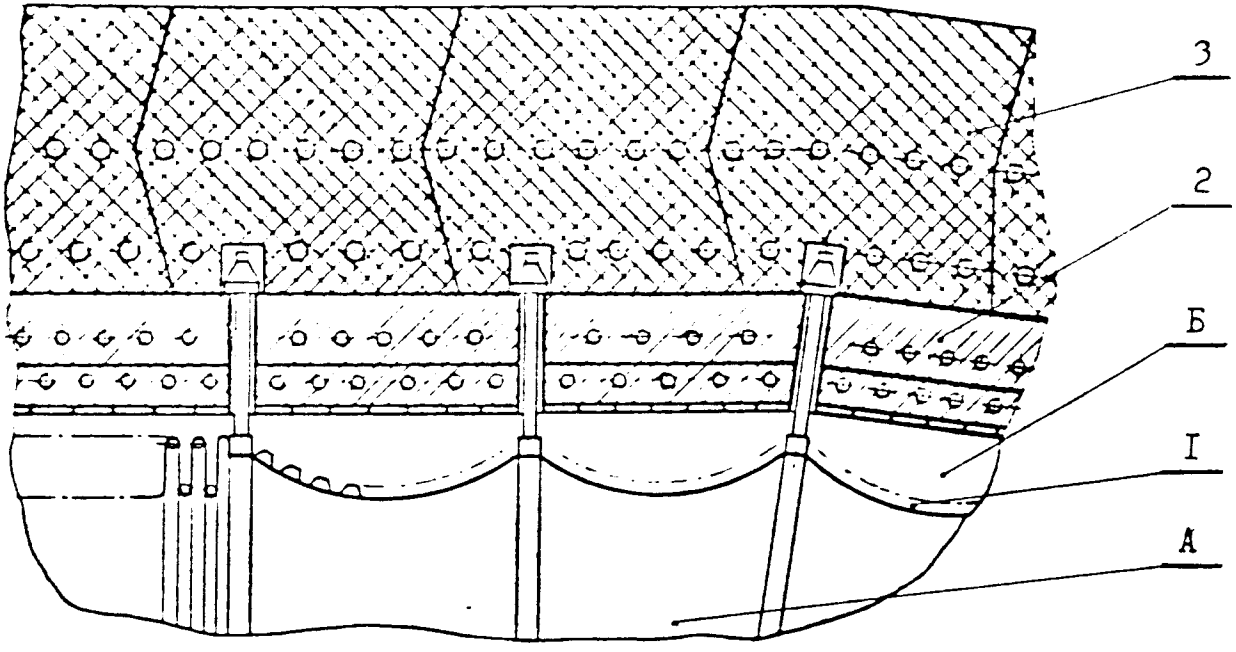

Рис.Ш.4. Элемент вакуумной камеры:

I - разрядная камера; 2 - наружная (промежуточная) камера; 3 - радиационная защита; А - рабочий (высоковакуумный) объем; Б - промежуточный вакуумный объем

Figure III.4 Section of Vacuum Chamber

1 - discharge chamber
2 - intermedi-te chamber
3 - shield, A - high vacuum region B - intermediate vacuum region

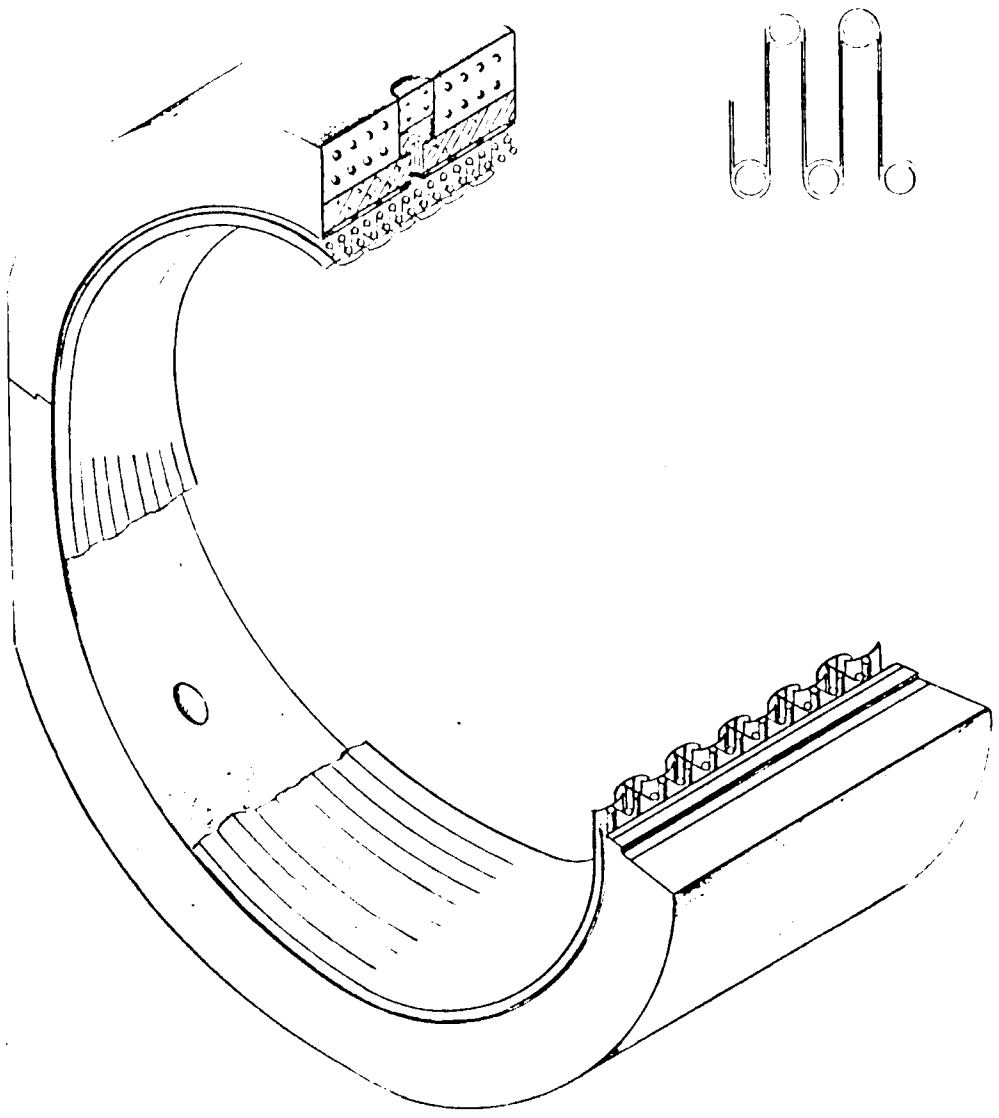

Рис.Ш.5. Секция вакуумной камеры

Figure III.5 Section of vacuum chamber (different design)

- compactness
- making use of the shield material for structure
- making better use of available space within the TF coils
- combine the cooling for the intermediate chamber and the shield.

The intermediate chamber wall is made of a thin walled lattice with each lattice compartment filled with shield material. The chamber comes apart in two halves with the separation on a horizontal plane to provide access to the joints between blocks.

3. Vacuum Pumping System for T-20

Vacuum Pumping of the discharge Chamber

The vacuum system for the discharge chamber must provide for evacuation from atmospheric pressure and maintaining the chamber at 2×10^{-8} torr at the operating temperature of the wall. In order to achieve this low pressure, we anticipate to perform a series of operations to clean and degas the chamber wall. During the construction of the chamber, the components will be electropolished, cleaned ultrasonically and degreased of any lubricants that may have been used during forming of the bellows. Lowering specific outgassing rate from the chamber wall to 10^{-12} - 10^{-13} torr l/cm^2 sec at room temperature and to 10^{-10} torr l/cm^2 sec at the operating temperature, will be accomplished by baking the chamber at $600^{O}C$ preparatory to conducting experiments, and training the chamber wall by means of discharge in inert gasses. To obtain the design pressure in the degassed chamber, an effective pumping speed of 5×10^4 l/sec will be required. For pumping down the chamber between pulses in no more than 100 sec, the needed effective pumping speed is not less than 6×10^4 l/sec.

Table III.1

Main Features of Vaccum System for the Discharge Chamber Using Commercial Pumps and Varying the Number of Pumping Blocks

Number of Blocks	Size of Vacuum Duct mm	Type of Pumps	Effective Pumping Speed l/sec.	Time Needed to Pump from 10^{-3}-10^{-8} torr, (sec)	Cryopanel Area m^2	Liquid He boil-off.
4	d = 1200	Turbo Molecular and Vac-ion.	$(6.1 - 1.9) \times 10^4$	80 - 260	6.0	5.0
	l = 3500	Mercury diffusion and vac-ion Cryosorption.	1.7×10^4	280		
			6×10^4	80		
6	d = 850	Same as above	$(5 - 2.7) \times 10^4$	120 - 180	6.0	5.0
	l = 3500		2.5×10^4	190		
				80		
8	d = 550	Same as above	$(5 - 3.1) \times 10^4$	120 - 160	6.0	5.0
	l = 3000		2.9×10^4	170		
			6.0×10^4	80		

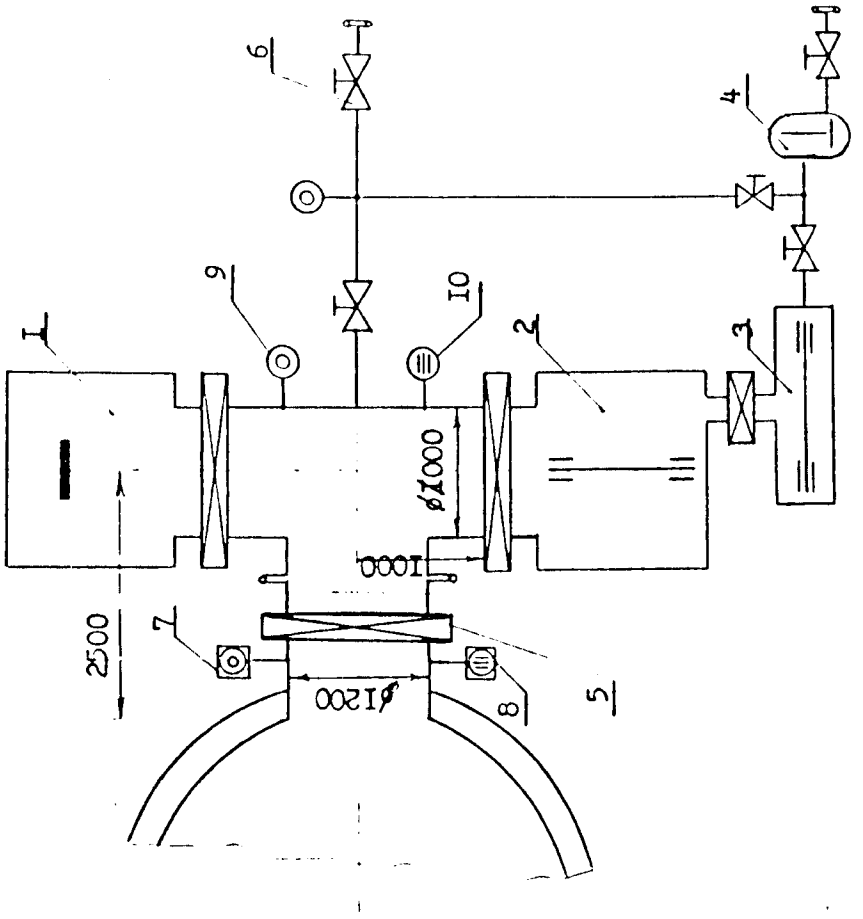

Fig. III.6 Schematic of a pumping block for discharge chamber.

1. vac-ion pump
2,3. Turbo molecular pumps
4. roots blower
5. fast acting gate valve,
6. vacuum valve
7. noise free pressure gauges
8. noise free man-spectrometer
9. commercial pressure gauges
10. commercial man=spectrometer

For evacuation in the range 10^{-3} - 10^{-8} torr under conditions which exclude a large inventory of tritium, it is proposed that turbomolecular or mercury diffusion pumps be used to augment the active surface panels, at the final stage of the pump down cycle when the pressure is lower than 10^{-6} torr (see Table III.1). As a primary evacuating system, we are examining a scheme consisting of four pumping stations distributed equally around the perimeter. These stations will have turbomolecular and vac-ion pumps with a pumping speed of 2×10^4 l/sec for N_2 each (see Fig. III.6). Backing up the high vacuum turbomolecular pumps will be other turbomolecular pumps with a pumping speed of 5×10^3 l/sec. These will provide an oil free fore-vacuum which is needed in this pressure range. The pumped out gasses are then collected into a reservoir.

The pumpout lines will have gate valves which close in the order of one sec and seal hermetically in 10 sec. Turbomolecular pumps are used to evacuate the discharge chamber from 10^{-3} - 10^{-6} torr (see Fig. III.2 from point E to point F), and for lower pressures, the turbomolecular pumps are augmented with titanium vac-ion pumps (see Fig. III.2 F - G). The inventory of titanium in the vac-ion pumps is adequate to last the lifetime of the machine (10^5 pulses). Each pump will have lost about 0.2 gm of titanium during this period.

In order to gain experience for future Tokamak fusion reactors, it is proposed that an experimental pumping station be used on T-20 based on the principle of cryosorbtion on layers of condensed gasses. This experimental station will be used to study and determine cryosorbtion pumping of D_2 , T_2 and He, for determining the structural properties of the cryosorbants and the optimum temperature time

relationships for regenerating the pumps. The relative arrangement of the cryopanels at different temperatures must insure a maximum rate of sorbtion and aid in the subsequent separation of the gas mixtures.

An inert gas is admitted into the discharge chamber at the end of a burn cycle to reduce the possibility of localized overheating of the chamber wall.

Evacuation System for the Intermediate Chamber

The aim of the intermediate vacuum is to thermally isolate the discharge chamber and thus avoid the diffusion of tritium through the cold wall of the intermediate chamber. The pumping load is determined by the out gassing of the hot discharge chamber wall and the amount of gas diffusing through it. The out gassing rate of a degassed stainless steel is 10^{-10} torr l/cm^2 sec; the cooled wall of the intermediate chamber produces a negligible amount of out-gassing. The diffusion of gasses through the wall consisting mainly of D_2 and T_2 reaches a maximum during the pumping period between pulses. The total pumping speed for the intermediate chamber is 5×10^3 l/sec; the pressure rise during a pulse is from 1×10^{-6} torr to 1×10^{-4} torr (Fig. III.4). The amount of T_2 pumped during one pulse does not exceed 6.6×10^{-4} gm.

Differential Pumping System for RF Wave Guides.

The differential pumping system is needed for obtaining the required discharge in the RF generators which communicate with the discharge chamber through a system of wave guides. The need for having a common vacuum system for the chamber and the wave guides

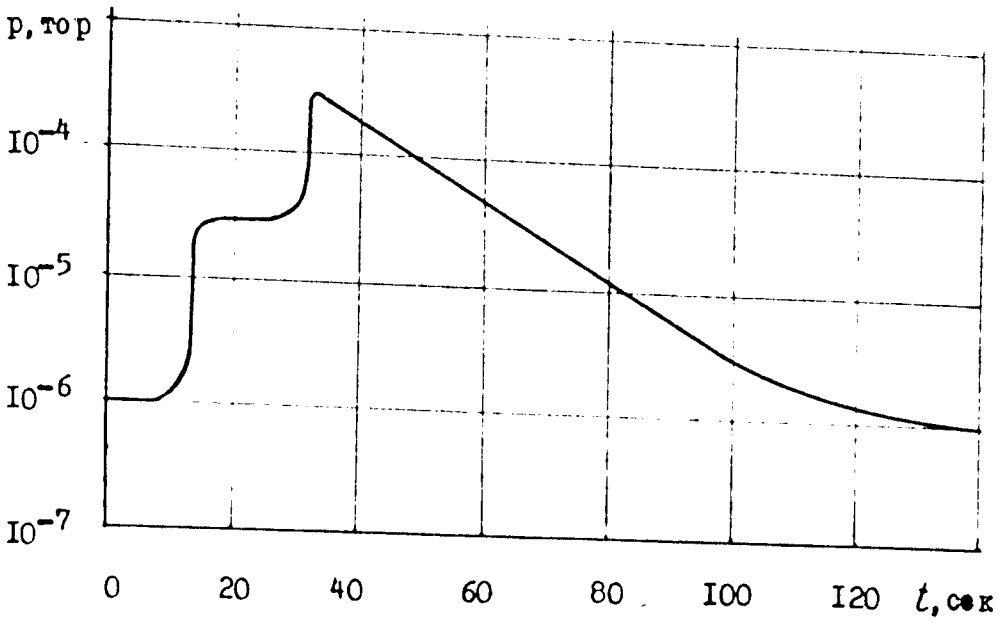

Рис.Ш.7. Циклограмма откачки наружной камеры

Fig. III.7. Pumpout curve for intermediate chamber.

comes from the fact that there are no RF windows which are vacuum tight. Each eight wave guides are served by one vac-ion pump at a speed of 10^3 l/sec. This system will maintain a pressure of 10^{-6} torr in the vicinity of the RF injector during a burn cycle. The amount of tritium collected in each pump after 10^5 pulses is ~ 12 gms.

4. Gas Injection and Control of Vacuum Parameters

The system of gas injection is intended for final clean up, measurement and injection into the discharge chamber of working gasses (D_2, T_2, H_2, He and A), either individually or as mixtures. The number of particles injected into the chamber during a pulse can vary from 10^{18} - 10^{24}, depending on the experiment. This system of gas injection is made up of standardized units controlled by an electronic computer.

The injection system (see Fig. III.8) consists of several symmetrically arranged and interconnected units for purifying and preparing fuel mixtures (UPPF) and injection units (IU). The number of operating units is determined by the pressure uniformity of the gas being injected into the chamber (see Fig. III.9).

A (UPPF) block (see Fig. III.10) consists of a monopolar mass-spectrometer, a vacuum gauge, automatic pressure regulators, a 100 l/sec turbomolecular pump, a heated fitting for passing and controlling gasses for injecting recycled DT mixtures from the tritium cycle.

The injection units are made up of a heated valve which insures the passage of a programmed amount of gas, a vacuum fitting, accumulators for injecting inert gasses into the chamber and vacuum gauges for automatic monitoring and controlling the proper pressure in the system.

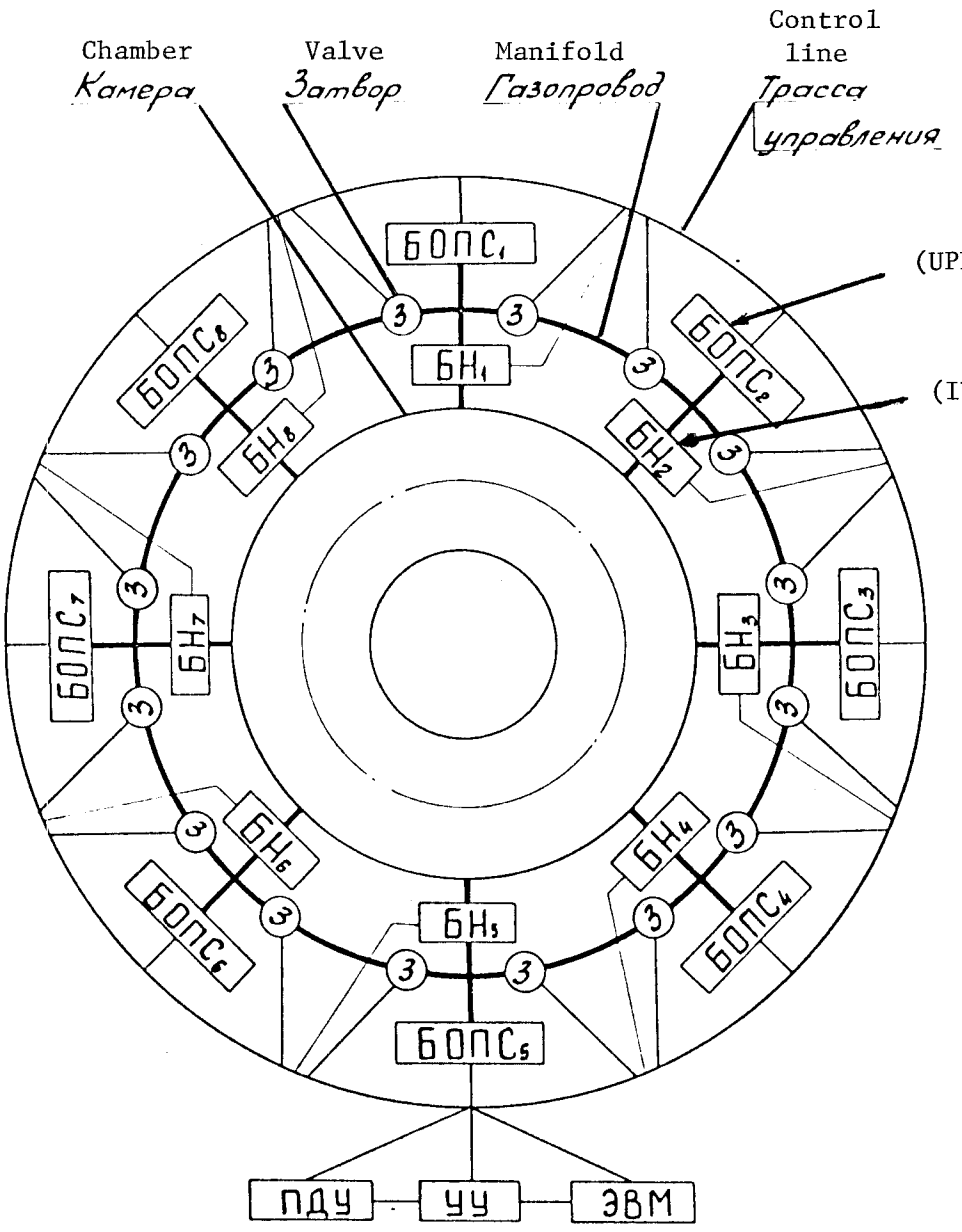

Рис.Ш.8. Блок-схема системы напуска газа

Fig. III.8 Block diagram of gas injection system.

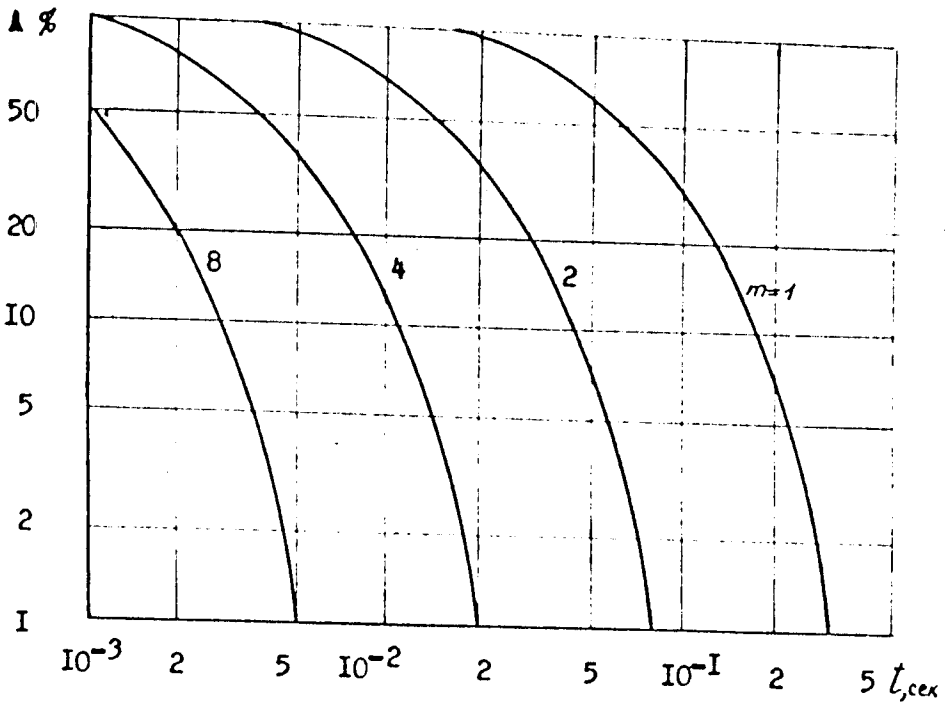

Рис.Ш.9. Кинетическая зависимость относительной неоднородности концентрации газа при напуске через m блоков

Fig. III.9 Non-uniformity of gas concentration due to kinetic effects as a function of the number of block.

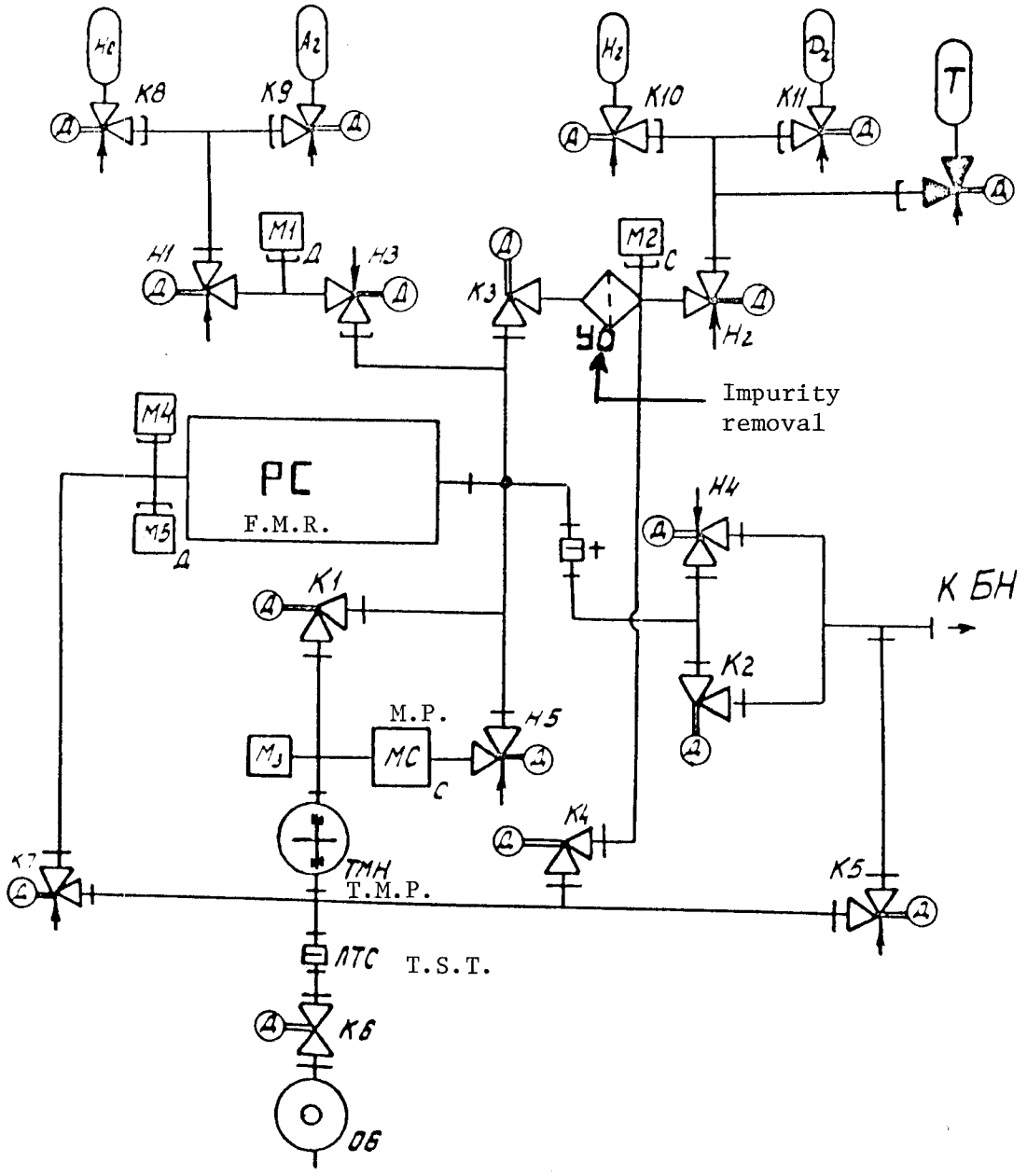

Fig. III.10. The main vacuum system (UPPF)
K_{1-11} heated control valves,

H_{1-5} control accumulation

M_{1-5} pressure gauges and converters

I.R. - Impurity removal system. F.M.R. - fuel mixture reservoir. T.S.T. - thermosorption trap. T.M.P. - turbomolecular pump. M.P. - mechanical pump.

For automatic control of the amount of gas injected, redundant regulators, duplicating the control, will be used.

For measuring the neutral gas pressure in the chamber during a burn cycle, a pulsed noise free ionization guage will be used, which will make pressure measurements of the neutral gas in the vicinity of the plasma in the range 5×10^{-3} torr - 1×10^{-9} torr. Controlling the background gasses during a burn cycle will be done by a mass-spectrometer capable of operating in a radiation environment.

The pressure and partial pressure of the background gasses in the range $1 - 10^{-8}$ torr in the discharge and intermediate chamber, in the pumps, vacuum lines and other elements of the vacuum system will be done with commercial vacuum gauges and mass-spectrometers with analog outputs.

The plan for measuring and leak checking of the vacuum chamber is the following:

1) Step by step control of leak tightness during construction of the joints and other details. The more critical joints, we intend to test with a stream of helium gas and repeated thermal cycling.
2) Mass-spectrometer leak checking at the time of assembly.
3) Periodic checks of the leak tightness by inserting a gas which is not normally present during experiments, such as neon, which would be picked up by the uniformly spaced external mass-spectrometers, thus insuring the location of leaks.

5. Tritium Cycle and Evaluation of Tritium Diffusion

Principle features of the tritium cycle

The function of the tritium cycle is to purify the effluents from the discharge chamber, consisting of DT mixtures and other

gasses, and to prepare new mixtures for subsequent use. The sequence of operations and the placement of elements is shown on Fig. III.11.

Gas consisting of 45% D and T, and 45% Ar, He, H , H_2O, CH_4, CO_2 and others is pumped through four vacuum lines into a common 100 l tank (3) by four oil free mechanical pumps.

Gas Purification

From tank (3) the gaseous mixture goes through a chemical purification of its contaminants. Purification will be done with either molten alkaly metals, cupric oxide or hard metals (Ti, Mn, etc). For purifying the DT mixture by hard metalic sorbents, the amount of metal used is 3-4 Kg for 100 l of contaminants.

For cleaning up H_2 mixtures of contaminants, $\approx$ 160 kg of sorbent material will be used at 2-5 gm/cm^3 over the duration of 10^5 pulses.

The sorbent material contained in two series connected banks (4) will be used at 750° - 900° C.

The purified mixture containing hydrogen isotopes, helium and argon is collected in vessel (6) and then goes to a thermal diffusion process where H_2 , He and Ar are removed (8).

If the H_2 content is low, then the gaseous mixture after undergoing chemical purification goes through columns where the D_2 and T_2 is absorbed and the He and Ar passes through. The absorbing material can either be porous titanium or powdered uranium, and the amount is 150 - 300 gm needed to absorb $\approx$ 40 l of DT mixture ($\sim$100 pulses). Like the chemical columns, the absorbing material is contained in two series connected banks. Absorption of the DT

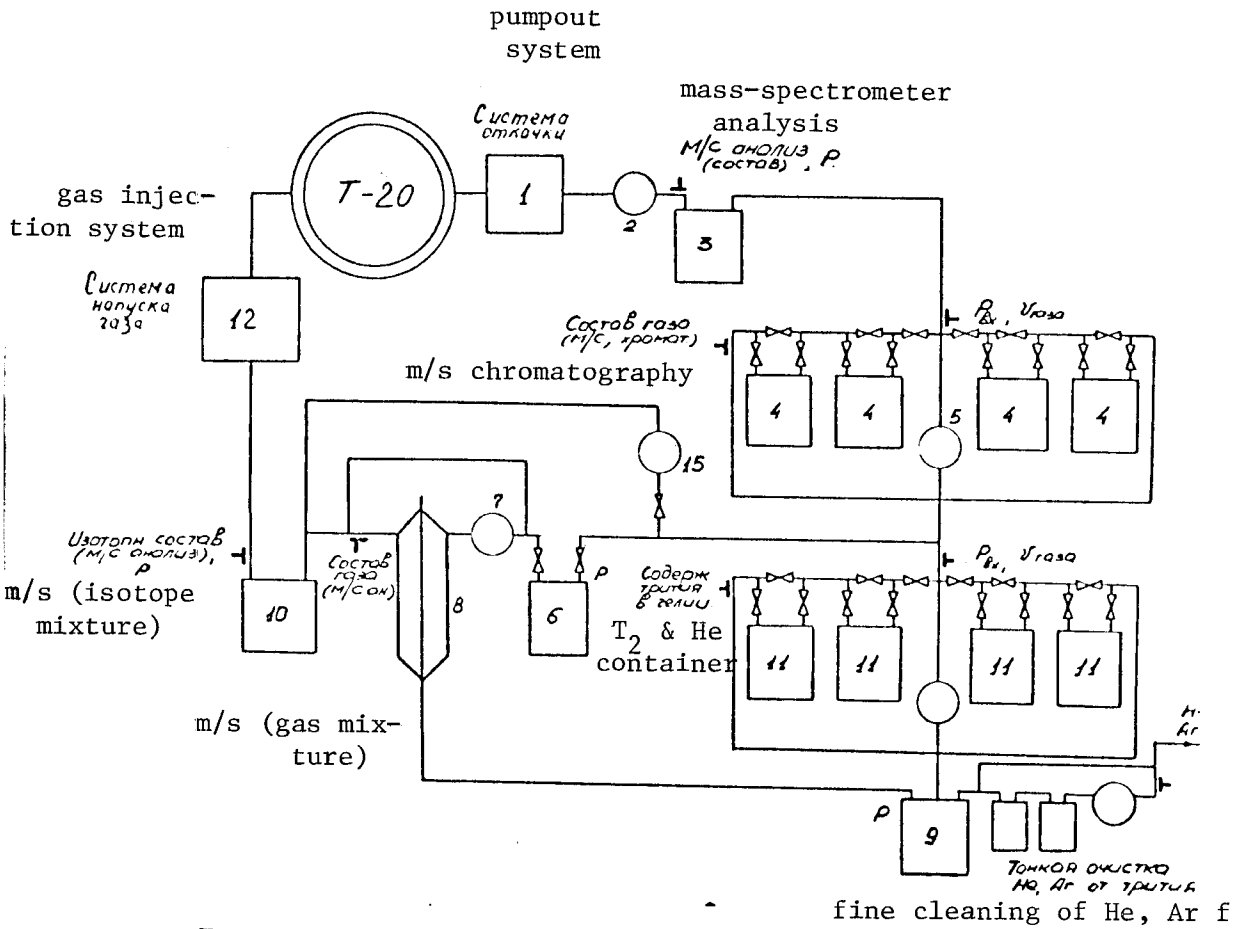

Рис.Ш.II. Технологическая схема тритиевого цикла

Fig. III. 11. Block diagram of the tritium cycle.

on titanium occurs at 300°C and on uranium powder at room temperature. Regeneration of the DT mixture is done at 700°C and 500°C respectively. The amount of tritium not released in regeneration is not more than 0.1% and the amount released with the He and Ar does not exceed 10^{-2}% (activity 10^{-4} C/l). Similarly, the amount of tritium absorbed with impurities during hydrogen purification is $\sim$0.1%.

The total amount of helium accumulating in the DT mixture during 10^5 pulses is not more than 1% of the DT mixture used, i.e. $\sim 0.5m^3$. By diluting the helium with argon, injected at the end of a cycle, the volume of gas increases by a factor of 100. To be able to dump this helium in the atmosphere, a more thorough purification from tritium should be made. This tritium may have been picked up from the cupric oxide or was absorbed on the zeolite.

In order to provide uninterrupted operation of the clean up cycle (4) and the absorbers (11), the columns are arranged in two parallel lines.

For separating and concentrating the tritium, we will use the method of thermal diffusion.

Evaluation of tritium release by diffusion

Diffusion of tritium through the discharge chamber wall is an exponential function of its temperature (Table III.2).

Table III.2

Diffusion of tritium through the discharge chamber wall (partial pressure of T_2 is 5×10^{-4} torr, wall thickness 1mm)

Wall temp. C	Diffusion		Activity
	cm^3/sec	cm^3/pulse	Ci/pulse
100	7.2×10^{-4}	2.2×10^{-2}	5.5×10^{-2}
200	1.8×10^{-3}	5.4×10^{-2}	0.14
300	2.9×10^{-3}	8.7×10^{-2}	0.22
400	5.1×10^{-3}	1.53×10^{-1}	0.37
500	2.5×10^{-2}	7.5×10^{-1}	1.9
600	8.4×10^{-2}	2.5	6.2
700	0.23	6.9	17.2
800	0.51	15.3	38.2

The amount of tritium diffusing from the discharge chamber to the intermediate chamber through a 1mm wall during 100 pulses, with a change in the wall temperature from 100° C to 500° C rises from 5 to 190 C. If the wall thickness is increased to 10mm, the amount diffusing is reduced by an order of magnitude.

Because of the large amount of tritium diffusing into the intermediate chamber, the vacuum system for it will need a separate tritium removal cycle.

Calculations of tritium diffusion through a 1mm thick intermediate chamber wall at 50 C and a pressure range of 10^{-7} - 10^{-5} torr indicates (Table III.3) that with a pressure change from 10^{-7} to 10^{-5} torr, the diffusion of tritium into the surroundings goes from 0.03 C/hr to 0.3 C/hr.

Table III.3

Diffusion of T_2 through intermediate chamber wall per hour (wall thickness 1,mm, wall temp. 50°C)

Pressure P,torr	Diffusion cm^3/hr	Activity Ci/hr
10^{-7}	1.3×10^{-2}	0.032
10^{-6}	4.1×10^{-2}	0.10
10^{-5}	1.3×10^{-1}	0.32

The obtained values of tritium flow were derived for clean unoxidized steel surfaces. Oxidation on the backside of the chamber wall will reduce diffusion of tritium to the surroundings by two orders of magnitude.

All components which have sizeable quantities of tritium will be housed in areas designated class I. However, components which are hermetically sealed, and have protective measures against tritium diffusion may be housed in areas designated class II.

In all portions of the building containing the machine, including service areas there will be dosimeters monitoring the tritium concentration in the air. This control is done separately for gaseous tritium, oxidized tritium and aerosols containing tritium from 0.1

Experimental Thermonuclear Installation

TOKAMAK - 20

Preliminary Study (First draft)

Vol. II, part 2
Engineering Solutions

National Committee for the Utilization of Atomic Energy Soviet Ministry, USSR.

I. V. Kurchatov Atomic Energy Institute
D. V. Yefremev Scientific Research Institute for Electrophysical Apparatus.

MOSCOW 1975

Translated by Igor N. Sviatoslavsky
University of Wisconsin Fusion Design Study Group

UWFDM-129

Experimental Thermonuclear Installation

TOKAMAK - 20

Preliminary Study (First Draft)

Vol. II, part 2

Engineering Solutions

National Committee for the Utilization of Atomic Energy Soviet Ministry, USSR

I. V. Kurchatov Atomic Energy Institute
D. V. Yefremev Scientific Research Institute for Electrophysical Apparatus

MOSCOW 1975

Translated by Igor N. Sviatoslavsky
University of Wisconsin Fusion Design Study Group

UWFDM-129

This is Part 2 of Volume II of the Tokamak 20 report as translated by Igor N. Sviatoslavsky.

Table of Contents
(Cont.)

IV. Plasma Heating Methods

1. General State

Ohmic heating of the plasma in T-20 lasts about two sec during which the temperature reaches $T_i \approx 3$ KeV. As this temperature is reached, the heating efficiency goes down because the current becomes limited by hydrodynamic plasma instabilities and the electrical resistance of the plasma decreases sharply with temperature. Further plasma heating is done by methods which are effective independently of plasma temperature. Of all the possible methods for plasma heating, the most promising are neutral beam injection and RF heating.

Experiments on T-20 will be conddcted in two stages. The first stage will concentrate on hydrogen and deuterium plasma (no tritium). The second stage will be devoted to obtaining a fusion reaction giving about 10^{19} neutrons/sec by heating DT plasma to 10 KeV, or producing a two component plasma by injection of deuterium atoms at 160 KeV into a tritium plasma target at Te $\approx$ 5 KeV. Plasma heating with neutral beams or RF, depending on the required plasma parameters, can be obtained in several ways at either experimental stage.

Taking τ_E = 2 sec, n $\approx 5 \times 10^{13}$ cm^{-3} ($n\tau_E \approx 10^{14}$), if the plasma receives 50 MW of power in 2 sec, its temperature will rise from 3 - 10 KeV. Assuming that the coupling efficiency of the energy by the investigated heating methods to the plasma ions is 85%, then the total energy expended is 60 MW.

This 60 MW of energy, by either neutral beams or RF takes place for 2 - 3 sec after the ohmic heating. Further expenditure

of power depends on the experiment, but does not exceed 13 sec.

During power injection with 80 KeV deuterium atoms, the amount injected is 750 equiv. atoms. This corresponds to 4.5×10^{21} particles/sec. At an initial charge of 2×10^{22} particles in a volume of $400 m^3$, the injected particles will double this number in about 5 sec. This may limit the length of injection, however, at an energy of 80 KeV, about half of the injected atoms will be captured in the plasma by charge exchange, therefore we can expect that the chamber wall will experience a flux of atoms at 10 KeV. We should note that neutral beam injection at 160 KeV has the following advantages:

- the number of particles admitted into the Tokamak chamber for the same amount of power is decreased in half as compared to 80 KeV.
- atom capture in the plasma is by ionization rather than charge exchange and thus, the flux of charge exchange atoms incident on the chamber wall decreases.

However, 80 KeV neutral beam injectors have a higher duty factor.

For plasma heating with HF and UHF electromagnetic waves, the following methods hold the most promise.

1) UHF heating at a fequency close to the electron cyclotron ($\omega \approx \omega_{ce}$).

2) UHF heating in the range of the lower hybrid frequencies ($\omega \approx \sqrt{\omega_{ce} \cdot \omega_{ci}}$);

3) Heating in the ion-cyclotron resonance frequency and its harmonics, and in the magnetic sonic resonance ($\omega \approx \omega_{ci}$).

It should be noted that since for the anticipated plasma parameters, the time for energy exchange between ions and electrons is about one sec, it does not make any difference which component of the plasma receives the energy.

However, with electron heating one might expect less plasma contamination, since the chamber wall sputtering by electrons is two orders of magnitude less than with ions. Further, RF heating does not need neutral beam injection and thus, there is no 10 KeV charge exchange atom flux incident on the wall.

The planned complex of plasma heating has many possibilities for experimenting, depending on the attained $n\tau_\epsilon$:

1. During the heating of a DT plasma for the given conditions of $n\tau_\epsilon = 10^{14}$, injected power of 60 MW and T_i = 10 KeV, it is possible to insure a $Q \approx 2$. Thus, of the 100 MW of power coming from the fusion reaction, about 20 MW will be by α-particles which will produce supplementary heating of the plasma. Consequently, after 2 - 3 sec after the start of heating, the amount of injected power in this case can be decreased.
2. If confinement time τ_ϵ is less than 2 sec, let us say one sec, then with 60 MW power injected and a plasma temperature $T_i \approx 10$ KeV ($n\tau_\epsilon \approx 2.5 \times 10^{13}$ we can expect a Q = 1.
3. If for τ_ϵ = 1 sec, the plasma temperature does not exceed 5 KeV, then for a nominal value $n \approx 5 \times 10^{13}$ cm^{-3} ($n\tau_\epsilon = 5 \times 10^{13}$) the value of Q fall to about 0.3.

In these cases plasma heating is done by 80 KeV neutral beam injection or by one of the RF systems described above

4. If the 160 KeV neutral beam injectors are used, keeping the power at 60 MW, τ_ϵ = 2 sec and T_i = 10 KeV then $Q \approx 4$.

5. With the same conditions as in (4) but τ_ϵ = 1 sec, $Q \approx 1.5$.

6. If at a higher plasma temperature, the ion thermal conductivity does not decrease and transition into the banana regime does not take place ($\tau_\epsilon' < 1$ sec) then to maintain the electron temperature at 5 KeV it is reasonable to use the UHF system at the ion-cyclotron frequency to inject 60 MW of power. Simultaneous injection of 50 MW via the 160 KeV neutral beam injectors will have to take place. In this regime of two component plasma, one might expect a $Q > 1$. This mode of operation is suitable from the standpoint of maintaining good vacuum conditions in the chamber and reducing the undesirable loading on the chamber wall.

2. Neutral Beam Injection System

The creation and injection into T-20 of 60 MW of 80 KeV and 50 MW of 160 KeV neutral beams is accomplished by eight injectors whichhave integral systems of power supply and vacuum pumps. Five injectors are 80 KeV and the remaining three, 160 KeV. On the first stage of experiments, all eight injectors will be used at 80 KeV, with a combined power of 100 MW. The change in the power of neutral beams can be done discreetly every 3 MW.

The neutral beams are admitted into the chamber of T-20 through eight windows (25 x 250 cm^2) situated two to a quadrant between TF coils (see Fig. IV-1). The direction is tangent to the radius $R - \frac{a}{2} = 4$ m, both with and against the plasma current.

The path of neutral beams in the plasma is 12 m, and the spread of the beam does not exceed $+1.5^{o}$. The 80 KeV beam is attenuated a factor of 20 and the 160 KeV, a factor of 13. Energy deposited on the opposite wall is 125 watt/cm^2 and 250 watt/cm^2 respectively.

It is proposed that 80 KeV beam injection take place 2 - 3 sec after ohmic heating of the plasma. Further energy supply would depend on the experiment. Injection of 160 KeV neutral beams will last about 10 sec.

Construction of Injector

The injection complex in T-20 includes a 160 KeV neutral beam injector. The only difference in the two injection systems is in the ion optics. Fig. IV-2 shows a basic schematic of the injector which is common to both energies in T-20.

Generation of the positive ions is in four ion sources (1) arranged on top of each other, namely in the direction of the small dimension of the beam port. Each source has its own optics. (2) Neutralization of the ion beam is accomplished by passing it through a gas which flows from the source to the neutralizing chamber. (3) The ion source and the neutralizer are shielded from the magnetic field and a venetian blind arrangement (4) is used to shield the drift region directly behind the neutralizer.

Separation of the charged components of the beam is done in the stray field of T-20, or with the aid of a special coil system. (A picture of the stray field in T-20 is given in Fig. II.8).

The positively charged atomic ions curve in the stray field beyond the neutralizer and strike the current collector (5), which in some designs of the injector are getter pumps. Positive molecular ions and negative ions strike the water cooled venet n blind type of current collectors (6) and (7).

Evacuation of the injector is by turbomolecular pumps and cryopanels (8). Between the chamber of T-20 and the injector there is a fast acting screen (9) a gate value (10) and a coupling (11).

Besides this, each injector has:

1 - A system for measuring atom and ion beam parameters

2 - A power supply

3 - A cooling water supply

4 - A system for controlling, locking, shielding and regulating the injector.

A general view of the injector and overall dimensions are given in Fig. IV.3. Its principal parameters are given in Table IV.1.

Table IV.1

Principal Parameters of the Injection System

Energy of the atoms	KeV	80	160
Power injected into the plasma	MW	60	50
Number of injectors		5	3
Parameters of a single injector			
Power at exit from injector	MW	12	16
Flow of atoms at exit from injector	Equiv. atoms	150	100
Coefficient of ion-atom conversation	"	0.67	0.37

Table IV.1 (cont.)

Transport efficiency of the atom beams	Equiv. Atoms	0.75	0.75
Efficiency of acceleration		0.50	0.28
Power of the initial ion beam	MW	25	60
Number of ion sources		4	4
Parameters of an ion source			
Needed ion beam, not less than	A	80	90
The discharge: Potential	V	60	60
Current	kA	10	10
Power	kW	600	600
Filament power	kW	150	150
Electric Power Supply			
High Voltage Rectifiers			
For a single source:			
Voltage	kV	80	160
Current	A	100	100
Power	MW	8	16
For a single injector, Power	MW	32	64
Total power for all types of injectors	MW	160	192
Low Voltage Supply			
Power supply for a single ion source	MW	1.35	1.35
Power supply for a single injector	MW	5.4	5.4
Total power for all the injectors	MW	27	16.4
Power supply of the whole injection system not including the rectifier efficiency, vacuum pumping power and auxiliary needs of the system	MW	187	208.4
Total	MW		400

Ion Source and the Ion Optics

For the first design of an injector, we have adopted a single type of ion source for both types of injectors (80 and 160 KeV), namely an ion source which does not have an external magnetic field but has a low pressure straight diffusion arc discharge with an indirectly heated cathode (Fig IV.4). The maximum ion current available from the source is 100 A. The anode is a rectangular frame (2) which surrounds the cathode (1). The ion optical system (3), emitter (4) and the flanges (5) with the gas distribution system are under a "floating" potential or under a potential which is controlled by the resistance.

The emitter is a plate with two rows of slits 8 cm long and 0.2 cm wide, through which the charged particles are selected. It has a void area of about 30%. Areas betweeen the slits are cooled with forced water under pressure and are in the form of hard soldered preformed tubes, or they may be molybdenum tubes. Areas between the rows of slits are also water cooled. The emission electrode has external dimensions of 20 x 48 cm^2.

The positive ion current density from the plasma edge is not greater than 0.5 A/cm^2. Plasma uniformity in the region of the emission slits is not less than 0.5% and is obtained by the proper placement of the cathodes, stabilizing the discharge current and gas pressure to ±.05% and ±1% respectively. Such stable discharge parameters in conjunction with properly selected geometry for the ion optical system allows the formation of elementary ion beams with a divergence of $2 - 3^{o}$.

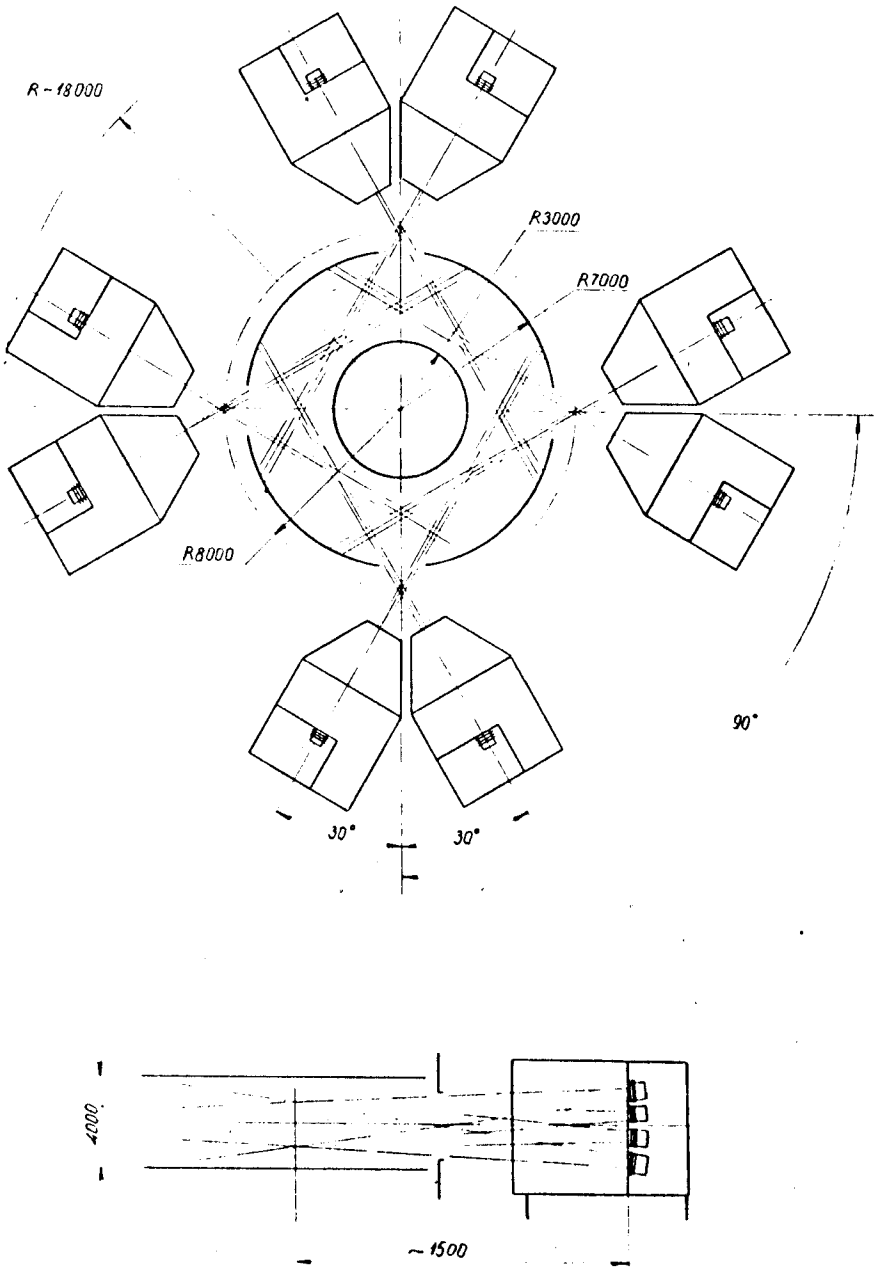

Рис.IУ.I. Общая компоновка инжекторов

Fig. IV.1 General Assembly of the Injectors

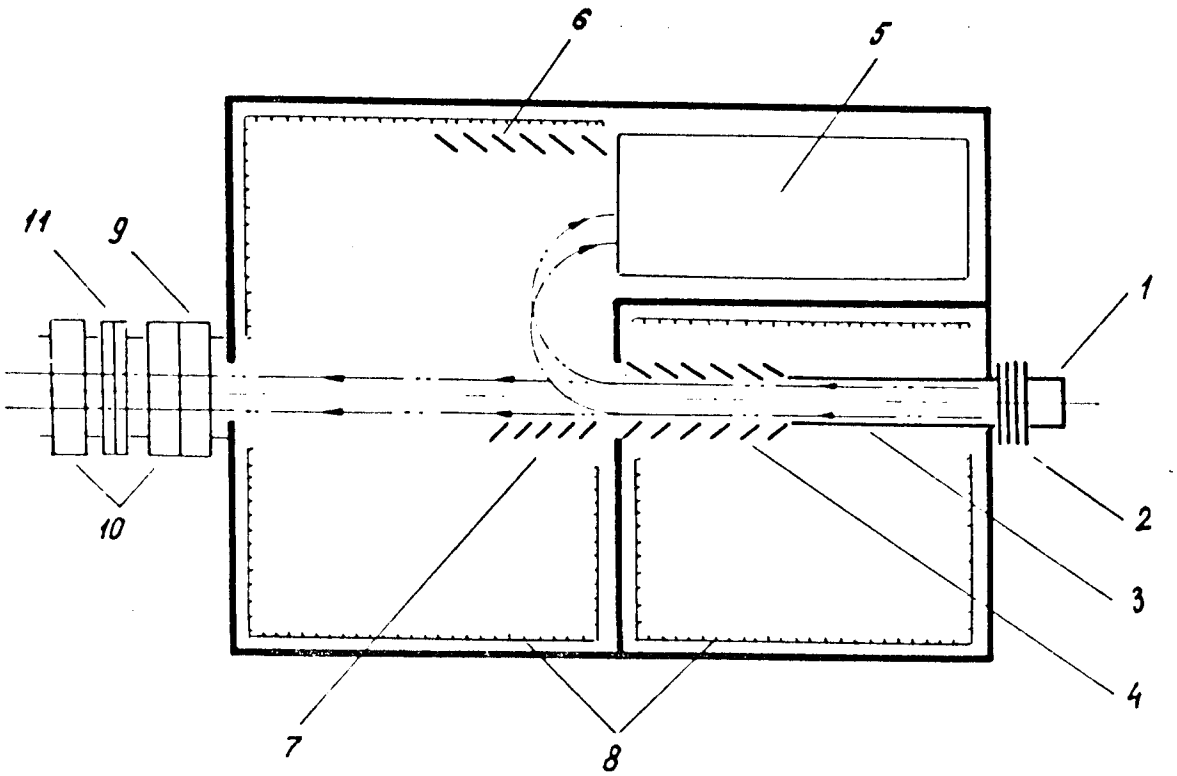

Fig. IV.2 Principle Diagram of the Injector

1 - ion source; 2 - ion optical system;

3 - neutralizer; 4 - screen; 5 - D_1^+ collector;

6 - $D_{2,3}^+$ collector; 7 - D_1^- collector; 8 - cryopanel;

9 - shutter; 10 - valves; 11 - adapter

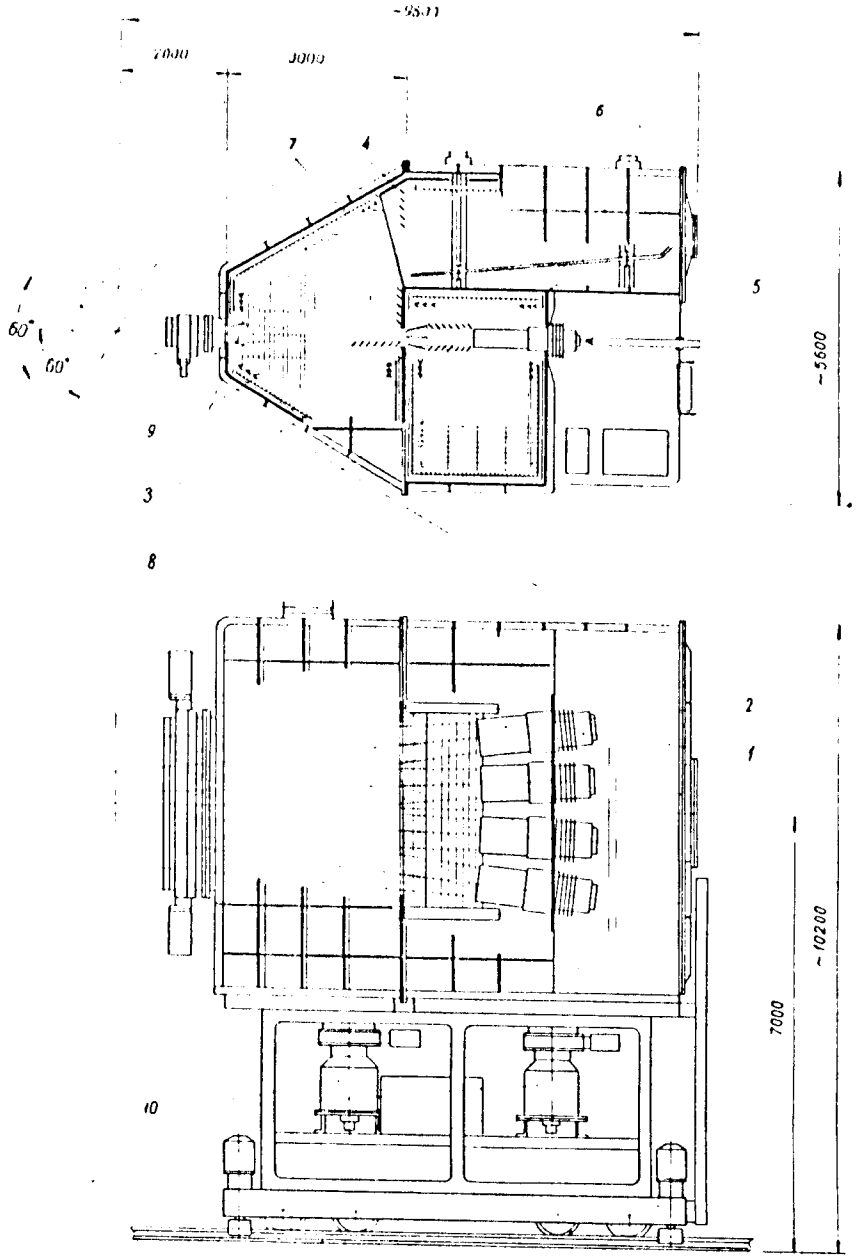

Fig. IV.3 General View of Injector

1 - ion source; 2 - neutralizer; 3 - collimator; 4 - screen; 5 - D_1^+ collector; 6 - cooled panel; 7 - $D_{2,3}^+$, D_1^- collector; 8 - cryopanel; 9 - nitrogen screen;10 - turbomolecular pump

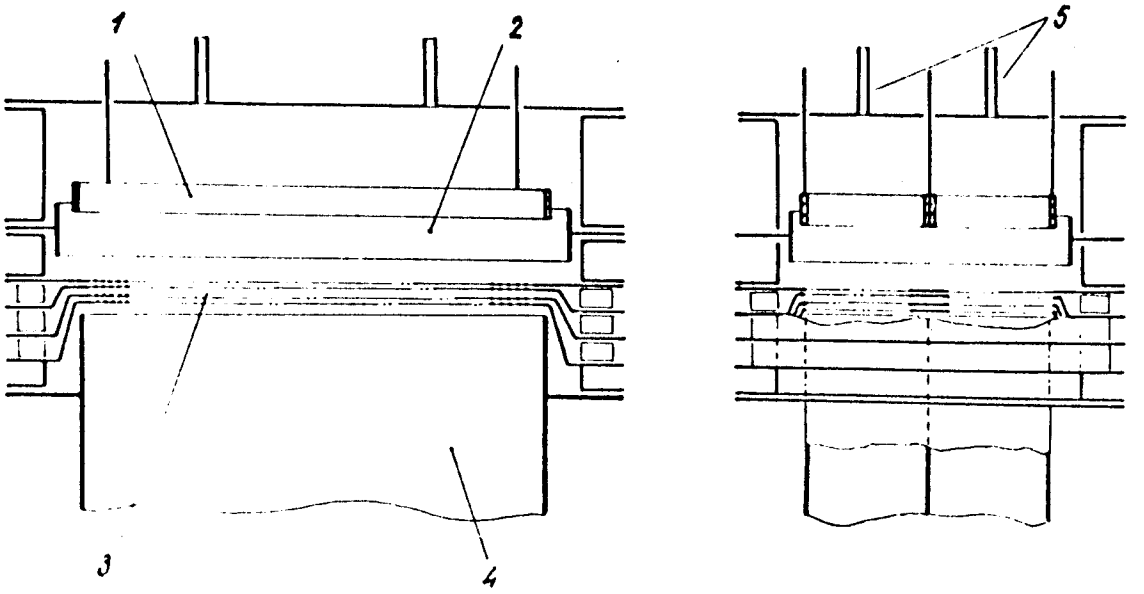

Рис.IУ.4. Принципиальная схема ионного источника:
I - катод; 2 - анод; 3 - ионно-оптическая система; 4 - нейтрализатор; 5 - трубки напуска газа

Fig. IV.4 Principle diagram of the ion source
1 - cathode; 2 - anode; 3 - ion optical system;
4 - neutralizer; 5 - gas inlet tube

Typical composition of the ion beam from the source is 75% D^+, 15% D_2^+ and 10% D_3^+. The gas efficiency in the source is about 30%.

Operating conditions of the ion source are:

1 - Current in the arc discharge 10 kA

2 - Voltage at discharge 60 V

3 - Power in the cathode heater 150 kW

4 - Power dissipated in the source 900 kW

The ion optical system of the source consists of three or four slitted electrodes. The slits in the electrodes coincide with the slits in the emitter. Initial formation and selection of elementary ion beams occurs at a voltage drop of 40 kV across the first gap, ($d_1 = f(n, Te, U)$, where d_1 is the width of the gap, $j \leq 0.5$ A/cm^2. Acceleration to 80 and 160 KeV occurs in the second gap. Use of two accelerating gaps (d_1 and d_2) preserves the current density at high accelerating voltages and by the fact that the gap width is limited by breakdown voltage U_{br}.

$$U_{br} \approx c \cdot d_{1;2}^{\alpha}, \qquad 0.5 < \alpha < 1.0$$

The accelerating electrodes of the optical system of each ion source have a void fraction of 30-40%. Areas between the slits are cooled with water. Beam losses on the electrodes is calculated to be <1%.

For focusing the beam extracted from the large area of the emitter, it is proposed to slightly curve the surface of the

electrodes and to displace the relative locations of the slits in the emitter and the first accelerating electrode. The retarding electrode holds back the flow of electrons and takes some part in beam shaping.

The ion source and its optical system have a common external magnetic screen. In addition there are electrostatic screens between the ion sources. The magnetic field from external sources must not exceed 10 Oe in the region of the ion source and its optical system. The distance between the emitters of adjacent sources is about 26 cm.

Neutralizer

As the ion beam goes through the gas target neutralizer, dissociation between the molecular ions and neutralization of the charged components occurs with an efficiency of ion to atom conversion of 0.67 and 0.37 for 80 and 160 KeV ions respectively.

Each ion source has a neutralizer which is a rectangular tube 26 x 60 cm^2 in cross section and 120 cm long. It is divided into two parts on the inside. The walls and partition of the neutralizer are water cooled.

The magnetic field inside the neutralizer does not exceed 10 Oe because of the effect of the screen and the 2.5 cm thick walls.

Pressure distribution in the neutralizer channels and in the adjacent drift region is shown in Fig. IV.6.

Separation of Charged Components

The beam exiting from the neutralizer consisting of particles of several energy levels must be cleaned of any charged components. Two versions of injectors are under consideration, differing in the mode of molecular ion separation. The first version makes use of the stray fields in T-20 (see Fig. IV.3), and the second version has a special magnetic system which separates and localizes the different charged particles of different energies in special places. In the latter version, attention has to be given to the effect of the separation field on the magnetic field in the chamber of T-20.

In the version selected, the one using the stray field in T-20, there is a problem of locating the injectors for proper acceptance of the D_1^+ ion beams which have densities of 12 kW/cm^2 and 4-5 kW/cm^2 for the 160 KeV and 80 KeV beams respectively. The position of the beam changes as a function of the plasma current. Thus, at a maximum plasma current of 6 MA, the magnetic field in the separation region is 650 Oe and the radii of curvature of the ions are 125 cm and 88 cm for the 160 KeV and 80 KeV ions respectively. For a plasma current of 2 MA the radii of curvature get so large that it becomes difficult to position the collectors for the $D_{2,3}^+$ beams and for this reason we have recommended that beam injection take place within the narrow range of 4-6 MA plasma current.

In the event that the stray field will be inadequate, separation will be accomplished with a special coil in the plane of the large beam dimension. The separator poles in this case

are 500 x 110 cm^2 for a gap of about 50 cm. Magnetic field in the gap is 800 Oe and 550 Oe for the 160 KeV and 80 KeV beams respectively. Radius of curvature for the D_1^+ ions is 100 cm for both energies. The flux of D_1^+ ion at 160 and 80 KeV will turn through 180^o and is collected on a special collector.

Collector

The D_1^+ ion collector is made in the form of a cooled plate positioned at 3^o to the ion trajectory, which lowers the power loading on the collector surface by a factor of 20. This plate, besides being a collector, is also a sorption pump since its surface is covered with a getter which is sputtered under the action of the beam (thermal and kinetic sputtering). Across from the collector is a corrugated and, either water or N_2 cooled screen which acts as the sorption panel.

The collector and the sorption panel terminate in the magnetic shield and can be displaced and rotated as a whole relative to the ion beam trajectory. The collector produces a field non-uniformity of ±3% on top of the variation in the regular field during a pulse in T-20. The D_1^+ ion energy can vary by ±4% as a result. Provisions for adjusting the plate can accommodate up to a 30% maximum variation of the field.

The collector plate is made in the form of a "C" with the base plate dimensions being 280 x 400 cm^2, side plates 50 x 400 cm^2, the sorption screen 300 x 450 cm^2 with a total area of $\sim 3 \times 10^5$ cm^2, which insures the collection of gasses from the recombination of the D_1^+ ion beam of 300 A intensity and maintains a pressure of 10^{-5} torr in the collector.

Other charged components have a substantially smaller power density and thus do not present any difficulty.

In the future, collectors for the various charged components of the ion beam will be insulated and will float at a regulated potential so that the energy of the charged particles could be recovered.

Beam Diagnostics

The beam diagnostics system will allow the separate measurements of the intensity, power, distribution of intensity and power in a transverse section of an atom and D_1^+ ion beam, and the phase characteristics of these beams at their nominal energy. (D_2^+, D_3^+ and dissociation ions are not measured.) Measurements are based on calorimetric and electric methods for beam diagnostics.

The system for measuring beam parameters consists of two collectors, one for atoms and the other for D_1^+ ions. These collectors are plates placed at an angle of 3^o to the D_1^o and D_1^+ beams.

Both collectors have rows of slits uniformly distributed across the plates with individual receivers behind each slit for measuring the beam intensity.

A part of the slits measures the phase characteristics of the D_1^o and D_1^+ beams and thus provides the control for the operation of the ion-optical system.

The vacuum system for the injector has the following main features[1]:

---

1) These vacuum parameters are for injector operation at E_i = 160 KeV which are more stringent.

Flow of deuterium into the ion source (mol/sec)	8×10^{21}
Coefficient of gas ion conversion of ion source	0.3
Partial constituents of the ion beam D_1^+	75%
D_2^+	15%
D_3^+	10%
Neutral deuterium molecules accompanying the ion beam (Q_o, mol/sec)	6.4×10^{21}
Neutralization chamber, - tube cross section	20 x 200 cm^2 x 120 cm long
Density of the neutral gas in the neutralization chamber (δ cm^{-2})	10^{16}
Fast deuterium atom flux at the exit from tube,	100 eq. at. (E_i = 160 KeV) 150 eq. at.(E_i = 80 KeV)
Flow of neutral gas from the injector to the discharge chamber (torr. l/sec)	0.7
Atom inlet tube, rectangular cross section	(25 x 200) cm^2 x 150 cm long
Background pressure in injector, (torr)	5×10^{-8}
Total effective pumping speed of the cryopanels (on deuterium)	2.4×10^6 l/sec
Regeneration frequency of cryopanels - every	5×10^3 cycles
Cryopanel area, (m^2)	70
Area of N_2 radiation shields (m^2)	200
Liquid helium usage (4.2K) (l/hr)	45
Liquid N_2 usage (l/hr)	130
Closing time of gate valves (sec)	2

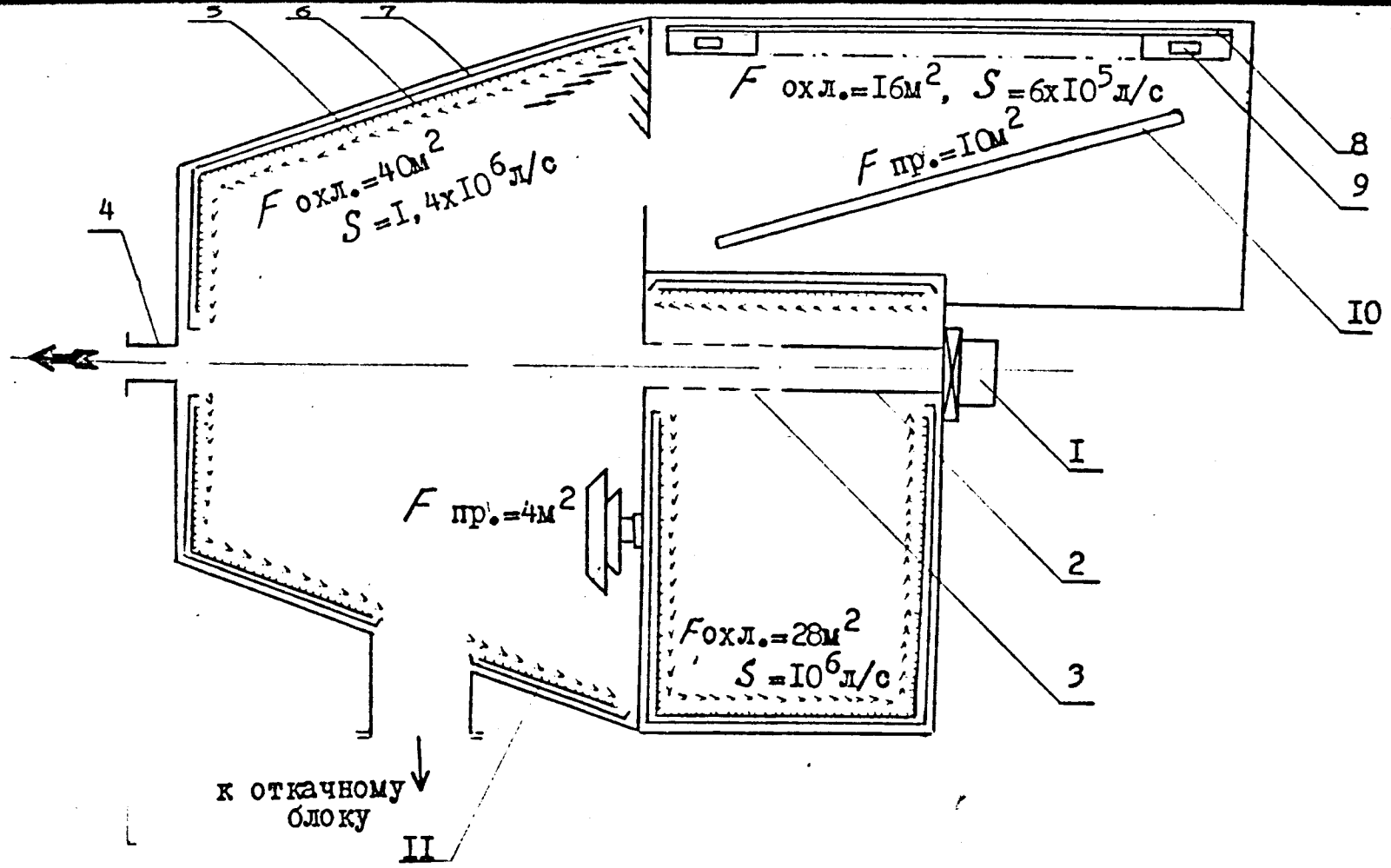

Fig. IV.5 Construction of the Vacuum System for the Injector of E_i = 160 KeV

1 - ion source; 2 - neutralizer; 3 - magnetic shield
4 - beam port; 5 - venetian blind screen; 6 - cryopanel;
7 - solid screen; 8 - sorption surface; 9 - arc evaporator;
10 - positive ion collector; 11 - negative ion collector

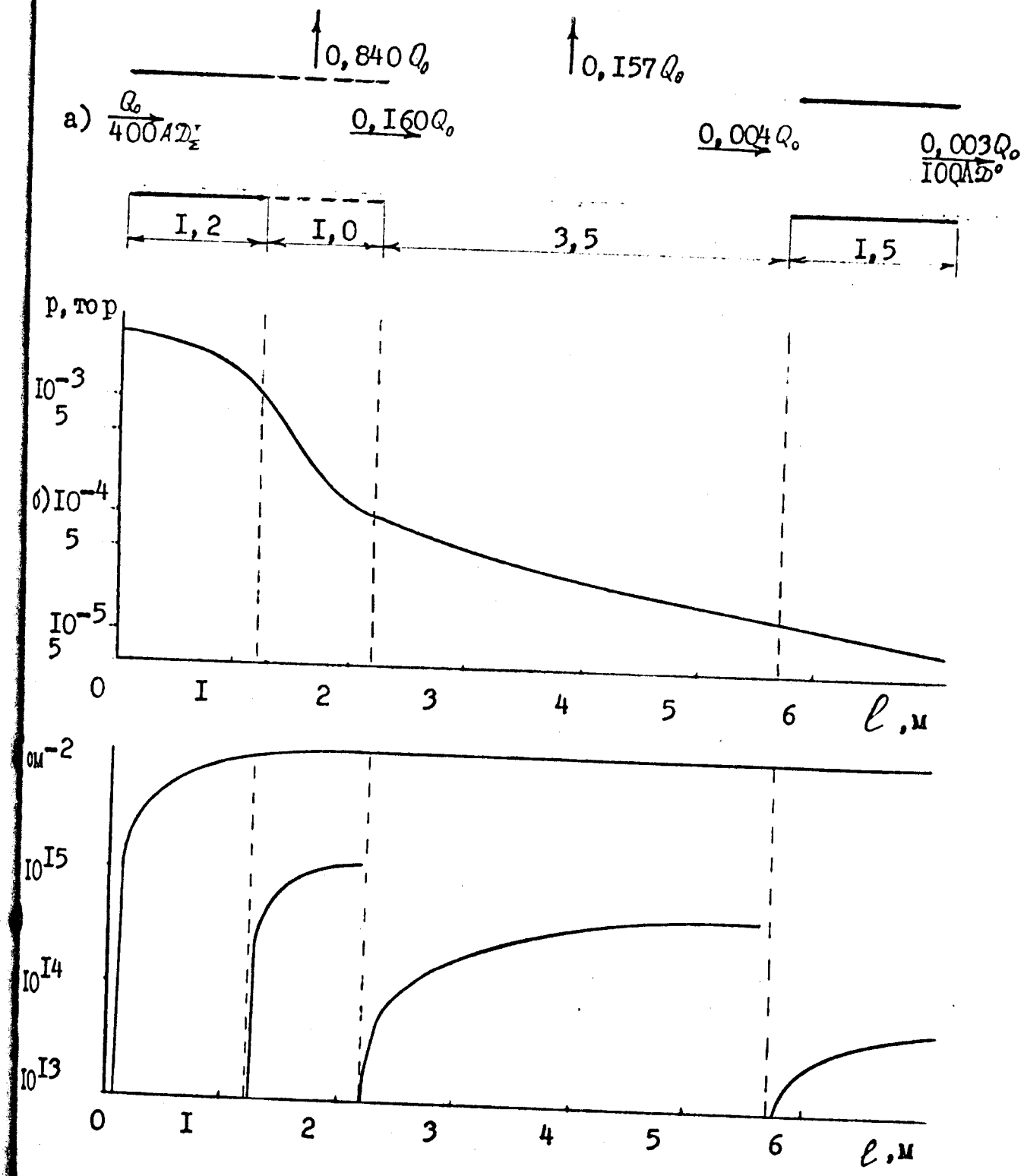

Fig. IV.6 Distribution of Neutral and Charged Particle Fluxes

(a) pressure, (b) integrated density of the neutral gas (c) along injection port for T = 300 K, M = 4, E_i = 160 KeV

The space distributions of the ion beam, the fast atom beam, density and pressure of neutral gas along the beam line is shown in Fig. IV.6.

Pumping of gasses produced in the ion collector chambers after separation by the stray field in T-20 will be in the following manner:

1 - Positive ions: Water cooled titanium strips, which will sputter with the aid of discharge arcs as well as by the beam itself.

2 - Negative ions: Pumping by regenerative titanium strips. Regeneration period - every 10^4 cycles.

3 - For pumping the injector during high temperature conditioning and regeneration of the ion collectors, and for periodic pumping out of the helium collecting within the injectors, a pumping module similar to that used in the discharge chamber will be used.

4 - For pressure control, gas analysis and vacuum alarm signals, a multichannel commercial instrument will be used which will interface with a computer.

Injector Power Supply

The power supply for the injectors also provides power to the VHF and HF plasma heating and it is therefore reasonable to analyze it at the end of this chapter. However, the main parameters of the power supply system are given in Table IV.1.

Injector Water Supply

The water supply for the injector is divided into two sub-systems: the first is for cooling elements which are at a high potential (greater than 1 kV) and the other for low voltage elements (1 kV).

The cooling water for the ion source and the optical system electrodes is connected through electrical isolators. Water pressure for the ion source is 10 Kg/cm^2 and for the optical systems, 80 Kg/cm^2. The pressure is maintained by pumps insulated against 160 and 80 KV respectively.

Cooling water for the ion collectors at a maximum energy will have a pressure of 10 Kg/cm^2. The amount of water needed for cooling the ion sources and the optical systems is 300 l/sec. That needed for cooling the collectors is 3000 l/sec. Other injector parts will require an additional 100 l/sec.

For a maximum allowable water temperature of 90° C, the water flow for a single 160 KeV injector is 3.4m^3/sec and for one 80 KeV injector, 1.7m^3/sec for a single pulse.

Instantaneous water flow for all the injectors is 19m^3/sec during a pulse. Average flow is about 1m^3/sec.

System of Alarms and Injector Control

The following parameters will be controlled: cathode filament current, arc discharge current, the potential on the arc and all the electrodes in the ion optical system, currents in the ion optical system, gas pressure in the ion source and in the neutralizer. In the three pumping regions there will be control

of the remnant gasses, the current and power density of the atom and ion beams, temperature of the injector elements, temperature and pressure of the cooling water and the cryopanel temperature. The activity and radiation level in the effluent gasses, in the isolator region and other places will be monitored.

Collection, recording and data analysis on the operation of the injectors will be done automatically in conjunction with a computer. All the data will be available in printed form.

Control of the injectors will be accomplished automatically according to the program on T-20. It is possible that some hand tuning of the injectors will be done during the shake-down period.

Each injector will have the following alarm and interlock systems: 1) Vacuum alarm; 2) Cooling water alarm; 3) Valve interlocks; 4) Interlocks on shield position; 5) Collector interlocks; 6) Interlocks against injector element overheating; 7) Interlocks against electrical breakdown; 8) Interlocks in the high voltage system; 9) Alarms to indicate an excessively high voltage in the magnetic shield system; 10) Magnetic field alarm.

3. Radio Frequency Heating

A. Plasma heating in the electron-cyclotron resonance range.

For a mangetic field of ≈ 3.5T, it is imperative to use the $\lambda \approx 3$ mm frequency band. At the frequency $(\omega \approx \omega_{ce})$ there exist effective mechanisms for RF energy absorption, namely synchrotron damping and linear transformation. However, in a

device the size of T-20 at Te $\approx$ 3-10 KeV, the dissipation of an extraordianry wave is so great that it is difficult to produce heating in the inner regions of the plasma torus. For this reason we have used the computer to calculate the synchrotron damping of an ordinary wave propogating through the plasma from outside the torus. In this operating range for T-20, $\omega_{pe} < \omega_{ce}$ an ordinary wave will freely propagate through all sections of the plasma. The main difficulty in utilizing this frequency range is the development of high power UHF generators. In view of this, it would seem reasonable to use as many low power generators as the geometry of the facility will allow. Obviously, the individual inputs must insure the independent operation of the generators.

In each of the eight spaces between TF coils, it would be possible to distribute ten waveguide ports on the outer surface of the torus. Calculations have been made to determine wave trajectories and damping during propagation along the median plane and at 45^{o} to it.

In order to minimize the effects of refraction, it seems reasonable to direct the waves along the radius of the plasma torus. However, practical radiation systems have a finite beam width. In view of this we have considered wave trajectories which have a spread of 10^{o} at the plasma surface. We show that if the RF energy is directed at 60^{o} to the magnetic field, there is a complete energy absorption during a single traversal by the wave of the synchrotron resonance zone. Undesirable heating by "runaway" electrons can be considerably reduced by selecting

the proper direction for this current. In Fig. IV.7 are shown typical trajectories of two waves within the plasma cross section. Calculations were made for an average density $\bar{n} = 5 \times 10^{13}/cm^3$ and $T_e = 5$ KeV. It can be seen that if the radiation systems are situated on the outer chamber surface within an angle of $\pm 45^\circ$ to the median plane, the effects of refraction will cause all the wave trajectories to intersect within $r < a/3$. Figure IV.8 shows the dependence $\ln \frac{W(r_{max})}{W(r)}$ for waves, propagating at an angle of 60° to the toroidal magnetic field. Here $W(r_{max})$ is the wave energy at the plasma edge, $W(r)$ the value of energy at a given radius. Curves one and two are for $T_e = 10$ KeV for wave trajectories shown in Fig. IV.7. Curves three and four are the same but for $T_e = 5$ KeV. In Fig. IV.9 and IV.10 is shown the distribution of RF waveguides. Some of these waveguides can be used to pre-ionize the plasma.

Evaluations have shown that RF use at the electron cyclotron frequency at a rate of 10^7 W for 10^{-3} sec can produce a preliminary ionization in the central region of the discharge chamber. A current rise at a rate of 10^7 A/sec will insure the containment of the plasma, a condition which is needed for the sustainment of the discharge. The pre-ionization RF waveguide inlets can be situated separately from the main heating system or integral with it as shown in Fig. IV.9. These waveguides must excite an extraordinary wave propagating to the cyclotron resonance zone where $\omega_{ce} > \omega_o$. The dimension of the RF waveguide port is 15 cm and is picked on the basis of the

Fig. IV.7 Wave trajectory W_{ce} (projected) in the plasma cross section

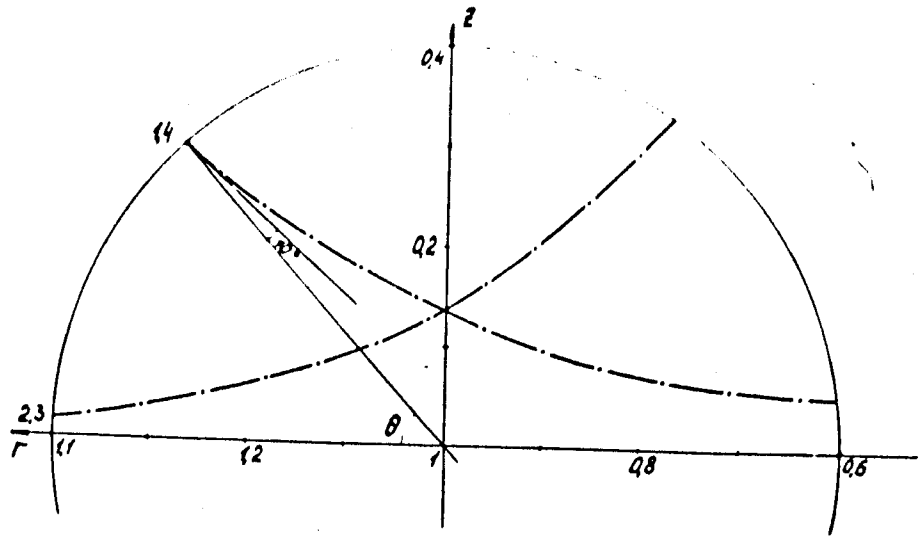

Рис.IУ.7. Траектории волны ω_{He} (проекция) в сечении плазменного шнура

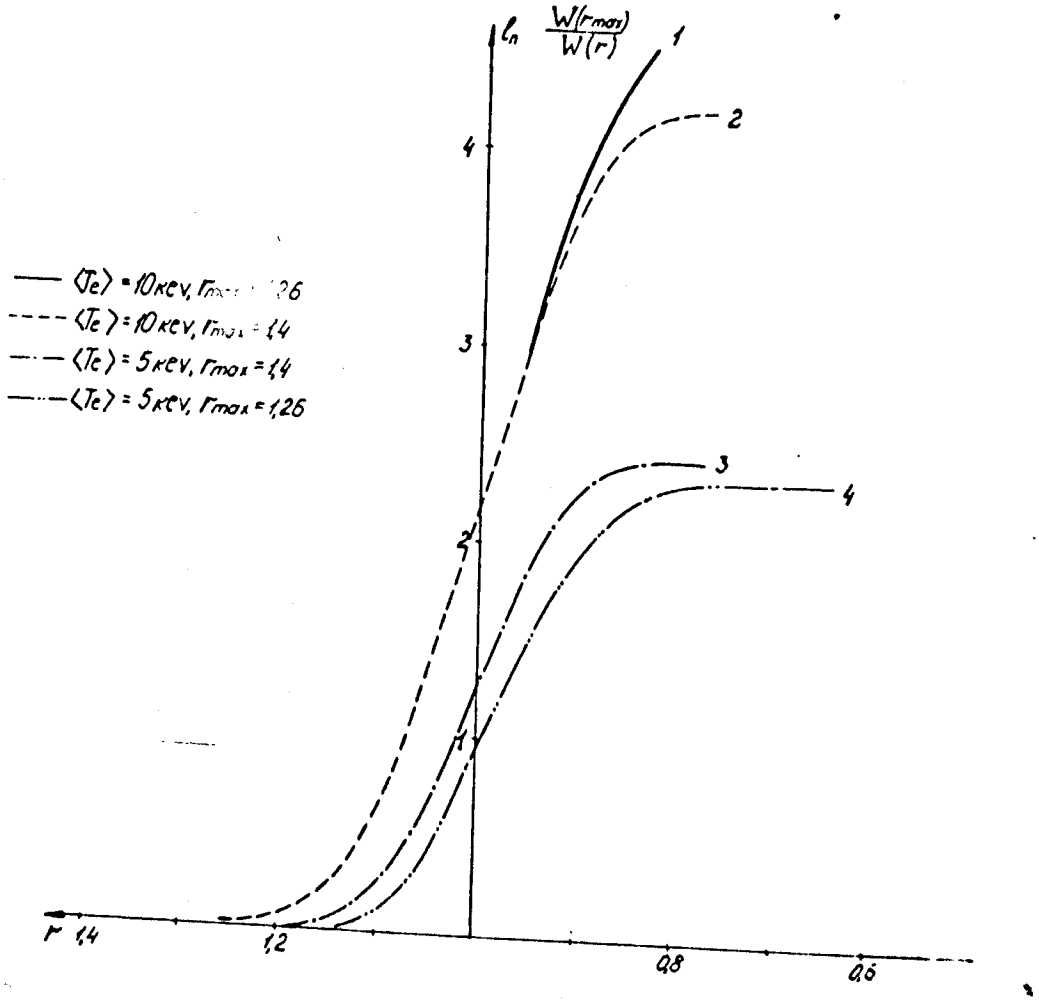

Fig. IV.8 Wave absoprtion W_{ce} along the minor radius of the plasma toroid.

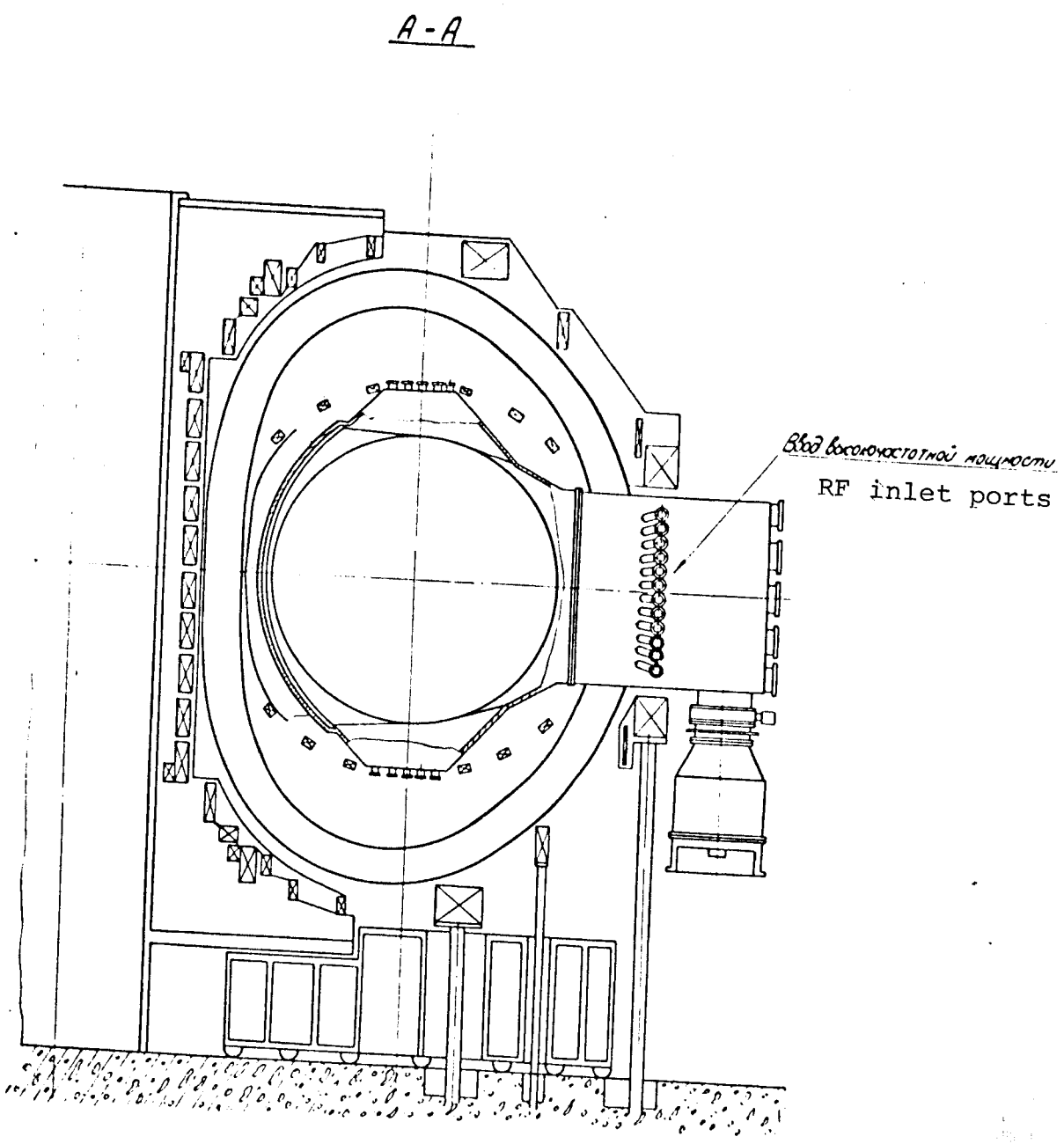

Рис.IУ.9. Расположение ВЧ-вводов мощности
Fig. IУ.9 Distribution of RF ports

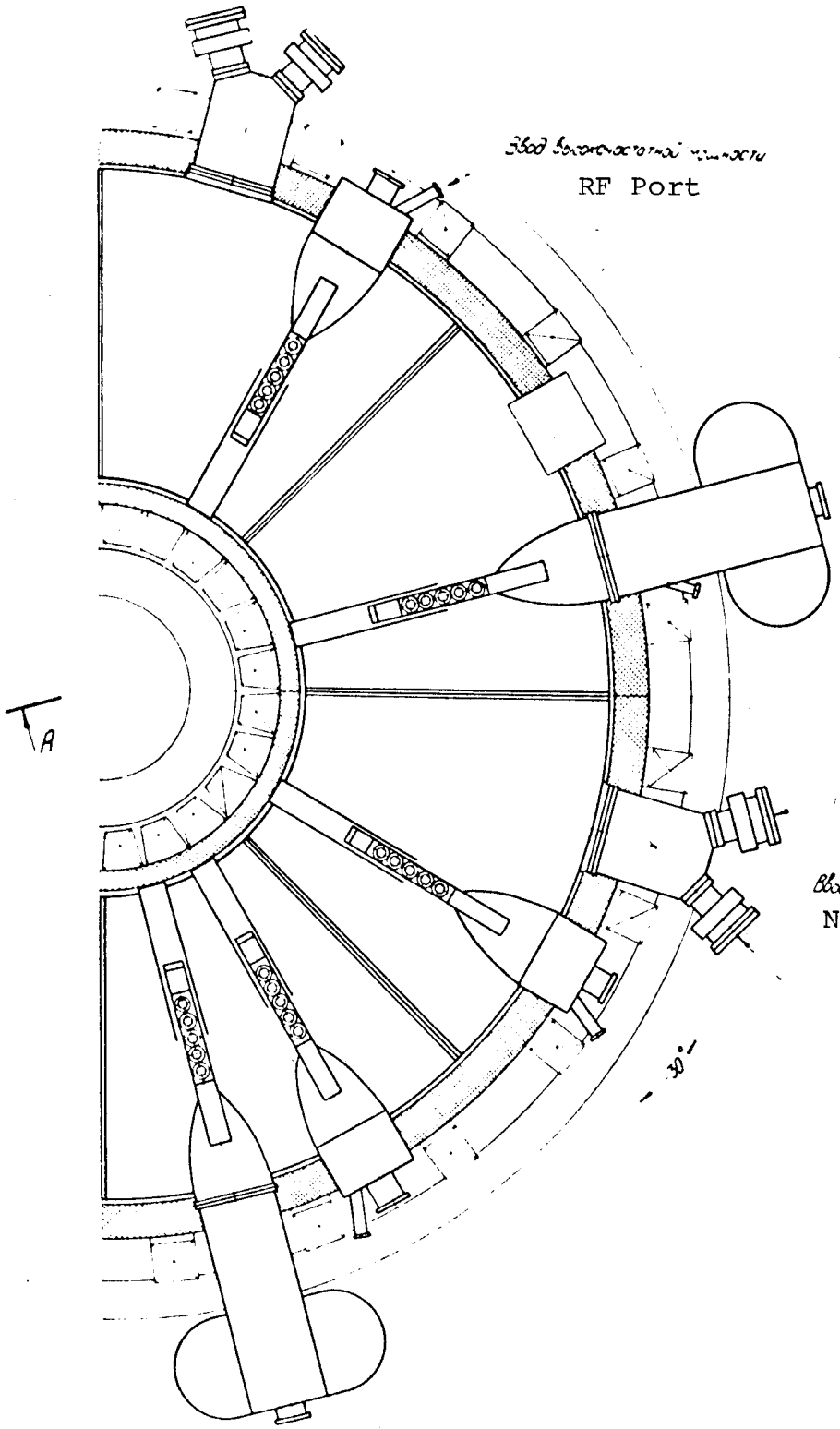

Рис.IУ.I0. Расположение ВЧ-вводов мощности
Fig. IV.10 Distribution of RF ports

allowable power density of 5 kW/cm^2. (At this RF power density, no breakdown has been observed in present experiments on Tokamak devices.)

A. Plasma Heating in the Lower Hybrid Frequency Range

The frequency range in question is $f \approx 10^9$ cycles ($\lambda \approx 30$ cm). The virtue of this method is the fact that it is possible to have effective electromagnetic energy dissipation by means of a linear transformation of the electromagnetic wave into a plasma wave and also in that high power generators of this frequency are easier to build than the millimeter range.

One of the problems in the use of this frequency range for plasma heating appears to be the transport of electromagnetic energy inside the plasma and the creation of the necessary conditions so that this energy will reach the lower hybrid resonance threshold without being dissipated in the surface layers of the plasma.

In order to insure penetration of the electromagnetic energy into the central region of the plasma, the linear theory of wave-plasma interaction imposes some rather strict restrictions on the allowable values of longitudinal wave damping.

$$N_{\parallel \min} < N < 2.2$$

With the presence of a large number of "runaway" electrons, dissipation of a wave propagating in the same direction as the electrons can increase considerably. This can be avoided in principle, if the wave is made to propagate in the opposite direction.

A more suitable arrangement for injecting energy into the plasma and one which conforms to the above formulated requirements is a system of phased waveguides. Calculations indicate that the wave spectrum excited by such a system is relatively narrow and therefore satisfies the required condition. Besides, it is easy to obtain the proper direction of wave propagation by relative phasing of the waveguides. A drawback of such a system is the possibility of having sharp reflections in the waveguides if they are not properly matched with the impedence at the plasma surface.

If there is improper impedence matching, reflections in the waveguides will amount to 80-90%. Avoiding such reflections by conventional methods implies an increase in the field potential of the waveguide and correspondingly, the limit on the power supplied by each waveguide will be more severe because of the problem of breakdown.

Another convenient method of power supply can be imagined, which depends on the fact that it is possible to have an electromagnetic wave propagating between the plasma surface and the corrugated metalic wall of the containment chamber. Damping of such a wave is determined by the plasma surface impedence and by the depth of the metal wall corrugations. Proper damping can be achieved by selecting the correct depth of corrugations.

RF injection in the lower hybrid frequency range is proposed to be accomplished through four ports into the chamber. The width and height of each window is 0.5m by 2m respectively. The RF power transmitted through each port at an operating

frequency of 1000 MC is 15 MW. Two versions of wave launching systems have been considered, an active radiator and a passive system.

The first RF antenna version is a collection of phased waveguide radiators. The radiating ends of the waveguides must be oriented such that the electric component of the high frequency wave (parallel to the narrow dimension of the waveguide) is directed along the magnetic field of the machine. It is proposed that there be six ports horizontally (narrow dimension of waveguide is 8 cm) and eight ports vertically (wide dimension is 25 cm). All waveguides in one vertical row will radiate in phase. Adjacent waveguides in the horizontal rows will be driven out of phase (Fig. IV.11).

Such a system of waveguides will produce a standing wave pattern with an effective damping of 1.8. The damped waves excited in the plasma will propagate along the magnetic field in both directions away from the RF port. The amount of power supplied by each waveguide is 0.3 MW. The maximum potential across the narrow walls of the waveguides (not taking into account reflections) wil be equal to 14 kV and the electric field potential 1.8 kV/cm.

All the waveguides will be differentially pumped from below. Waveguides in one vertical row are joined together by a gridwork of ports. The vacuum connection on the external RF tube is made at the transition point of the coaxial RF tube leading to the generator. Corresponding elements and ferrite connections which protect the generator from reflected power can be integrated into the coaxial system.

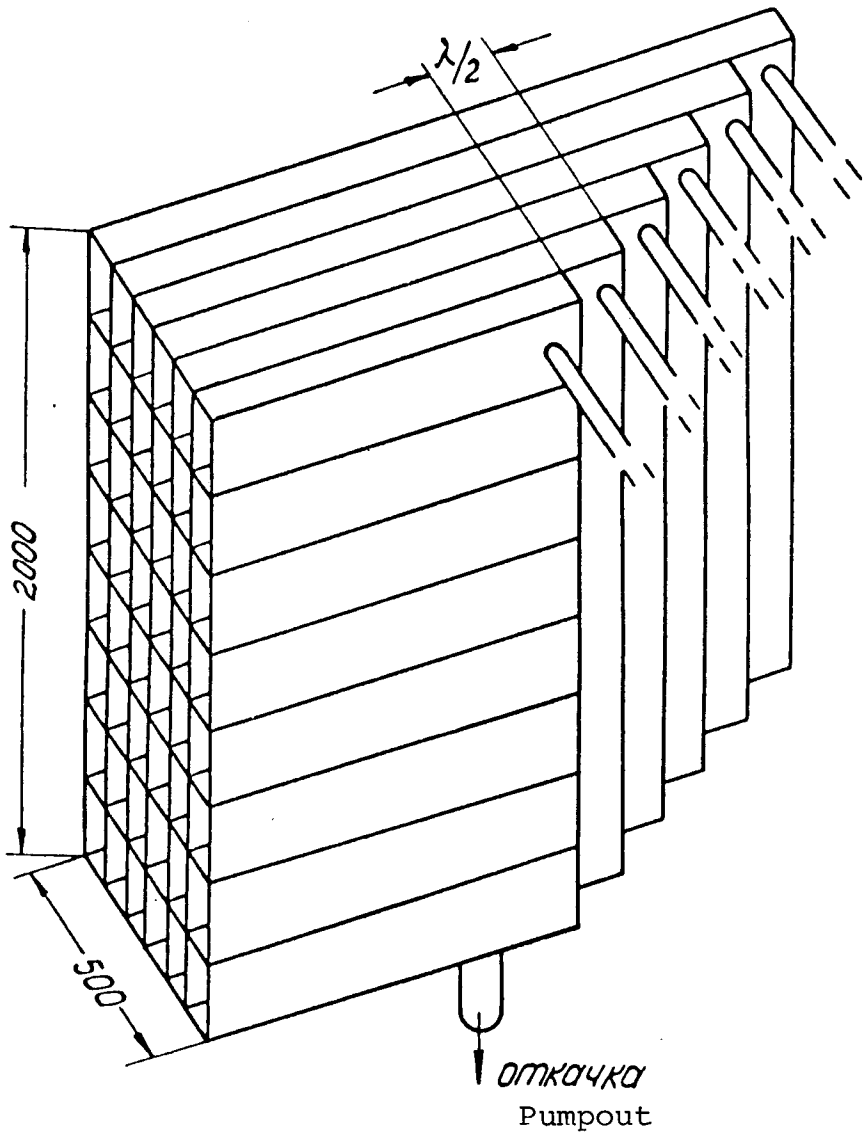

Рис.IУ.II. Комплект волноводных излучателей

Fig. IУ.11 Complex of waveguide radiators

The necessary phase shift between adjacent ports can be accomplished by properly selecting the length of the waveguide sections. In order for adjacent ports to be out of phase, the length of the waveguide must be different by one half wavelength. Since it is necessary to excite a directed wave in the plasma, the field pattern at the exit from the waveguide must have the appearance of a travelling wave. For this reason the phase shift between adjacent waveguides must be $\pi/2$. In order to obtain the required damping, the radiating ends of the waveguides will have to be made half as big and their total number doubled.

It should be mentioned that for such a system, changing the operating frequency over a large range will not change the effective damping. The power in the external regions leading to the waveguides must be in phase. It would therefore make no difference if one 15 MW generator is used or several smaller generators.

The main disadvantage of this system is the difficulty of tuning, that is matching the radiators to the strongly reflecting plasma while observing the phase relationships.

The second variety of antenna is much simpler to construct and regulate. It makes use of a passive retarding system. In this variety the RF power is introduced along a narrow waveguide gap, which could be replaced by a set of vertical waveguides such as the ones described above. The rest of the opening must be closed off by a ribbed metalic surface which has a retarding capability. Calculations show that for

producing retardation of 1.5 - 2 the height of the ribs should be 2.6 cm and the distance between them 2.0 cm. At the same time we assume that the plasma density increases linearly from the edge of the retarding system reaching a value of $10^{13}/cm^3$ at the midsection of the diaphragm. The matching of the external source to the plasma is simplified here, since there are no phase relationships to observe and the number of waveguides is reduced sharply. However, the total power per waveguide increases (up to 2 MW) and consequently the electric field potential in the waveguide is larger and a question as to the effectiveness of retardation from the plasma density distribution near the wall arises. The final choice for the RF antenna will be made after more detailed calculations and experiments are performed.

No provision will be made in the preliminary study for RF injection to provide plasma heating in the ion cyclotron resonance and its harmonics and in the magnetic sonic resonance regions. These systems can be developed during the experimental program on the basis of the use of proposed (in the preliminary report) injection system for RF heating and the ports into the chamber intended for neutral beam injection.

4. Power Supplies for Plasma Heating

For T-20 it is proposed that the same power supplies used for neutral beam injection, to a large extent, can also be used to supply power to the RF generators.

At the present time, the development of the needed generators appears to be within the state of the art. There are well known prerequisites for the building of generators operating in the electron-cyclotron frequency range (3mm wavelength), and the lower hybrid resonance range (30 cm wavelength). It also appears possible to build powerful generators operating on the ion-cyclotron frequency range.

It may be expected that the efficiency of generators operating in the millimeter range can be no less than 20% while it is well know that generators of ten cm or and larger wavelengths can have efficiencies up to 60%. Assuming the losses in the waveguides from the generator to the plasma as being 62%, then the power needed for the millimeter range generator will be 400 MW and the 10 cm and longer wavelength ranges, 150 MW for a total power coupled to the plasma of 50 MW. From these rough estimates, and the estimated needs of the neutral beam injectors it appears that the power supply system can operate in the following modes presented in Table IV.2. The modes presented in Table IV.2 correspond to:

Ia - neutral beam heating with a total power dissipated in the plasma of $\approx$ 60 MW (τ_E = 2 sec).

Ib - neutral beam heating with a total power dissipated in the plasma of $\approx$100 MW (τ_E = 2 sec).

II - two component Tokamak mode with neutral beam injection.

IIIa, IIIb and IIIc - RF heating with total power dissipated in the plasma $\approx$ 60 MW.

IV - two component Tokamak mode with both RF and neutral beam heating. This system can only work if the generator frequency is around 40%.

Table IV.2

Operating Mode	Total Power	Max. Voltage	Polarity	Max. Pulse length	Remarks
1	2	3	4	5	6
1a	160 MW	80 kV	positive	13 sec	Neutral beam
1b	260 MW	80 kV	positive	13 sec	injection at 80 KeV
II	160 MW	80 kV	positve	13 sec	Neutral beam injection at 80 KeV
	190 MW	160 kV	positve	10 sec	Neutral beam injection at 160 KeV
IIIa	400 MW	80 kV	negative	13 sec	RF generator power supply at electron-cyclotron frequency
IIIb	160 MW	30 kV	negative	13 sec	RF generator power supply at the lower hybrid frequency
IIIc	160 MW	20 kV	positive	13 sec	RF generator power supply at the ion-cyclotron frequency
IV	210 MW	80 kV	negative	13 sec	RF generator power supply at the electron-cyclotron frequency
	190 MW	160 kV	positive	10 sec	Neutral beam injection at 160 KeV

As can be seen from Table IV.2, the maximum power needed by the joint plasma heating schemes (IV mode) is 400 MW. Taking the power at 80% efficiency to allow for regulation and stabilization, the total amount required from the power grid is 500 MW.

It should be pointed out that during DT operation, after four seconds of heating it would be possible to partially reduce the level of power needed by either switching off some injectors or RF generators. In a mode of operation when only RF plasma heating will be used (III mode) we are considering the use of only one of the three types of generators, millimeter, decimeter or the radio transmition frequency.

We therefore propose to have a unified power supply which can operate the neutral beam injectors as well as any of three types of RF generators.

To characterize the power supply system for plasma heating we will enumerate the important features which insure the operation of the neutral beam injectors.

The power supply for each injector module (32 modules) consists of a high voltage source, a power supply for the arc discharge, the cathode, the gas injection system and the gas pressure regulator.

1. It is proposed that the high voltage source for each injector module operating at 80 KeV (24 modules) consist of four sources having the following parameters:

a)	source of accelerating voltage I	40 kV
	load current not larger than	100 A
	voltage stability including pulsing	±0.5%

b) source of accelerating voltage II	40 kV
load current not larger than	100 A
voltage stability including pulsing	±1.5%
c) source of decelerating voltage I	10 kV
load current not larger than	5 A
voltage stability including pulsing	±3%
d) source of decelerating voltage II	5 kV
load current not larger than	5 A
voltage stability including pulsing	±3%
2. Maximum pulse length	13 sec
Pulse rate, each	5 min
3. Rise and decay time of the voltage	10 m sec
4. Protection against breakdown in the accelerating system up to one and a half times increase in the current due to normal or a doubled voltage rise rate.	
Voltage switching off time	20 sec
Voltage turn on time after breakdown	20 m sec

5. The power supply must provide for smooth regulation of the accelerating voltage from 10 kV to the maximum value.

6. We are considering the possibility of switching the power supply for the three injectors from 160 kV to 80 kV.

7. Also under consideration is continuous operation at high voltage of the accelerating system during the conditioning period with a current limitation up to $10^{-4} I_H$.

The voltage on the decelerating electrode should not drop below 80% from the nominal value during the short period (about one m sec) when the current rises to 100 A.

II. It is contemplated that the high voltage supply system for the 160 KeV injector modules (12 modules) will vary from the supply for the 80 KeV injectors only in the second stage of high voltage supply. Instead of a 40 kV source, there will be a 120 kV source stabilized to ±1.5% at a load of 100 A.

III. Power supplies for the arc, cathode and the pulsed gas port system with its pressure regulator for each injector module are insulated from the ground and held at either 80 kV or 160 kV. They will have the following parameters.

a) Arc power supply

1. Number of ion source modules	32
2. Arc breakdown voltage	120 V
3. Arc burn voltage	60 V
4. Current	10 kA
5. Stability of the arc current taking pulsing into account	±1%
Current regulation range	1 - 10 kA

b) Cathode power supply

Heating the cathode of each ion source module will require 150 kW and is done at 400 Hz. A scheme for bringing the cathode into operation has to be considered.

The power required for the pulsed gas port system and pressure regulation in the discharge chamber is 2 kW for each module.

V. Control Systems

The dependable and effective operation of all the systems, realization of the given modes of operation, the conduction of the necessary experiments, protection of components and the safety of personnel requires that there be a centralized automatic operation and control system. Equipment and components of various systems will be housed in several buildings scattered over a large area. For this reason, the overall control for the machine must be well developed and have besides a central control room, other control panels located at the various other machine systems. The monitoring and analysis of the existing control systems by various electrophysical means will allow the following functions to be performed relative to the operation of T-20:

1. Independent regulation of any selected parameter.
2. The possibility of independent measurement,to a given degree of accuracy and discreetness,any selected parameter.
3. Complicated manipulation of several devices according to a previously determined program, such as consecutive switching on of various devices which are interdependent in time and amplitude relationships.
4. Complex measurements of several (group) parameters with the possibility of analyzing the results, in the event when the needed parameter is determined by several measurements, but a separately taken parameter of this group does not supply the operator with the needed information.

5. Periodic measurements and control of different parameters and conditions of various systems, which will provide data to help trouble shoot a failure mode or an emergency situation.
6. Periodic tuning (correction) of various parameters to compensate for drift in system components.
7. Production of complicated control functions by various components, for example, during the formation of currents and magnetic fields which vary according to a given function.
8. Optimization of the controls by means of feedback with the aid of a computer.
9. The possibility of analyzing the machine to determine the dependencies of its parameters on the parameters of other systems, in order to find the most effective means of control.

We should add, that in addition to the above functions, the control system must perform other tasks brought on by the peculiarities of the machine and the nature of the experiment performed. Among them are:

- Provide information to all interested parties on the current status of the machine and on the near future plan for changing the mode of operation.
- Storage, analysis and documentation of all available information.
- The possibility of changing the mode of operation to an extent which was not originally planned.
- Protection of system components and creation of a safe environment for operating personnel and users.

It is quite obvious that such a control system must be very flexible and highly developed, depending very strongly on a computer. The control system can be broken down into the following sub-systems:

1. Collection and storage of information on the condition and mode of operation of the machine.
2. Formation and input of controlling data into the different systems of the machine.
3. Collection, processing and analysis of experimental results (information on plasma diagnostics).
4. Organization of massive amounts of information for use by operators.
5. Channels of communication between different machine systems to allow exchange of information.
6. A sub-system of protection and emergency shutdown of the machine.

In this way, the control system for T-20 is standard in many ways. It must be organized into three stages of control (Fig. V.1).

First Stage - Control and operation functions of the machine during all planned modes of operation under the chief operator at the central control panel.

Second Stage - Control and operation functions of each technical system during the shakedown period performed by the local operator at the individual control points.

Third Stage - Control and operation functions of the equipment in each technical system during maintenance and overhaul

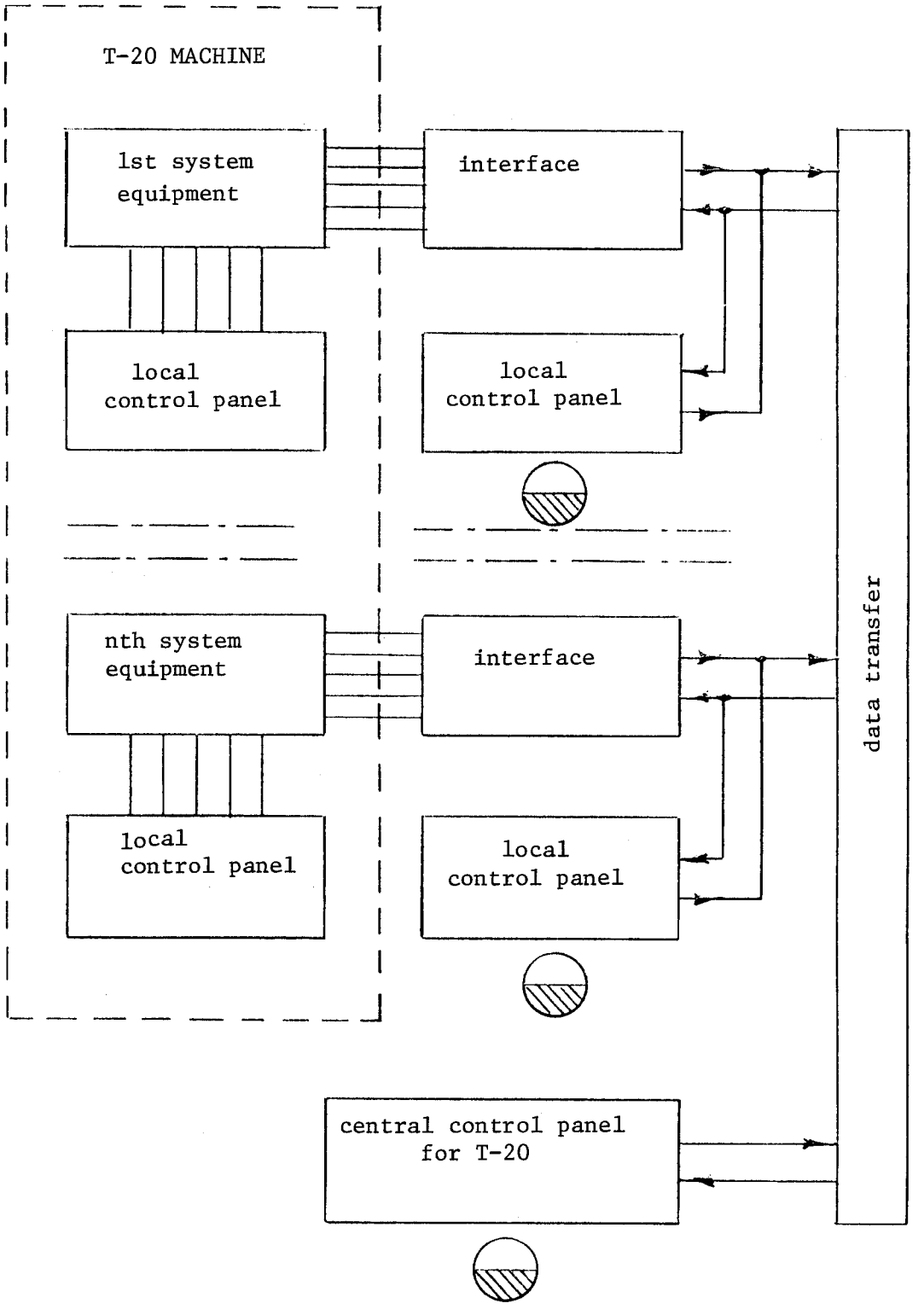
T-20 MACHINE
1st system equipment
interface
local control panel
local control panel
nth system equipment
interface
local control panel
local control panel
data transfer
central control panel for T-20

Fig. V.1

periods performed by service personnel assigned to the given system with the aid of local control panels.

All the local control points must be equipped with special necessary means for the collection and preliminary processing of information and transmission of controlling data to the different system components. In order to simplify the amount of interaction between systems, the control and operation equipment were separated. The system insures the exchange of information between local control points and the central control panel.

The interface between the local equipment and its control points consists of a collection of components which measure the various parameters and turn out the control signals.

Typically, the components consist of various digital to analog and analog to digital converters, counters, recorders, switchboards, level converters, amplifiers and others. The equipment at each local control panel includes various displays on vacuum ray tubes which formulate command signals as well as indicators for digital and graphical information; teletype, switch panels for address selection, printout equipment on paper tape and oscillograms etc. Depending on the nature and the amount of information derived from the equipment, the local control panel may be equipped with a minicomputer of the ES-1010, ASVT-M6000 or the "Electronica-100E" class.

The central control station must be equipped with several powerful computers with large memories. Computers of the ES-1030 class or equivalent could be used. The central control

station is more complex than the local control panels. It will include such items as graph plotters, multi-channel recorders, multi-functional signal generators etc.

During the shakedown and maintenance periods, as well as during preparation of the system for a certain mode of operation, the control and operation functions will depend on the personnel which are normally assigned to that particular system. The local control panels will be an indispensible part of the overall control system. It must be equipped with the necessary technical control equipment, alarm circuits, etc. and must be capable of performing the following functions:

1. Turning on and off system equipment.
2. Checking the operational integrity of the equipment.
3. Preparation of the equipment for inclusion in the overall machine system.
4. Connecting and disconnecting system power outlets with other networks of the machine.
5. Control of the condition and mode of operation of the equipment.
6. Disconnecting the networks from the local control panels and transferring the control function to the central control system.

All the technical systems of the machine will have the necessary amount of regulators and monitors. The regulators, as a rule, are operated by digital code information. It is also possible to operate them with analog signals such as DC potentials provided by special digital to analog converters.

The monitors are divided into three levels, depending on the parameter observed:

1. First level of monitors are the emergency system conditions which threaten to deactivate equipment or harm operating personnel.
2. Second level of monitors keep track of certain limits of operation which do not threaten either equipment or personnel but do disrupt normal operation of the system.
3. The third level of monitors provide information on the normal operation of the system.

The first and second level monitors have alarms activated by contact relays, while the third level monitors, as a rule, provide an output in the form of binary digits.

It would be possible to use monitors which provide an analog output in the form of a DC potential. In that case the analog signals are normalized and converted to digital form.

Monitors of the first and second level as well as the various interlock circuits which protect the condition of the equipment are integrated with the emergency shutdown system. This system is built according to a strict functional design and is divided into several levels which correspond to different modes of operation of the machine. Depending on the complexity of the equipment and its function in the system, the outputs of the interlock circuits are grouped into several interlock circuits. The output of the interlock circuit leads to two normally open block contact relays or

switches which are closed during operation and open when an interlock circuit is activated.

A group of block contacts comprises a successive chain feeding an interlock circuit relay. The other group of the same block contacts generates a signal about the condition of the interlock circuit: if the interlock circuit was not activated (did not work) it gives a level signal "I"; if it was activated it gives a level signal "O". Thus for normal operation a signal "I" is generated while for an emergency situation a signal "O" is generated. The emergency signal will also exist in the case of a malfunction in the interlock circuit (eg. power failure, or a short etc.).

The large number of interlocks and the complexity of the operational circuits between different parts of the system make it difficult for the operator to locate the faulty component. An indispensible piece of information for the operator is the location of the interlock circuit which was activated first, since it triggers the emergency shut down of system components as well as other interlock circuits. Thus, each system must have, in general, several local interlock circuits (see Fig. V.2) integrated into the overall interlock system, and each local circuit must be equipped with a device which can identify the first alarm triggered. The controls of the group relays in the overall interlock circuit are a part of the emergency machine shutdown circuit.

Thus the actuation of the block contact in any circuit produces the opening of the group relay contacts and the

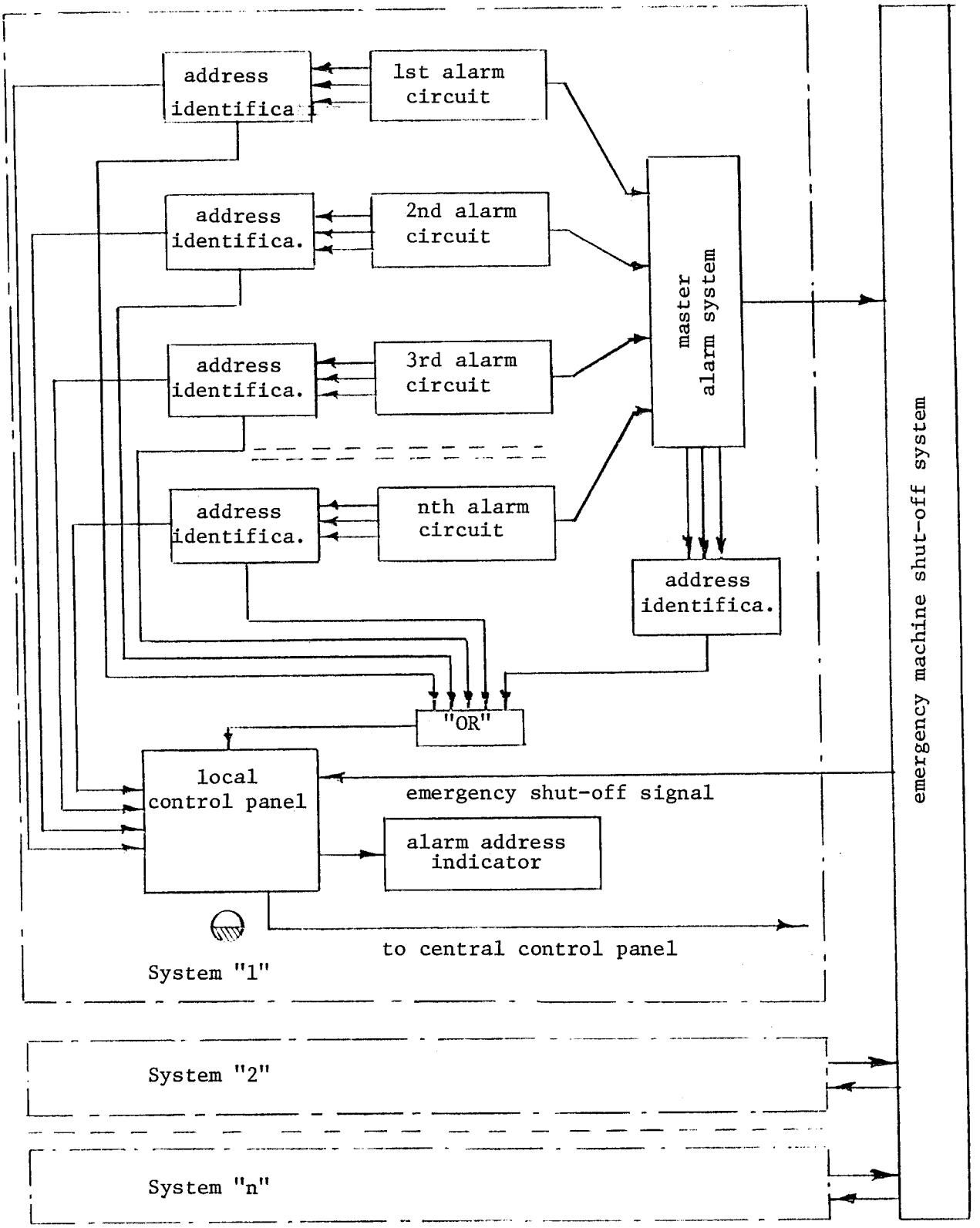
address identifica.
1st alarm circuit
address identifica.
2nd alarm circuit
address identifica.
3rd alarm circuit
address identifica.
nth alarm circuit
master alarm system
address identifica.
"OR"
local control panel
emergency shut-off signal
alarm address indicator
to central control panel
System "1"
System "2"
System "n"
emergency machine shut-off system

Fig. V.2

consequent appearance of an emergency signal at the output of the overall interlock circuit. This signal enters the emergency machine shutdown circuit where commands are then issued for shutdown of the affected components or systems (including those where an alarm circuit was triggered). The "0" signal (emergency situation) appears at the outlet of the circuit which determines the location of the alarm through the "or" logic grid, and is sent to the local control panel indicator which informs the operator of the presence and location of the fault. At the same time the signal also appears on the central control panel.

A great deal of attention has to be devoted to the control and operation system with regards to insuring the safety of personnel, in particular during DT operation and blanket handling. It is therefore imperative that all the equipment and elements of the machine as well as the operating and service areas, furniture and the surrounding air must be under continuous careful control to insure radiation safety and must be closely integrated into the control system of the machine.

The central control operator must at all times have complete information on the degree of contamination of all equipment and buildings. To this end there will be a wide network of control and measurement dosimeters which will monitor fixed equipment located in critical areas as well as the movable systems. All the fixed equipment dosimeters must be equipped with remote control indicators on the central control panel and with a light and enunciator signal equipment which will

give an alarm if the radiation level exceeds the allowable dose. Each local control panel must have an activity level indicator of its own which will be interlocked with a system guarding access to the affected area. Before turning the machine on, the central control panel operator must satisfy himself that all personnel have left all the dangerous areas and must take measures to insure that no one can enter those areas during machine operation. Television cameras will be used to implement those safeguards with monitors at the central control panel, and the doors leading to those areas will be directly interlocked with machine operation, the locks being remotely activated from the central control panel.

If it becomes necessary to perform work on the machine between cycles, the central control panel operator will determine the boundary of the accessible zone and will provide the limitations on the length of exposure for personnel in this zone before giving permission for the work to commence. The entrances into these areas must be equipped with counters which will record the number of people admitted. Thus, if the number of people leaving the area does not agree with the number entering, a signal is generated which will prevent the turning on of the machine. Any equipment leaving the dangerous zone must pass through a special dosimetric box, so that its degree of contamination may be determined.

It is proposed that the T-20 machine be equipped with the following channels of communication:

1. Microwave or telephone communication between the central operator and the local control panel for transmission of operating instructions.

2. Loudspeakers for transmission of operating and administrative instructions in all operation and service areas.
3. A television system for visual observation of operating personnel, especially in dangerous areas.
4. A telephone communication system for transmission of urgent information such as a fire, an explosion or any dangerous situation.
5. Separate channels of communication utilizing head phones and contact speakers for use by personnel to communicate with control panel operators during machine tuning or checking out of components and diagnostic equipment.

All these communication channels must be built on the basis of a multilevel system. Thus, highest priority will be given to emergency information and information originating at the central control room of the machine.

Appendix I
Vertical Field Coil Calculations

Calculation of the VF coils was performed in two steps. In the preliminary step, when all the machine parameters where not yet completely established, we were faced with finding the number and distribution of discreet circular coils and the currents necessary for generating a magnetic field of ≈ 3 G at the vacuum chamber center and a decay index $n = -\frac{r}{B} \cdot \frac{\partial B}{\partial r}$ in the chamber of ≈ 0.5. These control coils were to be situated externally to the D shaped TF coils at a distance of not less than 0.15 m from them, at $r \geq 5.5$ m and $z \geq 1.5$ m ($z \leq 1.5$ m). Regions $4.5 \text{ m} < r < 5.5$ m and $-1.5 \text{ m} < z < 1.5$ m were reserved for other purposes. The region $r < 4.5$ m although not excluded from use for VF coils was crowded with OH windings.

The transverse cross section of the conductors was assumed to be infinitely small and the VF coil was analyzed as a system of separate, circular infinitely small coil bundles. As is well known, the magnetic field components created by a straight circular current in cylindrical coordinates r, φ, z are determined by the product of the current in the coil and a form factor depending only on the coordinates of the coil and the point of observation. Because of symmetry, we will examine only the upper half of the coils. Let S be the number of field observation points situated in a symmetric plane and ℓ, the number of coils in the upper half of the VF system. The field distribution in the plane of symmetry is determined by a system of linear equations relating the magnitude of the currents in the straight circular coils:

$$B_1 = q_{11} \cdot i_1 + q_{12} \cdot i_2 + \ldots\ldots + q_{1e} \cdot i_e$$

$$B_2 = q_{21} \cdot i_1 + q_{22} \cdot i_2 + \ldots\ldots + q_{2e} \cdot i_e \qquad \text{(II.1.1)}$$

$$B_s = q_{s1} \cdot i_1 + q_{s2} \cdot i_2 + \ldots\ldots + q_{se} \cdot i_e$$

The linear dependence of the magnetic field components on the magnitude of the current in the circular coils lends itself to linear programming methods for calculating the VF coils.

At first it is reasonable to determine the magnitude and current distribution which would create a field slightly different from that required. For this we solved a Chebishev approximation system of equations which lends itself to linear programming.[1)]

We will rewrite the system of equations (II.1.1) in the following way:

$$\eta_K(i) \equiv q_{K1} \cdot i_1 + q_{K2} \cdot i_2 + \ldots\ldots + q_{Ke} \cdot i_e - B_K = 0 \qquad \text{(II.1.2)}$$

$$(K = 1, \ldots\ldots s)$$

and we will seek the Chebishev point of this system i* (i_1^*, i_2^*, ... , i_e^*), for which

$$\max_{e \le K \le S} \left| \eta_K(i^*) \right| = \inf_i \max_{e \le K \le S} \left| \eta_K(i) \right| \qquad \text{(II.1.3)}$$

We introduce a new variable i_{e+1} and require that

---

1) S.I. Zykhovitskii, L.I. Ardeeva. "Linear and Convex Programming" Published in "Nanka", M., 1967.

$$|\eta_K(i)| \leq i_{\ell+1} \qquad (K = 1, \ldots, S)$$

ie

$$-\eta_K + i_{\ell+1} \equiv -q_{K1} \cdot i_1 - q_{K2} \cdot i_2 - \ldots - q_{K\ell} \cdot i_\ell + i_{\ell+1} + B_K \geq 0 \qquad \text{(II.1.4)}$$

$$\eta_K + i_{\ell+1} \equiv q_{K1} \cdot i_1 + q_{K2} \cdot i_2 + \ldots + q_{K\ell} \cdot i_\ell + i_{\ell+1} - B_K \geq 0$$

Now we solve the problem of linear programming by minimizing the linear form

$$Z = i_{\ell+1} \qquad \text{(II.1.5)}$$

with limitation (II.1.4) or by maximizing the linear form

$$\bar{Z} = -Z = -i_{\ell+1} \qquad \text{(II.1.6)}$$

with the same limitation as

$$\min Z = -\max \bar{Z} \qquad \text{(II.1.7)}$$

The number of observation points was picked as 23, (S = 23). They were distributed in the plane of symmetry at 20 cm intervals from r = 2.8 m to r = 7.2 m. The coordinates of the straight circular currents (ℓ = 21) were selected along the surface of the TF coil about 8 - 12 cm away, placed at equal intervals in places designated for VF coils. Solution of the system of equations (II.1.4 - II.1.6) by linear programming has shown that a magnetic field slightly different from the one needed can be created by coils with the following coordinates r = 3.14 m, z = 4.2 m (i = 3757 kA) and r = 8.26 m, z = 1.72 m (i = 1402 kA); the currents in the remaining coils were equal to zero. The maximum deviation of the field from the required value was $\approx$ 0.1 kG.

The problem was solved by the simplex method with a maximum and minimum limitation on the value of the currents.

$$i_{min} \leq i_K \leq i_{max} \qquad (K = 1, \ldots \ell) \qquad \text{(II.1.8)}$$

i_{min} was taken as zero, namely, we only considered positive currents; i_{max} was taken equal to 10,000, 720, 600, 480 kA. The presented result is for i_{max} = 10,000 kA; for the remaining values of i_{max}, the field deviation exceeded 0.1 kG.

The results of the solution to (II.1.4 - II.1.6) with various i_{max} show that a magnetic field close to the desired one can be created by currents in several coils for which the coordinates were determined. The currents, however, turned out very high and besides, the field decay index at the edge of the vacuum chamber at r = 7.1 m was ≈ 2.

Since the field decay index in the problem (II.1.4 - II.1.6) was not taken into account, it was decided to solve the same problem in a different way, namely optimizing the decay index while maintaining the field deviation from the desired value at a minimum. It was established that for the indicated trial coils, the decay index at r = 7.1 m must be not less than 1.7.

Since the currents needed to create a field close to the desired one were unacceptable because of their magnitude, we decided to optimize the VF coil for needed power, setting reasonable limits on the deviation of the field.

The following problem was solved by linear programming: namely, minimization of the linear form

$$z = r_1 \cdot i_1 + r_2 \cdot i_2 + \ldots + r_\ell \cdot i_\ell \qquad \text{(II.1.9)}$$

where r is the radial coordinate of the trial currents with the the following limitations:

1) Field deviation

$$-\Delta B \leq -q_{K1} \cdot i_1 - q_{K2} \cdot i_2 - \ldots - q_{K\ell} \cdot i_\ell + B_K \leq \Delta B \qquad \text{(II.1.10)}$$
$$(K = 1, \ldots 5)$$

2) Deviation of the field decay index

$$A'_{K1} \cdot i_1 + A'_{K2} \cdot i_2 + \ldots + A'_{K\ell} \cdot i_\ell \leq 0 \qquad \text{(II.1.11)}$$

$$A''_{K1} \cdot i_1 + A''_{K2} \cdot i_2 + \ldots + A''_{K\ell} \cdot i_\ell \geq 0$$
$$(K = 1, \ldots 5-1)$$

where

$$A'_{mn} = b_1^{(m)} \cdot \tfrac{1}{2} q_{m-1;n} + a_1^{(m)} \cdot \tfrac{1}{2} q_{mn};$$

$$A''_{mn} = b_2^{(m)} \cdot \tfrac{1}{2} q_{m-1;n} + a_2^{(m)} \cdot \tfrac{1}{2} q_{mn};$$

$$a_1^{(m)} = n_1 + \frac{r_{m-1} + r_m}{r_m - r_{m-1}}; \qquad a_2^{(m)} = n_2 + \frac{r_{m-1} + r_m}{r_m - r_{m-1}}$$

$$b_1^{(m)} = n_1 + \frac{r_{m-1} + r_m}{r_m - r_{m-1}}; \qquad b_2^{(m)} = n_2 - \frac{r_{m-1} + r_m}{r_m - r_{m-1}}$$

Here r_{m-1} and r_m are radial coordinates of adjacent observation points, n_1 and n_2 are limiting values of the decay index. Allowable values of Δ B where from 0.12 - 0.5 kG; n_1 was equal to zero and n_2 was varied linearly from 0.8 for r = 2.9 m to 2.3 for r = 7.1 m.

A satisfactory result was obtained for $\Delta B = 0.3$kG. A field which has a maximum deviation of 0.3 kG can be realized with straight circular currents with the following coordinates:

1. r = 2.9m $\mathcal{Z}$ = 4.08m (i_1 = 720 kA)
2. r = 5.72m $\mathcal{Z}$ = 4.40m (i_2 = 720 kA)
3. r = 5.92m $\mathcal{Z}$ = 4.33m (i_3 = 381 kA)
4. r = 6.10m $\mathcal{Z}$ = 4.24m (i_4 = 262 kA)
5. r = 8.23m $\mathcal{Z}$ = 1.92m (i_5 = 625 kA)
6. r = 8.30m $\mathcal{Z}$ = 1.74m (i_6 = 720 kA)

It is evident that the second, third and fourth coils are close together as are the fifth and sixth.

The obtained results were used in the second step for calculating the VF coils, when the physical and constructional parameters were more accurately known. The field at the denter of the vacuum chamber was taken as 4.2 kG; the coil cross-sectional area was determined to be 30 x 280 mm^2 and the maximum supply current as 120 kA. The method of linear programming was used in the second stage of calculations also. Solutions for equations (II.1.9 - II.1.11) were sought with the limitation $\Delta B = 0.3$ kG, $n_1 = 0$, $n_2 = 0.8 - 2.3$, and the coordinates of the coil centers were taken as three separate groups, more representative of the actual case, based on information derived in the first stage of the calculation.

Appendix II

Automatic Control of the Location of the Plasma Toroid in T-20

In T-20, as well as in other fusion reactors, it is reasonable to maintain an equilibrium location of the plasma toroid with the aid of automatically controlled magnetic fields. In the absence of a copper sheath, the following parameters should be closely controlled during a discharge:
(a) the equilibrium horizontal position of the plasma toroid
(b) preservation of the plasma shape and
(c) stabilization of the plasma toroid in the vertical direction.
To accomplish this, it would be necessary to use magnetic field control systems such as feedback as well as other means of automatic control (variation of the exitation etc.).

Experience has shown that the use of automatic regulation for maintaining equilibrium of a plasma toroid within a high degree of accuracy entails a system which would allow simultaneous control of several components of the transverse magnetic field. A reasonable approach is to control the following components of the field: a) Dipole (vertical) component $H_{\perp}$, to insure stability along the major radius;
b) Quadrupole H_q, which creates the necessary vertical field gradient in the horizontal plane of symmetry, thus controlling the cross sectional shape of the plasma;
c) Horizontal component $H_{\parallel}$ which establishes equilibrium of the plasma toroid relative to the horizontal plane.

All these fields must be as uniform as possible around the circumference of the toroid in the azimuthal direction.

1. General Principles of the Control System for Regulating the Position of the Plasma Toroid in the Discharge Chamber

The control system for regulating the position of the plasma toroid will consist of the following sub-systems:

I. Horizontal direction control sub-system

II. Cross-sectional plasma shape control sub-system

III. Vertical direction control sub-system

The horizontal control sub-system must insure the creation of a transverse magnetic field on the toroidal axis equal to $H_\perp \approx H_{\varphi_0}$, where $H\varphi_0$ is the value of the toroidal field at the upper and lower extremities of the plasma. For T-20, $H\varphi_0 = 6 \times 10^{-1}$ T. If one were to create such a field exclusively with automatic compensation coils based on feedback, then for extremely fast responses, very large amounts of power will be needed in the controlling equipment.

It is therefore useful to seek a means of alleviating this heavy requirement on the automatic compensating system. We should take into account the experimentally observed time dependent dipole component of the vertical field which insures plasma equilibrium in the horizontal direction and which, although an intermitent function changing from discharge to discharge, nevertheless falls within a limited region as shown in Fig. 1.

The cross-hatched region in Fig. 1 represents the area in which the dipole component of the vertical field lies, while the dashed line gives a possible equilibrium value of the vertical field. The solid line gives one set of the calculated values.

It is proposed that the main portion of the dipole component of the vertical field be generated according to a predetermined program. The compensation needed by the vertical field to maintain an equilibrium position of the plasma will be generated by the automatic compensation system. A similar scheme can be used by the sub-system designed for creating the quadrupole component of the magnetic field which is used to give the proper cross sectional shape to the plasma toroid. As regards the vertical control sub-system, it should be recalled that T-20 has a horizontal plane symmetry and consequently, vertical instabilities in general will occur infrequently. As a result, it seems reasonable to use an automatic compensating system based on feedback, without any preliminary programming.

Let us now examine the general principles for building the system in question.

In building the equipment needed to program the vertical field, it is necessary to provide the capability for changing the program within the above indicated dynamic range in the intervals between pulses or a series of pulses. This will make it possible to produce a program which will give a field with the least deviation from that needed for stability.

Correspondingly, because of the more accurate programming, the dynamic range covered by the automatic compensating system will be smaller. This will reduce the load on the automatic compensating system and consequently, make it faster and more accurate.

To generate the controlling components of the vertical field (vertical, horizontal and quadrupole) it is necessary to locate coils external to the vacuum chamber. These coils, hereafter referred to as compensating coils can be located between the shield and the TF coils, or they can be external to the TF coils. Naturally, for better magnetic coupling with plasma, it would be more suitable to place the compensating coils closer to the discharge chamber. However, this kind of placement can lead to large mechanical forces existing on the compensating coils, determined by the equation

$$F = \pi n . b_c . I_c . B_z$$

where n is the number of turns in the compensating coil; I_c is the current in the coil; b_c the minor toroidal radius on which the coil is located and B_z is the vertical field strength. For T-20, the value F can reach $5 - 10 \times 10^3$ Tonnes. It would be necessary to take special measures for attaching these coils which will complicate the construction as well as the assembly and disassembly. External coils carrying larger currents would have to be used which will reduce their coupling with the plasma. At the same time it would increase the power requirement in the coils.

The automatic compensating coils will have to be located between the shield and the TF coils. Since the currents in them are relatively small, the forces acting on the flat junctions between coils are considerably smaller (< 500 T). Fastening of such coils is not very difficult. On the other hand, if these coils were to be located outside the TF coils, then they would require the development of powerful regulators, which in this case appears unreasonable.

The above considerations have thus led us to the following scheme for locating the VF coils (Fig. 2).

VF_1 - is the coil programmed to give a poloidal field with the necessary gradient.

VF_2 - is the coil which gives an automatic uniform compensating poloidal field.

VF_3 - is the coil which gives an automatic compensating quadrupole magnetic field component for maintaining a properly shaped plasma toroid.

VF_4 - is the coil which gives an automatic compensating field for vertical position control.

Each of the compensating coils has an independent converter or an automatically controlled power supply. For more effective control, it is necessary that VF_1 be magnetically decoupled in operating frequency from VF_2 and VF_3. This can be accomplished either by an experimental set up to find the proper coil orientation or by an external decoupling arrangement.

The system for the automatic compensation of the plasma toroid in the TO-1 Tokamak used feedback to keep the plasma

centered on axis. Such a system in principle insured equilibrium, however, an accurate means for horizontal stability was not achieved. As the plasma parameters changed and as the currents in the OH coils and the fields in the adjoining magnetic elements decayed, the position of the magnetic axis changed drastically. Taking this into account, special measures are being taken in T-20 by the use of a more sophisticated compensating system for the control of the equilibrium position of the plasma toroid relative to the major radius. This system will maintain an accurate position of the plasma toroid relative to the geometric axis of the machine during the duration of the pulse. The controlling mechanism will not only be the deviation of the plasma toroid from the magnetic axis but other changing plasma parameters as well. At the same time, tighter regulation will be observed taking into account the inertial effects of the machine elements. In other words, if the correction process is to be organized properly, it is necessary to have a good model of the controlled object, allowing for accurate formulation of compensating signals. Such a model of the controlled object, consists of an analog computer complex which formulates the required compensating signals and actuates automatic regulators. All of these sub-systems will form a fast acting multicircuit arrangement of controls.

At the same time the system will have a slow acting circuit which will allow us to vary the given dynamic range within certain limits, in the programmed external coils. This can be done between pulses.

The indicated system of automatic regulation places an additional requirement on the measurement apparatus. In the past (TO-1), we have used measurement systems which allowed us to regulate the deviation of the plasma toroid from the magnetic axis. This is inadequate in T-20. Thus, in addition to this sort of information, which is obtained by current free coils of the same shape as VF_2, VF_3 and VF_4, it would be necessary to obtain continuous information on the plasma current and certain other plasma parameters such as the ratio of the stagnation gas pressure to the magnetic pressure, charges in the diamagnetic flux of the toroidal field, self inductance of the plasma toroid etc. In addition, we must understand the decay modes of the currents in adjacent components induced by the time varying fields of the VF coils and the plasma itself. In other words, one must know the transfer functions of the decaying and reflected fields of all the energized elements in the machine.

2. Operating Scheme for Automatic Regulation of the Position of the Plasma Toroid

The control system which regulated the position of the plasma toroid in T-20 insures the equilibrium of the plasma relative to the major radius and stabilization of this equilibrium position. The controlled parameters are: the position of the toroid relative to the geometric axis of the chamber and the major radius of the toroid, the position of the toroid relative to the horizontal plane of symmetry and the cross-sectional shape of the plasma.

On Fig. 3 is shown a block diagram of the control scheme which accomplishes the above requirements. This system can be described as a multicircuit, self tuning and regulating arrangement acting on the controlled object. It consists of three major parts (Fig. 3a), the controlled object (O), the computing complex (CC) and the regulator (R). The diagram also shows the device which generates the program (P) for the VF coils.

As previously mentioned, the control system is divided into three sub-systems. Each sub-system will be traced out on the operating schematic (Fig. 3b) as a separate controlling circuit.

Sub-system (I) which controls the position of the plasma toroid in the horizontal direction is contained in circuits 2, 5 and 6. Sub-system (II) which controls the cross sectional shape of the plasma is contained in circuits 1, 4 and 7. Finally, sub-system (III) which controls the vertical position of the plasma is confined to circuit 3.

As was previously indicated, sub-systems I and II act in combination on the plasma toroid. Circuits 6 and 7 are used to control the plasma toroid position by the use of the vertical magnetic field which varies according to a predetermined program. Adjustment of this program between pulses or series of pulses is made by means of circuits 1 and 2. Circuits 4 and 5 are used for operational control of the plasma toroid during discharge.

Circuits 6 and 7 are not related to the automatic position control system and will not be discussed further.

The controlled object (O) consists of a system of loops with transfer functions: W_{OR}^*, W_{OQ}^* are coil transfer functions which generate the programmed dipole and quadrupole components of the vertical field respectively; W_{OR}, W_{OQ}, W_{OZ} are coil transfer functions which produce automatically regulated dipole, quadrupole and horizontal components of the vertical field respectively.

The dynamics of the plasma toroid within the above degrees of freedom and its interaction with the surroundings is represented in the form of loops with the corresponding transfer function W_R^*, W_Q^*, W_R, W_Q, W_Z.

The control object also includes the external electromagnetic decoupling system (MDS) of the vertical field coil VF, (for which transfer functions W_{OR}^* and W_{OQ}^* apply) with coils VF_2 (W_{OR}) and VF_3 (W_{OQ}).

The regulator R includes the system of independent energy converters which are represented as loops with transfer functions: W_{CR}^*, W_{CQ}^*, W_{CR}, W_{CQ}, W_{CZ}.

The computing complex (CC) consists of the following blocks: PM, a partial object model; SM, the standard object model; DB difference block; CSB controlling signal block.

According to the function of each sub-system, the current status of the controlled object is described by three outputs: $\Delta_R(t)$, the displacement of the plasma toroid axis from the geometric axis of the discharge chamber; $\Delta_Z(t)$, the vertical displacement of the plasma horizontal plane from the chamber

horizontal plane; $\Delta_q(t)$ a general coordinate output characterizing the change in the cross-sectional elliptical shape of the plasma.

All the parameters which effect the equilibrium of the plasma toroid can be divided into two groups: factors which are continuously present and factors which are present during start up. The first group inclues I_o, the plasma current; a, minor plasma radius; ℓ_{io}, ℓ_{il} coefficients of plasma self-inductance corresponding to the longitudinal and transverse constituents of the plasma current respectively; B_{Io} the ratio of the average gas stagnation pressure to the magnetic field pressure. The second group of parameters form the initial toroidal geometry at the moment of plasma discharge.

We propose to have measuring devices which will produce complete information on the condition of the controlled object, relative to the coordinate system Δ_R, Δ_q, Δ_z, and the pertinent parameters I_o, a, ℓ_{io}, ℓ_{il} and B_{Io}. At the same time, gages will display independent signals of some of the above parameters, which are represented on the schematic at the vector $\vec{Q}$ (Δ_R, Δ_q, Δ_z, I_o, a, ℓ_{io}, ℓ_{il} and B_{Io}). The quantities I_R, I_q and I_Z on the schematic are currents in VF_2, VF_3 and VF_4 respectively; δI_R, δI_q are induced currents in VF_2 and VF_3 resulting from incomplete electromagnetic decoupling between these coils and the VF_1 coil in the external decoupling circuit (MDS). These currents comprise vector $\vec{u}$ which acts on the control object.

Vectors $\vec{u}$ and $\vec{Q}$ are only preliminary data concerning the control object. On the basis of this data, and with the aid of the computing complex, it would be possible to identify the object and formulate the best controlling function by means of the regulator (R).

The computing complex will solve the following main problems:

1. Analysis of the measured parameters regarding the location of the control object and the reactions on it with the aim of obtaining more complete information. This problem is solved with the aid of the partial object model (PM). The resulting signal at the output of (PM) consists of (a) coordinate vector $\vec{x}$ (Δ_R, Δ_q, Δ_z) representing the status of the object and (b) a vector function of the constantly present parameters $\vec{f}$ (I_o, a, ℓ_{io}, ℓ_{il} and B_{Io}).

In addition, the (PM) block performs a total separation of the currents I_R, I_q, I_z, δI_R and δI_q, formulates the vector $\vec{u}$ which characterizes the present values of currents in the VF coils generated by regulator (R) and the currents induced in them by electromagnetic coupling

The (PM) block also generates a vector signal of the generalized parameters which characterizes all the changes in the plasma controlling quantities of the plasma toroid.

2. Identification of the controlled object with the aim of formulating the best controlling signal and improving the programmed magnetic field generated by the currents in the

external VF coils. This problem is solved with the aid of an analyzer block (A) which analyzes the vector signals of the present parameters and compares them with those of the full standard model (SM). The analyzer (A) generates the signals for tuning the model object, that is the signals for adjusting the regulator output and the signal for improving the program of the external coils (vectors $\vec{y}$ and $\vec{z}$). The full standard model is really a mathematical model of the control system for the plasma toroid position, which provides the basis for the correction signals $\vec{U}_o$ (t) and ΔU_R and ΔU_q. These dependencies will be narrowed down as operating experience on the model is gained.

The difference block (DF) determines the variation in the parameters, $\vec{\varepsilon}$, obtained by comparison of the standard model with the actual measured parameters of the controlled object.

The controlling signal block (CSB) acts to change the controlling signal in order to zero in on the final model. The output of the (CSB) produces a signal ΔU which diminishes as the model is refined.

3. Controlling and Measuring Coils of the Automatic Control System

We examine the system of vertical field coils VF_2, VF_3 and VF_4 intended to stabilize the location of the plasma toroid and its cross sectional shape as well as coils MF_2, MF_3 and MF_4 which measure the vertical, quadrupole and horizontal components of the magnetic field respectively. Each of the coils mentioned, either creates or measures the respective components

of the vertical field. Thus, the position of the coils around the minor radius of the torus is critical to the functions for which they are intended. In addition, all these coils must be as uniform as possible in the φ direction (toroidal direction).

To stabilize the plasma toroid relative to possible changes in the major radius, it is necessary to have a vertical field. Taking into account that in T-20, the value of $\frac{a}{R} = 0.4$ (i.e. aspect ratio is large), the vertical field must be nonuniform with R. The degree of decay depends on the current distribution along the plasma cross section. Therefore, during the discharge process as the current distribution changes in the plasma cross section the vertical field gradient must change. It is also necessary to point out that the penetration of the dipole and quadrupole components of the magnetic field into the chamber have a certain time constant. These considerations as well as the need for keeping a low profile for the plasma cross-sectional shape, necessitates the independent creation of a uniform vertical and a gradient component of the vertical field. It appears that the main change in the transverse shape of the plasma cross section is related to the $m = 2$ mode, which is associated with the appearance of an elliptically shaped plasma. For this reason we propose to have two independent coils for the creation of the vertical field. One coil will create a uniform vertical field and the second, a quadrupole component of the transverse field. By controlling the currents in each of the

coils independently, it will be possible to stabilize the position of the plasma toroid on the machine axis and maintain the circular shape of the plasma.

It is well known that a uniform transverse field in a cylindrical geometry can be created by cosinosoidal current distribution with m = 1. In the case of a toroid, this rule changes. Correspondingly, a quadrupole component of the magnetic field in a cylindrical geometry can be created with nonuniform current distribution which is also cosinosoidal with m = 2. This also has to be changed for a toroidal geometry. The coil which generates the horizontal magnetic field serves to stabilize the plasma toroidal position in the vertical direction. This field should be as uniform as possible.

The shape of the measuring coils is similar to the shape of the VF coils, but they can be placed in a different way. They can, for example, be located either between the chamber and the shield, or in the diagnostic ports. These coils are only used to measure the respective components of the magnetic field. They are practically current free and consequently do not experience electromagnetic forces and can be located in regions of large neutron flux.

4. Magnetic Calculations of the Automatic Control of the Position of the Plasma Toroid

Calculations were performed in the following manner:
a) solution of the problem of special distribution and assembly of the VF_2, VF_3 and VF_4 coils in the available space.

b) calculation of the inductances, currents, power etc. taking into account the positions of the coils and the magnetic field requirements.
c) optimization calculations with regard to minimizing power requirements in the control circuits and maximizing the reproducibility of the magnetic fields.

The principle of super-position was used to calculate the fields and the elementary source was taken as the current in a circular coil. Field strengths and currents in the VF coils were obtained by solving a system of algebraic equations. The optimum position for VF_2, VF_3 and VF_4 from the standpoint of conservation of power is shown in Fig. 2.

The obtained distribution of VF coils insures the reproducibility of the transverse magnetic field in the plasma cross section over the diameter of the machine to within 20% for VF_2, which creates the vertical field, 25% for VF_3, which creates the quadrupole component and 10% for VF_4, which creates the horizontal magnetic field. Regardless of the indicated deviation in the reproducibility of the correcting fields, we expect that with their aid, we will achieve a stable equilibrium position and reduce the possibility of plasma cross-sectional shape distortion by a factor of 3 - 5.

It would be possible to improve the reproducibility of the components of the transverse field maintaining the same power requirement in the control system, if the restricted areas (shown cross-hatched in Fig. 2) were made smaller.

Another means of accomplishing the same aim, (to about 1% accuracy) is by a more complex distribution of the current in the coils (by using counter currents). However, this will inevitably lead to a higher power requirement. Preliminary indications are that the power level will increase $\approx$ 70% for the vertical, 100% for the quadrupole and 50% for the horizontal components of the field. The results of calculations for the VF control coils and their electrical and mechanical parameters are presented in Table I. Analysis of the ohmic heating of the VF_2, VF_3 and VF_4 control coils shows, that with adequate neutron shielding, they can operate without forced cooling.

5. Current Regulation in Control Coils of the Transverse Magnetic Field.

Preliminary values of power for figuring the current regulation in the control coils as taken from Table I were: 62 MVA for VF_2, 23 MVA for VF_3 and 15 MVA for VF_4. The total power is 100 MVA. The power supply voltages and currents are 30 kV, 2.1kA for VF_2, 25 kV, 0.9 kA for VF_3 and 20 kV, 0.75 kA for VF_4.

For the given currents and voltages the operating mode of the final phase of the regulator should be regarded as the key which determines whether the control field coil will have the power supply voltage across it, or if the voltage will be shunted through low impedance circuits within the regulator. A characteristic of this type of operation is that the low impedance of the coil circuit gives it a rather large time

constant for the decay of currents induced by uncontrolled displacements of the plasma toroid. Thus, for example, the smallest time constant (for VF_2) is $\tau = \frac{L}{R} \approx 1$ sec. This is about the order of time (without correction) it would take the plasma to move a distance equal to the minor radius. In 10 - 20 m sec of uncontrolled mode, the plasma can move a distance of ±5 cm, which is entirely tolerable for this machine.

The time constant of the vacuum chamber, although not yet determined, will probably not exceed $\tau_c \approx 0.5$ sec and thus cannot be counted on to give any damping action. There is no need to take into account plasma displacement without magnetic field penetration of the chamber wall and coil, caused by changes in plasma temperature and current in the stationary regime. It is true, the allowable plasma displacement (±5 cm) due to these factors can happen in less than 0.3 - 0.5 sec, but this time is much greater than the response time of the current regulator and will therefore not take place.

On the basis of the above data, it is possible to assert that a response time of 10 - 20 m sec for the regulator of the vertical field current is entirely adequate since the plasma displacement in this time space is within tolerable limits. Realization of such a response may be impeded by the time constant of the chamber. If it is the order of $\tau_c \approx 100$ m sec, then for handling fast disturbances, say $\tau \approx$ 10 - 20 m sec, the dynamic range of the regulation will be reduced (5 - 10 times).

Response times not less than those indicated can be produced on a simple multiphase controlled rectifier utilizing thyristors. This scheme has the following advantages: it does not require intermediate devices to rectify the alernating current supplied to theccircuits, neither does it require intermediate energy storage systems; the possibility of using commercially available multiphase power transformers of the required capacity;the use of contemporary switching elements with relatively low losses. All these advantages point out the need for developing a current regulator of the multiphase controlled rectifier type, in particular since the design of a linear amplifier capable of handling 50 MVA is difficult at the present time.

A block diagram of the regulator is shown in Fig. 4. The energy supplied is converted into multiphase voltages by power transformers, goes through a thyristor controlled multiphase rectifier (2) on the way to the load (4) (one of the coils) which fortunately is inductive. In order to achieve the desired current in the load, it has truncated cosinusoidal voltage pulses of various lengths and amplitudes applied to it. These pulses are generated in (2). The control of the firing of the thyristors in rectifier (2) originates in block (3) which insures that the thyristors fire in phase with the system of multiphase outputs of the transformer. Block (3) is regulated by the circuit in block (6) where the actual current is compared with the desired current in the load. The integrating loop (5) smooths out the pulses. The regulator circuit will

also have an amplifier (7) for the incoming signal, a high frequency filter (8) and a filter control circuit (9). Block (10) is a protection circuit for the rectifier and the load, as well as the signal generator and the supply for the low powered circuits.

Time curves depicting the principle of operation of the regulator is shown in Fig. 5. The signal for increasing the current occurs at t_1. Starting with t_3 it is possible to make a controlled reduction of the current in the load by applying a reverse phase voltage. Between t_2 and t_3, the load receives a forward phase voltage pulse lasting $\tilde{\tau}_{max}$ = 5 m sec (cross-hatched region on Fig. 5). Thus, reduction of the current in the load before t_2 is not possible, however, this period lies within the indicated fast response time of the regulator.

Table I

Table of Calculated Parameters of the System

Parameters of VF control coils	Preliminary number of turns / coil	Coil cross section	Field strength at given current	Current in coil	Self inductance	Resistance	Voltage components		Power components		Energy / pulse	Force on junction between coils
							Inductive	Active	Re-active	Active		
		mm^2	kA/m	kA	H	m	V	V	MVA	MW	MJ	Tonnes
VF_2	100	30 X 20	300 Oe (24)	263	55	0.05	289.3	13.15	58.7	3.45	25	400
VF_3	40	60 X 30	120 Oe (9.6)	338	154	0.05	624	1.7	21.1	0.57	1.23	25
VF_4	50	40X 30	150 Oe (12)	343	79.4	0.05	418	1.7	14.3	0.58	1.22	120

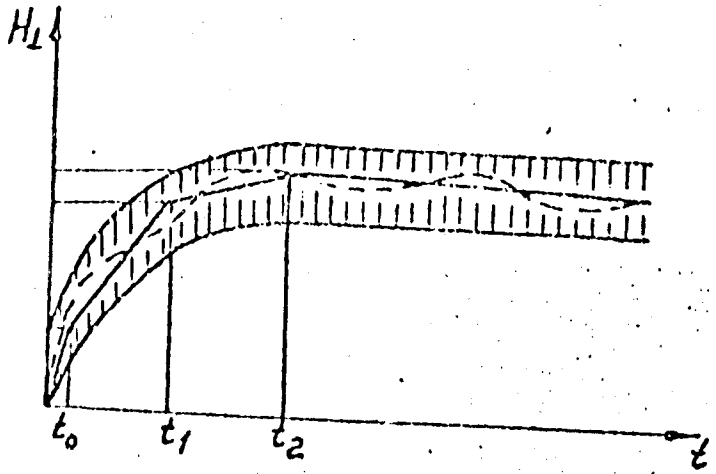

Рис. 1

Fig. 1

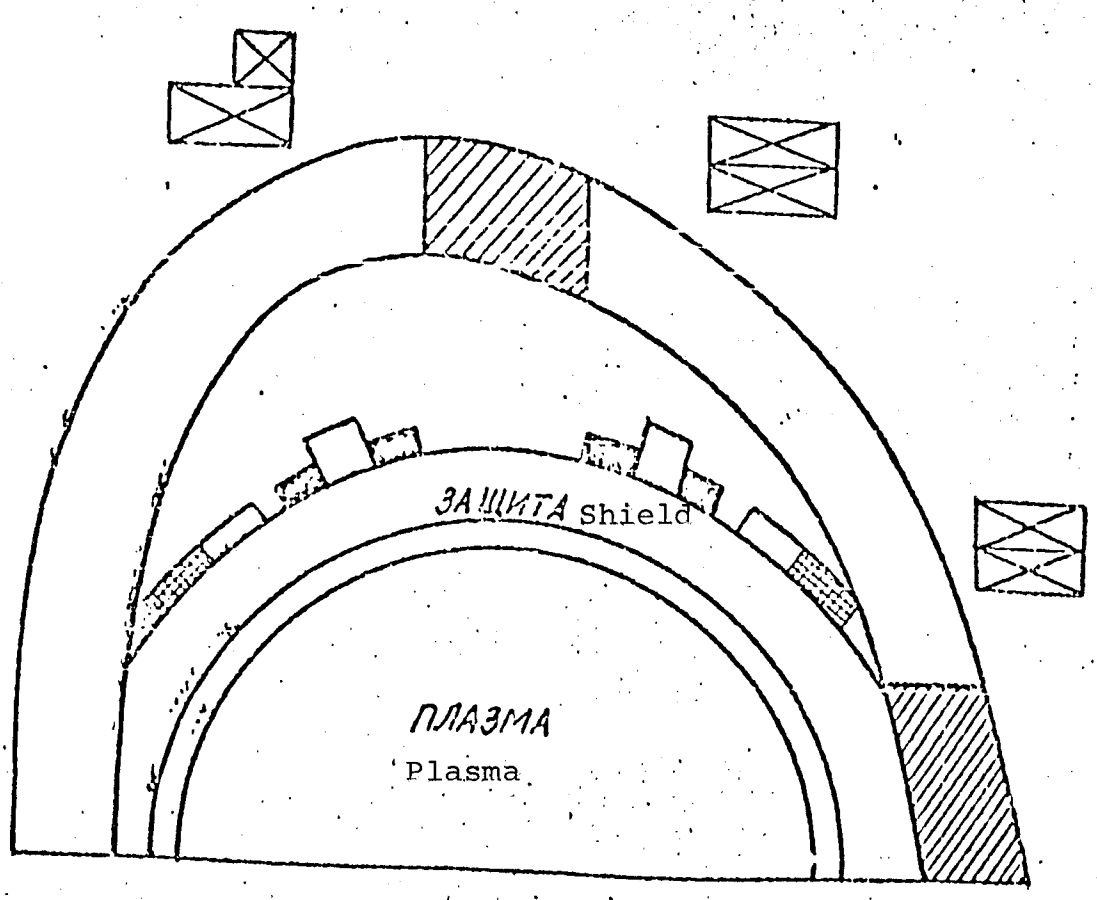

Fig. 2 Рис. 2

Расположение управляющих обмоток

Distribution of controlling coils

— $УО_1$, — $УО_2$, — $УО_3$, — $УО_4$

VF1 VF2 VF3 VF4

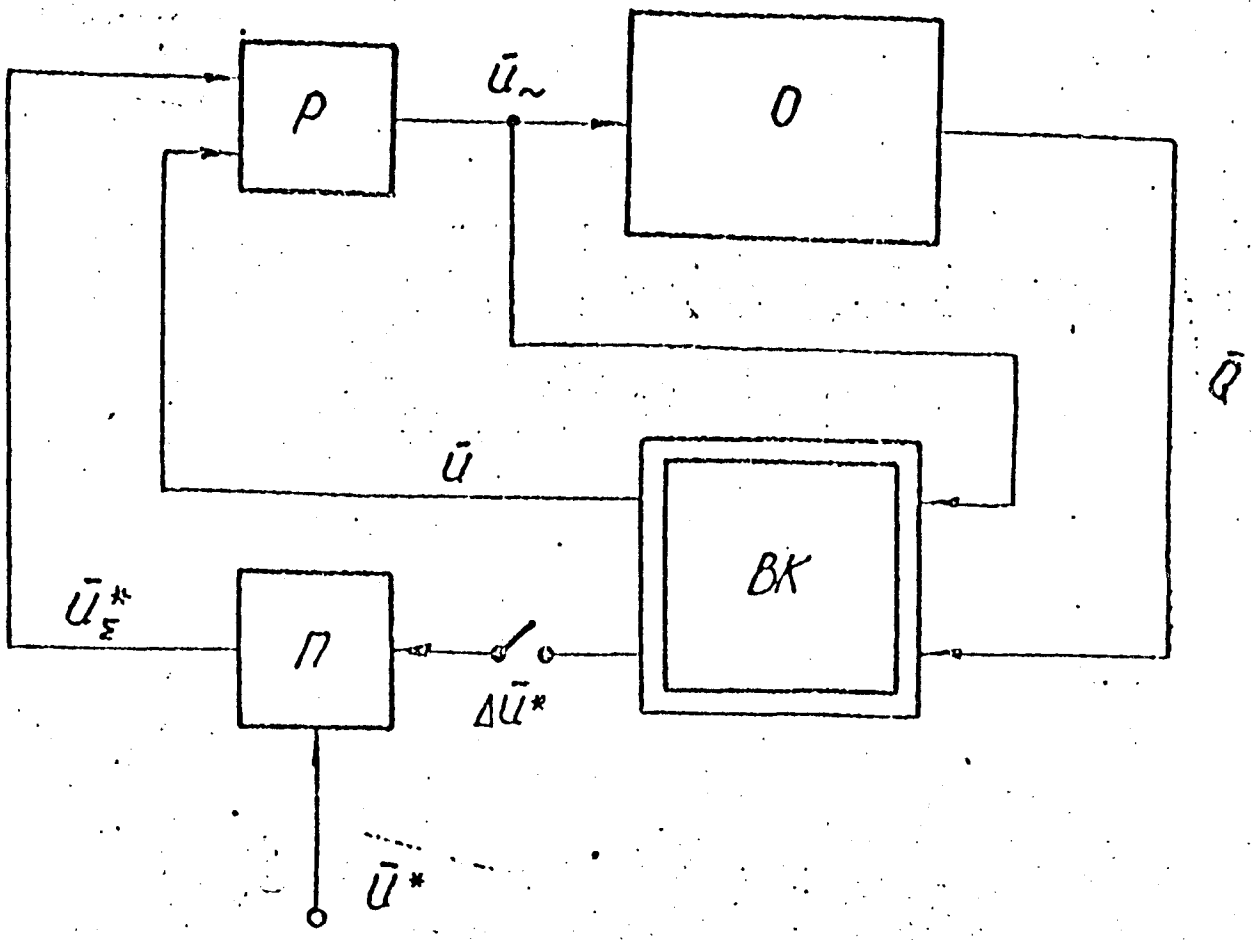

Fig. 3a Рис. 3а

Блок-схема системы управления

Block diagram of the control system

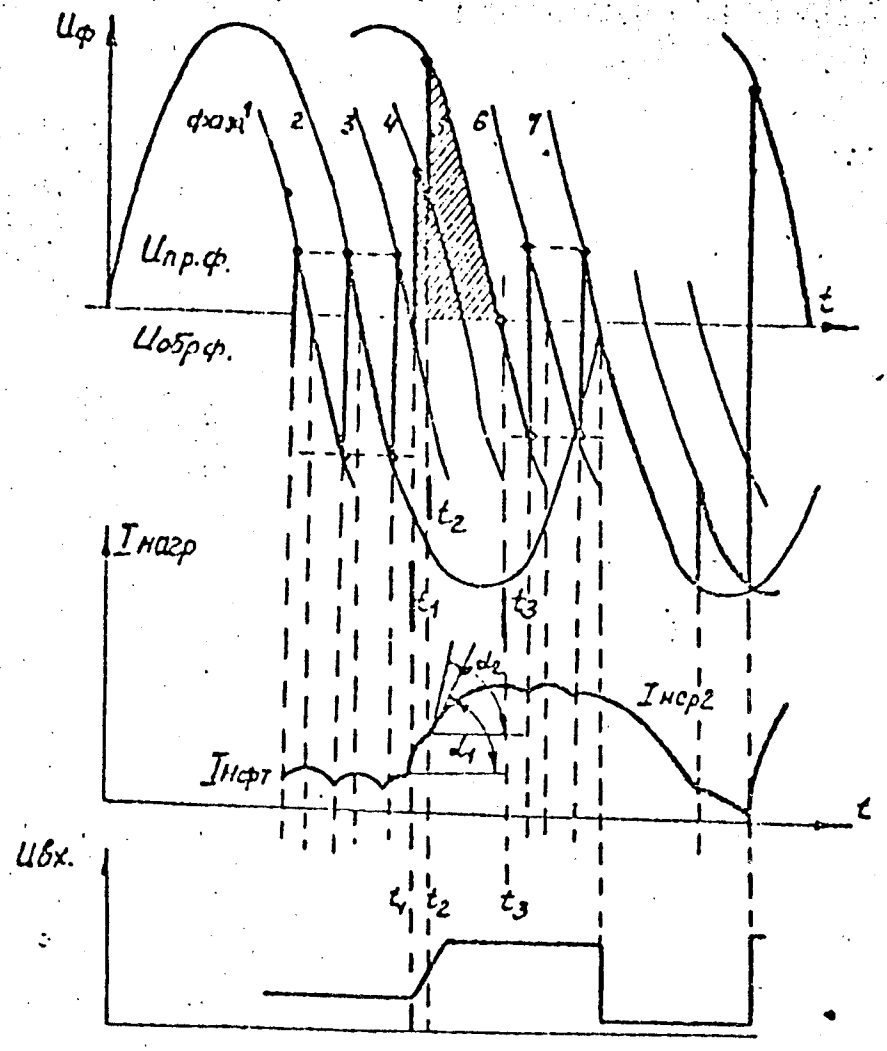

Fig. 5 Operating Parameters of the Controlling Circuit as a Function of Time

$U_{for.ph.}$ Forward phase voltage applied to the load

$U_{rev.ph}$ Reverse phase voltage applied to the load which compensate the emf due to the self inductance of the load

t_1 The moment when the signal appears to increase the current in the load.

t_2 Time of switching to a faster current rise.

t_3 Time when the current reaches the nominal value.

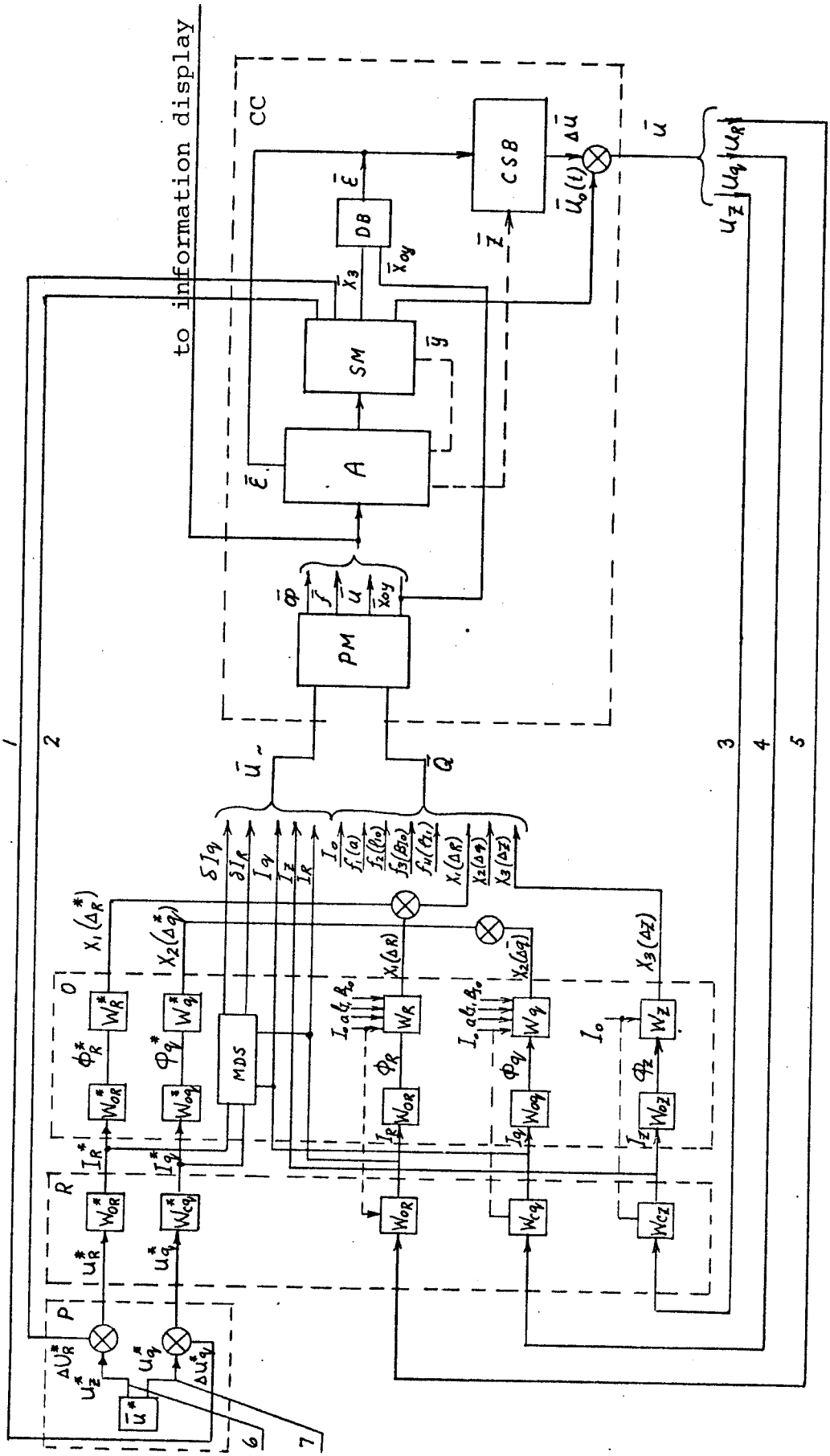

Fig. 3b

Functional diagram of the control system

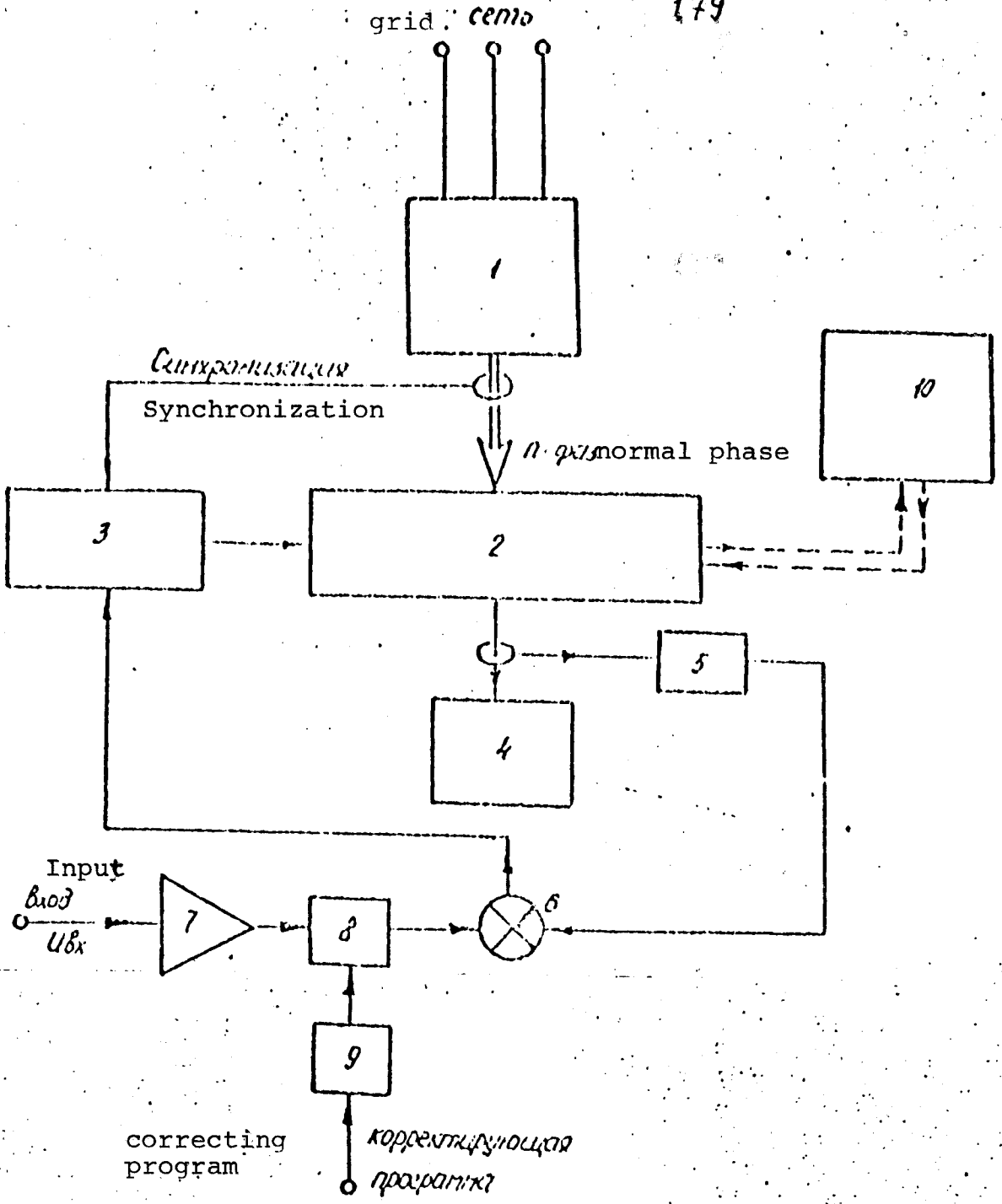

Рис 4.

Блок-схема регулятора

Fig. 4.

Block-diagram of the regulator

ЭКСПЕРИМЕНТАЛЬНАЯ ТЕРМОЯДЕРНАЯ УСТАНОВКА „ТОКАМАК-20"

ТОМ 1

Государственный комитет по использованию
атомной энергии при Совете Министров СССР

Институт атомной энергии имени И.В.Курчатова

Научно-исследовательский институт электрофизической
аппаратуры имени Д.В.Ефремова

ЭКСПЕРИМЕНТАЛЬНАЯ ТЕРМОЯДЕРНАЯ УСТАНОВКА "ТОКАМАК-20"

Материалы эскизного проекта (первый этап)

Том I

ФИЗИЧЕСКОЕ ОБОСНОВАНИЕ

Москва
1975

В разработке физического обоснования проекта Т-20 принимали участие:

Аликаев В.В.

Глухих В.А.

Днестровский Ю.Н.

Иванов Д.П.

Кадомцев Б.Б.

Мирнов С.В.

Моносзон Н.А.

Муховатов В.С.

Попков Г.Н.

Семашко Н.Н.

Стрелков В.С.

Чураков Г.Ф.

Шафранов В.Д.

О Г Л А В Л Е Н И Е

Аннотация

Т-20 представляет собой экспериментальную термоядерную установку, предназначенную для исследования физических процессов в плазме с термоядерными параметрами ($n\tau_E \approx 10^{14}$ см$^{-3}$сек, $T > 7$ кэв) и позволяющую длительно работать в условиях дейтерий-тритиевого эксперимента. Наряду с решением физических задач установка Т-20 позволит провести моделирование и выбор основных инженерных решений, которые должны будут быть приняты при разработке проекта энергетического термоядерного реактора на основе токамака.

Основные параметры установки (размеры плазмы и протекающий по ней ток, мощность питания установки и дополнительных методов нагрева) выбираются таким образом, чтобы в дейтерий-тритиевой плазме осуществлялась мощная термоядерная реакция с энергией, выделенной в нейтронах, масштаба вложенной в плазму.

Параметры плазмы ($n\tau_E$ и T) в Т-20 практически совпадают с параметрами плазмы, необходимыми для гибридного реактора-токамака с урановым бланкетом и могут быть прямо экстраполированы (без промежуточного этапа) на "чистый" энергетический реактор.

I.2. Успешное развитие исследований на токамаках, и в частности вывод о том, время жизни плазмы должно возрастать с её размерами, позволили наметить следующий шаг в программе токамаков. Этот шаг будет осуществлен вводом в строй в середине 1975 года двух крупных установок : Т-10 (ИАЭ) и PLT (Принстон).

На Т-10 по сравнению с Т-4 будет вдвое увеличен радиус плазменного шнура и почти в четыре раза увеличен ток в плазме (с 0,2 до 0,7 ма). Ожидается, что на Т-10 удастся поднять величину $n\tau$ до 10^{13} и температуру ионов до 1,5 ÷ 2,0 кэв.

I.3. В настоящее время ведется проектирование трех крупных токамаков следующего поколения : JET (Объединенный Европейский Тор), ТСТ - (двухкомпонентный тор, Принстон) и JT-60 (токамак с объемом плазмы в 60 $м^3$, Япония). Установка JET рассчитывается на ток 3 ма (с возможностью доведения его до 5 ма), ТСТ - до 2,5 ма, JT-60 - до 3 ма. В установках JET и ТСТ планируется в качестве последнего этапа проведение экспериментов по осуществлению термоядерной реакции в дейтериево-тритиевой плазме. Предполагается, что все эти установки будут сооружены и введены в строй до 1980 года.

2. Установка Т-20 и её цели

2.I. Исходя из последовательности шагов $n\tau \approx I0^{I2}$ (Т-4), $n\tau \cong I0^{I3}$ (Т-I0) представляется естественным поставить целью достижение величины $n\tau \approx I0^{I4}$ на следующем шаге, т.е. Т-20. При температуре плазмы Т = 8-I0 кэв величина $n\tau = I0^{I4}$ обеспечивает выделение энергии в Д-Т реакции (включая энергию I4,I Мэв нейтронов) больше вложенной в плазму. Другими словами, величина Q , равная отношению мощности Д-Т реакции к мощности, вкладываемой в плазму, превышает единицу. Величина $n\tau = I0^{I4}$ вполне достаточна для промышленного бридерного реактора с ураном в бланкете. Она несколько меньше критерия Лоусона ($n\tau = 3.I0^{I4}$) зажигания термоядерной реакции, но представляется вполне естественным, что экстраполяция в три-пять раз на "чистый" энергетический реактор может быть сделана от $n\tau = I0^{I4}$ прямо без промежуточного этапа.

Итак, одной из основных целей установки Т-20 является достижение $n\tau_E \approx I0^{I4}$ см$^{-3}$сек (τ_E - энергетическое время жизни) при температуре плазмы выше 7 кэв, т.е. осуществление демонстрационного эксперимента с выделением энергии в термоядерной Д-Т реакции масштаба вложенных в плазму.

2.2. При достижении плазмы с термоядерными параметрами ($n\tau_E \approx I0^{I4}$сек см$^{-3}$, $T > 7$ кэв) установка Т-20 позволит исследовать физические процессы в реагирующей дейтериево-тритиевой плазме. В частности, на этой установке можно исследовать процессы удержания заряженных продуктов термоядерной реакции, т.е. α - частиц, и их влияние на термоядерную

реакцию, что необходимо для выяснения вопроса о зажигании и самоподдержании реакции в Д-Т плазме.

2.3. При осуществлении режима часто повторяющихся импульсов и при длительной работе в этом режиме установка Т-20 позволит провести исследование различных конструкций модулей бланкетов для нейтронно-физических экспериментов и провести моделирование элементов будущего энергетического термоядерного реактора на основе токамака.

3. Выбор основных параметров Т-20

3.1. Параметры установки Т-20 определяются поставленной целью, т.е. возможностью длительной работы с реагирующей Д-Т плазмой, техническими возможностями реализации этих параметров.

3.2. Одним из основных параметров установок типа Токамак является величина протекающего по плазме тока I. По оптимистическим оценкам величина $n\tau = 10^{14}$ может быть достигнута только при токе более трех мегаампер. Именно на такой ток рассчитываются установки JET и JT-60, примерно такой же величины ток может достигаться в ТСТ. Если ввести некоторый запас, учитывающий неточность наших знаний, то следовало бы принять для тока более высокое значение. Планируя, кроме того, возможность длительной работы с Д-Т плазмой и проведение

инженерно-технологических исследований на Т-20, представляется целесообразным выбрать величину тока $I = 5\text{-}6$ Ма.

3.3. При токе $I \approx 3$ Ма не все α -частицы от Д-Т реакции удерживаются в системе, заметная их доля может сразу уходить на стенки. Из соображений возможности удержания значительной доли α - частиц и замедления их внутри плазменного шнура величину тока I также целесообразно поднять выше 3 Ма. При $I = 6$ Ма в плазме будет удерживаться более 90% α - частиц.

3.4. Выбор максимального тока I до 6 Ма определяет и остальные параметры установки, если учесть при этом технические возможности их реализации.

3.5. Основные параметры установки Т-20

1. Большой радиус тора : $R = 5$ м
2. Малый радиус (круглого) плазменного шнура по диафрагме : $a = 2$ м.
3. Объем плазмы $V = 400$ м^3, поверхность плазмы $S = 400$ м^2
4. Максимальный ток разряда : $I = 6$ Ма
5. Магнитное поле по центру разрядной камеры : $H_z = 35$ кэ
6. Длительность протекания тока в плазме : $t_J = 20$ сек
7. Ожидаемые значения

   Температуры плазмы

   при омическом нагреве : $T = 3$ кэв

   при дополнительном нагреве : $T = 10$ кэв

   Энергетического времени жизни $\tau_E = 2$ сек

параметра удержания $n\tau_E = 10^{14}$ сек см$^{-3}$

средней плотности $n = 5.10^{13}$ см$^{-3}$

β_p полоидального при Т = 10 кэв : $\beta_p = 1$

запаса устойчивости $q = 2,3$

числа частиц в установке $N_e = 10^{22}$

8. Энергосодержание плазмы $W_p = 10^8$ дж

Ожидаемая мощность потерь $P = W_p / \tau_E = 50$ мвт

Средняя тепловая нагрузка на стенки $p_w = P/S = 12,5$ вт/см^2

9. Ожидаемое количество нейтронов в импульсе на Д-Т смеси $10^{20} \div 10^{21}$ (поток нейтронов до 10^{13} нейтр./см^2 сек)

4. Удержание плазмы в Т-20

4.1. Изложим теперь те соображения, которые приводят к приведенным выше предполагаемым параметрам Т-20. Основным показателем эффективности магнитной термоизоляции плазмы является энергетическое время жизни τ_E. Эту величину можно оценить либо на основе экстраполяции существующих эмпирических соотношений, либо опираясь на ту или иную теоретическую модель. Мы обсудим здесь различные возможные варианты.

4.2. Прямая эмпирическая экстраполяция может быть проведена, основываясь на эмпирической зависимости $\tau_E = 7.10^{-9}\, a\, I$ (т.е. $\tau_E \sim a^2 H_\theta$, где $H_\theta = I/5a$ – поле тока на краю разряда в эстедах, I – ток в амперах). Эта зависимость соответствует лучшим результатам по удержанию плазмы на токамаках, и в этом смысле она, скорее всего, дает верхний предел

для τ_E. Для выбранных параметров a, I эмпирическая формула дает значение τ_E = 8,4 сек. Уже сейчас имеются экспериментальные данные, в которых τ_E в два-три раза меньше, чем дается эмпирической зависимостью $\tau_E \sim aI$. Поэтому более реальным кажется принять τ_E = 3÷4 сек, что при энергозапасе $W_p = 10^8$ дж. соответствует мощности потерь 25 ÷ ÷ 30 мвт.

Следует заметить, что эмпирическая формула $\tau_E \sim a^2 H_\theta$ не имеет какого-либо физического обоснования, и кроме того, она не учитывает потерь на излучение примесями, которые будут становиться более сильными по мере повышения температуры.

4.3. Другой подход может быть основан на тех или иных теоретических моделях, которые дают удовлетворительное описание уже существующих данных. Некоторые из этих моделей обсуждаются в Приложении I. Так, например, достаточно оптимистическая модель, предполагающая псведоклассическую теплопроводность у электронов и неоклассическую у ионов (с заходом в глубоко бесстолкновительную банановую область) приводят к временам удержания в несколько десятков секунд. Более пессимистическая "шестишаговая модель", в которой учтены теоретически предсказываемые, но экспериментально пока не исследованные неустойчивости на запертых частицах, приводят при H_2 = 35 кэ и токе I = 6 Ма к величине $n\tau_E \approx 10^{14}$ при T = 7 кэв β_p =I, и $\bar{z}$ = I, причем $n\tau_E$ очень быстро возрастает по мере уменьшения температуры и увеличения плотности (кроме того, $n\tau_E$ линейно вырастает с $\bar{z}$).

4.4. При обсуждении вопроса об экстраполяции имеющихся у нас знаний на более крупные размеры установок целесообразно привлечь соображения подобия в системах типа токамак. Можно показать, что полностью ионизованная плазма в токамаках характеризуется восемью безразмерными параметрами. При джоулевом нагреве два из этих параметров, например, β_p и $\theta = T_e/T_i$, являются зависимыми, т.е. функциями остальных шести. Из этих шести параметров дебаевское число N_d (число частиц в сфере дебаевского радиуса) представляется несущественным для рассматриваемого круга вопросов, а отношение электронной массы и ионной, $\mu = m_e/m_i$, можно считать постоянным. Четыре из оставшихся параметров представляют собой аспектное отношение $A = R/a$, коэффициент запаса $q = aH_z/RH_\theta$, и два параметра, характеризующие продольное и поперечное удержание плазмы : $\nu = qR/\lambda_e$, $K = \rho/a$, где λ_e – средний свободный пробег электронов, ρ – ларморовский радиус ионов (его удобно отнести к электронной температуре). A и q являются параметрами с ограниченным интервалом изменения, так что их практически можно считать постоянными. Таким образом, только ν и K являются определяющими параметрами.

Величина ν уже в существующих установках изменяется в довольно широких пределах, она характеризует степень углубления в бесстолкновительную банановую область. В установке Т-20 предполагаемые параметры соответствуют глубоко банановой области, так что существующие результаты, относящиеся для ионов к области плато, на бесстолкновительную область прямо экстраполированы быть не могут.

Зависимость от параметра K кажется менее критичной. Доказанный на существующих установках диффузионный характер

утечки, что соответствует зависимости $\tau_E \sim K^{-2}$, вряд ли изменится при переходе к Т-20, у которой параметр $K \sim \sqrt{T}/I$ уменьшится всего лишь в пять раз по сравнению с ТФР и в три-четыре раза по сравнению с Т-10.

Таким образом, наибольшая неопределенность при прогнозировании τ_E для Т-20 возникает из-за вступления в банановую область для ионов. Частично эта неопределенность будет прояснена и, возможно, устранена ближайшими экспериментами на Т-10 и PLT.

4.5. Для дальнейших рассуждений удобно привести сводку численных значений для некоторых характерных величин. Начнем с электропроводности σ. Учитывая захват электронов из-за тороидальности и возможное наличие примесей, введем в формулу Спитцера для σ фактор аномальности A_R:

$$\sigma = \frac{1,1\cdot 10^{13}}{A_R} T^{3/2}_{\text{эв}}\ \text{сек}^{-1} = \frac{12}{R} T^{3/2}\ \text{ом}^{-1}\text{см}^{-1},$$

где T – температура в электрон-вольтах. Полагая $A_R = 10$, получаем при T = 10 кэв $\sigma = 1,2\cdot 10^6$ ом$^{-1}$ см$^{-1}$, а при T = 3 кэв $\sigma = 1,6\cdot 10^5$ ом$^{-1}$ см$^{-1}$ (скиновое время шнура равно соответственно 90 сек и 15 сек.) Таким образом, мощность джоулева нагрева $P_J = 2RI^2/\sigma a^2 = 1$ кв при T = 10 кэв и $P_J = 5$ мвт при T = 3 кэв, другими словами, она очень мала.

Далее (T = 10 кэв) : длина пробега электронов до столкновений с ионами $\lambda_{ei} \approx \frac{3\cdot 10^{12}}{A_R n} T^2 \approx 6\cdot 10^5$ см

Тепловая скорость электронов $v_e = 6\cdot 10^7 \sqrt{T} = 6\cdot 10^9 \frac{\text{см}}{\text{сек}}$

Частота электрон-ионных столкновений $\nu_{ei} = v_e/\lambda_{ei} \approx 10^4$ сек$^{-1}$

Время обмена энергией $\tau_{eq} \approx 0,8$ сек.

Параметр столкновительности $\nu = qR/\lambda_e \approx 2\cdot 10^{-3}$

Время замедления 80 кэв ионов $\tau_D \approx 0{,}3$ сек.

Заметим, что граница между областями "плато" и "банановой диффузией" лежит при $\nu \approx (r/R)^{3/2} \sim 10^{-1}$, так что при T = I0 кэв плазма Т-20 уходит глубоко в банановую область (на два порядка по ν).

Приведем еще Бомовское время $\tau_B = \frac{\pi a^2 H_z e}{cT} = 5.10^{-3}$ сек при T = I0 кэв и время теплопроводности ионов на плато $\tau_{pi} \cong \frac{a^2 R}{6 q \rho^2 v_i} \cong 0{,}1$ сек при T = I0 кэв (здесь ρ - ларморовский радиус ионов, v_i - их тепловая скорость). При температуре T = 3 кэв величина $\tau_{pi} = 0{,}5$ сек, она становится больше времени обмена энергией между электронами и ионами при этой температуре $\tau_{ei} \approx 0{,}2$ сек.

Время замедления α - частиц τ_α масштаба I сек. Мощность их энерговыделения при T = I0 кэв $P_\alpha \approx 15 \div 25$ мвт.

4.6. Утечка энергии из плазмы может осуществляться электронной и ионной теплопроводностью, нейтралами перезарядки, излучением чистой водородной плазмы (тормозным и магнитотормозным) и излучением на примесях. В чистой плазме с большими линейными размерами все механизмы утечки энергии, кроме теплопроводности, оказываются небольшими (см. Приложение I). Поэтому рассмотрим именно теплопроводность.

Во всех существующих экспериментах на токамаках преобладает электронный канал переноса энергии. Соответственно, в Т-20 при джоулевом нагреве и выключенной ионной теплопроводности можно было бы ожидать примерно такое же состояние плазмы, которое имеется в настоящее время. А именно, в широком интервале

изменения параметра $\nu = qR/\lambda_e$ величина β_p изменяется слабо, и как правило, она не опускается ниже значения 0,2 + 0.3. При умеренном оптимизме допустим, что β_p в Т-20 при джоулевом нагреве и выключенной ионной теплопроводности достигнет значения $\beta_p = 0{,}3$, что соответствует энергозапасу плазмы $W_p = 3.10^7$ дж и температуре Т = 3 кэв. При этом время жизни $\tau_E = W_p/P_y = 3.10^7 / 5.10^6 = 6$ сек.

При повышении температуры плазмы время жизни τ_E и мощность потерь по электронному каналу может несколько измениться. Например, если верна псевдоклассическая зависимость $\chi_e \sim \rho_{e\theta}^2 \nu_e$, то электронное время жизни должно возрастать с температурой как $\sqrt{T}$ и соответственно, мощность потерь $\sim nT/\tau_E \sim \sqrt{T}$ может возрасти доI0 мвт.

4.7. Обратимся теперь к ионам. Во всех современных токамаках ионы находятся в режиме "плато" неоклассической теории процессов переноса и величина их теплопроводности хорошо согласуется с теоретической. Если бы в Т-20 сохранился уровень теплопроводности для плато, то мы получили бы для мощности потерь на ионах $P_i = W_p/2\tau_{pi} = 100$ мвт при Т = 3 кэв и $P_i = 500$ мвт при Т = I0 кэв, что выходит за рамки разумных величин. Таким образом, для возможности осуществления эксперимента при Т = I0 кэв необходимо достигнуть понижения ионной теплопроводности по крайней мере на порядок величины по сравнению с величиной на плато. Неоклассическая теория при ожидаемой величине $\nu \sim I0^{-3}$, т.е. в глубоко банановой области, предсказывает величину, на два порядка большую, чем τ_{pi}, т.е. $\tau_{Ei} \sim$ I0 сек, и соответственно мощность потерь $P_i \sim 5$ мвт.

Эти числа кажутся слишком оптимистическими, поскольку в глубоко банановой области могут возбуждаться слабые ионные неустойчивости, в первую очередь, дрейфово-температурная и на запертых ионах. В крутом торе Т-20 с аспектным отношением $A = R/a = 2{,}5$ дрейфово-температурная неустойчивость допускает увеличение τ_{Ei} в несколько раз по сравнению с τ_{pi}, а неустойчивость на запертых ионах допускает величину $n\tau_E \cong 10^{14}$см$^{-3}$сек при $T = 7$ кэв и $\beta_p = 1$, $\bar{z} = 1$.

Учитывая очень большую неопределенность в этом пункте (которая может быть снята ближайшими экспериментами на Т-10 и PLT), мы приняли значения $\tau_E = 2$ сек и $n\tau_E = 10^{14}$см$^{-3}$сек но при этом нужно иметь в виду, что эти значения могут отличаться в два-три раза в ту или другую сторону от реальных значений на Т-20.

4.8. При рассмотрении ионного теплопереноса следует учитывать неоклассическую теплопроводность на ионах, запертых на неоднородностях (гофрировке) продольного магнитного поля. Обозначим величину гофрировки через $\delta = (H_{max} - H_{min})/2H$. Тогда по неоклассической оценке теплопроводность на гофрировке должна приводить к времени $\tau_{\delta i} \approx \nu\delta^{-3/2}\tau_{pi}$. При $\nu \sim 10^{-3}$ и $\tau_{pi} \approx 0{,}1$ сек величина δ должна быть меньше 0,1%, чтобы $\tau_{\delta i}$ поднималась до значения, масштаба нескольких секунд. Таким образом, величина δ в основной части плазменного шнура должна быть заведомо меньше 0,1%.

4.9. Излучение на примесях в высокотемпературной плазме представляет собой один из главных каналов утечки энергии. Согласно последним теоретическим данным (см. Приложение 3) равновесное излучение на примесях в районе $T = 10$ кэв сравнительно слабо зависит от температуры и может быть аппроксимировано соотношением $P_z = 6.10^{-30} n_e n_z z^2$ ватт/см^3, где n_z - - плотность примесей с атомным номером z . При плотности $n_e = 5.10^{13}$ отсюда получаем для всего объема $P_z = 6 \bar{z}$ мвт, где $\bar{z} = \sum_z \frac{n_z}{n_e} z^2$ - эффективное зарядовое число ионов. Отсюда видно, что по мере повышения $\bar{z}$ вклад потерь на излучение становится всё более весомым, достигая, например, 30 мвт при $\bar{z} = 5$. Вероятно, именно значение $P_z \approx 30$ мвт является верхней границей для разумной допустимой мощности потерь на излучение (напомним, что мощность от нагрева α - частицами Д-Т реакций может составлять 15 ÷ 25 мвт).

5. Примеси

5.1. Проблема загрязнения плазмы примесями является чрезвычайно серьезной для большинства стационарных систем, в том числе и для токамаков. Наряду с удержанием плазмы и её нагревом защита от примесей составляет одну из трех основных задач на пути к термоядерному реактору. Установка Т-20, будучи коротко-импульсной (длительность импульса не превышает нескольких энергетических времен), нацелена на решение только двух задач - нагрева и удержания плазмы, но она, разумеется, должна

обеспечить при этом получение достаточно чистой Д-Т плазмы.

5.2. Существующие экспериментальные данные об уровне загрязнения плазмы в токамаках и поведении примесей в плазменном шнуре не вполне определенны. Обычной величиной считается наличие нескольких процентов легких и долей процента тяжелых примесей, так что величина $\bar{z}$ может доходить до значений $3 \div 4$. С точки зрения излучения на примесях этот уровень кажется допустимым и для Т-20.

Не вполне ясен вопрос о возможном процессе накопления примесей во время разряда. Аккумулирование примесей в процессе разряда и их концентрация вблизи оси плазменного шнура были обнаружены в устойчивых разрядах токамака Т-4. С другой стороны, например, на ТФР при небольшом росте плотности плазмы со временем наблюдается постоянная во времени концентрация примесей, соответствующая величине $\bar{z} = 4$, и авторы делают вывод о том, что темп накопления примесей на два порядка меньше, чем поток примесей со стенок камеры на поверхность плазмы.

5.3. В установке Т-20 средний поток энергии на стенки принят равным I2,5 ватт/см^2 (при джоулевом нагреве и $T = 3$ кэв. Эта величина на порядок меньше). По порядку величины он совпадает с величиной потока энергии в современных крупных токамаках, таких как Т-4 и ТФР. Поэтому можно ожидать, что в плазме Т-20 с температурой I0 кэв темп поступления примесей будет примерно таким же, как и на Т-4, ТФР (если камера и диафрагмы будут сделаны из применявшихся до сих пор материалов). А так как малый радиус плазменного шнура в Т-20 на порядок больше, чем

в Т-4, ТФР, то можно ожидать на порядок более медленного поступления примесей в I $см^3$ плазмы. На ТФР уровень $\bar{z} = 4$ сохраняется в течение 0,4 секунды, так что в Т-20 можно надеяться на время в несколько секунд до накопления примесей до уровня $\bar{z} = 4 \div 5$. Это время достаточно для проведения эксперимента.

5.4. В первом варианте вакуумной камеры Т-20 не предполагается установка дивертора для снижения уровня примесей (хотя такая возможность и предусматривается на последующих этапах работы). Не исключено также, что первый вариант камеры окажется не достаточно оптимальным с точки выбора материалов для его отдельных элементов, взаимодействующих с плазмой : самой камеры, диафрагм (неподвижных и движущихся), экранов и т.п. Поэтому в конструкции установки должна быть предусмотрена возможность замены камеры или её элементов в процессе экспериментов. При разработке камеры и её элементов следует учитывать особенности переноса энергии в плазме и путей поступления в нее примесей.

5.5. При взаимодействии плазмы со стенками существует несколько каналов освобождения примесей и поступления их в плазму :

1. Таяние и, возможно, испарение сильно нагреваемых элементов камеры (например, диафрагм)
2. Распыление материала энергичными ионами
3. Десорбция газов и разложение химических соединений под действием электронного удара
4. Выбивание атомов примеси рентгеновским и ультрафиолетовым излучением

5. Распыление материалов нейтронами от Д-Т реакций

6. Блистеринг, т.е. шелушение материала, главным образом, из-за воздействия α - частиц от Д-Т реакций.

5.6. Эти механизмы явно не равноценны по своему воздействию на плазму. Блистеринг, например, начинается с доз масштаба 0,1 кулона, т.е. при полном числе α - частиц $\sim 10^{13} \div 10^{14}$ частиц за импульс на 1 $см^2$ поверхности он начинается после $\sim 10^3$ Д-Т импульсов. Поэтому для первой серии экспериментов с небольшим числом импульсов он не опасен, но в дальнейшем может оказаться очень существенным. Так как α - частицы заряжены и вероятно будут собираться на выступающие части камеры (диафрагмы), то должна быть предусмотрена смена диафрагм, если это понадобится (заметим, что при очень больших дозах, больше $1 \div 2$ кулон/$см^2$ блистеринг ослабевает). Можно надеяться также, что при параметрах Т-20 большая часть α - частиц будет успевать отдавать энергию плазме.

5.7. В отношении нейтронного распыления полной ясности нет, так как соответствующие данные для коэффициента распыления S_n колеблются от 10^{-3} до 0,25. Даже при $S_n \sim 10^{-1}$ поток примесей масштаба 10^{12} частиц/ $см^2$ сек (при нейтронном потоке 10^{13} нейтр/ $см^2$ сек) кажется небольшим.

5.8. Поступление примесей при падении на поверхность γ - квантов кажется наиболее безобидным из всех механизмов и поэтому излучение на примесях является наиболее благоприятным с точки зрения примесей механизмом съема энергии с плазмы.

Соответствующим механизмом загрязнения можно пренебречь.

5.9. Поступление примесей за счет электронных ударов при хорошей тренировке камеры может быть снижено до вполне приемлего уровня. Если добиться коэффициента десорбции $C \sim 10^{-5} - 10^{-4}$ (т.е. дойти до очень хорошего уровня чистоты стенки), то на один джоуль энергии, передаваемой стенками электронами с энергией ~ I00 эв освободится масштаба 10^{12} частиц примесей , , что составляет около 10^{14} частиц/см^2 за импульс и кажется допустимой величиной.

Во всех современных токамаках энергия, вываливающаяся на диафрагмы, поступает, в основном, в форме электронного тока с энергией ~ I00 эв. Тем самым осуществляется съем энергии из плазмы механизмом, наиболее благоприятным с точки зрения распыления материала. Это преимущество должно быть сохранено и в конструкции камеры и диафрагм Т-20.

5.I0. Распыление материала быстрыми ионами представляет собой один из наиболее серьезных каналов поступления примесей в плазму. В Т-20 распыление будет производиться, во-первых, ионами с энергией 30 - I00 эв на границе плазмы (например, падающих на диафрагмы), во-вторых, ионами с энергией I-3 кэв, возникающих из-за перезарядки падающих на границу плазмы атомов холодного газа, и, в-третьих, ионами с энергией около I0 кэв, возникающих при перезарядке во внутренних областях шнура атомов от внешней инжекции (с энергией 80 или I60 кэв). (Кроме этого, напротив каждого инжектора будет происходить

бомбежка стенки энергичными нейтронами с энергией 80 или I60 кэв, но эту часть стенки можно углубить и сделать сильно охлаждаемой для сорбции выбитых примесей). Поток энергии от атомов с энергией I0 кэв может составлять несколько процентов от мощности инжекторов, т.е. составлять величину до I ватт/см^2. Так как коэффициент распыления нержавеющей стали при этой энергии составляет около 2%, то соответствующий поток примесей может быть масштаба $I0^{I3}$ частиц/см^2 сек, так что за импульс инжекции в течение I0 сек на поверхность плазмы поступит $I0^{I4}$ частиц/см^2, что составляет 2% от числа ионов водорода. Такой уровень примесей для плазмы не допустим, и здесь можно надеяться только на экспериментально наблюдаемый механизм экранировки плазмы от примесей, так что поступление примесей в центральные части разряда значительно меньше потока примесей на границу плазмы.

Еще более серьезно обстоит дело с более мягкой областью спектра ионов. В интервале энергий от I00 эв до нескольких кэв распыление нержавеющей стали ионами может освободить около $I0^{I4}$ частиц/джоуль. Если ионами переносится масштаба I0% потока энергии на стенку, то это соответствует скорости поступления примесей на поверхность разряда около $I0^{I4}$частиц/см^{2}сек.

5.II. Таким образом, ожидаемый поток примесей на поверхность плазмы в камере из нержавеющей стали оказывается очень высоким. Экспериментально наблюдаемый эффект экранировки плазмы от примесей (поток примесей в центральную область значительно меньше потока примесей на поверхность плазмы) может заметно улучшить ситуацию, но вместе с тем совершенно настоятельно возникает необходимость подбора более оптимальных материалов

для стенки камеры и диафрагм.

5.I2. Газение стенок и испарение элементов камеры при больших тепловых нагрузках ∈ может составить гораздо более серьезную проблему в Т-20, чем во всех существующих токамаках. Выбор теплового режима стенок камеры и теплоснимающих элементов (диафрагм) должен быть произведен на стадии эскизного проектирования установки.

6. Начальная и конечная стадии процесса

6.I. Следует ожидать, что начальная стадия разряда в Т-20 должна заметно отличаться от начальной стадии в существующих токамаках.

Основная причина этого - большой размер установки и, как следствие, высокая степень скинирования разрядного тока.

В существующих токамаках пробой происходит по всему сечению камеры и затем разрядный ток увеличивается до номинального за времена $\sim 3 \div 30$ мсек со скоростью $\sim 10^7$ а/сек. При этом он имеет тенденцию к скинированию. Однако скиновая конфигурация разрядного тока оказывается неустойчивой относительно развития резонансных винтовых возмущений при целочисленных значениях $q(a)$.

6.2. Развитие этих неустойчивостей, по-видимому, способствует проникновению тока внутрь плазмы. С другой стороны, неустойчивости ведут к увеличению взаимодействия плазмы со стенкой и к поступлению примесей.

6.3. Масштаб энергии, выделяющейся при этом на стенке, можно оценить как $\sim \frac{\Delta L I^2}{2}$, где : ΔL – изменение индуктивности плазменного шнура при переходе от скинированного распределения $j(r)$ к параболическому. Для Т-20 эта величина может составить $\sim$ 100 мгдж. Если учесть импульсный характер развития неустойчивости, можно ожидать импульсное выделение энергии на стенке масштаба сотен меговатт. В такой ситуации возможно испарение материала разрядной камеры.

6.4. Проведенный расчет (Приложение I) показывает, что эффект скинирования не удаётся снять простым введением аномального сопротивления с коэффициентом $A_R = 10$ (обычно этого достаточно, чтобы для существующих токамаков расчет не приводил к значительному скинированию). Даже введение $A_R = 50$ *не* меняет ситуацию.

Оба расчета обнаруживают сильное скинирование, которое должно сохраниться в значительной части основной стадии разряда ($\tau_{ск} = 0{,}9\ \frac{\sigma a^2}{c^2}$).

6.5. Чтобы избежать скинирования, для Т-20 предлагается другой вариант возбуждения разрядного тока, а именно, с применением раздвигающейся диафрагмы, которая позволяла бы менять малый радиус плазменного шнура в процессе наращивания разрядного тока. При этом предполагается, что в тени диафрагмы электропроводность низка и плотность тока пренебрежимо мала.

6.6. Роль подобной диафрагмы могла бы играть стенка камеры в сочетании с поперечными магнитными полями, программированными соответствующим образом во времени.

6.7. Непременным условием такого формирования является подача рабочего газа (α_2 , T_2) на границу расширяющегося плазменного шнура. Газ будет ионизоваться вблизи границы, и, таким образом, мы будем иметь возможность программировать распределение n_e (r).

6.8. Начальный радиус плазмы предполагается выбрать масштаба существующих токамаков – 30 – 50 см с плотностью $n_e \sim 10^{13}$ см$^{-3}$. Скорость расширения диафрагмы следует выбрать порядка диффузионной (~ 10 м/сек), можно ожидать, что в этом случае тепловые нагрузки на диафрагму (или стенку) окажутся минимальными.

6.9. Для улучшения условий создания исходной плазмы следует предусмотреть предварительную ионизацию по оси камеры. Если на оси камеры создать плазму с плотностью $n_e \sim 10^{12}$см$^{-3}$ и $T_e \sim 30$ эв, то при скорости нарастания тока 10^7 а/сек за время ~ 100 мк сек ток достигнет значения, необходимого для удержания такой плазмы. За это время плазма не увеличит существенно своих поперечных размеров. Локализованную на оси предионизацию можно создать системой, предназначенной для нагрева плазмы на электронно-циклотронном резонансе.

6.10. В конечной стадии разряда после выключения систем нагрева за 2 ÷ 3 сек произойдет охлаждение плазмы до температуры в 1 ÷ 2 кэв, то есть, величина ее тепловой энергии окажется сравнительно мала.

Задача состоит в том, чтобы за несколько секунд снять магнитную энергию $\frac{\mathcal{L}_i I^2}{2}$, заключенную в шнуре, не допуская

отрицательного тока на периферии и "консервации" энергии внутри шнура.

6.II. Этого, казалось бы, можно достичь снижением полного тока с одновременной подачей на границу шнура какого-либо из инертных газов, например, аргона. (Можно надеяться, что его последующее удаление со стенки удается осуществить простым прогревом камеры до 600°С). Охлаждение периферии необходимо для снижения электропроводности вблизи границы до $I \div 3.10^{16}$ $сек^{-1}$.

Можно полагать, что такая операция окажется эффективной при интегральной подаче аргона на уровне $\sim$ I0% от полного начального числа электронов.

6.I2. Кроме того, отрицательный ток вблизи периферии шнура можно ограничить , снизив электропроводность внешних слоёв плазмы путем введения в шнур механической диафрагмы или, прижимая шнур к стенке поперечными полями. Операция - обратная начальной стадии. Возможно совместное применение всех трех методов.

7. Методы нагрева плазмы в установке Т-20.

7.I. Джоулев нагрев в течение первых 2 сек может довести температуру плазмы до $T \approx 3$ кэв. При достижении этой температуры эффективность джоулева нагрева упадет, поскольку величина тока ограничена условием гидромагнитной устойчивости, а сопротивление плазмы быстро уменьшается с температурой. Дальнейший

нагрев плазмы должен проводиться с помощью методов, эффективность которых мало зависит от температуры плазмы. Из возможных методов нагрева в настоящее время наиболее перопективны и экспериментально развиты инжекция быстрых атомов и ВЧ и СВЧ методы.

При принятых выше параметрах $n = 5.10^{13}$ см$^{-3}$, τ_ε = 2сек, подъем температуры от 3 кэв до 10 кэв можно осуществить введением в плазму мощности $\sim$ 50 мвт в течение 2-3 секунд. Примем, что эффективность передачи ионам вводимой в камеру мощности составляет около 0,85. Тогда вводимая в камеру мощность должна составлять 60 мвт.

7.2. Временная программа нагрева. В течение первых 2 сек. джоулев нагрев и достижение температуры плазмы 3 кэв ; в течение последующих 2 - 3 сек ввод мощности 60 мвт с помощью инжекции атомов или ВЧ методов и достижении температуры плазмы 10 кэв. Дальнейший ввод мощности (его величина и длительность) определяется условиями эксперимента, но не превышает общей длительности 15 сек.

7.3. Нагрев с помощью инжекции быстрых атомов (дейтерия). Энергия атомов принимается равной 80 кэв, поток атомов - 750 экв. а , что соответствует вводу в камеру $4,5.10^{21}$ част/сек При начальном количестве частиц в объеме 400 м^3 около 2.10^{22} при инжекции произойдет удвоение числа частиц в объеме за 5 сек, что может ограничить длительность инжекции при энергии атомов 80 кэв, и заставит перейти к инжекции более энергичных атомов с энергией 160 кэв.

7.4. Система инжекции составляется из следующих двух типов инжекторов :

Энергий атомов дейтерия .	кэВ	80	I60
Мощность потока атомов на выходе из инжектора	Мвт	I2,5	I6
Поток атомов	экв.А	I60	I00
Мощность, подводимая к инжектору:			
высокое напряжение	Мвт	32	64
низкое напряжение	Мвт	5,4	5,4

Для создания потока атомов с энергией 80 кэВ и мощностью 60 Мвт требуется 5 инжекторов с общей мощностью питания около I90 Мвт. Три инжектора с энергией атомов I60 кэв обеспечат введение мощности около 50 Мвт., при этом мощность электрического питания составит около 2I0 Мвт.

Общая вводимая мощность с потоками атомов 80 и I60 кэВ одновременно достигнет II0 Мвт, а мощность, подводимая к инжекторам составит около 400 Мвт.

При необходимости можно три инжектора I60 кэВ перевести в режим работы 80 кэв. В этом случае общая мощность 80 кэв атомов составит около I00 Мвт, а подводимая мощность к инжекторам достигнет 300 Мвт.

7.5. Заметим, что инжекция атомов с энергией I60 кэВ обладает определенными достоинствами :

I). Количество частиц, вводимых в камеру Токамака, при неизменной мощности инжекции уменьшается вдвое, по сравнению с 80 кэв ;

2) Захват вводимых атомов в плазме обусловлен в основном ионизацией (а не перезарядкой) и вследствие этого уменьшается

поток перезарядных атомов на стенки камеры ;

Однако, инжекторы с 80 кэв атомами раньше могут быть введены в строй, и поэтому именно они планируются на первой стадии.

7.6. Ввод энергии нейтральными пучками осуществляется с помощью нескольких инжекторов, имеющих самостоятельные системы электрического питания и средства вакуумной откачки. Такой принцип позволяет обеспечить одновременное введение потоков атомов двух энергий (80 и I60 кэв), а также дает возможность изменять мощности инжекции.

Исходя из геометрической симметрии катушек тороидального поля выбирается четыре промежутка (через 90^{o}) для установки восьми инжекторов (по два в каждом промежутке с противоположным по отношению к току в плазме направлением пучка). Направление инжекции выбирается по касательной к окружности радиуса $R - \frac{a}{2} = 4$ м. Длина пучка в плазме достигает I2 м.

Сквозь плазму проходит поток атомов, ослабленный по интенсивности в 20 раз (при энергии 80 кэв и I3 раз при I60 кэв). При этом на стенке камеры, противоположной входному окну каждого инжектора выделяется удельная мощность около I25 вт/см^2 при 80 кэв и 250 вт/см^2 при I60 кэв.

При энергии атомов 90 кэв сечения ионизации на ионах и перезарядки примерно равны, так что около половины вводимых в плазму атомов совершит перезарядку и образующиеся в результате этого нейтралы с энергией I0 кэв могут выйти на стенку. Таким образом, около 5% вводимой в плазму мощности может выделяться на стенках в виде их бомбежки I0 кэв нейтралами

(соответствующая нагрузка составляет около I ватта/см^2).

7.7. Нагрев с помощью ВЧ и СВЧ методов. Наиболее перспективны следующие методы :

I) СВЧ нагрев при частотах, близких к электронно- циклотронной ($\omega \sim \omega_{He}$) ;

2) СВЧ нагрев в диапазоне нижних гибридных частот ($\omega \cong \sqrt{\omega_{He}\,\omega_{Hi}}$)

3) Нагрев с помощью ионно-циклотронного резонанса и его гармоник, а также магнито-звуковой резонанс ($\omega < \omega_{Hi}$).

При проектных параметрах плазмы время обмена энергией между ионами и электронами меньше I сек, и поэтому безразлично в какую из компонент плазмы вкладывается энергия.

7.8. Электронно-циклотронный нагрев плазмы.

При значениях магнитного поля 35 кгс необходимо использовать диапазон частот с $\lambda \sim$ 3 мм. Согласно расчетам поглощение обыкновенной волны, распространяющейся с внешней стороны тора под углом к основному полю $\sim 60^{\circ}$, может быть практически полным в зоне циклотронного резонанса. Главной трудностью при использовании диапазона миллиметровых волн для нагрева плазмы является необходимость в разработке СВЧ генераторов большой мощности. В то же время вполне реально использовать большое количество генераторов, энергия от которых вводится через такое же количество отверстий. При излучении ВЧ энергии под углом в 60° к магнитному полю происходит полное поглощение ВЧ энергии при одном прохождении волной зоны циклотронного резонанса, поэтому нагрев "убегающих" электронов может быть значительно уменьшен выбором нужного направления тока.

Для ввода ВЧ энергии необходимо использовать около I00

патрубков, расположенных в промежутках между катушками тороидального поля. В каждом промежутке с внешней стороны тора располагается по несколько круглых патрубков, излучающих ВЧ энергию с фокусировкой на ось тора под углом 60° к направлению основного магнитного поля.

Следует отметить, что при нагреве электронов можно ожидать меньшего загрязнения плазмы, поскольку поверхностное распыление стенки камеры при электронной бомбардировке на два порядка меньше, чем при ионной. Кроме этого, при ВЧ нагреве не вводится поток нейтральных частиц в камеру и не возникает потока перезарядных атомов с энергией 10 кэв.

7.9. СВЧ нагрев в диапазоне нижних гибридных частот.

Эффективный линейный механизм поглощения связан с трансформацией электромагнитной волны в плазменную. Для обеспечения проникновения вводимых в плазму волн необходимо использовать продольное замедление. В этом случае следует ожидать нагрева как ионов, так и электронов в окрестности нижнегибридного резонанса. ВЧ энергия может вводиться с помощью систем фазированных волноводов, помещенных в окна, которые используются также для инжекторов быстрых атомов. В необходимом диапазоне частот ($f \sim 1000$ мггц), задача создания генераторов необходимой мощности значительно проще, чем в области миллиметровых волн.

7.10. Нагрев в диапазоне ионно-циклотронного резонанса и его гармоник. В эскизном проекте не предусматривается специальная проработка системы ввода ВЧ энергии. Эти системы могут быть разработаны на стадии технического проекта с использованием системы питания ВЧ нагрева и окон для инжекции быстрых атомов.

7.II. Для питания ВЧ и СВЧ генераторов и инжекторов целесообразно использовать общую систему электрического питания высоким напряжением. В случае применения для нагрева плазмы только ВЧ методов можно использовать всю систему питания инжекторов с общей мощностью 400 Мвт. В этом случае можно получить 80 Мвт ВЧ мощности при КПД генераторов около 20%, который достигается практически во всех типах генераторов.

В режиме двух компонентной плазмы при одновременной работе СВЧ нагрева и I60 кэв инжекторов для питания СВЧ генераторов может быть использована система питания 80 кэв инжекторов с мощностью около I90 Мвт. В этом случае для получения СВЧ мощности в 60 Мвт необходимы генераторы с КПД не менее 30%.

7.I2. Планируемый для Т-20 комплекс методов нагрева обладает большими возможностями для маневрирования в зависимости от того, какая величина будет получена для $n\tau_E$:

I) При осуществлении нагрева дейтерий-тритиевой плазмы в предполагаемых условиях $n\tau_E = 10^{14}$ см$^{-3}$сек вводимая мощность 60 Мвт, при Т = I0 кэв может обеспечить величину $Q = 2$, (величина Q определяется как отношение полной энергии, выделяемой в Д-Т реакции, к энергии, вводимой в плазму). При этом из I00 Мвт выделяющейся мощности от ДТ реакции около 20 Мвт составит мощность α - частиц, которая может привести к дополнительному нагреву плазмы. Следовательно, вводимая извне мощность в этом случае может быть уменьшена спустя 2-3 сек после начала основного нагрева.

2) Если энергетическое время τ_E окажется менее 2 сек, например I сек, то при сохранении вводимой мощности 60 Мвт и температуры плазмы Т = I0 кэв ($n\tau \approx 2{,}5.10^{13}$) можно ожидать

достижения $Q = 1$.

3) Если при $\tau_\varepsilon = 1$ сек температура плазмы не превысит 5 кэв, то при номинальном значении концентрации $n = 5.10^{13}$ см$^{-3}$ ($n\tau = 5.10^{13}$) значение Q упадет приблизительно до 0,3.

В этих случаях нагрев плазмы может осуществляться с помощью инжекции атомов с энергией 80 кэв или одним из выше перечисленных СВЧ и ВЧ методов.

4) При использовании для нагрева плазмы атомов с энергией 160 кэв и сохранении мощности 60 Мвт в условиях $\tau_\varepsilon = 2$ сек, $T = 10$ кэв можно ожидать $Q \approx 4$.

5) В условиях, аналогичных 4), но при меньшем энергетическом времени $\tau_\varepsilon = 1$ сек можно ожидать значения $Q \approx 1{,}5$.

6) Если при увеличении температуры плазмы ионная теплопроводность не уменьшится и не удастся перейти в "банановый" режим (энергетическое время жизни ионов $\tau_{\varepsilon i} \ll 2$ сек), то существует возможность поддержания температуры электронов на уровне 5 кэв с помощью электронно-циклотронного резонанса на уровне 60 Мвт с одновременной инжекцией в плазму потока атомов с энергией 160 кэв и мощностью до 50 Мвт. В этом режиме двух - компонентной плазмы можно ожидать значения $Q > 1$. При этих условиях используются достоинства обоих методов нагрева с точки зрения вакуумных условий в камере и нагрузок на стенки камеры, но становятся очень напряженными условия на стенках.

8. Программа исследований и режимы работы.

8.I. Исследования на установке Токамак-20 можно разбить на следующие направления :

I. Исследование физики удержания и нагрева водородной плазмы при термоядерных параметрах.

2. Исследование реагирующей дейтериево-тритиевой плазмы, включая удержание α - частиц от Д-т реакции.

3. Электродинамические исследования.

4. Нейтронно-физические и материаловедческие исследования.

5. Технологические исследования.

Эксперименты по различным направлениям в значительной мере могут проводиться параллельно, что обуславливает необходимость широко разветвленного, диагностического комплекса и четкой координации работ.

8.2. Исследования водородной плазмы при термоядерных параметрах.

Этот цикл исследований предполагается провести на водороде во избежание сильной активации камеры. Естественная примесь дейтерия к водороду даст при проектных параметрах импульса $I0^{II}$ - $I0^{I2}$ нейтронов за импульс.

Такие активности безопасны с смысле работы персонала, активации материалов и работы аппаратуры.

Основное внимание в этом цикле должно быть уделено определению теплопроводности и диффузии плазмы при термоядерных параметрах, достижение которых намечено осуществить с помощью ВЧ нагрева или инжекции нейтральных частиц. В ходе этих

исследований необходимо определить причины, ограничивающие нагрев и приводящие к потерям энергии из плазмы, а именно : степень устойчивости или неустойчивости, скорость поступления примесей. На основе этих исследований необходимо провести исследования по оптимизации режима, которые включают в себя. Определение режимов с наименьшим взаимодействием плазмы со стенкой, испытание различных типов диафрагм или, если возникнет необходимость, дивертороров.

На основе полученных данных должны быть даны методы расчета параметров термоядерного реактора, структуры энерго - баланса.

8.3. Исследования дейтериево-тритиевой плазмы. Опыты с дейтериево-тритиевой плазмой предусматривают, прежде всего, физические исследования по удержанию α - частиц и передаче энергии их плазме. На основании этих исследований должны быть получены условия выхода реактора в самоподдерживающийся режим. Так как самоподдерживающийся режим не является единственно-возможным, в ходе исследований должны быть определены параметры и целесообразность осуществления реактора с постоянным дополнительным нагревом и двухкомпонентного реактора. Для этого должны быть проведены исследования двухкомпонентного режима и режима с постоянным дополнительным нагревом.

8.4. Реактор будущей термоядерной электростанции должен обладать максимально большим энергетическим циклом. В ходе исследований на установке Т-20 должны быть выработаны рекомендации по оптимизации энергетического цикла. С этой целью должны быть исследованы методы дополнительного напуска

дейтериево-тритиевой смеси в ходе рабочего импульса возможность очистки плазмы от продуктов реакции, разработаны меры стабилизации температурного режима.

8.5. Электродинамические исследования.

Целью этого направления исследований является изучение взаимодействия плазменного образования с внешними электромагнитными полями. В процессе экспериментов должно быть изучено распределение тока в плазме. Разработаны методы борьбы со скинированием тока в начальной стадии процесса, режим ввода плазменного образования в термоядерные параметры. В настоящее время экспериментально подтверждена возможность работы установок типа токамак при различных q вплоть до $q < 2$. Однако уменьшение q с 3 до 1-2 приводит к некоторому снижению энергетического времени жизни. В ходе экспериментов на токамаке-20 предстоит выбрать оптимальное q для последующих термоядерных реакторов. Также необходимо определить предельные значения β_p и методы поддержания температурного режима плазмы в районе β_p, близких к критическим. Большое энергосодержание плазмы, особенно в индуктивной составляющей, требуют тщательной отработки режима гашения разряда. С этой целью должны быть ~~в~~ поставлены специальные эксперименты.

8.6. Нейтронофизические и материаловедческие исследования.

Это направление исследований ставит своей целью отработку модулей бланкета будущих термоядерных реакторов, как для чистых реакторов, так и для реакторов гибридного типа. В ходе экспериментов предстоит, прежде всего, определить коэффициенты

воспроизводства трития для различных типов и конструкций бланкета, измерить нейтронные поля, испытать материалы первой стенки под воздействием полного комплекса факторов (нейтронное излучение, бомбардировка α - частицами, бомбардировка быстрыми атомами, электронами , γ - излучением, синхротронное излучение). В ходе этих исследований должны быть испытаны различные теплоносители и конструкционные материалы. Следует отметить, что установка Т-20 не предназначена для испытания конструкций и материалов на максимально допустимый интегральный поток нейтронов.

8.7. Технологические исследования.

Благодаря тому, что большинство инженерных систем установки Токамак-20 будут являться прототипами систем будущего реактора электростанции, на установке Т-20 предполагается провести широкий комплекс технологических исследований. К этим исследованиям относится отработка тритиевого цикла, включая выделение трития из бланкета и продуктов откачки, подготовку рабочего вещества ; теплофизические исследования на опытных модулях бланкета. В ходе экспериментов должны быть отработаны автоматические системы управления, алгоритмы и аппаратурная часть, определены характеристики надежности отдельных систем термоядерного реактора и оптимальные размеры резервирования, должен быть определен диагностический комплекс термоядерного реактора, позволяющий минимальными средствами надежно контролировать его работу.

8.8. Режимы работы.

Режимы работы установки можно разделить на режимы технологической подготовки установки и рабочие режимы.

Предусматриваются два режима технологической подготовки : прогрев внутренней вакуумной камеры до 600°С и тренировочный режим с током до I,5 Ма.

Программой исследований предусматриваются три этапа работы установки.

Работа в режиме " а " (первые I,5-2 года)

I0000 рабочих импульсов на водородной плазме с интервалами между импульсами I5 минут (предусматривается возможность получения серий из 50 импульсов с частотой следования I импульс в 5 минут).

Работа в режиме " б " (0,5 ÷ I,5 года)

I000 рабочих импульсов на дейтериево-тритиевой плазме с интервалами между импульсами I5 минут.

Работа в режиме " в " (2 ÷ 3 года)

I00.000 импульсов на дейтериево-тритиевой плазме с интервалами между импульсами не более 5 минут с длительностью непрерывной работы в режиме 3 ÷ 5 часов.

Указанные выше этапы предполагается осуществить последовательно. При переходе от одного режима к другому должна быть предусмотрена возможность замены элементов камеры.

ПРИЛОЖЕНИЕ I

Краткий обзор расчетов энергобаланса для установки Т-20 (Ю.Н.Днестровский) .

На основе одномерных моделей энергетического баланса был проведен анализ нагрева плазмы в ходе разряда. В расчетах использовались "псевдоклассическая" ("псевдоклассика" для электронов, "неоклассика" для ионов) и "бомовская" модели теплопроводности. Учитывались также нагрев плазмы с помощью инжекции пучка быстрых нейтралов, охлаждение за счет притока холодных нейтралов из вакуума, циклотронное и тормозное излучение, передача энергии от α - частиц плазме.

Для основного расчетного варианта использовались следующие значения параметров

$$R = 400, \quad a = 150, \quad H = 40 \text{ кэ} \qquad (I)$$

При $q = 2$ этим параметрам соответствует ток $I = 5.6$ МА , принятый в основном варианте установки.

В первой серии расчетов время подъема тока составляло 600 мсек. Вычисления показали, что даже при $Z_{eff} = 10$ плазма быстро прогревается и происходит сильное скинирование тока. Температура электронов за $t \sim 1$ сек возрастает до значений $T_e \sim 3$ кэв и распределение тока вмораживается. Увеличение Z_{eff} еще в 5 раз качественно не изменяет картины процесса. Скиновое время и в этом случае превышает 10 - 20 сек.

Таким образом, для создания относительно равномерного распределения тока по сечению плазмы необходимо принять специальные меры : ввести раздвижную диафрагму или формировать

плазму с помощью поперечных магнитных полей. В дальнейших сериях вычислений предполагалось, что такие меры приняты и начальное распределение тока считалось параболическим.

Диффузией частиц плазмы мы в расчетах пренебрегали, задавая профиль плотности формулой : $n(x) = n_{max}(1 - 0.8\, r^2/a^2)$.

Расчеты по оптимистической "псевдоклассической" модели приводят к следующей картине поведения разряда. При плотности $n_{max} = 6.10^{13}$ см$^{-3}$, если дополнительный нагрев отсутствует, температура плазмы за время 10 - 15 сек устанавливается на уровне $T_i \sim T_e \sim 3$ кэв. Для достижения температуры $T_i \sim 12$ кэв за время $\Delta t \sim 5$ сек нужно ввести дополнительную энергию $W \sim 3.10^7$ дж.

При температуре частиц меньшей 10-15 кэв основные потери определяются механизмом ионной теплопроводности и энергетическое время жизни τ_E составляет около 10 сек. При большей температуре электронов вступает в игру циклотронное излучение. При $T_e > 40$ кэв потери по циклотронному каналу превышают остальные потери из плазмы. Полное энергетическое время жизни при возрастании T_e от 15 кэв до 40 кэв падает в 2 раза, спускаясь до значений $\tau_E \sim 5$ сек. Мощность циклотронных потерь W_{ce} при $T_e = 20$ кэв составляет 4 Мвт, а при $T_e = 40$ кэв $W_{ce} = 11$ Мвт. (Рис. 4)

Для выяснения вопроса о возможности и надежности зажигания d-t реакции в расчеты вводился феноменологический параметр k_α, определяющий долю энергии α - частиц, передаваемую плазме (электронам). Предполагалось, что за время $\Delta t = 5$ сек в плазму с помощью инжектора нейтральных

атомов вводится энергия $3\text{–}5.10^7$ дж. (энергия инжектируемых частиц $E_0 = 100$ кэв , ток $i \approx 100$ а). После отключения инжектора реакция продолжает развиваться даже при $k_\alpha = 0.5$. Стационарное состояние при $k_\alpha = 1$ устанавливается за время $t = 30 \div 40$ сек, при $k_\alpha = 0.5$ - за время $t = 60\text{–}80$ сек. При небольших значениях коэффициента передачи $k_\alpha \cong 0.01$ температура плазмы спадает с характерным временем порядка 20 - 30 сек.

Малые потери по ионному каналу в рассматриваемой модели (без учета гофрировки магнитного поля) приводят к весьма высоким температурам части в стационарном состоянии : при $n = 6.10^{13}$ см$^{-3}$ $T_e \sim 60$ кэв, $T_i \sim 50$ кэв , при $n = 12.10^{13}$ см$^{-3}$ $T_e \sim T_i \sim 80$ кэв. В последнем случае для зажигания реакции достаточно дополнительной энергии $W \approx 10^8$ дж, вводимой за время $\Delta t = 5$ сек. Однако, развитие реакции при $n = 12.10^{13}$ см$^{-3}$ ведет к большим значениям $\beta_I \sim 8\text{–}10$ и нарушению условий равновесия и устойчивости плазмы в торе.

Снижение величины магнитного поля до значения $H = 30$ кэ и соответствующее уменьшение тока до $I = 4.2$ Ма увеличивает ионную теплопроводность и снижает ионную температуру. В результате условия самоподдержания реакции при плотности $n = 6.10^{13}$ см$^{-3}$ становятся более критичными : после выключения инжектора при $k_\alpha = 1$ реакция развивается хорошо, а при $k_\alpha = 0.5$ реакция "тлеет", очень медленно разгораясь.

Если малый радиус камеры снижается до значений $a = 100$ см то зажигания реакции не происходит. После отключения инжекции

при $T_i \sim 25$ кэв ионы перестают нагреваться даже при $k_\alpha = 1$. При $k_\alpha = 0.5$ реакция гаснет с характерным временем $t \sim 10 - 15$ сек.

При вычислениях по "бомовской" модели предполагалось, что коэффициенты теплопроводности определяются формулами

$$\chi_{i,e} = \frac{1}{\mathscr{K}} \chi^{B}_{i,e} \qquad \left(\chi^{B}_{i,e} = \frac{c\, T_{i,e}}{16\, eH} \right),$$

где $\mathscr{K}$ - феноменологический коэффициент.
В современных установках $\mathscr{K} \sim 30 - 100$.

Расчеты энергобаланса для основного варианта (I) проводились для $\mathscr{K} = 10^2 - 10^3$. Предполагалось также, что дополнительный нагрев плазмы производится непрерывной инжекцией пучка горячих нейтралов с энергией $E_0 = 100$ кэв и током $i = 100$ а.

Для плотности $n = 6.10^{13}$ см$^{-3}$ расчеты показали, что при $\mathscr{K} \sim 600$ реакция не является самоподдерживающейся. За время $t \sim 5$ сек пучок нагревает плазму до температуры $T_i \sim 10$-12 кэв, однако, при этом $n \tau_E \sim 8$-9.10^{13}, что недостаточно для дальнейшего развития реакции. Лишь при $\mathscr{K} \sim$ 600-700 энергия, выделяемая с α - частицами, сравнивается с энергией пучка горячих нейтралов. При увеличении плотности плазмы до значения 12.10^{13} см$^{-3}$ и тока инжектора до $i = 200$ А порог зажигания по параметру $\mathscr{K}$ снижается в 2-2.5 раза.

В ходе расчетов выяснялось поведение холодных нейтралов, идущих со стенок камеры, и их роль в энергобалансе. В периферийном слое плазмы толщиной $l \sim 20$-30 см, где температура нейтралов не очень велика, происходит быстрый спад их плотности

на 2 порядка. Во внутренних слоях плазмы поведение плотности нейтралов хорошо описывается диффузионным приближением. При $T_i \sim 10$ кэв плотность нейтралов в центре плазмы на 5 порядков меньше, чем на периферии.

В энергетическом балансе холодные нейтралы начинают играть заметную роль, начиная с плотности нейтралов в вакууме $N_0 \sim 10^9 см^{-3}$. Их влияние особенно существенно на периферии шнура. При $N_0 \sim 10^{10} см^{-3}$ ионы плазмы из-за перезарядки остаются холодными ($T_i \sim T_i^{wall}$) в приповерхностном слое толщиной порядка 10 см. Для модели бомовской теплопроводности в стационарном режиме при $\mathcal{R} = 800$ нейтралы с плотностью $N_0 = 10^{10} см^{-3}$ снижают T_{imax} с 15 кэв до 10 кэв, а полное энергетическое время на 30-40% (с $\tau_E \sim 1.8$ сек до $\tau_E \sim 1.2$ сек.).

Для оценки роли гофрировки магнитного поля в энергобалансе использовались следующие модели для коэффициентов ионной теплопроводности

$$\chi_i = \chi^{neo} + \chi^{ripple} \quad и \quad \chi = \frac{1}{\mathcal{R}} \chi^{Bohm} + \chi^{ripple}$$

Вычисления по первой модели показали, что при увеличении глубины гофрировки 2δ от 0 до 0.02 энергетическое время в диапазоне $T_i = 10$-30 кэв падает от значений $\tau_E = 7$-8 сек до $\tau_E = 3.5 - 4$ сек. Расчеты по второй модели проводились при $\mathcal{R} = 800$. В этом случае при $T_{imax} = 10$ кэв значения энергетического времени уменьшаются от $\tau_E = 2.6$ сек ($\delta = 0$) до $\tau_E = 1.6$ сек ($2\delta = 0.10$).

В обоих моделях парциальное энергетическое время гофрировки при $2\delta = 0.02$ и $T_{imax} = 10$ кэв составляет

τ_E^{ripple} 8–15 сек. Таким образом значение $\delta = 0.01$ на границе плазмы является максимально допустимым, при котором эффекты гофрировки не сказываются заметным образом на энергобалансе.

ПРИЛОЖЕНИЕ 2.

Расчет эффективности поглощения энергии обыкновенной волны в установке Т-20 .

(Ю.Н.Днестровский, Г.В.Переверзев, В.В.Параил)

Решалась задача о поглощении обыкновенных электромагнитных волн с частотой Ω , равной электронной циклотронной частоте (в центре плазменного столба) в установке Т-20. Плазме считалась бесстолкновительной с параметрами : $n_e = \frac{3}{2} n_0 \left(1 - \frac{r^2}{a^2}\right)$ ($n_0 = 5.10^{13}$ см$^{-3}$), $T_e = \frac{3}{2} T_0 \left(1 - \frac{r^2}{a^2}\right)$ ($T = 3; 5; 10$ кеV), $H = H_0 \left(1 - \frac{r}{R} \cos\vartheta\right)$ ($H_0 = 35$ кгс), $R = 5$ м, $a = 2$ м , $\Omega = \omega_{He} (r = 0)$.

Считалось, что волна поглощается за счет линейного циклотронного механизма затухания. Поскольку обыкновенная волна имеет почти круговую поляризацию с направлением вращения, противоположном вращению электронов в магнитном поле, то декремент ее затухания очень мал ($\varkappa/k \leq 10^{-3}$ при $\Omega \simeq \omega_{He}$). На ЭВМ рассчитывалась траектория волны, проникающей в плазму со стороны малого магнитного поля, и поглощение ее энергии вдоль луча в зависимости от величины угла θ на границе плазмы ; $\theta = \{\vec{k}\hat{\vec{H}}\}$.

Показано, что для углов $\theta \gtrsim 50^\circ$ рефракция слабо влияет на распространение волны и траектория проходит вблизи центра плазменного столба. При $\theta \lesssim 60^\circ$ за один проход поглощается практически вся энергия волны (так при $T_0 = 10$ кеV при $\theta = 60^\circ$ $\ln \frac{W_{нач}}{W_{кон}} = 4{,}1$; при $\theta = 70^\circ$ $\ln \frac{W_{нач}}{W_{кон}} = 1{,}8$). Оказывается, что основная доля энергии поглощается электронами с энергией $E \lesssim T_0$, т.е. идет на нагрев основной

компоненты плазмы ; зона нагрева локализована в области $\frac{\Omega-\omega_{He}}{\Omega}\ll 1$, т.е. $\frac{\Delta r}{a}\leq\frac{1}{4}$, что позволяет в принципе менять локализацию зоны нагрева, меняя величину поля H_0 или частоту волн. В расчетах учитывалось возможное наличие в плазме пучка ускоренных электронов с энергией $T_в\simeq$ 250 кэ и $n_в/n_e=10^{-2}$. Расчеты показали, что при $T_0\geq$ 3 кэ доля энергии, теряемой волной на пучке, пренебрежимо мала по сравнению с энергией, идущей на нагрев основной компоненты плазмы.

ПРИЛОЖЕНИЕ 3.

Зависимость радиационных потерь термоядерной плазмы от атомного номера примеси и температуры

(В.И.Гервидс, В.И.Коган)

Рассчитаны зависимости радиационных потерь термоядерной плазмы от атомного номера примеси Z и электронной температуры T_e, а также зависимость от Z "летальной" относительной концентрации примеси в DT -реакторе. Результаты такого расчета необходимы (в сочетании с соответствующей зависимостью от Z коэффициента распыления) для оптимального выбора материала стенки и диафрагмы термоядерного реактора.

Модель. Расчеты велись на основе модели коронального равновесия для постоянных и однородных n_e, n^* и T_e / n_e и n^* - концентрации электронов и примеси. Сама корональная модель, как показывает сравнение с результатами расчетов по более общей столкновительно-радиационной модели, хорошо применима при низких n_e, высоких T_e и больших Z, специфичных для плазмы термоядерного реактора, а ее стационарный предел / $t \to \infty$ / обеспечивается выполнением критерия Лоусона $n_e \tau \gtrsim 10^{14}$ см$^{-3}$сек.

Ионизационное состояние примесей. О глубине "обдирки" различных примесей можно судить по приведенным в таблице I для температуры T_e = 10 кэв относительным концентрациям различных ионов титана, железа, молибдена и вольфрама. Звездочкой отмечены значения концентраций наиболее "репрезентативных" ионов.

Таблица I

Z	Заряд иона $K = Z - N$							
	Относительная концентрация иона							
22	22 0,66*	2I 0,30	20 0,04					
26	26 0,28	25 0,48*	24 0,23	23 0,0I				
42	42 0,00	4I 0,0I	40 0,47*	39 0,37	38 0,I3	37 0,02		
74	65 0,03	64 0,I3	63 0,24	62 0,29*	6I 0,I8	60 0,08	59 0,03	58 0,0I

Из таблицы I видно, что при рассматриваемых температурах ядра даже самых тяжелых примесей способны удержать лишь число электронов $N \lesssim$ I0, так что $N \ll Z$. Это, в частности, резко упрощает учет экранировки в тормозном излучении.

Радиационные потери. На рис. I - 3 представлены результаты расчетов мощности радиационных потерь на тормозное, рекомбинационное и линейчатое излучения / и их сумма /, отнесенных к одной частице примеси и к одному электрону. Немонотонности кривых связаны с проходом гелие- и неоноподобных оболочек. Слабая зависимость суммарных потерь $Q^{сум}$ от T_e объясняется наличием в них как растущих, так и убывающих с T_e слагаемых.

Постепенная смена характера зависимости $Q^{сум}$ от заряда ядра Z / сначала примерно $\sim Z^4$, затем $\sim Z^3$ и, наконец, $\sim Z^2$ / обусловлена сменой ролей тормозного, рекомбинационного и линейчатого механизмов излучения.

Как видно из рис.3, при сравнительно небольших Z / когда обдирка примеси оказывается практически полной / $Q^{сум}(Z)$ хорошо апроксимируется трехчленной формулой

$$\frac{Q^{сум}}{n_e n^*} = 1{,}5\cdot 10^{-25} Z^2 T_e^{1/2} + 6\cdot 10^{-24} Z^4 T_e^{-1/2} + 8\cdot 10^{-23} Z^6 T_e^{-3/2}$$

(Васильев, Долгов-Савельев, Коган, 1962), учитывающей тормозное и рекомбинационное излучения в приближении голого ядра / $Q^{торм} \sim Z^2 T_e^{1/2}$, $Q^{рек} \sim Z^4 T_e^{-1/2}$, а линейчатое излучение - в приближении $T_e \gg Z^2 Ry$ эв, когда относительная концентрация водородоподобных ионов уже мала / $Q^{лин} \sim Z^6 T_e^{-3/2}$ /. Двучленная формула

$$\frac{Q^{сум}}{n_e n^*} = 1{,}5\cdot 10^{-25} Z^2 T_e^{1/2} + 5\cdot 10^{-24} Z^4 T_e^{-1/2}$$

(Коган, 1959) соответствует приближению 100%-ной обдирки ; ее разумная порядковая точность объясняется частичной взаимной компенсацией полного неучета $Q^{лин}$ и завышения $Q^{рек}$.

"Летальные" концентрации. Используем наши результаты для выяснения зависимости от Z "летальной" относительной концентрации примеси $C(Z) = \frac{n^*}{n_e}$, определяемой как такая концентрация, начиная с которой суммарные радиационные потери превосходят термоядерное энерговыделение реакции DT / в α - частицах / при любой температуре. При этом предполагается, что $T_e = T_i$, а n_e - фиксировано (т.е. не зависит от n^*).

Результаты расчета C (Z) для $10 \leq Z \leq 80$ хорошо апроксимируются формулой $C(Z) \approx 2{,}75 \cdot Z^{-1{,}67}$. Для C, Fe, Mo, W она дает $C(6) \approx 13\%$, $C(26) \approx 1{,}3\%$, $C(42) \approx 0{,}6\%$, $C(74) \approx 0{,}2\%$.

Подписи к рисункам :

Рис.1 Зависимости от T_e: $Q^{торм}$ (кривые 1 и 5), $Q^{рек}$ (кривые 2 и 6), $Q^{лин}$ (кривые 3 и 7), $Q^{сум}$ (кривые 4 и 8) для углерода (сплошные кривые 1-4) и железа (пунктирные кривые 5-8).

Рис.2 То же, что и рис.1, для молибдена (сплошные кривые (1--4) и вольфрама (пунктирные кривые 5-8).

Рис.3 Зависимость $Q^{сум}$ от Z . 1 - T_e = 10 кэв, 2 - T_e =20кэв 3 - T_e = 40 кэв ; —·—·—·— - двучленная формула (Коган, 1959) ; —×—×—×— - трехчленная формула (Васильев, Долгов-Савельев, Коган, 1962), две последние кривые - для T_e = 10 кэв.

Рис.4 Зависимость W_L, W_{cc} и τ_E от температуры.

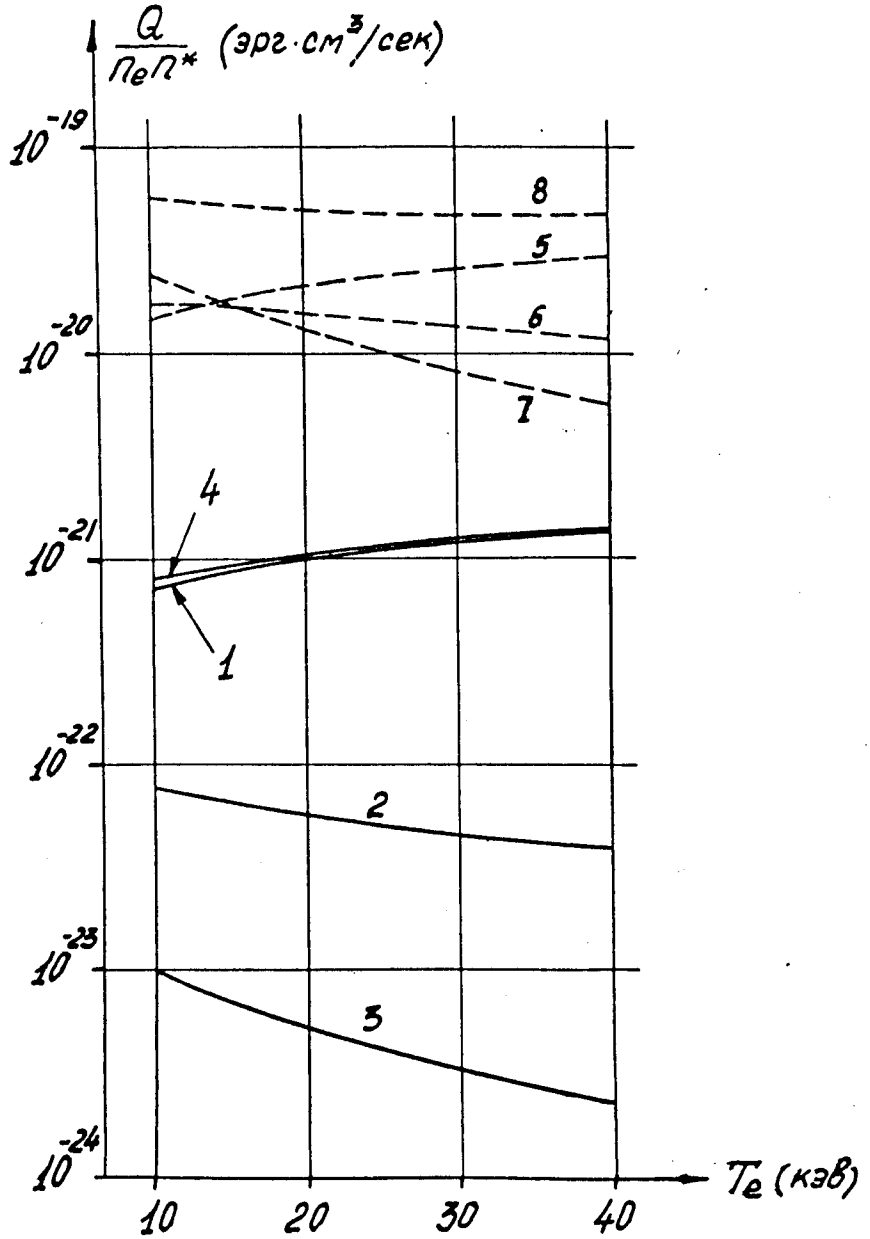
$\frac{Q}{n_e n^*}$ (эрг·см³/сек)
10^{-19}
10^{-20}
10^{-21}
10^{-22}
10^{-23}
10^{-24}
8
5
6
7
4
1
2
3
10
20
30
40
T_e (кэВ)

Рис.1

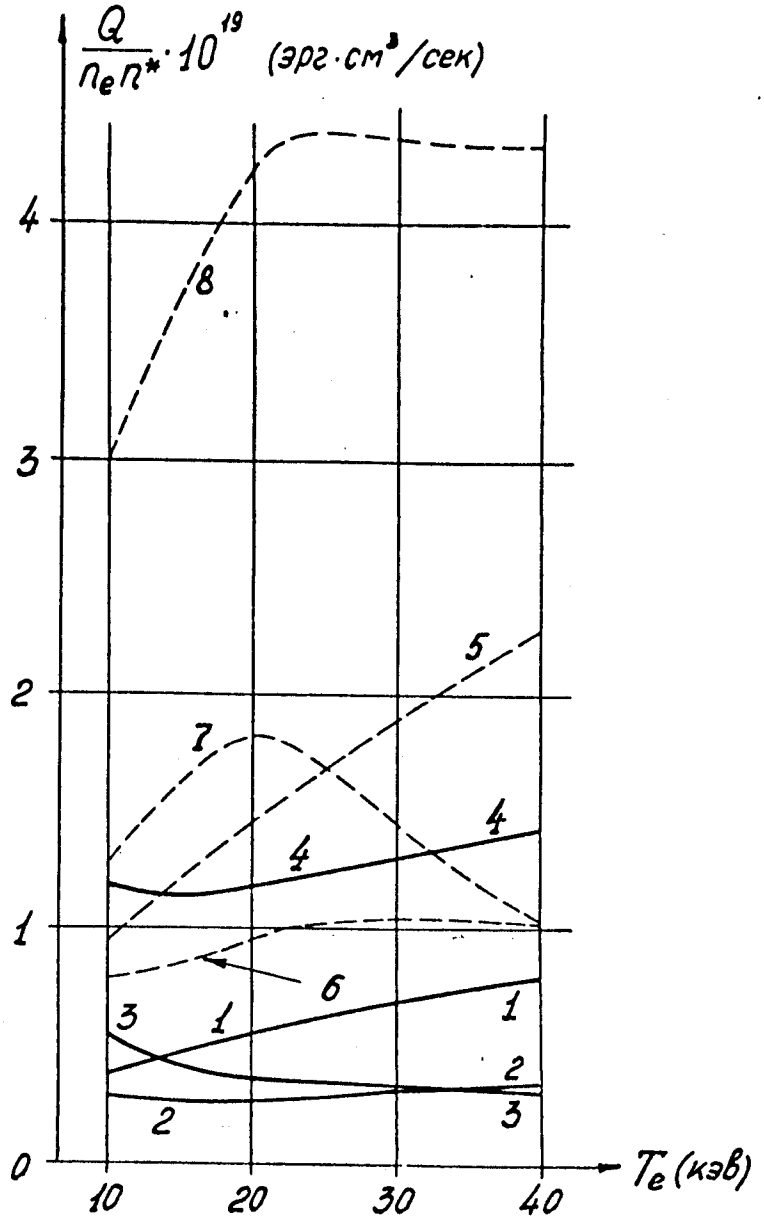
$\frac{Q}{n_e n^*} \cdot 10^{19}$ (эрг·см³/сек)
4
3
2
1
0
8
5
7
4
4
6
3
1
1
2
2
3
10
20
30
40
T_e (кэв)

Рис.2

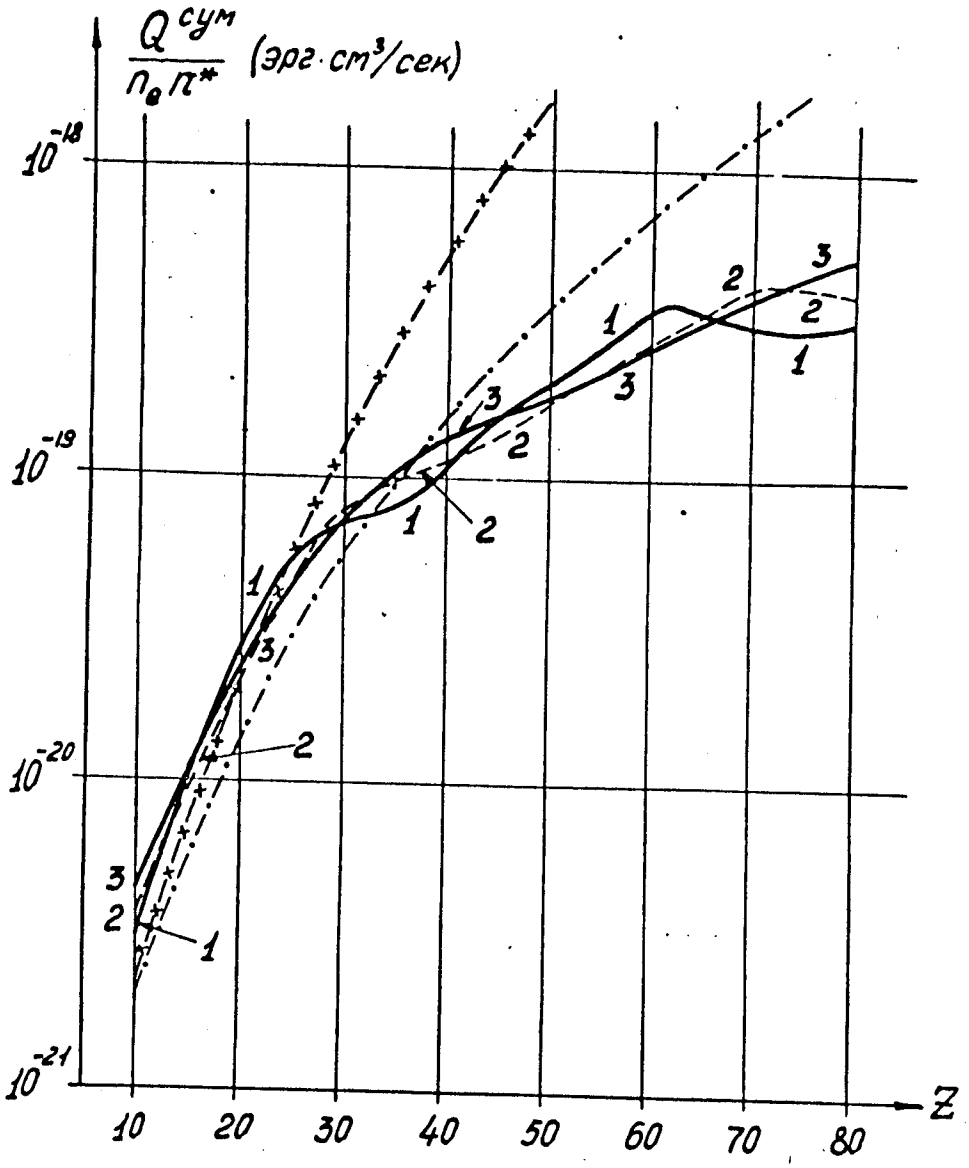
$\frac{Q^{сум}}{n_e \pi^*}$ (эрг·см³/сек)
10^{-18}
10^{-19}
10^{-20}
10^{-21}
10
20
30
40
50
60
70
80
Z
1
2
3

Рис.3

T-20

$R = 400$

$a = 150$

$H \doteq 4.0$

$n_{max} \doteq 6 \cdot 10^{13}$

W_α - мощность d-t реакций, выделяемая с α-частицами.

W_{ce} - циклотронное излучение из плазмы.

τ_E - полное энергетическое время жизни